Compartmentalized cAMP Signaling via the PDE4-Popeye Protein Complex

Amy Jane Tibbo

(BSc Hons)

Thesis submitted in fulfilment of the requirements for

Degree of Doctor of Philosophy

Institute of Cardiovascular and Medical Sciences,
College of Medical, Veterinary and Life Sciences,
University of Glasgow

April 2020

Abstract

The Popeye domain containing (POPDC) protein family are a unique family of transmembrane proteins with several proposed functions that are not fully understood. POPDC proteins are abundantly expressed in cardiac and skeletal muscle. Within the heart, POPDC1 has been shown to be highly expressed in the pace making centres and at moderate to low levels in the atria and ventricles. Given this localisation, a role for POPDC1 was hypothesised to be in the maintenance of normal heartbeat rhythm. Studies involving POPDC1 mutant mice and zebrafish provided evidence for this proposed function as the genetically modified model animals displayed cardiac arrhythmias as the predominant phenotype. Since POPDC proteins have been shown to be cAMP effectors, I set out to characterise their functions that that were regulated by cyclic nucleotide levels. As all the other known cAMP effector proteins such as PKA and EPAC form signalling complexes with phosphodiesterase (PDE) enzymes to limit cAMP concentrations in the vicinity of the cAMP effector, thus hindering their activation under basal conditions, the work presented in this thesis aimed to discover whether such a complex existed that contained POPDC and PDE4.

This thesis begins with characterisation of the molecular interaction between POPDC1 and PDE4A. It was hypothesised that a signalling complex containing POPDC1 and PDE4A would be formed as a regulatory mechanism to control cAMP concentrations in microdomains close to POPDC1 so modulating the activity of the protein. Co-immunoprecipitation studies along with proximity ligation assays confirmed the presence of this interaction in transiently transfected HEK293 cells, endogenously expressing neonatal rat ventricular myocytes (NRVM) and adult rabbit septal myocytes (ARSM). Fine mapping of the binding sites on each respective protein was carried out using peptide array technology. This allowed identification of key docking sites that mediate the interaction between POPDC1 and PDE4. Using the binding sequence for PDE4A on POPDC1, a cell penetrating disruptor peptide was created. It was proposed that the disruptor peptide would ‘unhook’ the POPDC1-PDE4A interaction, allowing for enhanced cAMP dynamics around POPDC1 therefore, modulating its interactions with other proteins such as the potassium channel TREK1. Using fluorescence resonance energy transfer (FRET) it was shown that the disruptor peptide led to a reduction in the

interaction between POPDC1 and TREK1, mimicking the effect of PDE4 inhibition with rolipram (4-[3-(cytopentyloxy)-4 methophenyl]-2-pyrrolidinone). Furthermore, treatment with the disruptor peptide in adult rabbit ventricular myocytes created a marked elongation of the cardiac repolarisation phase. It could be suggested that by blocking PDE4A binding to POPDC1, the subsequent increase in cAMP in its vicinity may lead to a reduction in the interaction between POPDC1 and TREK1. Given that the interaction with POPDC1 increases the current through the channel two-fold, the elongated repolarisation phase may be due to a decrease in K^+ efflux caused by the lack of POPDC1-TREK1 complex formation. This conclusion represents the first instance where PDE activity has been shown to influence POPDC function.

POPDC1 has previously been shown to be downregulated in human heart failure. Using a porcine model of myocardial infarction, I have demonstrated that there is an initial disease-induced reduction in POPDC1 expression levels that is lost after 3 months. In human patients suffering from heart failure, this loss in expression was not replicated. This data suggests that the initial reduction in POPDC1 creates a protective effect that helps the injury affected area of the heart in animal models.

A secondary aspect of this work was to investigate whether POPDC1 was subjected to any post translational modification (PTMs). PTMs are known to be able to modulate interactions between proteins through several mechanisms. *In silico* analysis of POPDC1 sequence revealed a high probability SUMOylation site (K119) and a PKA-dependent phosphorylation (T236) site which were confirmed using peptide array. Forced SUMOylation in NRVM further confirmed that Popdc1 is a SUMO substrate. It remains unclear at this time what the functional relevance of these PTMs are, but I hypothesize that either or both contribute towards the ability of POPDC1 to bind to different interaction partners by inducing a conformational change. This is the first study to show that POPDC1 is subjected to SUMOylation and phosphorylation.

The final part of this thesis reports work undertaken to determine the three-dimensional structure model of POPDC1. Currently, only indirect structural information about the protein is available, generated by homology modelling. Protein structure can often provide clues about putative protein function as well

as confirming that binding sites such as those identified in this work are surface exposed. Four expression constructs containing different fragments of POPDC1 were produced and the solubility of the proteins produced analysed. A construct containing only the Popeye domain was taken forward and highly purified samples were produced. Despite the quantity of recombinant protein, no structural analysis could take place as the protein aggregated in solution. Further testing of other constructs will be required to develop a construct that can be used to determine the structure of POPDC1.

In combination, the work described here provides a major contribution to the field showing, for the first time, that POPDC1 forms an interaction with PDE4A in the heart. I have also described novel methods and tools to investigate the functional correlates of the complex. In addition, this interaction underpins the first regulatory mechanism of POPDC1 to have been identified. Understanding the manner in which the POPDC1-PDE4A interaction affects cardiac pace making is necessary to pinpoint how POPDC1 contributes towards disease. This may lead to new therapeutic avenues that are able to target the POPDC1-PDE4A interaction.

Table of Contents

List of Figures

List of Tables

Acknowledgment

I would firstly like to give my deepest gratitude to my supervisor Professor George S. Baillie. Starting this project, I could never have imagined how far we could have come. George, you have been an amazing boss to have and I cannot thank you enough for all the support you have given me. I will miss your dad jokes, your ridicule and mostly, whisky Fridays! I feel lucky to have been a part of such an amazing lab group. Brian, as my second supervisor your help with the structural work has been incredible and I wish I could have worked more with you are your group. Gillian, words could not express how grateful I am that you took the time to read my thesis and offer advice! Thank you also to the MVLS DTP for their generous funding which has allowed me to carry out this work.

I would like to thank all the members of the Baillie lab group both past and present, it has been a complete honour to work alongside you all. The original crew; Ella, Bracy, Tara, Fiona and Gonzalo you guys were so welcoming and made this lab feel like a family. A massive thanks to my lab partner in crime, Tara. These past three years have been some of the best experiences of my life and it has been a joy to have come through this process together. To Alice, Galvin, Oom, and Jack, you guys have made the office such a laugh and I could not have imagined being able to make it to the end of this process without you lot. The Fuller lab, thank you for all the help you lot have given me, especially with the post translation modification experiments! Your expertise was invaluable.

Last but most not least, thank you to my wonderful family and friends who have been my support throughout the last three years. To my Mum and Dad, my sisters, and my grandparents, you have been the driving force behind me getting to where I am today, and I will never be able to thank you enough for everything you have done. To my amazing best friend Laura, thank you, you have been a rock who has helped and supported me throughout the years. Finally, to my amazing wife, Jen, without you there would be no thesis. Your love, advice and encouragement have dragged me the worst parts of this process. Thank you for standing beside me always.

Author's Declaration

I declare that the work presented in this thesis has been carried out by myself, except where otherwise cited or acknowledged. It is entirely my own composition and has not, in whole or part, been submitted for any other higher degree.

Amy Jane Tibbo

April 2020

Definitions/Abbreviations

ºC	degrees Celsius
25mer	25 amino acid peptide
5'AMP	5' - adenosine monophosphate
ß-AR	ß adrenergic receptor
AC	adenylyl cyclase
ACE	angiotensin converting enzyme
AD	Alzheimer's disease
ADP	adenosine diphosphate
AH	Akt homology
AKAP	A-kinase anchoring protein
ANOVA	a one-way analysis of variance
ANP	atrial natriuretic peptide
APD	action potential duration
ARSM	adult rabbit septal myocytes
ARVM	adult rabbit ventricular myocytes
ATP	adenosine triphosphate
AV	atrioventricular
AVN	atrioventricular node
BSA	bovine serum albumin
BVES	Blood vessel epicardial substance
C	catalytic subunit
CaCl2	calcium chloride
cAMP	cyclic 3',5' adenosine monophosphate
CAP	bacterial catabolite activator
CAV3	Caveolin 3
CBD	cAMP binding domain
cCMP	Cyclic, 3',5' cytidine monophosphate
CCS	cardiac conduction system
CD50	time from 50% contraction to 50% relaxation
CFP	cyan fluorescent protein
cGMP	cyclic 3',5' guanosine monophosphate
CL	chloride
cm	centimetre
CMC	critical micelle concentration
cmp	counts per minute
CNBD	cyclic nucleotide binding domain
CNGC	cyclic nucleotide gated channels
CNS	central nervous system
Co-IP	co-immunoprecipitation
CO2	carbon dioxide
COPD	chronic obstructive pulmonary disease
CREB	cAMP response element binding

CRP	cAMP response protein
DAG	diaglycerol
DAPI	4′,6-diamidino-2-phenylindole
DCM	dilative cardiomyopathy
ddH2O	double distilled water
dH2O	distilled water
DMEM	Dulbecco's modified eagle medium
DMSO	dimethyl sulfoxide
DNA	deoxyribose nucleic acid
DRG	dorsal root ganglion
E.coli	Escherichia coli
E1	SUMO activating enzyme
E2	SUMO conjugating enzyme, UBC9
E3	SUMO ligase
ECG	electrocardiogram
ECL	enhanced chemiluminescence
ECM	extracellular membrane
EDTA	ethylenediaminetetraacetic acid
EGF	epidermal growth factor
EGFR	epidermal growth factor receptor
EPAC	exchange proteins directly activated by cAMP
ER	endoplasmic reticulum
ERK	extracellular-signal-regulated kinase
FBS	foetal bovine serum
FFA	free fatty acids
FP	fluorescence polarisation
FRET	fluorescence resonance energy transfer
g	grams
GAL	Galectin-1
GAPDH	Glyceraldehyde 3-phosphate dehydrogenase
GDP	guanosine diphosphate
GEFT	guanine nucleotide exchange factor
GMP	guanosine monophosphate
GPCR	G-protein coupled receptors
GST	glutathione S-transferase
GTP	guanosine triphosphate
H2PO4	dihydrogen phosphate
HA	haemagglutinin
HCC	hepatocellular carcinoma
HCl	hydrochloric acid
HCN	hyperpolarisation-activated cyclic nucleotide-gated
HCNGC	hyperpolarisation-activated cyclic nucleotide-gated cation
HCSM	hydrophobic cluster dependent SUMOylation motif
HEK-293	human embryonic kidney-293 cells
HEPES	4-(2-hydroxyethyl)-1-piperazineethanesulfonic acid

HERG	human-ether-a-go-go-related gene
HF	Heart Failure
HIF	Hypoxia inducible factor
HIS	histidine
HRP	horseradish peroxidase
HSP	Heat shock protein
I_{ca}	inward Ca^{2+} current
IκBα	nuclear factor κ light polypeptide gene enhancer in B-cells inhibitor α
IBMX	3-isobutyl-1-methylxanthine
IF	immunofluorescence
IP	immunoprecipitation
IPTG	Isopropyl ß- d-1-thiogalactopyranoside
I/R injury	ischaemia/reperfusion injury
K_B	background potassium current
kDa	kilodalton
KO	knock-out
LAD	left anterior descending
LB	lysogeny broth
LTCC	L-type calcium channel
LSM	laser-scanning confocal microscope
LV	left ventricle
M	molar
M1	NRVM day 1 medium
M199	medium 1999
M2	NRVM day 2 medium
MAP	mitogen activated protein
MBP	Maltose-binding protein
MI	myocardial infarction
mg	milligram
Mg-ATP	magnesium adenosine triphosphate
MgCl2	magnesium chloride
MgSO4	magnesium sulphate
ml	millilitre
MS	mass spectrometry
N106	*N*-(4-methoxybenzo[d]thiazol-2-yl)-5-(4-methoxyphenyl)-1,3,4-oxadiazol-2-amine
NaCl	sodium chloride
NaF	sodium fluoride
NaOH	sodium hydroxide
NCS	neonatal calf serum
NCX	sodium calcium exchanger
NDSM	negatively charged amino acid-dependant SUMOylation motif
NEAA	minimum essential medium non-essential amino acids
NFκB	light chain enhancer of activated B cells
ng	nanogram

Ni-NTA	nickel-nitrilotriacetic acid
nm	nanometre
NO	nitric oxide
NKA	Na^+, K^+-ATPase
NMR	nuclear magnetic resonance spectroscopy
NPB	Nuclear Protein Buffer
NPC	nuclear pore complex
NRVM	neonatal rat ventricular myocytes
P/S	penicillin/streptomycin
PAT	protein acyltransferases
PBC	phosphate binding cassette
PBS	phospho-buffered saline
PCR	polymerase chain reaction
PDE	phosphodiesterase
PDI	protein disulphide isomerase
PDSM	phosphorylation dependent SUMOylation motif
PFA	paraformaldehyde
PIAS	protein inhibitor of activated STAT
PIP	POPDC interacting protein
PKA	protein kinase A
PKB	protein kinase B
PKC	protein kinase C
PKG	protein kinase G
PLA	proximity ligation assay
PLB	phospholamban
PLM	promyelocytic leukaemia
POPDC	Popeye domain containing protein
PTM	posttranslational modification
RAC	resin-assisted capture
RNA	ribonucleic acid
rpm	rotations per minute
ROS	reactive oxygen species
RPKM	reads per kilogram per million
RT	room temperature
RyR	ryanodine receptor
SA	sinoatrial
SAN	sinoatrial node
SDS	sodium dodecyl sulfate
SDS-PAGE	sodium dodecyl sulfate–polyacrylamide gel electrophoresis
SEM	standard error of the mean
SENP	sentrin-specific protease
SERCA	sarco/endoplasmic reticulum Ca2+-ATPase
SIM	SUMO interacting motif
SR	sarcoplasmic reticulum
SSS	sick sinus syndrome

SUMO	small ubiquitin-like modifier
TAPAS	tryptophan anchoring phosphatidic acid selective-binding domain 1
TBS	tris buffered saline
TBST	tris buffered saline with Tween-20
TCEP	tris(2-carboxyethyl) phosphine
TM	transmembrane
TNF	Tumour necrosis factor
TNFR	Tumour necrosis factor receptor
Tn	troponin
TnC	troponin C
TnI	troponin I
UBC9	SUMO conjugating enzyme, also referred to as E2
UCR	upstream conserved region
UF	unfractionated
VSMC	vascular smooth muscle cell
v/v	volume/volume
w/v	weight/volume
WB	western blot
WT	wild type
YFP	yellow fluorescent protein
µg	microgram
µl	microlitre
µm	micrometre
µM	micromolar

1 Introduction

1.1 Understanding the electrophysiology of the heart

1.1.1 Contractile apparatus

Muscle contractions are governed and executed by electrical stimulation. The rhythmic alteration between contraction and relaxation is the defined mechanistic basis for heart pump function. During normal cardiac cycle, the atria contract to move the blood into the ventricles which are relaxed. Upon the ventricles becoming filled, the ventricular myocardium contracts pushing blood into either the pulmonary artery, if exiting the right ventricle, or the aorta, if exiting the left ventricle. Relaxation of both the atria and ventricles allows the cardiac cycle to begin again.

Contractile apparatus is found in both cardiac and skeletal muscle. In both cell types there exists functional similarities and vastly significant differences. The most important shared feature is the presence of myofibrils which are responsible for the cell's ability to contract. Myofibrils are composed of sarcomeres arranged in a regularly repeating fashion. Each sarcomere is comprised of thick and thin filaments laid out in a manner that gives the appearance of the myofilaments being striated when examined microscopically. Thin filaments are mainly composed of actin, troponin and tropomyosin but also contain proteins such as the actin-binding protein nebulin, whereas thick filaments are mainly comprised of myosin molecules (Holland and Ohlendieck, 2013, van Eldik and Passier, 2013). There are several sarcomeric components that can also be identified for example Z-discs, which form the boundary of the sarcomere. Surrounding each Z-disc is the A (anisotropic) band and the I (isotropic) band with the M (middle) line running through the centre of the Z-disc. Anchored at Z-discs is titin, the largest protein known, functioning to connect the thick filaments to the Z-disc to increase the stability of the sarcomeres, which plays a crucial role in muscle elasticity and generation of passive muscle force (van Eldik and Passier, 2013, Fukuda et al., 2008, Gautel, 2011). Other components of the Z-discs include the telethorin (T-cap) which is known to bind to proteins within t-tubules to help with their development, structure and function (Zhang et al., 2009, Ibrahim et al., 2013). The physical event of a contraction involves the sliding of the thin filaments past the thick filaments. This in turn causes the shortening of the sarcomere and contraction of

the myofibril and the muscle. Mechanistically, the contraction is proposed to be delivered by the cross-bridge and swinging lever-arm hypothesis of muscle contraction (Holmes, 1997). This involves the myosin cross-bridges which are bound to actin. These complexes are dissociated by ATP binding to the ATPase, myosin, resulting in a conformation change of the myosin cross-bridge. Upon the hydrolysis of ATP to ADP + P_i, the conformation returns to its native state. Movement of the filaments creates a rowing like action of the myosin cross-bridge pulling the thin filament toward the M-line. Swinging-level theory addresses this by basing the movement of only the distal carboxy terminal portion of myosin keeping the main part of the cross-bridge attached to actin (Holmes, 1997).

1.1.2 Electrical activity in the heart

The rhythmic contraction of the heart is controlled by the propagation of electrical impulses controlled by the cardiac conduction system (CCS). To generate the cardiac contraction, an electrical impulse begins in the sinoatrial (SA) node, located within the wall of the right atrium, where it passes through the Bachman's bundle into the left atrium. Additionally, from the SA node the signal is passed to the atrioventricular (AV) node allowing the propagation of the impulse through the bundle of His and down the bundle branches. This impulse is delayed slightly to allow the blood from the atria to fill into the ventricles before contraction. The right bundle branch depolarizes the right ventricle while the left bundle branch depolarizes both the left ventricle and the interventricular septum (Anderson et al., 2009, Renwick et al., 1993). Depolarization generates the contraction and the expulsion of blood from the ventricles.

These physiological changes correlate with changes in action potential. This is namely down to changes in the ubiquitous second messenger Ca2+, which is central to cardiac electrical activity and is the direct activator of the sarcomere (Bers, 2002). The sarcomere is the basic functional unit of the muscle found within a myocyte. It consists of contractile elements; myosin, thick filaments that have globular heads that possess ATPase activity and actin, thin filaments arranged in an alpha helix woven between the myosin filaments. Tropomyosin acts a regulatory element which prevents the interaction between the myosin globular head and the actin during rest. Troponin, a complex of three proteins (T, I and C)

sits alongside the actin filaments. Troponin T (TnT), mediates the interaction between troponin and other contractile proteins, troponin I (TnI) inhibits the enzymatic capacity of myosin, and troponin C (TnC) can bind Ca2+ allowing for the regulation of contraction (Bers, 2002).

The electrical impulse passes through the conduction pathway leading to the depolarisation of the cardiomyocyte membrane. Following the membrane depolarisation, the L-type calcium channels (LTCC) on the membrane open allowing an initial influx of Ca2+ into the cell. This Ca2+ induces the opening of the ryanodine receptors (RyRs) located on the surface of the sarcoplasmic reticulum (SR). The SR functions as an intracellular Ca2+ store and its opening generates a greater influx of Ca2+ into the cytosol (Bers, 2002). It is this free Ca2+ that is responsible for mediating the contraction of the myocytes through the contractile proteins. TnC binds free Ca2+ and induces its conformational change in troponin exposing a site on actin that can now interact with the myosin globular head. This interaction leads to the hydrolysis of ATP supplying energy for the conformational change of the actin-myosin complex. The change promotes the movement of the myosin globular head and actin with the two filaments sliding past each other. This shortens the length of the sarcomere resulting in the contraction of the myocyte. The relaxation of the myocyte occurs when Ca2+ is released from TnC and contractile proteins return to their resting state. Ca2+ is then either taken up by SERCA into the SR for storage or expelled from the cell via the Na+/Ca2+ exchanger (NCX) (Kawase and Hajjar, 2008, Bers, 2002). The last cellular component contributing to the modulation of Ca2+ is the mitochondrial Ca2+ uniport which allows Ca2+ to enter the mitochondria leading

to another intracellular store. This process begins again during the next depolarisation event (Figure 1.1)(Bers, 2002).

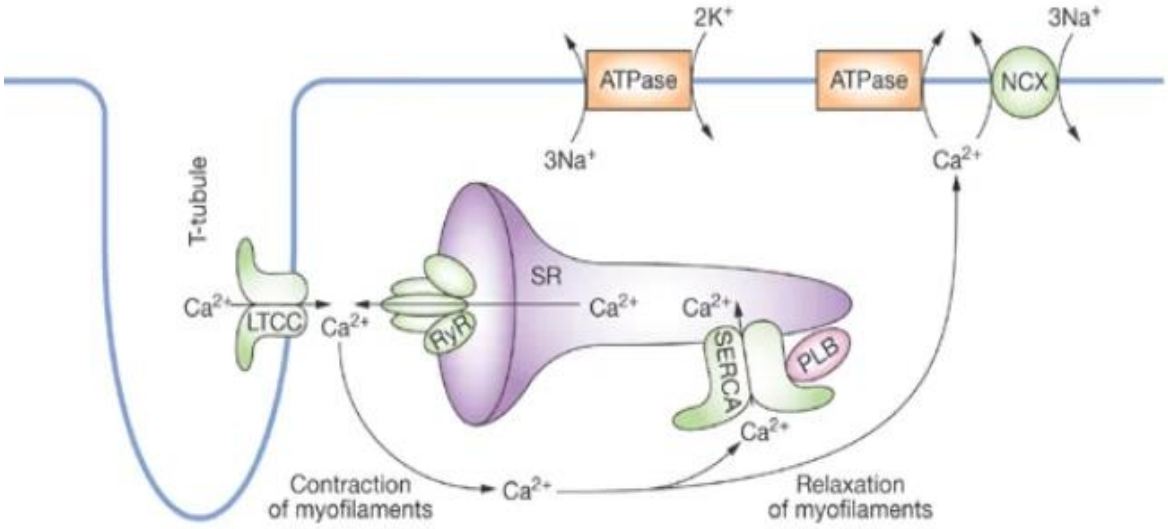

Figure 1.1 The excitation-contraction coupling. Ca^{2+} enters the cell via the activated L-type calcium channel (LTCC). This Ca^{2+} induces a conformational change in the ryanodine receptor (RyR) resulting in the release of Ca^{2+} from the sarcoplasmic reticulum (SR). Release Ca^{2+} interacts with contractile proteins to mediate cellular contraction. Relaxation of the cell occurs through the removal of Ca^{2+} from the cell via sarcoplasmic/endoplasmic reticulum calcium ATPase (SERCA) or sodium–calcium exchanger (NCX). (Kawase and Hajjar, 2008)

1.2 Cyclic Nucleotide Signalling

1.2.1 Second Messengers and Signal Transduction

Signal transduction is the process by which cells translate external cues into temporal physiological responses. Generally speaking, the activation of signal transduction begins with the interaction of an extracellular ligand, commonly a neurotransmitter, small molecule or a hormone, with a membrane bound receptor. The ligand binding initiates a distinct intracellular signalling pathway, which can involve a ubiquitous second messenger, which in turn drives signal transduction. These second messengers are the crucial link between the sensing of a stimuli by the receptors and the internal cellular effector proteins which can drive the creation of physical changes to respond appropriately to external environments (Sutherland, 1972). Second messengers include a wide variety of small molecules and ions that allow the cell to discretely respond to changes in extracellular environment. They can be rapidly generated or released to trigger

a pool of activated cellular effector proteins. For this sequence of events to work, there has to be an orchestrated signalling response driven by the activated receptor. Levels of second messenger molecules within the cell must be controlled both temporally and spatially to allow for compartmentalised signal transduction that is both effective and fleeting. The signalling response is complete when the concentrations of the second messenger is reduced back to a basal level following release of the second messenger from the cell, reuptake into a cellular store or by its degradation by specialised enzymes (reviewed in (Newton et al., 2016)). There are a variety of second messengers which include Ca^{2+}, diaglycerol (DAG), inositol triphosphate (IP_3) and cyclic nucleotides (Berridge, 1984, Sutherland, 1972). The two main forms of cyclic nucleotides involved in a wide range of cellular signalling are cyclic 3'5'-adenosine monophosphate (cAMP) and cyclic 3'5'-guanosine monophosphate (cGMP). Each are comprised of a nucleotide with a single phosphate that possesses two single bonds between the sugar and this phosphate. Although there are non-canonical cyclic nucleotides such as cyclic 3'5'-cytidine monophosphate (cCMP) and cyclic 3'5'-uracil monophosphate (cUMP); theses will not be discussed in this work as they are still relatively uncharacterised.

1.2.2 cAMP Signalling Pathway

The first discovery of a second messenger molecules was of cAMP (Sutherland and Rall, 1958). cAMP is an important second messenger molecule that is involved in a plethora of cellular processes. The cAMP signalling pathway begins with the binding of a specific ligand to a G-coupled protein receptor (GPCR) (Figure 1.2). Within the span of the human genome, approximately 4% of the total protein coding genome codes for GPCRs. These receptors possess both widespread expression patterns and a huge range of physiological roles. Generally, GPRCs contain a distinct extracellular N-terminal region, seven transmembrane domains and a cytosolic C-terminus. Housed within the N-terminal region is a ligand binding site which activates the receptor (Rosenbaum et al., 2009). The C-terminal region interacts with heterotrimeric G-proteins consisting of α, ß and γ subunits. G-proteins are normally referred to by their α subunit therefore the heterotrimeric version contains $G\alpha_s$, $G\alpha_i$ and $G\alpha_q$ subunit (Pierce et al., 2002). Each of these subunits possesses a distinct function within the signalling pathway. $G\alpha_s$ is known to positively interact with the cyclic

nucleotide catalysing enzyme adenylyl cyclase (AC). The converse can be said about $G\alpha_{i,}$ which negatively inhibits the activity of AC (Pierce et al., 2002). Lastly, $G\alpha_q$ works independently of both cAMP and AC pathways. It instead activates phospholipase C and signalling via the second messengers IP_3 and DAG. Upon ligand binding, the GPCR causes the α-subunit to release its attached guanosine diphosphate (GDP) and exchange it for a guanosine triphosphate (GTP) which drives a conformational change and subsequently the dissociation of the Gα subunit (Pierce et al., 2002). In addition to the α subunit signalling, the ßγ complex of the G-protein mediates alternative signalling pathways. The functional diversity within the GPCRs is due to the multiple ways in which the numerous genes encoding the subunits (sixteen α, five ß and twelve γ) combine (Pierce et al., 2002).

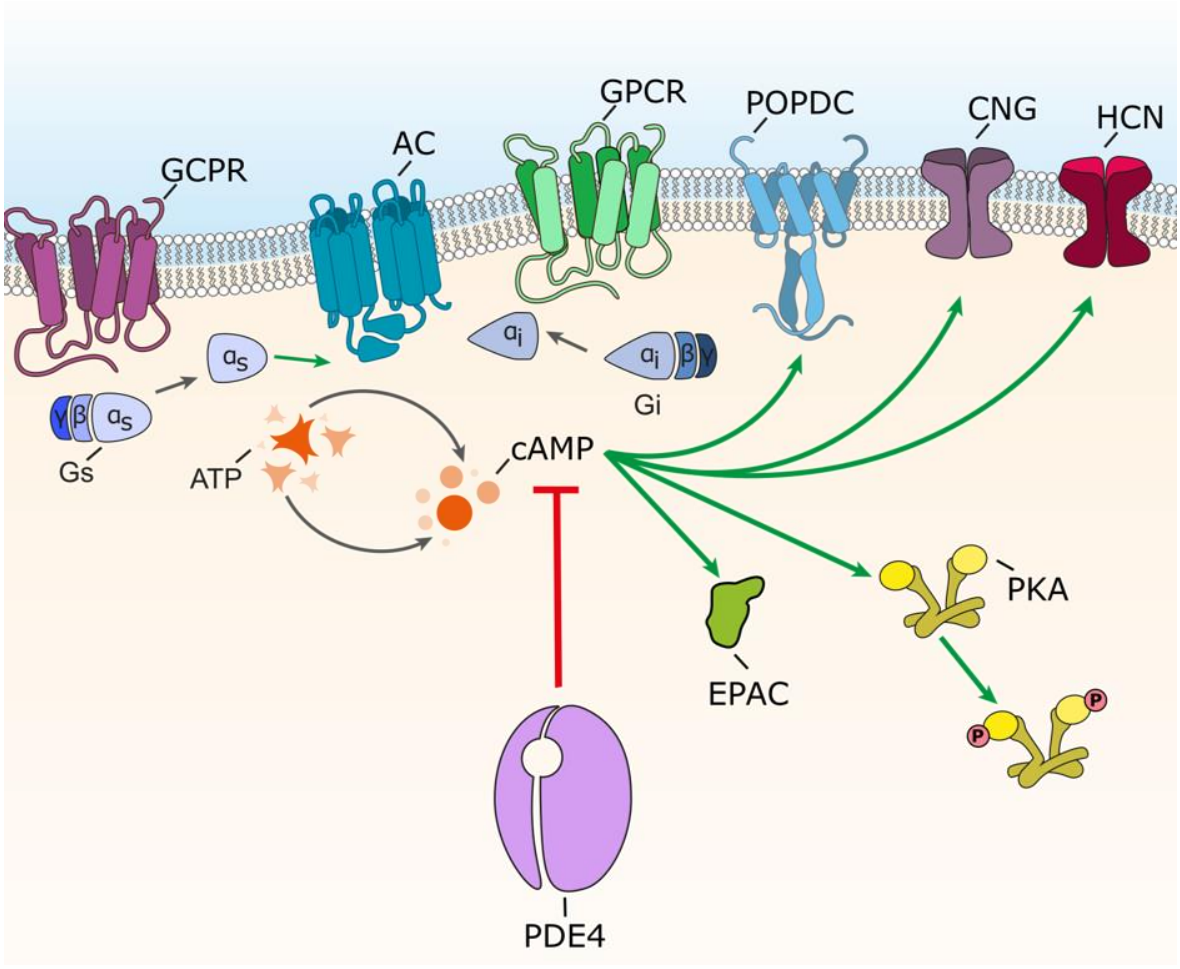

Figure 1.2 cAMP signalling pathway. Following the activation of membrane bound GPCRs, ACs are stimulated through the binding of the $G\alpha_s$ subunit leading to the generation of cAMP from ATP at the surface of the membrane. cAMP activates four main effector proteins: CNGC, PKA, EPAC, and POPDC, which are responsible for the mediation of many signalling pathways. The HCN channels are also known to be gated by cAMP and are of importance in cardiac cells. The only known enzyme able to hydrolyse cAMP is the superfamily of enzymes, PDEs. PDEs hydrolyse cAMP resulting in an inhibitory effect on the second messenger and its signalling pathways. (AC, adenylyl cyclase; ATP, adenosine tri-phosphate; GCPRs, G-protein coupled receptors; Gs, stimulatory G-protein; Gi, inhibitory G-protein; CNGC, cyclic nucleotide gated channel; EPAC, exchange protein directly activated by cAMP; POPDC, Popeye domain-containing protein; HCN, hyperpolarisation-activated cyclic nucleotide-gated channel; PDE, phosphodiesterase; PKA, protein kinase A).

GPCR classical signalling begins with the activation or inhibition of the membrane bound AC enzyme by $G\alpha_s$ or $G\alpha_i$, respectively. The most conserved AC structure in higher eukaryotes consists of a short N-terminal region and two cytoplasmic domains (C_1 and C_2) which contain two hydrophobic regions (M_1 and M_2). There is a total of twelve transmembrane (TM) helices that are dispersed within the cytoplasmic domains. The first six TM domains (TM1-TM6) are followed by a region containing a catalytic domain (C1a) followed by a C1b domain. A further TM region (TM7-12) follows, connected to a second catalytic

domain (C2a) and a C-terminal C2b region (Qi et al., 2019). Within the two cytoplasmic loops are conserved ATP binding regions which dimerise in order to form the catalytic part of the enzyme (Krupinski et al., 1989, Qi et al., 2019).

When AC is activated by association with $G\alpha_s$ it catalyses the production of cAMP from ATP (Figure 1.2). Interestingly, the catalytic site of the enzyme resembles that of DNA polymerase which suggests that it may function in a similar manner with a phosphoryl transfer mechanism (Tesmer et al., 1997, Zhang et al., 1997, Tang and Hurley, 1998). Contained within the catalytic site are two aspartate residues which can bind two Mg^{2+} atoms that facilitate the phosphoryl transfer. This in turn promotes the cyclisation of cAMP and the release of two phosphate groups (Willoughby and Cooper, 2007). The activity of AC results in a rapid increase in cAMP concentration around the inner surface of the plasma membrane. Since the original characterisation by Krupinski and colleagues (1989), a further eight structurally similar AC isoforms have been identified (Willoughby and Cooper, 2007).

1.2.3 cAMP effector proteins

As described, cAMP is produced by membrane bound ACs which are activated via Gs protein-mediated signalling. cAMP is known to act through interaction with and activation of four distinct classes of effector proteins: protein kinase A (PKA), exchange protein directly activated by cAMP (Epac), hyperpolarisation-activated cyclic nucleotide-gated cation (HCN) channels and Popeye domain containing (POPDC) proteins (see Figure 1.3).

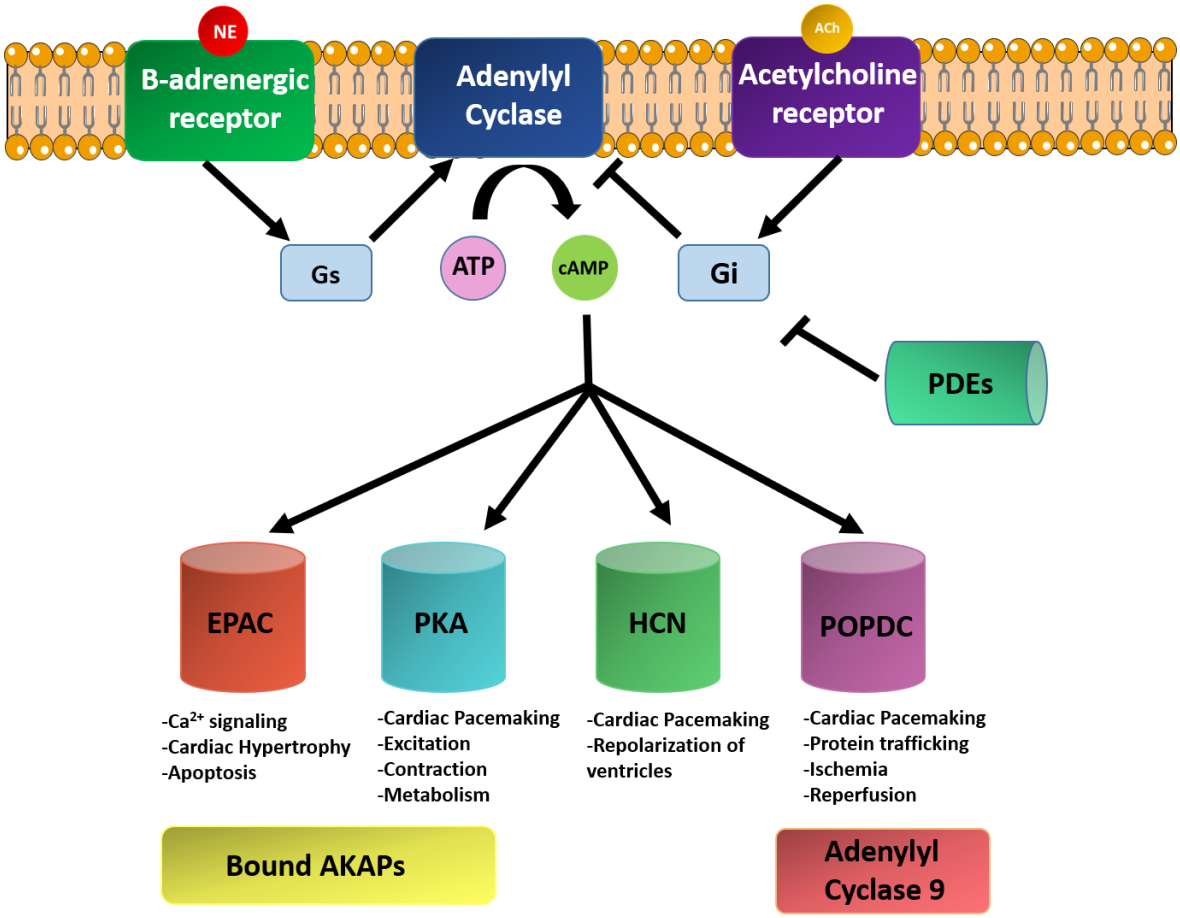

Figure 1.3 Signalling pathways of the four cAMP effector proteins and their main functions in the heart. Norepinephrine (NE) is secreted by sympathetic neurons and can bind to the β-adrenergic receptor embedded in the membrane of the cell. Binding leads to Gs activation and subsequent activation of Adenylyl Cyclase's (AC) generating cAMP. AC are inhibited through acetylcholine ligand binding to the muscarinic acetylcholine receptor. Upon receptor activation, Gi can be activated leading to the inhibition of AC decreasing cAMP production. Four main cAMP effector proteins sense these changes in cAMP levels; protein kinase A (PKA), exchange factor directly activated by cAMP (EPAC), hyperpolarization activated cyclic nucleotide gated (HCN) channel, the Popeye domain containing (POPDC) protein. PKA and EPAC are usually found bound to the same A-kinase anchoring protein (AKAP), whereas, POPDC1 and CNGCs are membrane bound. Listed below each effector protein are the main cardiac processes each is involved in. (Figure adapted from (Brand, 2018))

1.2.3.1 PKA

PKA was one of the first protein kinases to be discovered (Walsh et al., 1968). Interestingly, unlike most other eukaryotic protein kinases, PKA exists as a tetrameric enzyme consisting of two regulatory (R) subunits and two catalytic (C) subunits (Kemp et al., 1975). The C subunit of PKA can be phosphorylated at Threonine 197 (T197) which resides within the activation loop (Cheng et al., 1998, Cauthron et al., 1998). The C subunit is regulated by the interaction with the inhibitory R subunit. The R subunit binds to cAMP driving a conformational

change that leads to their dissociation from the C subunits. This dissociation allows for activation of the catalytic activity of the enzyme which can affect a range of diverse cellular processes by phosphorylating numerous cytoplasmic and nuclear proteins (Taylor et al., 1990). There are two known classes of PKA designated as PKA (I) and PKA (II) due to the differences that are found within R subunits, RI and RII respectively, that can interact with the identical C subunit (Taylor et al., 1990). Although both RI and RII contain tandem and highly conserved cAMP-binding domains (CBD) they differ in the N-terminal proteolytic hinge that allows their binding to the recognition site in the C subunit. In RII subunits there is a serine residue that can be autophosphorylated by the C subunit while the RI subunit possesses a pseudo phosphorylation site (Rosen and Erlichman, 1975).

PKA is a member of the family of serine/ threonine kinases that uses the active site to catalyse the transfer of a phosphate group from ATP to a threonine or serine residue on the target protein. Target threonine/serine residues are usually found integrated into a R-R-x-S/T-θ motif, where θ represents a hydrophobic amino acid and x represents any amino acid (Skalhegg and Tasken, 2000). As mentioned, this phosphorylation drives the activation of numerous cellular processes. For example, in the heart PKA is known to be an influential cAMP effector protein involved in excitation-contraction coupling (described in section 1.1) via direct phosphorylation and activation of L-type calcium channels (LTCC), troponin I (TnI), myosin binding protein C (MyBP-C), phospholamban (PB), and potassium channels (Wolff et al., 1996, Baryshnikova et al., 2008, Barefield and Sadayappan, 2010, Kurokawa et al., 2004).

1.2.3.2 Epac

A more recently identified cAMP effector protein is exchange protein directly activated by cAMP (Epac). It was found to have a cAMP binding domain homologous to that of PKA R subunits (de Rooij et al., 1998, Kawasaki et al., 1998). Epac is known to bind cAMP with high affinity and functions to activate the Ras family small GTPases Rap1 and Rap2 (Cheng et al., 2008). There are two isoforms of Epac, Epac1 and Epac2, which are the products of two independent genes in mammals and share extensive sequence homology. Both Epac1 and Epac2 possess distinctly different N-terminal regions whereas they share an

evolutionary conserved catalytic domain. Each isoform has a unique expression pattern with Epac1 being ubiquitously spread while Epac2 has a more restricted pattern of tissue expression (de Rooij et al., 1998, Kawasaki et al., 1998). These proteins are involved in many crucial cellular processes such as cell adhesion and migration through activation of integrins (Rangarajan et al., 2003, Han et al., 2006). Many of the processes that are driven by EPAC are also regulated by the activity of PKA. For example, PKA is also known to phosphorylate Rap1 at a site in the C-terminal however PKA phosphorylation is not necessary for the cAMP-dependent activation of Rap1 (de Rooij et al., 1998).

1.2.3.3 CNGC

Ions channels that are directly activated by cyclic nucleotides were first discovered during the hunt for the second messenger that is crucial in mediating the response of retinal photoreceptors (Haynes and Yau, 1985). These channels are predominantly activated by cyclic guanosine monophosphate (cGMP) (Liu et al., 1994). CNGCs belong to a superfamily of heterogeneous ion channels that are linked by the fact that they possess a common transmembrane and pore structure. Within the C-terminus there exists a binding site for 3'5'-cyclic nucleotide monophosphates (cNMPs) (Kaupp and Seifert, 2002).

Each CNGC is composed of four subunits which each contain six transmembrane domains followed by the C-terminus, which housing the cyclic nucleotide binding domain (CBD) (Kaupp and Seifert, 2002, Matulef and Zagotta, 2003). Binding of cNMPs to the CNCG results in the opening of the channel and subsequently the influx of cations into the cell.

The hyperpolarisation and cyclic nucleotide-gated channel (HCNGC) is of particular importance in the maintenance of the "funny" pacemaker current (I_f) in the heart (Ludwig et al., 1998, Santoro et al., 1998). There are four isoforms of HCN (HCN1-4), which are all known to be differentially expressed within the heart (Scicchitano et al., 2012). Channels are modulated by the direct action of cAMP binding which induces conformational changes that allow for the opening of the channel during hyperpolarisation of the cardiac membrane (DiFrancesco and Tortora, 1991). In addition, the binding of cAMP allows for the lowering of the threshold potential of the channel opening (DeBerg et al., 2016). During the

opening, the channels become permeable to Na^+ and K^+ ions that are close to the resting membrane potential of the cell producing the I_f current (Benarroch, 2013). Generation of the I_f current is responsible for the initial depolarisation of the cardiac action potential (DiFrancesco and Borer, 2007).

1.2.3.4 POPDC

The newest class of cAMP effectors to be identified are the Popeye domain containing (POPDC) gene family (Andrée et al., 2000, Reese et al., 1999).

1.3 Popeye domain containing protein family

Concomitant screening of cardiac cDNA libraries 18 years ago by two independent research groups lead to the discovery of Popeye- domain containing protein family (POPDC), a gene family with an enriched cardiac expression pattern (Reese et al., 1999, Andrée et al., 2000). The *POPDC* family consists of three isoforms; POPDC1 (also known as Blood Vessel Epicardial Substance, BVES), POPDC2 and POPDC3. These have expression profiles that often overlap with each other, but each has its own distinct expression level in specific tissues. For example, in the adult heart, POPDC1 is more highly expressed in the atria than in the ventricles and has elevated levels within the His bundle, the bundle branches, the Purkinje Fibres, sinoatrial node (SAN) and atrioventricular node (AVN) of the cardiac conduction system (Froese et al., 2012). In contrast, POPDC2 is equally expressed in both the atria and ventricles and at high levels within the same cardiac conduction components as POPDC1 (Froese et al., 2012).

As mentioned, POPDC1 and POPDC2 are both highly expressed in the heart and skeletal muscle whereas the expression pattern of POPDC3 has not been extensively examined yet (Froese et al., 2012). In addition to POPDC proteins' expression in heart cells and skeletal muscle cells, they have also been found in the smooth muscle lining of the uterus, bladder and the gastrointestinal tract, as well as in some neurons and specific epithelial cells such as those in the pyloric epithelium of the stomach (Brand et al, 2014).

1.3.1 Sequence and structure

In humans, both *POPDC1* and *POPDC3* are found on chromosome 6q21 with *POPDC3* upstream of POPDC1 (Schindler et al., 2012b). Separating the two genes is an intergenic sequence of around 20kb, which consists of an antisense RNA that overlaps with the start of *POPDC3*. *POPDC1* and *POPDC3* are both transcribed from a bidirectional promoter (Schindler et al., 2012b). The *POPDC2* gene, located on chromosome 3q13.33, appears to have arisen from gene duplication somewhere along the evolutionary path. It shares approximately 50% sequence homology with POPDC3, so it was therefore assumed that POPDC3 was duplicated (Andrée et al., 2000). In vertebrates, all three of the *POPDC* genes are present, however only two are present in lower chordates, echinoderms and non-vertebrates (Hager and Bader, 2009). Lin *et al* (2007) noted that Drosophila only contains one *POPDC* gene whereas in *Caenorhabditis elegans* there is no *Popdc* gene present at all noted it (Lin et al., 2007). Most animals have an identifiable POPDC homologue with a similar arrangement of sequence features that imply a conserved 3D structure. It is therefore evident that there is high evolutionary pressure to maintain the structure and subsequently the function of this family of proteins (Schindler and Brand, 2016).

While the three members of the POPDC family share between 25 and 50% amino acid sequence similarity, only limited similarity is observed between the POPDC family members and other cAMP effector proteins in vertebrates (Schindler and Brand, 2016). Significant sequence similarity has been found with the bacterial cAMP-regulated transcription factors, catabolite activator protein (CAP) and cAMP receptor protein (CRP), which have provided basis for structural modelling (Schindler and Brand, 2016).

The POPDC proteins are membrane-bound proteins whose isoforms range from 290-370 amino acids in length. POPDC1 is the best-characterized member of the family with respect to its structure. The extracellular amino terminus of POPDC spans around 27-40 amino acids in length and contains two N-glycosylation sites (Knight et al., 2003, Andrée et al., 2000). The role of this glycosylation remains unclear, but it has been hypothesised that it may contribute to the direct localization of the protein to the membrane or protect them from proteolytic degradation (Hager and Bader, 2009). The extracellular N-terminal is immediately followed by three proposed transmembrane α-helices which

transverse the cell membrane (Figure 1.4) (Schindler and Brand, 2016). The POPDC proteins contain an intracellular, cytoplasmic C-terminal region which contains the evolutionarily conserved 150 amino acid Popeye domain (Andrée et al., 2002a, Andrée et al., 2002b).

The Popeye domain is found within the cytoplasm and contains a phosphate-binding cassette (PBC) (Figure 1.4). The PBC of the POPDC family does not resemble any other cAMP binding proteins (Schindler *et al,* 2016). Through cAMP affinity pulldowns, radioligand binding assays and FRET analysis, Froese and colleagues determined that POPDC1 was able to bind to cAMP with a high affinity almost equalling that of PKA. Within the non-canonical PBC, there are two sequence motifs, DSPE and FQVT that have been implicated in POPDCs ability to bind cAMP (Froese et al., 2012). A charge-to-alanine mutation at D200 in POPDC1 has been shown to significantly reduce its ability to bind cAMP. Although the functional implications of POPDC1s ability to bind cAMP is not fully understood, it has been shown that cAMP binding modulates its interaction with TREK1. A dimerization motif also mapped to the Popeye domain that allows for homodimerization or heterodimerization of POPDC proteins at the membrane (Knight et al., 2003, Vasavada et al., 2004). Distal to the Popeye domain is the less conserved carboxyl terminal region. Although the three family members diverge from one another in this region there is interspecies conservation for each. The carboxy terminal region is also noteworthy for clusters of serine/threonine residues that can be phosphorylated in cells upon ß-adrenergic stimulation (Froese et al., 2012, Schindler and Brand, 2016).

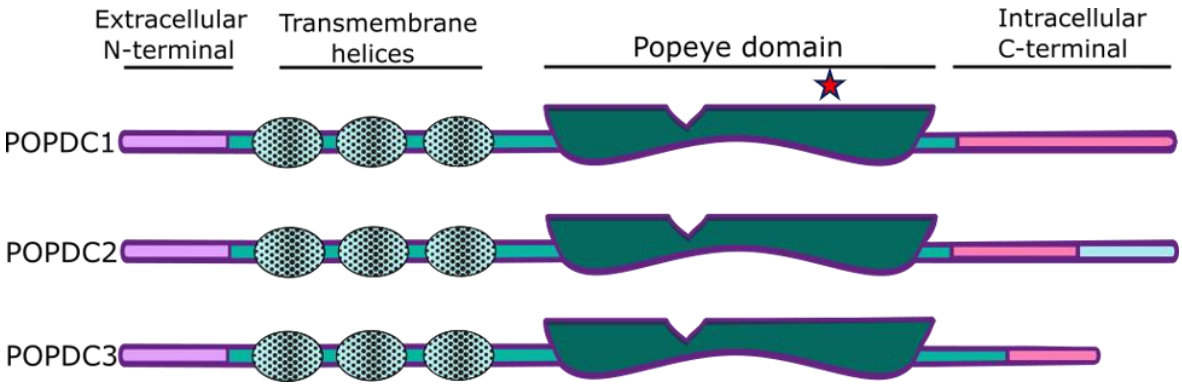

Figure 1.4 Schematic of the structure of Popeye containing proteins. The three POPDC isoforms share a similar protein structure with all containing a 20-40 amino acid extracellular N-terminal domain. This region is followed by a three proposed transmembrane (TM) domain. The cytoplasmic region of the protein contains the evolutionary conserved Popeye domain and the C-terminal domain, shown in pink. Within the Popeye domain is a non-canonical phosphate binding cassette (PBC) consisting of two tetrapeptides, DSPE and FQVT, which are essential for cAMP binding. At the end of the Popeye domain exists a dimerization motif. Mutations in the Popeye domain have been identified and the POPDC1 S201F mutation found in patients with muscle and heart disease has been shown with a red star. *POPDC2* generates three alternative splicing variants and a putative dimerization domain shown in blue.

1.3.2 Regulation of POPDC1 gene expression

1.3.2.1 EGF signalling supresses Popdc1

Currently, little is known about how *POPDC1* gene expression is regulated. However in Drosophila, Popdc1 is suppressed by the secretion of gurken, an epidermal growth factor (EGF)-like signalling molecule (Lin et al., 2007). This form of regulation has also been discovered in the gastric adenocarcinoma cell line SNU-216, which expresses all three of the POPDC isoforms as well as in several breast cancer cell lines where the addition of EGF results in the decrease of *POPDC*1 gene expression (Kim et al., 2010, Amunjela and Tucker, 2017b). Similarly, in cardiac myocytes cultured in serum, reduced levels of POPDC1-3 were rescued with the addition of the EGF antagonist tryphostin (Parnes et al., 2007). Neuregulin, an EGF-like signalling molecule, is secreted by endocardial cells and is responsible for the formation of the trabecular layer of developing ventricles (Parnes et al., 2007, Meyer and Birchmeier, 1995). *POPDC1* expression in this region is low which may mean that the neuregulin signalling depletes *POPDC1* during the suppression of apico-basal polarity of transforming myocytes during mid-gestation in mouse heart (Andrée et al., 2000, Andrée et al., 2002a).

1.3.2.2 Popdc1 expression can be suppressed by Netrin

Netrin-1 is a laminin-related neuronal guidance molecule which can be expressed in both neuronal and non-neuronal cell types. It has been identified that Netrin-1 is a negative regulator of POPDC1 expression through the modulation of the PI3-kinase/AKT signalling axis (Han et al., 2015). Netrin-1 is a specific inhibitor of the AKT pathway and this signalling cascade can re-establish POPDC1 expression. For example, several cancer types including hepatocellular carcinoma (HCC) have an increased Netrin-1 expression and an associated decrease in POPDC1 levels which may lead to tumour progression (Han et al., 2015).

1.3.2.3 The transcriptional regulation of the POPDC genes

Little work has been done to characterise the mechanisms by which the *POPDC* genes are transcriptionally regulated. It has however, been proposed that *POPDC1* might be the target of Pax3, a transcription factor important in muscle and neural development (Barber et al., 2002). The *POPDC2* promoter has also been investigated and was found to contain a binding site for the NK homeobox protein 2.5 (Nkx2.5) at an overlapping binding site for Meis homeobox 1 (Meis1) (Dupays et al., 2015). These two transcription factors are essential in vertebrate heart development and therefore in the normal physiology of the adult heart. In order to determine which transcription factor was most important in different heart tissues the differential binding of these transcription factors were probed using chromatin immunoprecipitation. Findings using the mouse *Popdc2* promoter identified that Nkx2.5 bound to the promoter in differentiated cardiac myocytes whereas Meis1 bound in the anterior heart field mesoderm (Dupays et al., 2015).

1.3.3 POPDC1 interactome

Our knowledge of POPDC1's range of interaction partners is growing as the protein is being investigated in different physiological settings by a number of groups. POPDC proteins, as mentioned previously, are expressed at high levels in cardiac and skeletal muscle and identification of direct binding partners will undoubtedly shine further light on the function role of these proteins. The first POPDC interacting protein (PIP) to be identified was the two-pore potassium

channel, TREK1 (TWIK-related K^+ channel 1) (Figure 1.5)(Froese et al., 2012). Evidence provided by the study by Froese and colleagues showed that POPDC1 modulated the gating properties of the channel which could potentially be altered in disease. This initial identification invigorated the idea that the POPDC proteins had a major role, not only in the normal function of cells in the heart and muscle, but also in the progression of disease pathology. To date, numerous PIPs have been identified with only some of their binding sites on POPDC1 being defined experimentally (Figure 1.5).

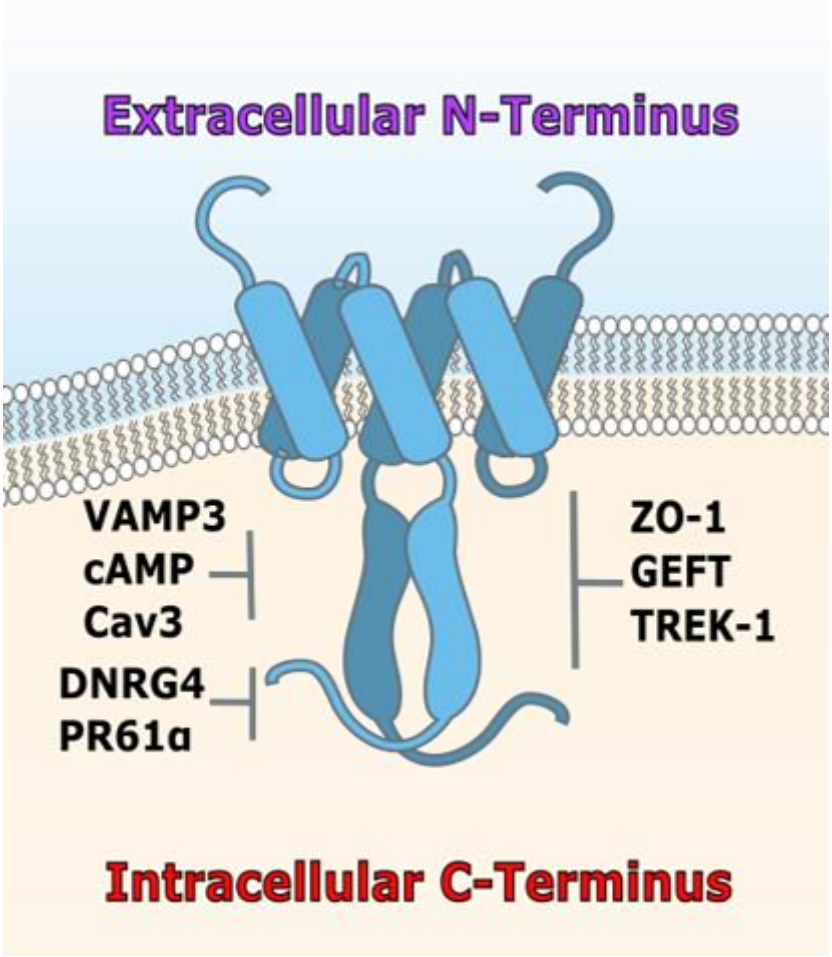

Figure 1.5 Interaction partners of POPDC1 and their proposed binding sites. POPDC1 consists of an extracellular N-terminus, three proposed transmembrane helices, and an intracellular C-terminus. POPDC1 is found dimerised at the membrane. Most of the interaction sites for POPDC1 are held within the highly conserved Popeye domain. Several of the main POPDC interacting partners (PIPs) that interact in this region are indicated including; VAMP3 (Vesicle-associated membrane protein 3), ZO-1 (zona occludens 1), cAMP, Cav3 (Caveolin 3), GEFT (guanine nucleotide exchange factor) and TREK1 (TWIK-related K^+ channel 1). There are currently two PIPs known to bind to the unstructured C-terminal tail, DNRG4 (downstream N-myc regulated gene 4) and PR61α.

1.3.3.1 POPDC1 interacts with the two-pore potassium channel TREK1

As POPDC proteins are localised to membranes it was hypothesised that they would interact with other membrane proteins. Numerous reports of POPDC mutants presenting with cardiac arrythmias have been shown in *Popdc1* null mutant mice and zebrafish morphants identifying a potential interaction with cardiac ion channels or pumps (Froese et al., 2012, Schindler et al., 2016b, De Ridder et al., 2019). A specific interaction was identified between POPDC1 and the two-pore potassium channel TREK1 (TWIK-related K^+ channel 1) which led to a two-fold increase in its current (Froese et al., 2012). Interestingly, this increase in current is believed to be due to enhanced membrane localisation of TREK-1. A bi-molecular FRET assay identified that TREK1s interaction with POPDC1 was sensitive to changes in cAMP concentrations like those caused by adrenergic stimulation, which caused a rapid reduction in FRET signal. This loss of interaction has been hypothesized to be caused by structural rearrangement of the Popeye domain upon cAMP binding (Froese et al., 2012). Furthermore, changes in conformation may allow for previously hidden binding sites to be exposed, further extending POPDC's interactome. Interestingly, the function of TREK-1 has not been fully elucidated. However, TREK1 is related to the K29 ion channel ORK1 in Drosophila and has been shown to be involved in the regulation of pace making activity in the heart (Lalevée et al., 2006). This would concur with data from a cardiac specific knock out for TREK-1 which gave rise to a stress induced sinus bradycardia phenotype, which resembles what is seen in *Popdc1* and *Popdc2* null mutants. This cardiac phenotype in *POPDC* mutants can be partly explained by the loss of the interaction between TREK-1 and POPDC (Froese et al., 2012, Schindler and Brand, 2016). In humans, the POPDC1^{S201F} mutant protein can be found in muscle tissue of patients with Limb-girdle muscular dystrophy 2X (LGMD2X). The mutant shows lack of membrane localisation and a reduction in cAMP binding to POPDC1^{S201F} (Schindler and Brand, 2016). When cAMP levels are increased in POPDC1^{S201F} muscle cells there is also a distinct reduction in the membrane localisation of TREK-1 (Schindler and Brand, 2016). This information taken together suggests that POPDC1's interaction with TREK-1 has two modulatory stages. The first is a rapid conformational change after cAMP binds to POPDC1 causing the dissociation of the two proteins. Second is a long-term reduction in the membrane trafficking of TREK-1. As such, it is hypothesised that POPDC proteins serve to modulate the

resting membrane potential of cardiac myocytes and subsequently influence their excitability. The physiological implications of this mechanism however remain unclear.

1.3.3.2 Popdc1 is important for control of cell proliferation

POPDC1 has been found to localise at the nuclear envelope as well as in the nucleoplasm in certain cell lines such as cardiac myocytes and epithelial breast cancer cells (Amunjela and Tucker, 2016b, Brand and Schindler, 2017). The nuclear localisation of POPDC1 may be a clue to identifying the mechanism by which POPDC1 regulates cell proliferation. POPDC1 was identified to have a direct interaction with Zonula Occludens- 1 (ZO-1), which was confirmed using GST pull-down (Osler et al., 2005). Z0-1 regulates the activity of zonula occuldens-1 associated nucleic acid – binding protein/ DNA binding protein A (ZONAB/DbpA) (Williams et al., 2011). ZO-1 is a tight junction adapter protein that is known to interact with actin, claudin, occludins and α-catenin and has been associated with the regulation of endothelial proliferation through ZONAB/DbpA (Balda and Matter, 2009, Pozzi and Zent, 2010). ZONAB/DbpA is a Y-box transcription factor that binds to ZO-1, in its SH3 domain, allowing for recruitment to tight junctions. It is a known regulator of cell cycle and proliferation genes such as cyclin D1 and HER2 and its expression in the nucleus results in an increase in cell proliferation (Balda and Matter, 2009, Lima et al., 2010, Pozzi and Zent, 2010, Balda et al., 2003). Correspondingly, when ZONAB/DbpA is bound to and transported by ZO-1 there is a marked decrease in the transcription of cell cycle and proliferation genes (Georgiadis et al., 2010, Williams et al., 2011). Interestingly, high ZO-1 levels are known to decrease cell proliferation and weak nuclear localisation of ZONAB/DbpA (Balda et al., 2003). Furthermore, high ZO-1 expression correlates to high POPDC1 expression (Russ et al., 2011, Osler et al., 2005). Conversely, this was corroborated by experiments showing a concomitant reduction of POPDC1 and ZO-1 expression in numerous cancer cell types (Amunjela and Tucker, 2017a, Amunjela and Tucker, 2017b, Hoover et al., 1998). A potential mechanism of action from the interaction between POPDC1 and ZO-1 could presumably be to inhibit the nuclear localisation of ZO-1 and therefore prevent cell proliferation (Amunjela et al., 2019). Forced expression of a truncated POPDC1 which did not contain the

integral Popeye domain or C-terminal part increased the nuclear localisation and transcriptional activity of ZONAB/DbpA further supporting the notion that dysregulated POPDC1 drives proliferation (Schindler et al., 2016a).

The interaction with ZO-1 and ZONAB/DbpA is not the only means by which POPDC1 is involved in cell proliferation. POPDC1 has been extensively shown to interact with multiple partners in pathways crucial to cell proliferation (Russ et al., 2011, Han et al., 2015, Amunjela and Tucker, 2017b, Parang et al., 2017, Kliminski et al., 2017, Jayagopal et al., 2011, Smith et al., 2008). Although this has been seen for all POPDC isoforms there is evidence that there is an isoform-specific role of each. For example, POPDC1 is thought to function as a tumour suppressor that can regulate and inhibit cell proliferation under normal physiological conditions (Amunjela et al., 2019). Interactions with the aforementioned ZO-1 as well as Wnt and c-myc add support to this hypothesis. The transcription factor c-myc is often overexpressed in various cancers and is known to regulate many cellular aspects from proliferation to epithelial/ mesenchymal transition (Toon et al., 2014, Koo et al., 2000, Cowling and Cole, 2007). POPDC1 was also shown by Parang and colleagues (2017) to promote the proteasomal degradation of c-myc through an interaction with PR61α containing -PP2A phosphatase complexes. Furthermore, the *POPDC1* promoter was found to be hypermethylated leading to its reduced expressed in patients with colitis-associated cancer (CAC) when compared to normal colonic tissue (Parang et al., 2017).

1.3.3.3 POPDC1 is integral in regulating cell-cell contact

The role of tight junctions is to regulate the passage of molecules through the cell membrane as well as blocking the diffusion of proteins through the apical membrane into the baso-lateral membrane and vice versa (Sawada et al., 2003). Popdc1, as previously mentioned, interacts with important tight junction proteins such as occludins and ZO-1. In human corneal epithelial cells POPDC1, through its interaction with ZO-1, sequesters the Rho guanine nucleotide exchange factor GEF-H1. It is hypothesised that POPDC1 combined with ZO-1 and cingulin uses the sequestered GEF-H1 at the plasma membrane as a means of modulating and controlling RhoA signalling (Russ et al., 2011). This concept is supported by evidence showing that upregulation of POPDC1 combined with

inactivation of the RhoA/Rock pathway was observed during the mesenchymal to epithelial transition in pig fibroblasts as well as in human hepatocellular carcinoma (Shi et al., 2013). This was confirmed using a RhoA-GTPase activation assay to prove that suppression of POPDC1 resulted in an increase in RhoA activity that promoted cell migration and invasion (Han et al., 2015). A similar scenario occurs in the control of cell contraction in the trabecular meshwork of the eye, where POPDC1 downregulates RhoA signalling leading to a decrease in the phosphorylation of myosin light chain. An increase in POPDC1 results in the increase in tight junction formation as well as increased transepithelial resistance (Russ et al., 2011, Russ et al., 2010). It has also been shown that in zebrafish, POPDC1 interacts with atypical protein kinase C (aPKC) which is known to play a role in the recruitment and tethering of multiple proteins to the tight junction signalling complex and in doing so maintains its integrity (Wu et al., 2012a). In addition to the formation and maintenance of tight junctions, POPDC1 is known to regulate adherens junctions through its interaction with the WNT signalling pathway. Adherens junctions function to modulate WNT signalling through the sequestering of ß-catenin at the cell membrane (Klinke et al., 2015, Francis et al., 2018). Interestingly, POPDC1 expression correlates with the expression and localisation of E-cadherin and ß-catenin (Williams et al., 2011). Moreover ZO-1, which is a major POPDC1 interacting protein, is known to interact with key components of adherens junctions such as N-cadherin as well as Connexin43, which is crucial to the formation of gap junctions (Palatinus et al., 2010). The overexpression of POPDC1 has been shown to increase the membrane localisation of ß-catenin while decreasing its cytoplasmic expression, whereas in POPDC1$^{-/-}$ mice there were marked increases in the cytoplasmic and nuclear level of ß-catenin (Williams et al., 2011, Parang et al., 2017). In addition the Wnt targets, Mmp7, Wisp2 and Rspo4, were increased in POPDC1$^{-/-}$ mice (Parang et al., 2017, Reddy et al., 2016).

It is of note that POPDC1 is known to localise to cell-cell contact points such as filopodia before the appearance of E-Cadherin. The transfection of POPDC1 into non-adherent L-cells results in the development of adhesive properties and aggregation of those cells (Wada et al., 2001). This evidence suggests that POPDC1's membrane localisation is under the regulation of epithelialization signalling pathways. Wada *et al.,* (2001) provided evidence that the inhibition

of POPDC1 disrupts epicardial migration as well as the formation of epithelial sheets in rat epicardial cell culture. The suggestion that POPDC1 possess a role in adhesion therefore may allude to a role for the protein in coronary vasculogenesis and development. In this vein, the current hypothesis is that POPDC1 plays a critical role in the regulation of cell adhesion during coronary vessel development(Wada et al., 2001). During the migration of mesenchymal cells to the developing vascular beds, POPDC1 accumulates in the perinuclear region. It is known that various cells within the epicardium respond to signals given off by cardiac muscle cells which may be facilitated and mediated by a co-factor for GATA transcription, FOG-2, that removes POPDC1 from the cell membrane (Tevosian et al., 2000, Wada et al., 2001). Upon vasculogenic mesenchyme reaching the forming channels within the myocardium, endothelium driven signals cause the movement of POPDC1 back to the membrane. This allows POPDC1 to participate in cell-cell adhesion in the developing smooth muscle cells (Wada et al., 2001).

1.3.3.4 POPDC1 in the regulation of cell shape and motility

In addition to its role in cell-cell adhesion, POPDC1's involvement in cell motility has been widely investigated and recognised. Using a yeast two-hybrid screen a Rho family guanine nucleotide exchange factor, GEFT, was identified as an interaction partner of POPDC1, which was later confirmed through direct GST-pull down (Smith et al., 2008). Overexpression of GEFT leads to a pronounced alteration and reorganisation of the cell cytoskeleton giving a marked change in the cell morphology (Guo et al., 2003). A POPDC1 construct with a truncated N-terminus lacking the transmembrane domain was transfected into NIH3T3 cells and led to a reduction in the speed of cell locomotion as well as altered cell shape; when transfected into C2C12 myoblasts there was a marked reduction in differentiation (Smith et al., 2008). The exact function of the interaction between POPDC1 and GEFT remains largely unclear but it is speculated that POPDC1 may affect the proper subcellular localisation of GEFT therefore modulate its activity by altered compartmentalisation.

POPDC1 is known to be downregulated in aggressive breast cancer cells in comparison to non-malignant control groups (Amunjela and Tucker, 2017a). It is hypothesised that the loss of POPDC1 at the cell membrane in breast cancer causes a reduction in POPDC-mediated tight junctions that promote cell migration, a result which has previously been shown in epithelial cells (Russ et al., 2011). Amunjela and Tucker (2017) described the promotion of cell migration in various aggressive, malignant breast cancer cell lines such as MCF7, MDA231 and SKRB3, with the overexpression of POPDC1 inhibiting migration (Amunjela and Tucker, 2017a). This, taken with the fact that the suppression of POPDC1 in glioblastoma, hepatocellular carcinoma, gastric and colorectal cancers leads to an increase in cell migration and invasion provides strong evidence that the loss of POPDC1 promotes a malignant phenotype in cancer (Parang et al., 2017, Kim et al., 2010, Amunjela and Tucker, 2016a, Williams et al., 2011). As known, cAMP interacts with POPDC1 stabilising it and upregulating its expression in MC7, MDA-MB-231 and SKBR3 breast cancer cells (Amunjela and Tucker, 2017a). Interestingly, cAMP inhibits cell migration and invasion in breast cancer cells (Spina et al., 2012, Bianco et al., 1997). Furthermore, elevating cAMP in MC7, MDA- MB-231 and SKBR3 after *POPDC1* has been knocked down restored both cell migration and proliferation thereby strengthening the hypothesis that cAMP, and by association POPDC1, mediates the inhibition of breast cancer migration (Amunjela and Tucker, 2017a).

1.3.3.5 POPDC1 interacts with Caveolin-3 to control caveolar formation

A more recently identified POPDC interacting protein (PIP) within the confines of the heart is the caveolae protein Caveolin 3 (Alcalay et al., 2013). Caveolae are small invaginations within the membrane that have integral roles in a variety of cellular processes such as signal transduction (reviewed in (Gazzerro et al., 2010). There are currently three identified isoforms of caveolin (Cav1, Cav2 and Cav3) (Stan, 2005). Of these isoforms, Cav3 has a muscle-specific expression and is localised to the sarcolemma in skeletal muscles as well as the sarcolemma and transverse tubules in cardiac myocytes (Song et al., 1996). It is proposed that POPDC1 functions to regulate the number and size of caveolae within the membrane, a notion that was supported by a reduction in the observed number of caveolae present, but an increase in their size, in *Popdc1* null mice (Alcalay et al., 2013). In addition, *Popdc1* null mice have alterations in Ca^{2+} transients as

well as increased susceptibility to ischemia-reperfusion injury due to Cav3's role in both vesicular trafficking and signal transduction (Alcalay et al., 2013). Importantly, the identified binding site for Cav3 on POPDC1 lies within the conserved Popeye domain which is proposed to undergo conformational change during the binding of cAMP (Rehmann et al., 2007). In concert with this is the knowledge that Cav3 conformation is dynamic and under the control of ß-adrenergic stimulation (Wypijewski et al., 2015). Therefore, the proposed model by which Cav3s interaction with POPDC1 takes place is via ß-adrenergic stimulated generation of cAMP that drives the conformational change of the Popeye domain of POPDC1 and allowing Cav3's binding. The bi-directional modulation of the interaction may affect the subcellular localisation of both Cav3 and POPDC1 and its interaction with other PIPs (Xiang, 2011).

1.3.3.6 POPDC1 functions to control vesicular transport

GST pull-down experiments identified another class of POPDC1 interacting proteins, the vesicle-associated membrane proteins Vamp2 and Vamp3 (Hager et al., 2010). It is reported the Vamp2 and Vamp 3 are promiscuous during development with the proteins replacing each other when one is absent (Deák et al., 2006). Vamp3 is a ubiquitously expressed SNAP Receptor (SNARE) proteins with cellular roles including vesicle membrane fusion and membrane trafficking of several proteins including ß-integrin and transferrin (Luftman et al., 2009, Proux-Gillardeaux et al., 2005). Interestingly, the expression of a truncated dominant-negative POPDC1 the construct decreased transferrin uptake, reduced beta-integrin internalisation and reduced in exocytosis in MDCK (Madin-Darby Canine Kidney) cells (Hager et al., 2010). Furthermore, it has been shown that *Popdc1* knockdown results in morphological changes that are comparable with integrin depletion, allowing the conclusion that POPDC1, through its interaction with Vamp3, is crucial for the control of important cellular process that require vesicle transport (Hager et al., 2010). Intriguingly, Vamp2 expression in the heart is a key mediator of atrial natriuretic peptide (ANP) from atrial myocytes (Ferlito et al., 2010). TREK1, a previous mentioned PIP, is also known to function within the ANP release pathway (McGrath and de Bold, 2009) suggesting crosstalk between these systems. It is also of note that VAMP2/3 has crucial roles in cell-to-cell adhesion through the control of recycling integrin receptors (Luftman et al., 2009).

POPDC1's role in vesicular transport is further supported by its interaction with N-myc downstream regulated gene 4 (NDRG4) (Benesh et al., 2013). Both POPDC1 and NDRG4 were found to be crucial in trafficking VAMP3 to the plasma membrane through the mediation of the movement of fibronectin via changes in the extracellular matrix (ECM) essential for epicardial cell movement (Benesh et al., 2013). This interaction is also crucial for the fusion of recycling endosomes at the cell surface. A vesicle fusion assay demonstrated that inhibition of the interaction between POPDC1 and NDRG4 triggered a disruption in Vamp3 positive lipid vesicles that docked to the cell surface (Benesh et al., 2013). In addition, disruption of the interaction resulted in a marked reduction in biotin-labelled fibronectin that is moved between the medium and the insoluble matrix. This provides further support for the notion that cargo delivery to the membrane requires POPDC1 and NDRG4 mediated vesicle fusion.

1.3.4 POPDC in the heart

The role of POPDC proteins within the heart has been investigated extensively with numerous mutant model organisms having been developed. The depletion of either *Popdc1* or *Popdc-2* in both mouse and zebrafish models has resulted in the development of severe cardiac arrhythmias (see Table 1)(Froese et al., 2012, Kirchmaier et al., 2012). *Popdc1*$^{-/-}$ and *Popdc2*$^{-/-}$ mice displayed stress-induced sinus bradycardia upon subjection to either physical or mental stress which is characterised by the increased occurrence of a sinus pauses where there is a loss of sinus node activity (Froese et al., 2012). This results in a widely variable heart rate. Interestingly, the development of bradycardia is age dependent. Young animals (3 months old) do not present with bradycardia but the severity of the arrythmia worsens with age (Froese et al., 2012). The electrophysiological phenotype is found in conjunction with structural degeneration of the SAN in both *Popdc1*$^{-/-}$ and *Popdc2*$^{-/-}$ mice (Froese et al., 2012). Degeneration is particularly significant in the inferior part of the SAN which is crucial in the control of cardiac pace making during adrenergic stimulation (Opthof, 1988). There is support for the concept that a lack of POPDC leads to a loss of pace-maker cells as there is a pronounced decrease in the volume of the sinus node and an increase in the number of fibroblasts and extracellular matrix (Froese et al., 2012).

Table 1 Cardiac and Skeletal muscle phenotypes in model organisms and patients.

Species	Mutation	Heart	Skeletal Muscle	References
Mouse	*Popdc1*$^{-/-}$	stress-induced sinus bradycardia	regeneration defect	(Froese et al., 2012)
	Popdc1$^{-/-}$	ischemia-reperfusion damage	not analysed	(Alcalay et al., 2013)
	Popdc2$^{-/-}$	Stress-induced sinus bradycardia	not analysed	(Froese et al., 2012)
Zebrafish	*popdc1* morphants	AV-block, pericardial effusion	muscular dystrophy	(Schindler et al., 2016b)
	popdc2 morphants	AV-block, pericardial effusion	muscular dystrophy	(Kirchmaier et al., 2012)
	popdc1^{S191F}	AV-block, pericardial effusion	muscular dystrophy	(Schindler et al., 2016b)
Human	*POPDC1*^{S201F}	2nd degree AV-block	limb-girdle MD	(Schindler et al., 2016b)
	POPDC1$^{del56\ V217\text{-}K272}$	1st degree AV-block	limb-girdle MD	(Nelson et al., 2017)
	POPDC2^{W188X}	3rd degree AV-block	no known phenotype	(Swan et al., 2019)

The phenotypes in mice are similar to those of sick sinus syndrome (SSS) in humans, a disease of the elderly. SSS patients, much like the *Popdc* null mutants, cannot regulate their heart beating frequency to physiological demands (Rodriguez and Schocken, 1990). Such a correlation has resulted in the hypothesis that the disease in humans may be caused by the dysfunction or dysregulation of POPDC proteins or gene. Recently mRNA expression of *POPDC1* and *POPDC3* has been shown to be reduced in failing hearts compared with normal hearts; however, the magnitude of the downregulation seen is highly variable between patients (Gingold-Belfer et al., 2011).

During myocardial ischemia/reperfusion (I/R), there are a number of damaging alterations in the myocardial ultrastructure, cardiac function, electrophysiology and energy metabolism (Ferdinandy et al., 2007). Alcalay *et al*., identified that

both the protein and the mRNA levels of POPDC1 were decreased during I/R (Alcalay et al., 2013). In *POPDC1* null mutants, the induction of myocardial I/R resulted in a markedly lower functional recovery when compared to their WT counterparts. In addition, cardiac myocytes isolated from POPDC1 null mutants showed an impaired Ca^{2+} transient and an increased vulnerability to oxidative stress (Alcalay et al., 2013). Furthermore, a study utilising siRNA knockdown of *POPDC1* revealed that it is required for the survival of cardiac myocytes in serum-deficient conditions (Kliminski et al., 2017). In addition, knockdown of *POPDC1* in neonatal cardiac myocytes increased the expression of cell death regulators Bcl-2/adenovirus E1B 19-kDA interacting protein (Bnip3) while reducing Rac1 activity. This is accompanied by the alteration in the interaction of FOX3 and NF-κB transcription factors with the promoter of Bnip3 (Kliminski et al., 2017). In summation, these results suggest that POPDC1 is a potential target for the enhancement of heart protection (Gingold-Belfer et al., 2011).

Interestingly, Schindler *et al*, identified a new *POPDC1* missense variant (S201F) through whole-exome sequencing of a family of four people presenting with cardiac arrythmias and limb-girdle muscular dystrophy (Schindler et al., 2016b). Forced expression of $POPDC1^{S201F}$ in murine cardiac muscle cells resulted in increased hyperpolarisation and upstroke velocity of the action potential (Schindler et al., 2016b). A homologous construct ($POPDC1^{S191F}$) in zebrafish resulted in the same heart and skeletal muscle phenotype present in the human condition (Schindler et al., 2016b). To date, this is the only study that has identified *POPDC* as a disease-causing gene in human heart disease.

Interestingly, in zebrafish the loss of P*opdc2* by morpholino oligonucleotide-mediated knockdown results in the chambers of the heart being misshapen. This is normally accompanied by the lack of trabeculation, pieces of muscle that extend into the left ventricle, reduced myofibrillar content and embryonic heart failure (Kirchmaier et al., 2012). In addition, single SAN cells display less cellular extensions which in turn reduces the size of the SAN tissue itself. Single-plane illumination microscopy (SPIM) identified that Ca^{2+} transients measured, using a transgenic calcium indicator reporter line (Tg(cmlc2:gCaMP)s878), showed *Popdc2* mutants suffered from severe arrythmias not seen in their WT counterparts (Kirchmaier et al., 2012). Cardiac repolarisation was particularly

affected in these animals. Accompanying the data seen in *Popdc2* null mice, *Popdc2* null zebrafish embryos have been shown to display SAN block and a substantial decrease in heart rate (Kirchmaier et al., 2012). However, the exact role of *popdc2* in the development of the heart and its conductive tissue is not fully understood.

1.4 PDEs

Cyclic nucleotide signalling has critical roles in the control of a wide variety of cellular responses (Tasken and Aandahl, 2004). However, termination of signalling through these pathways requires hydrolysis of the cyclic nucleotides to below the activation threshold of the cyclic nucleotide effector proteins. This can only be achieved via the action of cyclic nucleotide phosphodiesterases (PDEs). PDEs were identified shortly after the discovery of the second messenger, cAMP and are the only known protein able to metabolise cNMPs. They function by hydrolysing the 3'5'-phosphodiester bond within cAMP or cGMP converting it to 5'AMP or 5'GMP, respectively (Francis et al., 2011a).

The superfamily of mammalian PDEs is comprised of 21 genes that are grouped into 11 families. Each of these genes codes for multiple splice variants resulting in approximately 100 PDE isoforms (Maurice et al., 2014). These isoforms have widespread distribution patterns and possess distinct functions within the cell. Family members can also be categorised on their substrate specificity into three groups. PDE1, PDE2, PDE3, PDE10 and PDE11 can act on both cAMP and cGMP with a spectrum of affinity dependent upon the isoform (Conti and Beavo, 2007, Azevedo et al., 2014). PDE4, PDE7 and PDE8 are cAMP-specific while PDE5, PDE6 and PDE9 act upon cGMP alone (Azevedo et al., 2014, Conti and Beavo, 2007).

Despite the variability in localisation, function and substrate specificity, the structure of PDE isoforms is conserved to some degree. Typically, PDEs have an NH_2-terminal regulatory domain (R-domain) and a C-terminal catalytic (C) domain however PDE4 family members are known to have regulatory features in their C-domain (Bender and Beavo, 2006). There are a variety of other domains within PDEs that are known to provide regulatory control including;

calcium/calmodulin-binding domains (PDE1), GAF domains (PDE2, PDE5, PDE5, PDE10 and PDE11), PAS (Per-ARNT-Sim) domain (PDE8), the upstream conserved domains (PDE4), and the autoinhibitory domains (Francis et al., 2011a). UCR domains serve to directly regulate PDE4 activity (Burgin et al., 2010, Houslay and Adams, 2003, Houslay and Adams, 2010, Richter and Conti, 2002, Richter and Conti, 2004) as well as forming interactions with heterologous proteins (Collins et al., 2008, Houslay, 2010, McCahill et al., 2008, Murdoch et al., 2007). PDE regulatory domains are most commonly connected to each other and other domains by "linker regions" that are able to communicate changes in activity and structure between the portions of the PDE (Francis et al., 2011a).

Given the widespread role of the PDE superfamily within the cNMP signalling pathways it is not surprising that they are linked to the pathophysiology of many diseases. Ablation, and more recently forced activation, of their hydrolytic activities has been a target for therapeutic intervention in a number of disease areas. Since the 1960s when Rall and West identified that the caffeine derivative theophylline was able to potentiate cardiac inotropic responses there has been the emergence of several drugs onto the market that alter PDE activity (Rall and West, 1963).

1.4.1 PDE4ology

cAMP-specific PDE4s comprise the largest PDE family with over 20 isoforms which are the products of the alternative splicing of 4 genes (A, B, C and D) (Houslay and Adams, 2003, Conti et al., 2003, Houslay et al., 2005). PDE4s contain an isoform specific N-terminal transduction domain (TD), upstream conserved regions 1 and 2 (UCR1 and UCR2) which are linked by linker region 1 and 2 (LR1 and LR2) respectively, and the conserved C-terminal catalytic domain (Houslay et al., 2007). Isoforms are further segregated by the presence and size of the UCR1 and UCR2 domains (Figure 1.6).

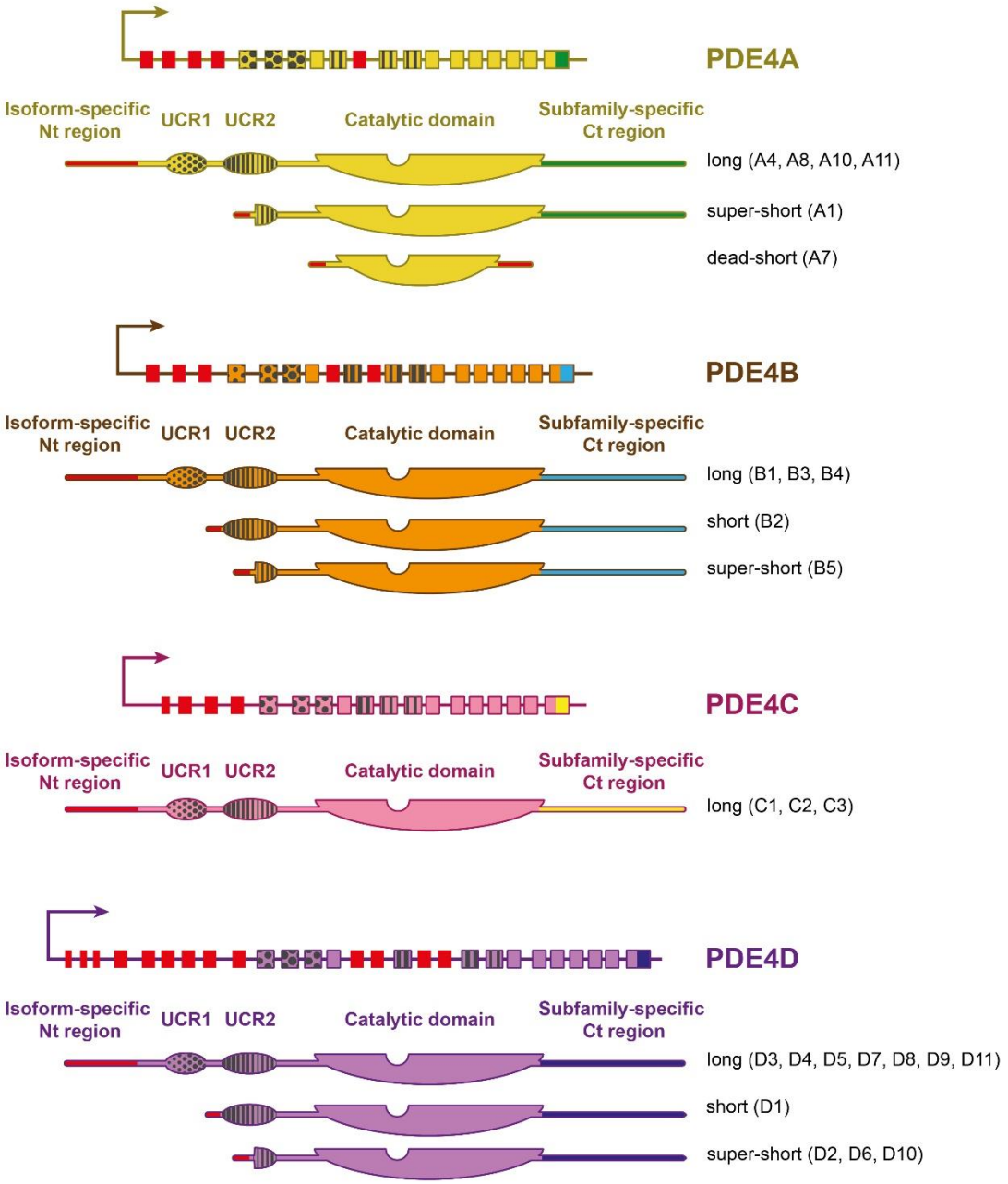

Figure 1.6 Schematic of PDE4 sub family structure. Schematic diagram showing the domain organisation of the PDE4 isoforms. All known isoforms contain a TD, LR1 and LR2 (not shown here) and a catalytic domain. Isoforms containing both upstream conserved regions (UCR1 and UCR2) are identified as long isoforms. The presence of a UCR2 region only identifies the family member as a short isoform. Family members with a truncated UCR2 and the lack of a UCR1 are known as super-short isoforms and those that lack any UCR1 are known as dead-short isoforms. (taken from (Tibbo et al., 2019).

Importantly, the TD is known to be important for the targeting the various PDE4 isoforms to specific subcellular localisation (Houslay et al., 2017) (Figure 1. 7). However, more recently it has been identified that other regions within the PDE4, such as the multifunctional docking site found at the end of the catalytic

domain, can direct subcellular localisation and protein partner diversity (Houslay et al., 2017). As mentioned in the above section, the UCR1 and UCR2 domains function to regulate the activity of PDE4s via phosphorylation by PKA in the UCRs, while ERK phosphorylates a site in the catalytic domain (Hoffmann et al., 1999, MacKenzie et al., 2002). Interestingly, PDE4 proteins are known to exist as dimers; dimerization has been shown to modulate the activity status of the enzyme. The UCR1/UCR2 domains of one long isoform partner can occlude the cAMP binding site of its partner in a dimer in a process known as 'trans-capping' (Burgin et al., 2010). Phosphorylation by PKA in the UCR1 domain or SUMOlyation at the start of the catalytic core can cause the locking of the PDE4 into a more active and unoccluded state. Phosphorylation by ERK MAP (mitogen activated protein) kinase at the end of the catalytic domain can force the dimer into an inactive conformation where the active site is occluded (Houslay and Adams, 2010). Lastly, the catalytic domain is known to contain a hydrophobic pocket which functions as the active site for the hydrolysis of cAMP once bound (Wang et al., 2007).

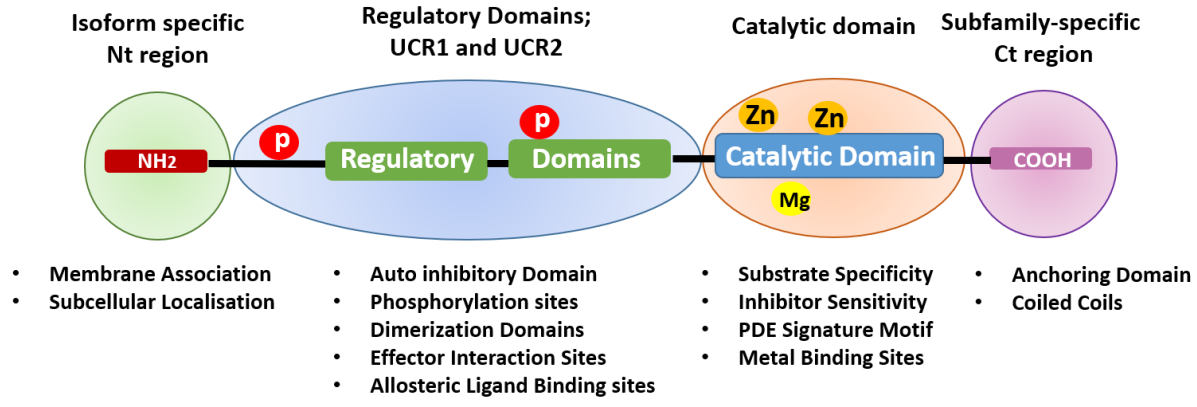

Figure 1. 7 Structure and domain function of PDE4 long isoform. The N-terminal domain contains the transmembrane helices allowing for the PDE localization. After the N-terminus are the regulatory domains of the PDE. These domains are responsible for auto inhibition, ligand binding, dimerization and the interaction sites of effector proteins. These N terminal regulatory regions contain the structural determinants that allow the various PDEs to bind different interaction partners for example the PDE4 protein contains an upstream conserved region (UCR) in addition to the catalytic domain. Immediately following this is the catalytic domain of the protein. This region is important for the binding of the metal ions that support the catalytic activity of PDEs as wells as the being involved in the specificity of PDEs interactions. The catalytic domains are followed by the C-terminus that is responsible for the anchoring of the PDE protein to its interaction partner

1.4.2 The role of PDEs in compartmentalised cAMP signalling

cAMP is a highly diffusible molecule that is synthesised intracellularly in response to extracellular stimuli interacting with cell-surface receptors. Formation of cAMP occurs at the inside surface of the plasma membrane by the membrane associated ACs. cAMP diffuses easily throughout the cell to spatially restricted cAMP effector proteins such as PKA and POPDC. Without control, the levels of cAMP would rise uniformly throughout the cell after any Gs-coupled receptor activation event, leading to the simultaneous activation of all cellular cAMP effector proteins. This would in turn lead to a lack of receptor specific responses meaning inappropriate signalling pathway activation and probably cell death. We know from recent work that cAMP gradients are shaped within cells to allow distinct, non-overlapping, receptor-specific responses. The mechanism by which this occurs was first researched by Burton and colleagues who determined that there are many different GPCRs within cardiac myocytes that lead to the same elevated level of cAMP upon activation yet produced very different outcomes (Hayes et al., 1980). Hayes and colleagues discovered that there was compartmentalised cellular signalling in which cAMP effector proteins are confined to specific compartments and their activation depends on their proximity to PDEs (Hayes et al., 1980, Hayes and Brunton, 1982).

Early attempts to investigate cyclic nucleotide dynamics via immunohistochemical methods led to the observation that there was compartmentalisation between the cAMP and cGMP signalling systems (Steiner et al., 1975, Ong et al., 1975). Although such experimentation verified the fact that cAMP signalling depended on compartmentalisation, it failed to provide any measurement that would quantify cAMP gradients present in cells. The development of optical probes was a transformative breakthrough in this regard as it allowed visualisation of cAMP gradients and showed them to be temporally and spatially segregated within living cells (Nikolaev and Lohse, 2006). These optical probes were developed to detect the dynamic movement of cAMP in real time using fluorescence resonance energy transfer (FRET). Possibly the most dramatic result from work using these techniques was the visualisation of discrete cAMP microdomains in cardiac myocytes after beta-adrenergic stimulation (Zaccolo and Pozzan, 2002). Clearly, cAMP levels were increased only in the vicinity of the sarcoplasmic membrane and this cAMP microdomain

was only able to activate PKA that was anchored near the transverse tubule. Importantly, all of this highly localised signalling was lost if a general PDE inhibitor was applied. Since this initial discovery FRET has been used to visualise the cAMP gradients surrounding all cyclic nucleotide effector proteins to identify how discrete signalling occurs within the cell as it diffuses from its origin at the membrane (Rich and Karpen, 2002, Nikolaev et al., 2004, Zhang et al., 2001). The development of targeted cAMP probes that localise to specific cellular locations has changed the way we conceptualise cAMP signalling.

In hand with the compartmentalisation of cAMP signalling is the compartmentalisation of PDEs themselves. If left unchecked the levels of cAMP would rise uniformly throughout the cell leading to the inappropriate activation of all cellular cyclic nucleotide effector proteins causing aberrant signalling pathway activation. As PDEs are the only known enzymes able to hydrolyse cAMP, their localisation to specific regions within the cell is crucial to the generation of intracellular gradients. The ability of PDEs to shape cAMP gradients is dependent on the fact that they can anchor themselves to selected microdomains within the cell. The localisation to discrete subcellular domains creates a compartmentalised system by which these enzymes can act as 'sinks', hydrolysing local cAMP and thus shaping the local cAMP gradient and limiting the diffusion of this second messenger molecule (Baillie, 2009). This allows for the creation of subcellular cAMP gradients which are solely dependent on the activation specific receptors. An example of this was shown in cardiac myocytes using cAMP optical reporters (Zaccolo and Pozzan, 2002). Cardiac myocytes were treated with ß-adrenergic agonists causing the generation of cAMP gradients throughout the cell. Upon treatment with the non-specific PDE inhibitor IBMX the distinct areas of low cAMP near PDEs were lost and the whole cell became swamped with a uniformly high level of cAMP. This confirmed the ability of localised PDEs to directly shape the cAMP gradient through their hydrolytic activity. Thus, a mechanism by which cAMP concentrations increase in the vicinity of specific cAMP effector proteins without causing the activation of all effectors within the cell is apparent. Anchoring of effectors to subcellular locales contributes to this mechanism. Upon the activation of an individual receptor, the concentration of cAMP rises allowing for the overwhelming of the tethered PDE and subsequent activation of the relevant effector protein. The

creation of this signalosome, which can contain unique combinations of effectors, either one or a subset of PDEs as well as localised scaffolding proteins such as AKAPs allows for the generation of multiple cAMP gradients simultaneously in different cellular locations irrespective of their distance to an AC (Maurice et al., 2014, Baillie, 2009) (Figure 1.8).

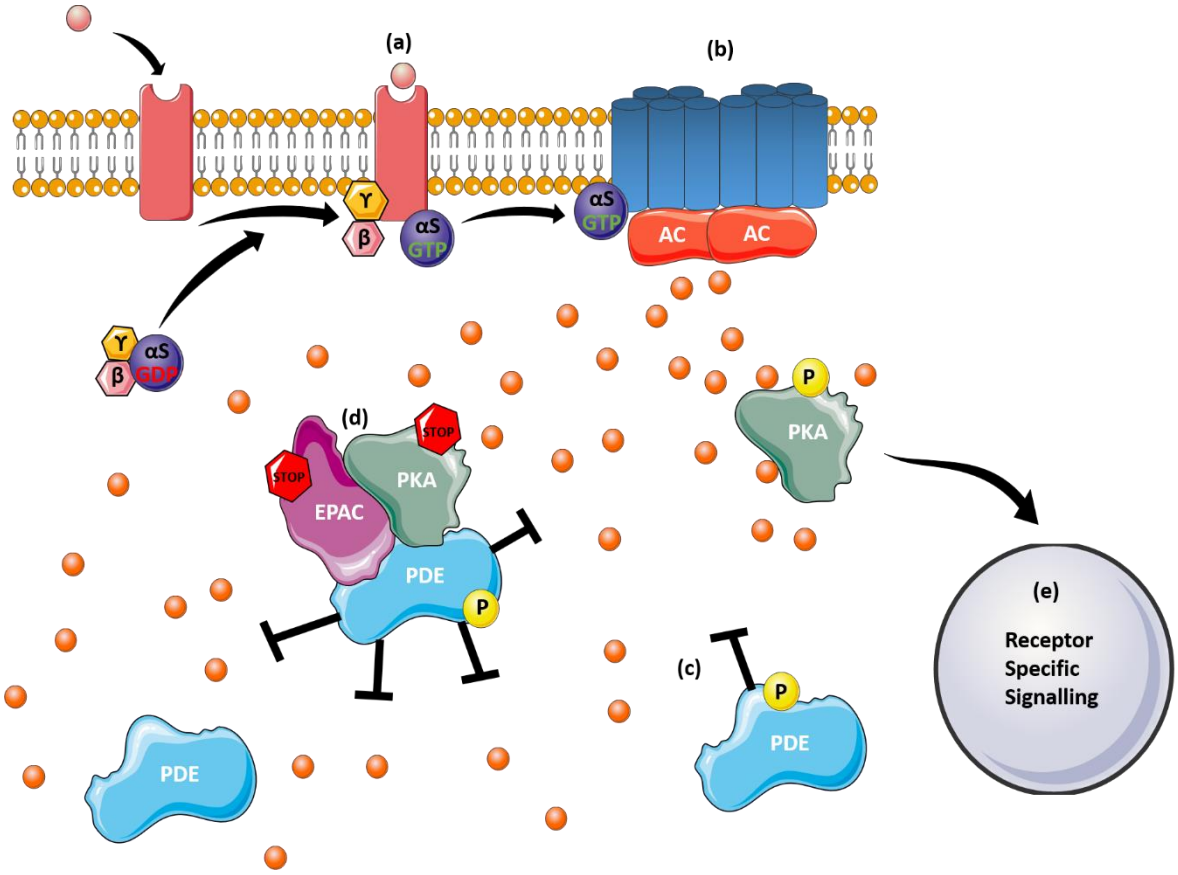

Figure 1.8 Diagrammatic representation of the compartmentalization of cAMP cellular signalling. (a) The binding of an appropriate ligand to the transmembrane spanning G- coupled protein receptor. Upon activation, Gα subunit of the receptor is released. (b) The enzyme adenylyl cyclase (AC) is bound by the Gα subunit and triggers the production of cAMP. (c) Phosphodiesterase's mediate the signal produced by cAMP by degrading cyclic nucleotides. (d) cAMP effectors (PKA and EPAC) form signalosomes with cAMP phosphodiesterase's (PDEs) meaning they can only be activated when the PDEs are 'swamped' by the cAMP produced by receptor activation. (e) Activated downstream effectors can drive cellular signalling pathways controlling numerous processes such as cellular growth, movement and differentiation.

1.4.3 Role of PDEs in the Cardiovascular System

The role of PDEs and cyclic nucleotide signalling in the heart has been extensively investigated. In the cardiomyocyte, elevation of cAMP controls the activity of several proteins (via PKA phosphorylation), including MyBP-C, PLB and TnI, which are responsible for excitation-contraction coupling as well as

sarcomere function (Kentish et al., 2001, MacLennan and Kranias, 2003, Nagayama et al., 2007). This however, means that chronic sympathetic stimulation of membrane-bound receptors leads to prolonged high levels of cellular cAMP driving pathways contributing towards hypertrophy and heart failure (Bobin et al., 2016). As such, researchers have attempted to identify therapeutic targets in this area and some of them have been identified as PDEs. Within the cardiovascular system, PDE3 and PDE4 are the predominant families but this may only be due to a lack of information about the functional roles of PDE1, PDE2, PDE5 and PDE9 in the context of heart disease (Bobin et al., 2016). Although many pre-clinical studies exist that have examined how inhibition of PDEs can help improve the pathophysiology of cardiac related diseases, there remains relatively few of these compounds that have been used clinically. One of the first investigations into the therapeutic role of PDE modulation for the treatment of heart disease started with the hypothesis that the inhibition of PDE3 could lead to the enhancement of both PKA and Epac dependant signalling pathways (Maurice et al., 2014). Inhibition of PDE3 resulted in increased contractility through the enhancement of the current from LTCC (Verde et al., 1999, Weishaar et al., 1987). The issue that was presented with broad PDE3 inhibition is that, due to excessive calcium entry and further internal release from the sarcoplasmic reticulum (SR), the development of arrhythmia was promoted (Bobin et al., 2016). The treatment of chronic heart failure patients with milrinone, a PDE3 inhibitor, was stopped due to this increased occurrence of ventricular arrythmias and an increase in morbidity and mortality (Packer et al., 1991, Baillie et al., 2019). PDE4 inhibition has also been extensively investigated. Treatment with the PDE4-specific inhibitor rolipram resulted in significantly increased heart rate and contractility as a result of the enhanced stroke volume, cardiac output, slope of ESPVR and ejection fraction in rat hearts through the activation of SERCA2a (Huang et al., 2019). However, it has been shown that the use of rolipram in humans resulted in a potent cAMP-mediated anti-inflammatory response which has led to a drive by pharmaceutical companies to develop inhibitors that can specifically be used for inflammation-related diseases (Torphy, 1998, Rabe, 2011). There are currently several PDE4 inhibitors approved for clinical use such as: Apremilast in the treatment of psoriasis and psoriatic arthritis and Roflumilast approved for the treatment of

chronic obstructive pulmonary disease (COPD) and asthma (reviewed in (Li et al., 2018)).

Within the confines of the cardiac system, the generation of cAMP is largely governed by ß-adrenergic signalling. In cardiomyocytes, the sympathetic activation driving this ß-adrenergic signalling functions largely to facilitate the fight or flight response (Fertig and Baillie, 2018). This occurs through the activation of the membrane bound GPCR subsequently activating an AC through association with the G_s-protein. The resulting production of cAMP from ATP activates effector proteins causing various downstream signalling pathways. Of these effectors, PKA is of great importance during excitation-contraction coupling in the heart as it phosphorylates many key proteins, including LTCC, ryanodine receptor (RyR), PLB, and TnI, controlling the pathway (Fertig and Baillie, 2018). The combination of the actions of these phosphorylated proteins leads to numerous positive inotropic and lusitropic effects which help increased heart function based on increase circulatory demands (Bers, 2002). Actions of these signalling proteins are tightly regulated in signalosomes by bound PDEs. Signalosomes not only contain PDEs, AKAPs, PKA substrate protein and PKA holoenzyme.

Specific PDE isoforms tethered to cardiac signalling complexes have been identified by several biochemical methods. Pharmacological intervention by inhibiting one family of PDEs, and measuring the subsequent change in the phosphorylation of cAMP substrates (Sin et al., 2011). This is usually followed by the development of knock-out animals which lack specific subfamilies for example PDE4D allowing for further characterisation of the role of that PDE family on the cAMP-controlled pathway (Lehnart et al., 2005). Another method by which the roles of specific isoforms have been investigated is through the development and use of siRNA to knockdown each member of the subfamily (Maurice et al., 2014). In doing this the specific isoform that is driving the regulation of cAMP-controlled phosphorylation in any given pathway could be identified. More recently, peptide array technology has been utilised to map specific binding sites of PDEs on their signalosome interaction partners allowing for the creation of cell-penetrating disruptor peptides (Lee et al., 2013). These peptides function to unhook the interaction in one specific signalosome removing

the control over cAMP levels giving further information about the role of a single "pool" of a single PDE isoform. As previously mentioned, FRET experiments using proteins tagged to fluorescent probes have alluded to how PDEs in signalosomes function in the regulation of discrete and localised signalling (Maurice et al., 2014). In this context, FRET is particularly informative as it can use cAMP-binding proteins/domains and targeting proteins to specifically show cAMP in very specific microdomains within a cell. In combination these approaches (cAMP FRET and disruptor peptide technology) have potential to identify specific isoforms of PDEs tethered to individual signalling complexes.

1.5 Post-translational Modifications

Post-translational modifications (PTM) of proteins are known to have many important regulatory roles that underpin cellular homeostasis. A PTM is the covalent attachment of a specific functional group to proteins. Currently there are nearly 200 identified PTMs and their dysregulation has been linked to many disease pathologies including cancer (Saraswathy and Ramalingam, 2011). Some of the main functions of PTMs are in the regulation of protein folding, protein stability and conformation. Interestingly, PTMs can either generate a reversible or irreversible change in activity. The most commonly found PTMs in life are phosphorylation and glycosylation and both are crucial to protein function. Additionally, SUMOlyation, which is the addition of small ubiquitin-like modifier (SUMO) protein to a substrate, has been shown to have a multitude of functional effects including subcellular localisation and degradation of proteins (Müller et al., 2001, Seeler and Dejean, 2003, Hannoun et al., 2010). A PTM that plays a major role in the degradation of proteins is ubiquitination. This is the addition of ubiquitin, a 76kD protein, covalently to lysine residues of the protein targeting it for degradation (Hayat, 2016). PTMs will be reviewed further in chapter 6.

1.5.1 Phosphorylation

Of importance to this work is the PTM of phosphorylation in the context of PDEs and it will be briefly described here. Approximately 30% of all cellular proteins within the human proteome are known to be phosphorylated (Saraswathy and

Ramalingam, 2011). Phosphorylation or dephosphorylation is a quick and extremely sensitive method by which the activity state of a protein can be altered. The action of two enzymes, phosphatase and a kinase are responsible for the removal and addition of a phosphate groups. The kinase will drive the addition of a phosphate group to the side chain of certain amino acids which are primarily serine (S) or threonine (T), while phosphates act oppositely to this by removing the phosphate. Phosphorylation of PDEs by either PKA or PKG is known to stimulate the catalytic ability of multiple enzymes including PDE3, PDE4, PDE5 and PDE8 (Figure 1.9)(reviewed in (Baillie et al., 2019)). Not only does this PTM affect the activity of the PDE but can also drive the change in its cellular localisation. This can be through changing the protein complexes that the PDE is found in.

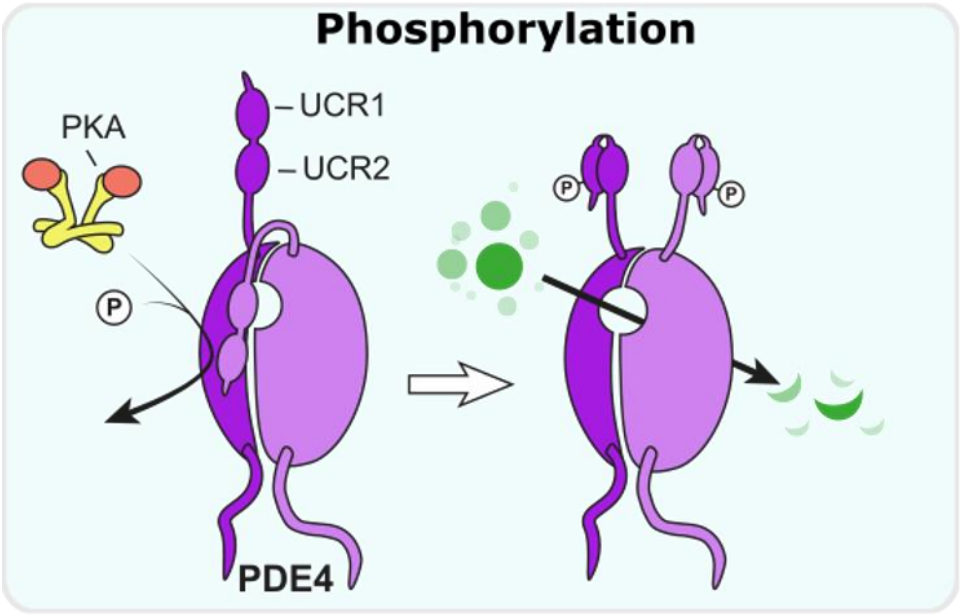

Figure 1.9 Phosphorylation of PDE4. The phosphorylation of PDE4 is an extensively identified means by which its activity is controlled. The phosphorylation of PDE4 by PKA activates its catalytic ability leading to the decrease in localised cAMP concentrations. (adapted from Baillie, Tejeda and Kelly, 2019).

In terms of changing the catalytic ability of PDEs, it has shown that the human PDE4A4 activity displays a four-fold increase in activity after phosphorylation by PKA (Laliberté et al., 2002). In addition, phosphorylation increases the sensitivity of the PDE to enantiomers of rolipram, the specific PDE4 inhibitor. The activation of PDEs will be investigated in this work.

1.6 Hypothesis and Aims

Since its original identification in 1999 and 2000, our understanding of how *POPDC* genes function within the cell has increased immensely (Reese et al., 1999, Andrée et al., 2000). In heart and skeletal muscle, some of the functions of POPDC1 have been elucidated however relatively little is known about its underlying mechanistic role in the heart and skeletal muscle. POPDC1 is proposed to be a key protein involved in the maintenance of cardiac pace-making due to its high levels in the pace-making regions of the heart. This is where the focus of my work lies.

Recently, POPDC proteins have been identified as a novel family of cAMP effector proteins (Froese et al., 2012). The known interaction with the potassium channel, TREK1, has been extensively investigated and is known to be a key interaction in heart and skeletal muscle. This interaction is facilitated by cAMP, as at basal concentrations the two proteins interact. As cAMP levels rise after stimulation of membrane-ACs, TREK1 becomes dissociated potentially due to the conformational change of the interaction domain on POPDC1 after binding cAMP (Froese et al., 2012). Once cAMP levels return to basal the interaction can be formed again allowing the potassium current to be altered. As Popdc1 is the newest cAMP effector protein to be identified, we hypothesis that it will form a complex with PDEs (PDE4 in particular) and other POPDC interacting proteins. The interaction with a PDE4, will facilitate the generation of a cAMP “sink” around POPDC1, severely restricting its access to the cyclic nucleotide. In turn this would allow for the regulation of POPDC1’s interaction with protein partners such as TREK1. This is important as POPDC1 is known to function by way of its protein-protein interactions.

Mutations in *POPDC1* have been identified in patients presenting with cardiomyopathy, a cardiac conduction disorder usually accompanied by muscular dystrophy. One aim of this thesis was to investigate the interaction between POPDC1 and PDE4 and use information gleaned to devise a cell-penetrating disruptor peptide to allow characterisation of the PDE4-POPDC1 signalosome function. I was also interested to determine how known POPDC1 mutations affected its interaction with PDE4.

Finally, as it is known that post-translational modification can alter the localisation, function and interactome of any protein, we sought to identify any PTMs that could potentially alter POPDC1. Such data would provide preliminary evidence that PTMs alter Popdc1 function and expansion of such a theme may identify disease related modifications that could be targeted therapeutically.

In summation, the hypothesis that I am testing is that POPDC1 function can be regulated by either interaction with PDEs or alteration by PTMS. My specific aims are:

1. To investigate whether POPDC1 interacts directly with PDE4 and if so to map the protein-protein interactions sites

2. To use information from the fine mapping of POPDC1-PDE4 interaction sites to devise a cell-permeable peptide that can effectively disrupt the complex.

3. To utilise the disruptor peptide in studies that propose a functional role for the POPDC1-PDE4 complex.

4. To try to determine the structure of the Popeye domain of POPDC1 and discover the sites of PTMs to better understand PDE4 binding mode and assess possible effects of PTMs on POPDC1 function.

2 Materials and Methods

2.1 General Laboratory Practice

All equipment and reagents were purchased from Sigma-Aldrich (Dorset, UK) unless stated otherwise. Any hazardous reagents were handled and disposed of according to the relevant Control of Hazardous to Heath regulations. Personal protective equipment was worn accordingly during all procedures.

Glassware, prior to use, was washed using Decon 75 detergent (Decon Laboratories Ltd, East Sussex, UK), thoroughly rinsed with distilled water and dried. Sterile disposable plastic dishes, containers and dispensers were used including microcentrifuge tubes (Grenier Bio-one, Stonehouse, UK), falcon tubes (Corning, Birmingham, UK), stripettes (Corning, Birmingham, UK) and pipette tips (Ranin, California, UK). Reagents, liquids, glassware and other laboratory items were sterilised by autoclaving in a Prestige Medical autoclave (Prestige Medical, Blackburn, UK). Chemicals for the preparation of buffers, solutions and media were weighed using a Mettler Toledo balance (sensitive to 0.01 g, Ohio, USA) or a Sartorious CP124S balance (sensitive to 0.0001 g, Bradford, UK). Unless otherwise stated, all solutions were prepared using distilled water. Solution pH was measured using a Mettler Toledo Seven Easy digital pH meter (Mettler Toledo, Ohio, USA) and adjusted to correct pH using either HCl or NaOH. All volumes were dispensed using a Gilson battery powered pipetting aid (1 – 25 mL) and Gilson and Gilson pipettes (0.2 -1000 µL; Gilson Medical Instruments, Staffordshire, UK). Centrifugation was carried out at appropriate temperature in a temperature controlled Sigma-Aldrich 1 – 14K rpm table top microcentrifuge (ThermoFisher Scientific, Paisley, UK), a ThermoFisher Scientific Cl31 multispeed centrifuge (ThermoFisher Scientific, Paisley, UK) or a Beckman Coulter Optima L – 80 XP ultracentrifuge (Beckman Coulter, High Wycombe, UK) depending on volume and speed requirements. Temperature sensitive incubations were carried out using a Grant OLS200 water bath (Grant Instruments, Cambridgeshire, UK), Techne Dri-Block DB2A heat block (Teche, Staffordshire, UK) or a Startorius CERTOMAT BS-1 (Sartorius Stedim BioOutsource Ltd, Glasgow, UK).

2.2 Isolation and Preparation of Plasmid DNA

All work encompassing the use of plasmid DNA was performed in a sterile environment using autoclaved buffers and media.

2.2.1 Transformation of Chemically Competent Cells

Chemically competent DH5α cells (Invitrogen, ThermoFisher Scientific) were stored at -80ºC and were thawed prior to use on ice. Typically, 1-5 ng of plasmid DNA was added to 50 µl and mixed gently by flicking the tube. Cells were incubated on ice for 30 minutes prior to a 30 second heat shock at 42ºC then returned to ice for a further 5 minutes. 450 µl of pre-warmed Luria-Bertani (LB) media (1% (w/v) Bacto-tryptone, 0.5% (w/v) Yeast Extract and 170 mM NaCl) supplemented with either 100 µg/ml Kanamycin or Ampicillin depending on the antibiotic resistance of the plasmid. Tubes were incubated, with vigorous shaking, for 1 hour at 37ºC. 50-200 µl of the transformation mixture was spread onto LB agar plates (LB media supplemented with 1.5% (w/v) agar and 100 µg/ml of appropriate antibiotic) and incubated overnight at 37ºC. Colonies present on plates after incubation period indicated the cells were successfully transformed with the plasmid DNA.

2.2.2 Preparation of Plasmid DNA

Single colonies present on the LB agar plates were picked in order to inoculate 5 ml of LB media supplemented with 100 µg/ml of appropriate antibiotic. Cultures were incubated at 37ºC overnight in an orbital shaker at 225 rpm. QIAprep Miniprep Kits were used to isolate the plasmid DNA from culture according to the manufacturer's protocol. In order to produce larger DNA collection, 500 ml of LB media was used containing 100 µg/ml of appropriate antibiotic was inoculated and the QIAprep Maxiprep Kit was used to isolate the plasmid DNA using the manufacturer's instructions. For both protocols purified plasmids were eluted in Nuclease-Free distilled water and stored at -20º

2.2.3 Storage of Plasmid DNA

For storage of plasmid DNA as a glycerol stock, 1ml of overnight culture described previously was mixed with 1ml 50% LB Media / 50% glycerol solution in

a sterile cryovial. Glycerol stocks were snap-frozen on dry ice and stored at -80ºC until needed. DH5α competent cells are suitable for long tern storage thus plasmid DNA preparation can be generated from glycerol stocks when required.

2.2.4 Quantification of DNA concentration

To determine the concentration of DNA isolated from the Miniprep or Maxiprep protocol a NanoDrop 3300 spectrophotometer (ThermoFisher Scientific) was used. The absorbance of the sample was measured at 260 nm and 280 nm. The absorbance at 260 nm was used to determine the concentration of double stranded DNA (dsDNA). The $A_{260/280}$ ration was used in order to validate the purity of the DNA sample.

2.3 Mammalian Cell Culture

Class II flow hoods (ThermoFisher) were used for all detailed cell culture procedures. Standard aseptic techniques were used, and all solutions and instruments were kept in sterile conditions. All reagents and media were purchased from Gibco unless stated otherwise, all plastics including flasks and plates were acquired from Corning (Sigma-Aldrich). To visualise cells for routine checks a phase contract inverted microscope (Leitz Diavert) was used.

2.3.1 HEK-293 cell culture

Human embryonic kidney (HEK) 293 cells were purchased from ATCC and HEK-293 PDE4A4 stable cell line established by Millipore. HEK-293 and HEK-293 PDE4A4 cells were cultured in high-glucose Dulbecco's Modified Eagle's Medium (DMEM) supplemented with 10% (v/v) foetal bovine serum, 1% (v/v)penicillin/streptomycin (P/S), 1% (v/v) L-Glutamine, 1% (v/v) minimum essential media non-essential amino acids (NEAA). HEK-293 PDE4A4 cell media is further supplemented with 500 µg/ml G418 (Promega). Culture conditions were 37ºC in a humidified atmosphere with 5% CO_2. Cells were split at 80-90% confluence and media was replaced every three days as required.

2.3.2 Passage of cells

When HEK-293 and HEK-239 PDE4A4 stable cells reached 80-90% confluency they were passaged. Culture media was aspirated from flasks and cells were washed with 5ml of sterile phosphate buffer saline (PBS), which was pre-warmed to 37ºC, per 75 cm^2 flask. 0.25% (w/v) trypsin – ethylenediaminetetraacetic acid (EDTA) solution was pre-warmed and added to the flask and incubated at 37ºC for 5 – 10 minutes until the cell monolayer had detached from the base of the flask. An equal volume of fresh culture media was added in order to neutralise the cell suspension. Volume was removed and centrifuged at 500 x g for 3 minutes at room temperature (RT). The cell pellet was resuspended in appropriate volume of fresh culture media and seeded as required.

2.3.3 Isolation and Maintenance of Neonatal Rat Ventricular Myocytes

Neonatal rat ventricular myocytes (NRVM) are a commonly used model to study cardiac processes due to the similarities between adult ventricular myocytes as well as the relative ease by which they can be isolated.

The preparation of neonatal rat cardiomyocytes was modified from the protocol described by Bogoyevitch *et al*. (1995) and Chlopeikova *et al*. (2001). 1-3-day old neonatal Sprague-Dawley rats were sacrificed by cervical dislocation and femoral artery dissection. Cardiomyocytes were dissociated from the ventricles by serial digestions with 0.3 mg/ml Type-2 Collagenase (Worthington) and 0.6 mg/ml pancreatin (Sigma) in a balanced salt solution (120 mM NaCl, 20 mM HEPES, 5.5 mM Glucose, 5.4 mM KCl, 1 mM NaH_2PO_4 and 0.8 mM $MgSO_4$ (pH 7.4)). The first digestion was carried out at 37ºC in a water bath shaking at 130 cycles per minute for 5 minutes. The supernatant was collected and discarded. Tissue was then incubated for 20 minutes at 37ºC in a water bath shaking at 200 cycles per minute. This digestion step was repeated 3-5 times or until the tissue was completely digested. Cell suspensions form every digestion were collected and centrifuged at 1250 rpm for 5 minutes and the pellet was resuspended in 2ml of New-born Calf Serum (NCS). Cells were kept at 37ºC in a humidified incubator with an atmosphere of 95% air and 5% CO_2. After final digestion the cell suspensions were pooled and centrifuged for 5 minutes at 1250 rpm. The pellet was resuspended in M1 plating media (67ml D-MEM; 25mM HEPES (Invitrogen),

17.5ml M-199 (Invitrogen), 10ml Horse serum, 5 ml New-born calf serum, 1ml Glutamine 200nM and 0.1ml Penicillin-streptomycin). As non-cardiomyocytes become attached easily, the cells were pre-plated on 10cm^2 dishes (Corning) for 2 hours to allow differential attachment of non-myocardial cells. Non-adhered cells were collected and centrifuged at 1250rpm for 5 minutes. Cells were counted and plated at a density of 1 x 10^6 cells per well of a 6 well plate that was pre-coated with sterile 1% (w/v) gelatin (Sigma-Aldrich). For immunocytochemistry, cells were seeded at 1.5 x 10^5 on mouse lamin (BD Bioscience) (100 µg/ml per coverslip).

After being allowed to grow in M1 Media for 18-24 hours the media was aspirated and replaced with M2 media (75ml D-MEM; 25mM HEPES (Invitrogen), 17ml M-199 (Invitrogen), 5ml Horse serum, 0.5ml New-born calf serum, 1ml Glutamine 200nM and 0.1ml Penicillin-streptomycin). All drug treatments and transfections were carried out in M2 media.

Cells derived from the same primary culture were used for each set of experimental comparisons (n=1). All experiments were performed at least three times with different primary cell isolates.

2.3.4 Adult Rabbit Ventricular Myocytes

Adult rabbit ventricular myocytes (ARVM) were isolated as described in (Donahue et al., 1998). All isolations were carried out by Aileen Rankin (University of Glasgow). Briefly, adult rabbits were injected with heparin to prevent coagulation and phenobarbital (50 mg/kg). The heart was dissected out of the animal and rinsed twice with ice-cold Krebs buffer (138.2 mM Na+, 5.4 mM K+, 1.2 mM Mg^{2+}, 1.0 mM Ca^{2+}, 144.4 mM Cl-, 1.2 mM SO_{42-}, 1.2 mM H_2PO_4, 20 mM HEPES, 15 mM glucose, saturated with O_2, pH7.4). A canula was inserted into the aorta to allow the heart to be suspended on a langendorff perfusion rig. The perfusion was retrograde through the ascending aorta into the coronary arteries. The hearts were perfused with Krebs buffer for 2.5 minutes at a rate of 30 mL/min immediately followed by Ca^{2+}-free Krebs buffer for 10 minutes at a rate of 10 mL/min. Perfusion of an enzyme solution (0.025 mM Ca^{2+}, 1 mg/ml collagenase B, -.1 mg/ml protease, 60 mM taurine, 8 mM glutamic acid, 2 mM carnitine in Krebs) allowed for the digestion of the myocardium. Immediately following digestion, ventricles were excised separating out the left, right and

septal regions and agitated by constant pipetting. Straining through a 200 µm nylon mesh filter removed any valve and tendon cells and tissue. Cells were "stepped up" in increased concentrations of Ca^{2+}, this was done in 4 consecutive steps with at least 10 minutes between to allow for equilibration. Cells were cultured in supplemented M199 media (5 mM creatine, 5 mM carnitine, 5 mM taurine, 0.1 mg/mL penicillin/streptomycin) in cell culture dishes coated 1 µg/cm^2 laminin. 1-2 hours after initial plating the media was replaced to remove dead cells in the culture.

2.3.5 Transient Transfections

Plasmids containing human *POPDC1*-Flag and mouse *Popdc1*-myc were kindly gifted by Dr Thomas Brand, Imperial College London. Dependant on which POPDC plasmid was being used, either the human PDE4A4-VSV or the rodent PD4A5-VSV were used for transfections. Plasmid DNA was transiently transfected into HEK-293, HEK-293 PDE4A4 Stables and primary NRVM in the present study. Both HEK-293 and HEK-293 PDE4A4 stable cell lines were passaged 24 hours prior to transfection to ensure cells reached 50-70% confluency on the day of transfection. Primary NRVM were allowed to incubate in M2 media for at least 2 hours before transfection was undertaken. Transfections in all cells were performed using Lipofectamine LTX transfection reagent (Invitrogen) following manufacturer's instructions. For HEK-293 cell lines, transfections were carried out in OptiMEM reduced serum media (Invitrogen) and in NRVM transfections were carried out in M2 media. Concentration of plasmid DNA and transfection reagent were scaled according to the size of the culture dish used. Cells were incubated with transfection medium for 18-48 hours in order to ensure maximal plasmid expression. For control, mock transfections were carried out without plasmid DNA.

2.4 Preparation of Cell Lysate

2.4.1 Whole Cell Lysates

Protein extracts were prepared from cardiomyocytes and HEK-293 cell lines. Culture media was aspirated from culture plates and the cells were washed thoroughly before the addition of lysis buffer. For this project two lysis buffers

were utilised; 3T3 lysis buffer (50 mM NaCl, 50 mM NaF, 25 mM HEPES, 5 mM EDTA, 30 mM sodium pyrophosphate, 10% (v/v) glycerol, 1% (v/v) Triton X-100; pH7.5) and a CO-IP buffer (50 mM Tris; pH8.0, 150 mM NaCl, 2 mM EDTA, 1% (v/v) Triton X-100, 0.25% (w/v) bovine gelatine (Sigma-Aldrich)) (Roland Schindler, Imperial College London). Both lysis buffers were supplemented with phosphatase and protease cocktail inhibitor tablet (Roche). Cells were scraped using a sterile scrapper and transferred into an ice-cold 1.5 ml microcentrifuge tube. Cells were pulled through a sterile 23G needle four to six times before being sonicated at 2 mW for 15 seconds. This step was repeated twice with a 15 second pause between sonication rounds to allow the sample to cool. Samples were then centrifuged at 14,000 x g for 30 minutes to remove any insoluble components and remove any debris.

2.4.2 Determination of Protein Concentration

To determine the concentration of the protein collected from whole cell lysing and purified proteins the Bradford dye-binding method (Bradford, 1976) was used. The quantification protocol utilises the change in colour and absorption maximum of Coomassie Brilliant Blue G-250 when bound to increasing protein concentrations. Briefly, A standard curve was constructed using various concentrations of Bovine serum albumin (BSA) from 0-5 µg. Each well of a 96 well plate was composed of 50 µL of 1:50 – 1:200 dilution of the protein sample and 200 µL of Bradford reagent (Biorad) prepared at a 1:5 dilution per manufacturer's instructions. All standards and samples were carried out in triplicate. Measurements were taken for 595 nm absorbance using Anthos 2010 plate reader fitted with a 595 nm filter. Analysis was performed using ADAP software and a standard curve was constructed using the measurements from BSA standards. Concentrations of protein samples could be derived from produced curve.

2.5 Subcellular Fractionation

Subcellular fractionation was performed using both transiently transfected HEK-293 cells and endogenously expressing NRVMs.

2.5.1 HEK-293 fractionation

HEK-293 cells were cultured on 10 cm^2 dishes before undergoing the transfection protocol outlined in section 2.3.5. Following a 24-hour incubation in transfection medium, the media was aspirated, and the plate was washed twice in ice-cold PBS. 500 µl of Fractionation buffer (20 mM HEPES; pH7.4, 10 mM KCl, 2 mM $MgCl_2$, 1 mM EDTA, 1 mM EGTA) and were incubated on ice for 15 minutes. Plates were scraped using a sterile cell scraper. Lysates were transferred to 1.5 ml Microcentrifuge tubes and samples were passed through a 23G needle at least 10 times. Samples were incubated on ice for a further 20minutes before centrifuging at 3000 rpm (720 x g) for 5 minutes. The supernatant was removed and added to a fresh 1.5ml microcentrifuge tube and contains the membrane, cytoplasm and mitochondrial fractions whilst the pellet contains the nuclear fraction. The nuclear fraction was washed with 500µl of fractionation buffer and passed through a 23G needle 10 times before centrifuging at 3000 rpm (720 x g) for 10 minutes. The supernatant was discarded, and the pellet was resuspended in 100µl of Nuclear Protein Buffer (NPB) (10 mM $NaCl_2$, 10 mM Tris-HCl; pH7.5, 2 mM $MgCl_2$, 0.5% NP-40). The supernatant containing the cytoplasm, membrane and mitochondrial fractions was processed next. Samples were centrifuged at 8000 rpm (10000 x g) for 5 minutes. The supernatant, containing the cytoplasm and membrane fractions, was added to a fresh 1.5 ml microcentrifuge tube. The pellet containing the mitochondrial fraction was processed in the same manner as the nuclear fraction. The cytoplasmic and membrane fraction were transferred to ultracentrifuge tubes and centrifuged at 40000 rpm (100000 x g) for 1 hour. The supernatant recovered from this step contains the cytoplasmic fraction whilst the pellet contains the membrane fraction. The pellet was washed by the addition of 400 µl of fractionation buffer and pulled through a 23G needle and centrifuged at 40000 rpm (100000 x g) for 45 minutes. Supernatant was discarded and the pellet was resuspended in 100 µl of Fractionation buffer, this was the membrane fraction.

Samples are normalised by volume before being run of SDS-PAGE gel. Whole cell and nuclear fractions were normalised by the addition of 10µl of sample to 70µl dH_2O and 20µl 5x Laemmli protein sample buffer (Bio-Rad). The plasma membrane and cytoplasmic fraction were normalized by the addition of 50 µl of sample to 30µl dH_2O and 5x Laemmli protein sample buffer (Bio-Rad). Samples are boiled for 10 minutes and stored at -20°C.

2.5.2 Neonatal Rat Ventricular Myocyte Fractionation

Neonatal Rat Ventricular Myocytes were harvested and cultured as outlined in section 2.3.3. These cells were used to investigate endogenous localisation of POPDC1 and PDE4A5 and as such were lysed after 2-hour incubation with M2 media. Samples were subjected to the same protocol as used for HEK-293 cells, outlined in section 2.5.1.

2.6 Expression of Recombinant Proteins

2.6.1 GB1 Fusion Protein

A GB1-POPDC1 fusion construct was used containing residues 123-266 of POPDC1 fused with a 58 residue GB1 peptide to improve solubility. The construct was cloned into a pLEICS-91 vector, an ampicillin resistance vector, at the T7 promoter (Provided by Professor Thomas Brand, Imperial College London). The vector containing the plasmid was transformed into BL21 competent *Escherichia Coli* (E. coli) (NEB) for protein expression using manufacturers protocol. BL21 cells containing the plasmid were inoculated into 10 ml of Luria-Bertani (LB) medium supplemented with 100 µg/ml ampicillin and grown overnight at 37°C in an orbital shaker. The overnight cultures were used to inoculate 500 ml of LB medium supplemented with 100 µg/ml ampicillin and grown until optical density (OD_{600}) was between 0.6 and 0.8. Once the OD_{600} reached this level it indicated that the culture was in the logarithmic phase, and the exponentially growing cells were then subjected to 1mM isopropyl-ß-D-thiogalactopyranoside (IPTG) to induce protein expression. Cultures were allowed to grow for a further 3 hours at 37°C in an orbital shaker. Cells were pelleted by centrifugation at 6000 x g for 10 minutes at 4°C. The supernatant was discarded, and the pelleted cells were resuspended in 10 ml (per 500 ml of culture) of lysis buffer (50 mM Tris-HCl;

pH8.0, 300 mM NaCl, 10 mM Imidazole) supplemented with protease cocktail inhibitor tablet (Roche). The resuspended cell pellet was snap frozen and stored at -80ºC overnight in order to improve lysing of cells. Imidazole was added to lysis buffers in order to minimise the binding of untagged and contaminating proteins to the purification beads, therefore increasing the purity of the target protein. Frozen lysate was thawed on ice prior to sonication using a probe sonicator at 40-60 kHz (Sonicator, Jencons, England) for 10 minutes. The sonication cycle was repeated 7 times with 30 seconds of sonication followed by 1 minute on ice. Following sonication, cell lysates were centrifuged at 6000 x g for 15 minutes at 4ºC. This allows for the collection of the soluble fraction and discarding of the insoluble and cell debris fraction. The supernatants collected were incubated end-over-end with pre-equilibrated nickel-nitrilotriacetic acid (Ni-NTA) resin (Qiagen) for 1 hour at 4ºC with gentle agitation. Lysate containing resin bound protein was transferred to a disposable Econo-Pac® Chromatography Column (Bio-Rad) and allowed to flow through. Resin was washed extensively with wash buffer (50 mM Tris-HCl, 300 mM NaCl; pH8.0) supplemented with 10mM imidazole in order to reduce unspecific protein binding. The fusion protein is eluted from the Ni-NTA resin using elution buffer (50 mM Tris-HCl, 300 mM NaCl; pH8.0) containing step wise increasing concentrations of imidazole (25-250 mM) to remove weaker binding contaminating proteins before eluting the target protein.

40 µl samples were collected from each step for analysis by SDS-PAGE and Coomassie staining to allow for quality control (described in sections 2.8.12.8.2, and 2.8.3). After analysis, the purest elutions (indicated by a single band on the gel) were pooled and concentrated using an appropriately sized centrifugal concentrator (Vivaspin; Sartorius Stedim Biotech). Buffer exchange was performed using dialysis buffer (5 % (v/v) Glycerol, 50 mM Tris-HCl, 100 mM NaCl; pH8.0) in order to remove Imidazole and concentrate the protein diafiltration. Once the desired concentration was obtained, the purified recombinant protein was stored as aliquots at -80ºC

2.6.2 Glutathione-S-transferase (GST) Fusion Protein

A construct containing the Popeye domain of POPDC1 fused with a GST tag was used for purification. Cells were grown, induced, harvested and lysed as

described in section 2.6.1. The GST fusion protein was purified using glutathione sepharose resin (Amersham Biosciences). The elution buffer used to remove the protein from the bound resin contained 10 mM reduced Glutathione and 50 mM Tris-HCl; pH8.0. The cell lysis, protein purification and concentration procedures were carried out as outlined in section 2.6.1.

2.6.3 Maltose-Binding Protein (MBP) Fusion Protein

Full-length PDE4A4 fused with MBP was cloned in pET30b vector, produced by the Baillie lab, before being transformed into BL21 competent *E. Coli* cells for protein expression. Cells were grown, induced, harvested and lyse as described in section 2.6.1. For purification of MBP fusion proteins, cells were resuspended in MBP binding buffer (20 mM Tris; pH 7.4, 200mM NaCl, 1 mM EDTA, 1 mM DTT) supplemented with cOmplete™, EDTA-free Protease Inhibitor Cocktail (Roche, UK). The purification was performed using amylose resin beads (New England Bioscience). Proteins were eluted from the resin using elution buffer comprised of MBP binding buffer with 10 mM Maltose. The cell lysis, protein elution and purification procedures were carried out as outlined in section 2.6.1.

2.7 Generation of constructs for structural analysis

2.7.1 Synthetic DNA

Synthetic DNA containing the full length human POPDC1 sequence was purchased from Genewiz (US). The fragment was codon optimised for expression in *E. coli*.

Synthetic POPDC1 gene:

5’ATGAATTACACCGAAAGTAGCCCGCTGCGTGAAAGCACCGCAATCGGCTTCACGCCCG
AACTGGAAAGCATTATCCCGGTGCCGAGCAATAAGACCACTTGTGAGAATTGGCGCGAA
ATCCACCATCTGGTTTTCCATGTTGCAAACATTTGCTTCGCCGTTGGTTTAGTTATTCCT
ACCACTTTACATTTACACATGATCTTTCTGCGCGGTATGCTGACTTTAGGTTGCACTTTA
TATATCGTTTGGGCCACTTTATATCGCTGCGCTTTAGATATCATGATTTGGAATAGCGTG
TTTTTAGGTGTGAACATTTTACATTTAAGCTATTTACTGTATAAGAAGCGTCCCGTTAAG
ATTGAAAAGGAGCTGAGCGGCATGTACCGTCGTTTATTCGAACCTCTGCGCGTGCCTCC
CGATCTGTTTCGCCGTCTGACTGGTCAATTCTGCATGATCCAGACTTTAAAGAAGGGCCA
AACCTATGCCGCCGAAGACAAAACCAGCGTTGATGACCGTTTAAGCATTTTACTGAAGGG

CAAAATGAAGGTGAGCTATCGTGGTCATTTTTTACACAACATTTATCCGTGCGCCTTCAT
CGATAGCCCGGAATTCCGTAGTACCCAGATGCACAAAGGCGAGAAGTTCCAAGTTACCA
TCATCGCCGACGACAATTGTCGTTTTTTATGCTGGAGCCGCGAGCGTCTGACCTATTTTC
TGGAGAGCGAGCCGTTTCTGTACGAGATCTTTCGCTATTTAATCGGTAAAGATATTACCA
ATAAGCTGTATTCTTTAAACGACCCGACTTTAAATGACAAAAAGGCCAAAAAATTAGAAC
ACCAGCTGTCTTTATGCACCCAGATTAGCATGCTGGAGATGCGCAACAGCATCGCCAGC
AGCAGTGATAGCGATGACGGTTTACATCAGTTTCTGCGTGGCACCAGCAGCATGAGTTC
TTTACATGTTAGCAGTCCGCATCAGCGTGCCAGCGCAAAAATGAAGCCGATTGAGGAAG
GTGCTGAAGATGATGACGACGTGTTTGAACCGGCAAGCCCGAACACTTTAAAAGTTCAT
CAGCTGCCG 3’

2.7.2 Molecular cloning

Fragments of POPDC1 cDNA were created and amplified by PCR using a set of primers designed to bind the protein at various domains and all reactions were carried out in a MJ Research PTC-200 Thermal Cycle (MJ Research, Nevada, USA) (Table 2). PCR reaction conditions were constant throughout all experiments with only the annealing temperatures changed depending on primers used. The PCR machine conditions were as follows: 95^{o}C for 2 mins, then 30 cycles of 95^{o}C for 30 seconds, primer specific annealing temperature (Table 2) for 30 seconds, 72^{o}C for 30 seconds, followed by 72^{o}C for 5 minutes then 4^{o}C on hold. Sequences 5’TAC TTC CAA TCC and 5’TAT CCA CCT TTA were added to the 5’ and 3’ primers respectively to allow for ligation independent cloning into the pNIC28-Bsa4 plasmid vector (appendix 1) (Keates et al., 2011). NEBuilder® HiFi DNA Assembly Cloning Kit was used following the manufacture’s protocol to insert the created fragments into the plasmid vector, which was linearized by BsaI digest. To ensure correct sequences were produced, fragments were initially transferred into DH5α competent cells (NEB) using manufacturers protocol. Positive colonies were subjected to colony PCR to confirm presence of transformed fragments prior to being transformed into BL21 (DE3) competent cells (NEB). A single colony was taken, resuspended in 10 µl dH_2O and added to a PCR reaction including; 10 mM 5’ primer (Table 2), 10 mM 3’ primer (Table 2), and taq polymerase master mix. Examination of the fragments by agarose gel electrophoresis identified successful transformations. Using Monarch® DNA Gel Extraction Kit (New England Biolabs, US), confirmed fragments were excised and extracted from the gel for transformation into BL21 (DE3) competent cells.

Successful BL21 (DE3) colonies were miniprepped and sequenced (Source Bioscience, UK; Eurofins Scientific, UK). From confirmed transformation reactions, single colonies were picked and grown in LB supplemented with 50 mg/mL kanamycin to allow for glycerol stocks to be produced. 1 mL of culture was added to 1 mL of sterilised 50 % glycerol and stored at -80 ^{o}C.

Table 2: Primers designed for synthetic POPDC1 fragment generation

Name	Sequence	Tm (^{O}C)
Full length 5'	TAC TTC CAA TCC ATG AAT TAC ACC GAA	52
Popeye domain 5'	TAC TTC CAA TCC AAG CGT CCC GTT AAG	55
Full length 3'	TAT CCA CCT TTA CGG CAG CTG ATG AAC	55
Popeye domain 3'	TAT CCA CCT TTA CTT AGG CCT TTT TGT C	52

2.7.3 Solubility testing

Expression screening was carried out to determine optimal solubility conditions for large scale purification. Scrapings from glycerol stocks were grown in 10 mL LB supplemented with 50 mg/mL of kanamycin overnight at 37^{o}C whilst shaking at 220-225 rpm. The following day, three 50 mL Conical Centrifuge Tubes (Corning, UK) with 10 mL of fresh LB were inoculated with 1 mL of the overnight culture and grown to OD_{600} 0.6 - 0.8 whilst shaking at 220-225 rpm. Prior to the induction of protein expression, 1 mL of the culture was removed and added to a fresh 1.5 mL Eppendorf. Samples were centrifuged at 14,000 x g for 10 minutes; the supernatant was discarded, and the pellet was stored at -20^{o} C. Protein expression was induced by the addition of one of three IPTG concentrations; 0.1 mM, 0.4 mM or 1 mM. Cultures were allowed to express for 3 hours at 37^{o}C or 16 hours at 16^{o}C whilst shaking at 220-225 rpm. At the end of the induction period an OD_{600} reading was taken to allow the samples for analysis via SDS-PAGE to be normalised. A 1 mL aliquot of the induced culture was taken and treated in the

same manner as the pre-induction sample. Prior to SDS-PAGE, samples were defrosted and 1 mL of Bugbuster® (Merck) was prepared and supplemented with 25 units of Benzonase (Sigma-Aldrich). 60 µL of Bugbuster® plus Benzonase was added to each pellet and pipette thoroughly to resuspend all cells. Samples were incubated at room temperature for 20 minutes to allow for lysis of the cell membrane. Each sample was made up to a final volume (µL) of 150 x OD_{600} with water. To a fresh Eppendorf, 5 µL was removed from each pre-induction and post-induction sample and a further 10 µL of nuclease-free water was added. These samples represent the total protein in both pre-induction and post-induction cultures. Eppendorf tubes were centrifuged at 14,000 x g for 5 minutes and the supernatant from each condition was transferred to a fresh 1.5 mL Eppendorf and 15 µL was transferred to a further labelled tube, this represents the soluble fraction. The pellet was resuspended in the original volume of water. 5 µL was transferred to a fresh Eppendorf and a further 10 µL of water was added, this sample represents the insoluble fraction. Immediately prior to running the gel, 5x Laemmli protein sample buffer (Bio-Rad) was added and tubes were heated at 60°C for 10 minutes. SDS-PAGE analysis was carried out as described in 2.8.1.

Each construct was subjected to all test conditions.

2.7.4 Large scale protein purification

After identification of optimal growth conditions in the solubility screening tests, large scale expression was carried out following the same protocol as described in 2.6.1 and 2.6.2).

Cultures were pelleted by centrifugation at 6000 x g for 15 minutes. Cell pellets were briefly frozen at -80°C, thawed and the pellets were resuspended in lysis buffer (20 mM Tris-HCl; 0.5 M NaCl, pH7.4). Lysate was transferred to a 50 mL Conical Centrifuge Tubes (Corning, UK) and samples were sonicated on ice for 30 minutes, with 15 seconds of sonication and 15 seconds on ice. Cell debris were pelleted by centrifugation at 16,000 x g for 45 minutes. During this time, 1 mL of Ni-NTA resin (Qiagen) was allowed to settle in disposable Econo-Pac® Chromatography Column (Bio-Rad) and washed thoroughly with water then equilibrated with binding buffer (20 mM Tris-HCl; 0.5 M NaCl; 5 mM Imidazole,

pH7.4). Two of these columns were stacked allowing for lysate to flow through Ni-NTA resin twice capturing as much of the expressed protein as possible. After centrifugation, the supernatant was added to columns and allowed to drip through. Flow through lysate was collected and a 15 µL sample was taken for quality control. The columns were separated and resin bed was washed five times with binding buffer (20 mM Tris-HCl; 0.5 M NaCl; 5 mM Imidazole, pH7.4) and a further three times with wash buffer (20 mM Tris-HCl; 0.5M NaCl; 20 mM Imidazole, pH7.4). Protein elutions were collected in 500 µL of elution buffer (20 mM Tris-HCl; 0.5M NaCl; 0.3 M Imidazole, pH7.4). 15 µL of each elution was taken for analysis on SDS-PAGE following protocol outlined in section 2.8.1. Immediately prior to running, 5x Laemmli protein sample buffer (Bio-Rad) was added and samples were heated to 60^{o}C.

2.8 Protein Analysis

2.8.1 SDS-PAGE

Sodium dodecyl sulphate polyacrylamide (SDS-PAGE) gel electrophoresis was carried to separate proteins according to their molecular weight. Briefly, equal concentrations of protein samples were denatured and reduced in 5x SDS-PAGE sample buffer (10% SDS, 300 mM Tris-CL; pH6.8, 0.05% bromophenol blue, 50% glycerol, 10% ß-mercaptoethanol). Samples containing sample buffer was boiled for 5 minutes at 92ºC for 5 minutes or 72ºC for 10 minutes. After briefly centrifuging at 14000 rpm, protein samples were resolved on precast polyacrylamide gels (4-12% NuPAGE Novex Bis-Tris, Invitrogen) immersed in MOPS or MES SDS running buffer according the predicted molecular weight of the protein. Pre-stained protein marker (Bio-Rad) was loaded prior to protein samples and the gel was run for 45 minutes to 1 hour at 200 V.

2.8.2 Coomassie Staining

For direct protein visualisation, SDS-PAGE gels were removed from the pre-cast cassette and stained with Coomassie blue stain (1.25 g in 500ml Coomassie Brilliant Blue, 44 % (v/v) methanol, 6 % (v/v) acetic acid in water). Gels were incubated for 20 minutes at room temperature with gentle agitation. Residual background Coomassie staining was removed using a destain solution (10 % (v/v)

methanol, 10 % (v/v) acetic acid). Gels were incubated for 5-6 hours at room temperature with gentle agitation or until single bands were clearly visible. To further clean the stain from the gel, they were allowed to sit in distilled water at 4ºC overnight. To prevent the gel for cracking during the drying process they were washed with sterile water with 10 % glycerol. The molecular weight of the proteins was estimated through referring to the protein marker.

2.8.3 Western Immunoblotting

For Western blotting, resolved proteins were electrotransferred onto 0.45 µm pore nitrocellulose membranes (Protan, Whatman GmbH) using X-Cell II blotting module (Invitrogen) in transfer buffer (NuPage) containing 20 % methanol for 2 hours at 30 V. Full transfer of the pre-stained molecular weight markers onto the nitrocellulose membrane indicates successful transfer. The membrane is then blocked in 5% (w/v) non-fat dry milk (Marvel) in TBS-T (20 mM Tris-Cl; pH 7.6, 150 mM NaCl, 0.1% Tween 20) for 1 hour at room temperature with gentle agitation. Membranes are then probed with specific primary antibodies diluted in 1% milk/TBS-T solution and incubated overnight at 4º C (Table 3). The membranes are washed three times for 10 minutes each in TBST before adding appropriate Alexa Fluor fluorescent secondary antibodies diluted 1:10,000, in 1 % milk/TBS-T solution (Table 4). After secondary antibody incubation, blots are scanned using the Odyssey Infrared Imaging System (LI-COR Biosciences, UK) for fluorescence detection of the secondary antibodies. Fluorescence signal intensity is quantified using the Odyssey application software (LI-COR Biosciences, UK).

Alternatively, blots could also be scanned using enhanced chemiluminescence (ECL). Appropriate horseradish peroxidase (HRP) conjugated anti-immunoglobin-G (IgG) secondary antibody, diluted to 1:5000 was added in place of an Alexa Fluor antibody. After secondary antibody incubation, membranes were washed and detected by enhanced chemiluminescent Western Blotting Substrate (ThermoFisher). Chemiluminescent images of immunodetected bands were taken on blue-light sensitive autoradiography X-ray films (Kodak BioMax MS, Carestream Heath Inc.) developed using the Kodak ® X-Omat Model 2000 processor. In some cases, membranes were imaged using the Bio-Rad Universal

hood II (Bio-Rad). Images developed by both methods were quantified using Quantity One software (Bio-Rad) and averaged from at least an n or 3.

Table 3: Primary antibody list. IF, immunofluorescence; IP, immunoprecipitation: PA, peptide array; WB, western blotting.

Primary Antibody	Host Species	Immunogen	Dilution	Supplier; Product Number	Application
POPDC1 (BVES)	Mouse monoclonal	Raised against amino acids 1-300 mapping at the N-terminus of BVES of human origin.	1:1000	Santa Cruz; sc-374081	WB; IF; IP; PA
BVES	Rabbit polyclonal	Raised against amino acids 112-360	1:1000	Proteintech; 12920-1-AP	WB; IF; IP
GAPDH	Mouse monoclonal	Glyceraldehyde-3-phosphate dehydrogenase (GAPDH) from rabbit muscle	1:5000	Millipore; MAB374	WB
Caveolin 3	Rabbit polyclonal	Synthetic peptide corresponding to Mouse Caveolin-3 aa 1-19	1:2000	Abcam; Ab2912	WB
c-Myc	Mouse monoclonal	A 32 amino acid synthetic peptide (aa 408-439) derived from the C-terminus of the human c-myc protein.	1:1000	ThermoFisher; 13-2500	WB; IF; IP; PA
GST	Mouse monoclonal	Hybridoma 2H3-D10 produced by the fusion of mouse myeloma cells and splenocytes from BALB/c mice immunized with a GST-fusion protein	1:1000	Sigma-Aldrich; SAB4200237	WB; IP; PA
MBP	Mouse monoclonal	Raised against an epitope of myelin basic protein between amino acids 84-89.	1:100-1:1000	Abcam; ab11223	WB; IP; PA
Pan-PDE4A	Rabbit serum	Conserved C-terminal region of rat PDE4A isoforms	1:1000	In-house	WB; IF; IP; PA
Pan-PDE4A	Mouse monoclonal	Conserved C-terminal region of human PDE4A	1:5000	In-house	WB
Pan-PDE4B	Sheep serum	Conserved C-terminal region of rat PDE4B isoforms of all species	1:5000	In-house	WB; IF; IP
Pan-PDE4D	Sheep serum	Conserved C-terminal region of PDE4D isoforms pf all species	1:5000	In-house	WB; IF; IP
Hexa-Histidine	Mouse	Recombinant hexa-Histidine tagged fusion protein	1:3000	Sigma; H1029	WB; PA

Phospho-(Ser/Thr) PKA Substrate	Rabbit polyclonal	Synthetic phospho-PKA substrate peptide	1:1000	Cell Signalling Technologies; 9621	WB; PA
Phospho-UCR1	Rabbit polyclonal	Raised against phosphorylation site at serine 54 in the UCR1 domain	1:1000	In-house	WB
SUMO1 (C-terminal)	Rabbit polyclonal	Synthetic peptide corresponding to aa 72-97 of human SUMO-1	1:1000	Enzo; BML-PW9460-0025	WB; PA
SUMO2/3 (N-terminal)	Rabbit polyclonal	Synthetic peptide corresponding to aa 1-15 of human SUMO-2	1:1000	Enzo; BML-PW9465-0025	PA
VSV	Rabbit polyclonal	A synthetic peptide corresponding to aa 501-511 of vesicular stomatitis virus glycoprotein (VSV-G).	1:1000	Abcam; Ab1874	WB; IF; IP; PA

Table 4. Secondary antibody list. HRP, horse radish peroxidase; IF, immunofluorescence; PA, peptide array; WB, western blot

Secondary Antibody	Host Species	Immunogen	Dilution	Supplier; Product Number	Application
Donkey anti-goat	Donkey	IgG	1:5000	Licor; 925-68074	WB
Donkey anti-mouse	Donkey	IgG	1:5000	Licor; 925-68072	WB
Donkey anti-rabbit	Donkey	IgG	1:5000	Licor; 925-68073	WB
Anti-mouse HRP	Sheep	IgG	1:5000	Sigma; NXA931	PA; WB
Anti-rabbit HRP	Goat	IgG	1:5000	Sigma; A6154	PA; WB
Anti-goat HRP	Donkey	IgG	1:5000	Sigma; AP180P	PA; WB
Goat anti-mouse 488	Goat	IgG H+L from mouse	1:500	Invitrogen; A21071	IF
Goat anti-rabbit 488	Rabbit	IgG H+L from rabbit	1:500	Invitrogen; A21121	IF
Donkey anti-Mouse 488	Donkey	IgG H+L from donkey	1:500	Abcam; Ab1501105	IF
Donkey anti-rabbit 546	Rabbit	IgG H+L from rabbit	1:500	Invitrogen; A10040	IF

2.9 Protein-Protein Interactions

2.9.1 Co-immunoprecipitations

2.9.1.1 HEK293 cells

Co-immunoprecipitations (Co-IPs) is an ex-vivo method for confirming the interaction between two or more proteins. Cell lysates were normalised to equal protein concentration (1 µg/µl) using the lysis buffer outlined in section 2.4.1. 300-500 µg of cell lysate were precleared for 30 minutes at 4 ºC using washed protein G sepharose beads (Invitrogen). Samples were centrifuged briefly at 14,000 rpm in order to pellet the beads. The supernatant was removed and added to a fresh 1.5 ml microcentrifuge tube containing protein G sepharose beads combined with an appropriate primary antibody (Table 3). Anti-myc antibody was used to precipitate overexpressing POPDC1-myc or PDE4 isoform. Volume was adjusted to 500µl with CO-IP lysis buffer. The resulting immunocomplexes were captured during an overnight incubation at 4 ºC with end-over-end rotation. Samples were centrifuged at 500 x g for 3 minutes at 4 ºC and washed with CO-IP lysis buffer five times to remove non-specific binding proteins. Immunocomplexes were eluted from the beads by boiling in 2 X SDS-PAGE sample buffer and subjected to SDS-PAGE and Western blotting to identify interacting proteins.

2.9.1.2 Neonatal Rat Ventricular Myocytes

Endogenous IPs from neonatal rat ventricular myocytes (NRVM) were performed at P1-4. Lysates were prepared as described in section 2.4.1 and 500 µg of lysate was adjusted to 500 µl with CO-IP lysis buffer. Anti-BVES (Santa Cruz) was added and incubated with protein G sepharose beads at 4 ºC overnight with end-over-end rotation. Negative controls were set up using mouse IgG antibody to identify any non-specific binding proteins. After incubation, samples were handled as described in section 2.9.1.1.

2.9.2 Solid Phase Peptide Array

2.9.2.1 Solid Phase Peptide Array Synthesis

Peptide arrays were produced via automatic SPOT synthesis as described by Kramer and Schneider-Mergener (1998) and Frank (2002) using the AutoSpot-Robot ASS 222 (Invatis Bioanalytical Instruments) followed by Fmoc (9-fluroenylmethohydroxycarbonyl) chemistry (Kramer and Schneider-Mergener, 1998, Frank, 2002). This is based on solid phase peptide synthesis method stated by Fields and Nobel (1990) (Fields and Noble, 1990). The main principle of this technique is the use of spots that are formed through the dispensation of a solvent droplet on the array membrane surface creating a vessel for the reaction. These peptide array membranes are able to bind endogenous, transfected and recombinant purified protein and identify potential active motifs in order to investigate certain cellular activities. A 25-mer library of overlapping peptides, each shifted by five amino acids at a time, were produced sequentially in order to increase the reliability of the screening. Immobilised spots containing the peptide sequences were directly synthesised on Whatman 50 Cellulose membranes and used as peptide arrays.

2.9.2.2 Peptide array overlay

The peptide arrays were flooded with 100 % ethanol briefly and equilibrate in TBS-T to equilibrate for 10 minutes. This incubation step is used to remove any impurities used to store the peptides during synthesis. Peptide arrays were blocked using 5 % (w/v) milk (Marvel) in 1X TBS-T for 1 hour at room temperature with agitation. Either an appropriate protein or substrate was used to overlay the peptide array. For both cell lysate, containing either POPDC1-FLAG or PDE4A4-VSV, and purified recombinant proteins, either POPDC1-GST or PDE4A4-MBP, were diluted in 1 % TBS-T at a concentration of 0.5 µM. The arrays were incubated overnight at 4 ºC with gentle agitation. Negative control arrays were performed using 1 % Milk (Marvel) in TBS-T in place of the protein of interest. Arrays were washed three times with TBS-T for 10 minutes. Any interaction between the spots and the overlaid protein was detected using an appropriate specific primary antibody against the overlaid protein (Table 3). Arrays were incubated at room temperature for 2 – 4 hours with gentle agitation and washed as previously described. Arrays were incubated in the appropriate

secondary antibody conjugated to horseradish peroxides (HRP) (Table 4) for 1 hour at room temperature with gentle shaking before they were imaged by ECL.

2.10 PDE Activity Assay

To investigate the activity of PDE4A4/5 when in complex with POPDC1, a radioactive assay of cAMP hydrolysis was performed using the method outlined by Marchmont and Houslay (1980) (Marchmont and Houslay, 1980). Samples were first incubated with an 8-[^{3}H]-labelled cAMP substrate which when hydrolysed by the PDE becomes [^{3}H]-5'-AMP. Snake venom (*Ophiophagus* Hannah) is utilised to hydrolyse the [^{3}H]-5'-AMP to [^{3}H]-adenosine. The unhydrolyzed cAMP is separated from the adenosine using an exchange resin which binds the 8-[^{3}H]-cAMP as it is negatively charged. The level of [^{3}H]-adenosine is measured by scintillation counting to establish the rate of cAMP hydrolysis.

2.10.1 Preparation of Dowex anion exchange resin

Dowex anion exchange resin was activated by immersing 100g in 1L 1 M NaOH and subjected to constant stirring for 20 minutes. The resin is allowed to settle and then washed extensively with dH_2O until reaching pH 9.0. The washing solution was removed, and the resin was mixed into 1L 1 M HCl for 15 minutes. Again, the resin was washed with dH_2o until the pH was brought up to pH 3.0. The Dowex anion resin was resuspended in an equal volume of dH_2O and stored at 4^{o}C until use. A 1:1:1Dowex:100% ethanol:dH_2O mixture was prepared immediately before use in the assay.

2.10.2 Preparation of Purified Recombinant Proteins

To carry out the PDE activity assay purified recombinant POPDC1-GST tagged and PDE4A4-MBP tagged were produced following the protocols outlined in section 2.6.2 and 2.6.3. For the optimization step and for the experimental assays, PDE4A4-MBP was used at 10 µg/ml. POPDC1-GST was used at increasing concentrations from 10 µg/ml to 50 µg/ml. All samples were diluted in KHEM buffer (50 mM KCl, 50 mM HEPES pH7.2, 10mM EGTA, 1.9 mM $MgCl_2$, supplemented with protease and phosphatase inhibitors).

2.10.3 PDE Assay protocol

All measurements used from this assay were performed in triplicate and carried out at 4 ^{o}C unless specified otherwise. The assay substrate solution was prepared by adding 2 µl of 1 mM cAMP and 3 µl of 8-[^{3}H]-cAMP per ml of PDE assay buffer (20 mM Tris-HCl pH7.4; 10mM $MgCl_2$) giving a final concentration of 2 µM and 3 µCi/ml respectively.

The required amount of protein, noted in section 2.10.2, was diluted in buffer A (20 mM tris-HCl, pH 7.4) to give a total final volume of 50 µl. Pilot studies were performed by adding increasing protein concentrations to give an activity result in the linear range (6000-15000 cpm) which gives the optimal protein concentration required for the assay. When testing the PDE4 inhibitor rolipram, buffer A was added to give a total volume of 40 µl and 10 µl of inhibitor at concentrations of 0.5 µM to 10 mM. The control for the assay to test the effect of POPDC1 addition on PDE activity was the replacement of POPDC1-GST with GST alone. This was to ensure that there was no effect being caused by the tag. For the inhibitor assay, POPDC1-GST was again replaced with GST alone and treated in the same way as the experimental sample and for no inhibitor controls, an equal volume of DMSO was added. 50 µl of the premade substrate mix was added to all tubes including the controls to give a final volume of 100 µl. Samples were vortexed and incubated at 30 ^{o}C for 10 minutes before boiling in a heat block for 2 minutes to quench the reaction through the inactivation of PDE4A4-MBP.

Samples were cooled on ice for 15 minutes prior to 25 µl of 1 mg/ml snake venom being added to each tube. Samples were mixed and incubated for 10 minutes at 30 ^{o}C. This step is to allow the conversion of the MP to adenosine. To bind any negatively charged unhydrolyzed cAMP, 400 µl DOWEX anion exchange resin was added per tube and samples were incubated on ice for 15 minutes with brief vortexing every 5 minutes. The resin was pelleted by centrifugation at 16000 x g for 3 minutes before 150 µl of each supernatant was combined with 1 ml of Fluro SAFE1 scintillation in a fresh Eppendorf. To calculate total counts per minute, two tubes were prepared using 50 µl substrate solution and scintillant. Tubes were vortexed thoroughly before being measured through scintillation counting (Wallac 1409 Liquid Scintillation Counter, PerkinElmer). Counting

assessed the levels of remaining 8-[^{3}H]-adenosine in the supernatant, which is proportional to the levels of cAMP that have been hydrolysed.

2.10.4 Calculation of PDE activity

The cAMP hydrolysing capacity of the PDE was calculated using the following formula:

$$\text{PDE activity} = \frac{2.61\ x\ \frac{(Av\ C - Av\ B)}{Av\ S} x\ N\ x\ 10^{12}\ x \frac{1000}{P}}{t}$$

Where:
A = Specific activity of the PDE (ρmole cAMP hydrolysed / min / mg protein
Av C = Average of 3 repeats of sample value (cpm)
Av B = Average of 3 repeats of blank value (cpm)
Av S = Average of 3 repeats of the standard value (cpm)
N = Amount of cAMP in the substrate mix (moles)
P = Amount of protein added (µg)
t = time (min)
2.61 corrects for the use of 150 µl of supernatant from the Dowex as the total volume of the supernatant was 391.5 µl.

Dose response curves were calculated using GraphPad Prism 6.

2.11 Microscopy Techniques

2.11.1 Immunocytochemical staining

HEK293 cells or primary neonatal rat ventricular myocytes were seeded onto sterile glass coverslips in 6 well plates and transfected using the method outlined in section 2.3.5. After 24-hour incubation on coverslips cells were fixed using 4% (w/v) Paraformaldehyde for 1 hour at room temperature with gentle agitation. Coverslips were then washed 3 times for 10 minutes with PBS and blocked for 1 hour at room temperature with blocking buffer (PBS supplemented with 0.5% BSA and 0.25% Triton X-100). Primary antibodies were added at a 1:500 or 1:1000 dilution in blocking buffer to the coverslips and incubated

overnight at 4^{oC} in a humidity chamber (Table 3). Coverslips were washed 3 times with PBS for 30 minutes each time. Alexa-Fluor secondary antibody was added to coverslips and incubated for 1 hour at room temperature in a humidity chamber. Cells are then washed a further 3 times as before. DAPI nuclear staining in mounting media was added to a glass slide and the coverslips were mounted face down and allowed to dry overnight in the dark. Imaging was performed using a Zeiss Pascal laser-scanning confocal microscope (LSM) 510 Meta. Images were acquired with Zeiss LSM Image Examiner and analysed on ImageJ.

2.11.2 Proximity Ligation Assay

To visualise protein-protein interactions in both endogenously and overexpressing cells *in situ,* Duolink® proximity ligation assay (PLA) was employed using the manufactures protocol. Briefly, cells were fixed, permeabilised and incubated with primary antibodies as outlined in section 2.11.1. Cells were incubated in a humidity chamber with PLA probes, which are secondary antibodies tagged with oligonucleotides, specific to the primary antibodies. Coverslips were washed in wash buffer provided before incubation with the ligase enzyme for 30 minutes. The ligase enzyme functions to hybridise the oligonucleotides only if they are in close proximity (> 40 nm) from each other. A further wash was performed before the coverslips were incubated with the polymerase enzyme for 100 minutes at 37 ºC in a humidity chamber allowing for the rolling circle amplification. The signal can then be detected as small red dots by microscopy outline previously.

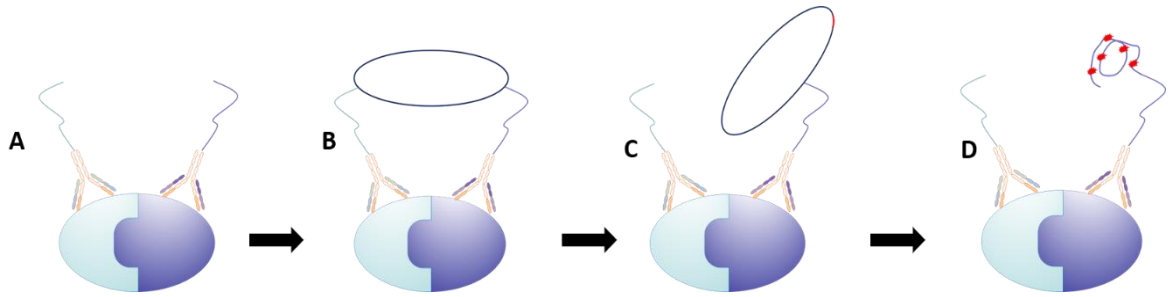

Figure 2.1 Schematic diagram Proximity Ligation Assay (PLA). **A** Cells are incubated with primary antibodies against the target proteins which are raised in two different host species. A set of PLA probes (PLUS and MINUS), which are bound to an oligonucleotide, recognising the host species are then applied. **B** If the proteins are in close proximity, the DNA strands from the opposing PLA probes can interact and are ligated together through a ligation reaction. **C** Rolling circle amplification is carried out through the addition of a DNA polymerase enzyme. **D** Cells are

then incubated with fluorescent probes to detect the DNA product of the amplification step, allowing for the visualisation of any interaction by confocal microscopy.

2.11.3 Fluorescence Resonance Energy Transfer

Fluorescence Resonance Energy Transfer (FRET) was utilised to monitor cAMP dynamics in live cells (Nikolaev and Lohse, 2006). Briefly, FRET describes the process by which there is the transfer of energy from a donor to an acceptor fluorophore. The donor then becomes excited by a particular wavelength it emits fluorescence at a characteristic wavelength. Interestingly, when the donor and acceptor are in close proximity their emissions spectrum overlap and the characteristic emission of the acceptor can be detected.

2.11.3.1 FRET probes

Given the lack of POPDC1/PDE4A bimolecular probes, the bimolecular sensors used within this work exploited the identified interaction between POPDC1 and TREK1. The POPDC1 sensor is fused to a CFP, donor, moiety while TREK1 is fused to the acceptor, YFP (Froese et al., 2012). In conditions of low cAMP these two fluorophores come into close proximity due to the interaction between POPDC1 and TREK1, so efficient transfer of energy from the donor to acceptor can occur leading to YFP's characteristic emission being detected and the decrease in the CFP emission. However, when the cellular concentration of cAMP is increased, cAMP can bind to POPDC1 causing a conformational change therefore increasing the distance between the donor and acceptor stopping the transfer of energy. This results in the CFP's characteristic emission being detected. Imaging records the ratio of donor to acceptor emissions in response to varying levels of cAMP.

Sensors used within this work were those produced and trialled by Froese and colleagues (Froese et al., 2012).

2.11.3.2 FRET Imaging

HEK293 cells were plated on sterilised 24 mm coverslips (VWR) at a low density to allow for single cells to be measured and clear background regions were

available to record. Transient transfections with FRET sensors were carried out 48hour prior to imaging according to previous protocols (Froese et al., 2012).

The coverslip was carefully removed from the culturing dish with watchmaker's forceps and inserted into a metal ring and sealed securely. Coverslips are washed three times with FRET saline (125 mM NaCl, 5 mM KCl, 1 mM Na_3PO_4, 1 mM $MgSO_4$, 20 mM HEPES, 5.5 mM glucose, 1 mM $CaCl_2$, pH7.4). A 300 µL bath of FRET saline was applied preventing the cells from drying out. The cells were then visualised on an Olympus IX71 Inverted Microscope under 40x or 60x immersion lenses (Zeiss). Image acquisitions were initiated, and real time measurements were taken. Stimulation with the AC activator, 25 µM forskolin or inhibition by 10 µM rolipram was carried out by diluting the drug in 300 µL FRET saline to allow for total dispersion. For later experiments, cells were treated with; 10 mM scrambled peptide, 10 mM disruptor peptide or DMSO, 2 hours prior to imaging.

Static measurements were taken in 5 second intervals for a total of 300 seconds to reduce the effects of photobleaching. A beam splitter was used to separate CFP and YFP so that images could be used to obtain a ratio of CFP to YFP in defined areas which had been drawn around single cells as well as clear background. The images were converted to mean intensity values allowing for ratios to be calculated. These ratios were used to determine the change in interaction between POPDC1 and TREK1 in various conditions.

2.12 *In Vitro* SUMOylation assay

To investigate whether proteins of interest were subjected to the posttranslational modification of SUMOylations, the predicted protein was subjected to an *in vitro* SUMOylation kit (Enzo). This kit provides the essential components of the SUMOylation pathway including SUMO activating enzyme (E1), UBC9 (SUMO E2), SUMO enzyme solutions (SUMO1, SUMO2, SUMO3), buffer, MgATP, and dH_2O. All samples were prepared on ice and the protocol was carried out using manufacturer's instructions. Reactions were carried out at 30^{o}C for 30 minutes with constant agitation. Samples were examined via SDS-PAGE and Western blotting. To determine successful SUMOylation, BVES/POPDC1 specific primary antibody (Santa Cruz) (Table3) was used to detect a band shift.

An appropriate fluorescent secondary antibody (Table 4) was used, and membranes were visualised using the Odyssey Infrared Imaging System (LI-COR Biosciences, UK) for fluorescence detection of the secondary antibodies. Fluorescence signal intensity is quantified using the Odyssey application software (LI-COR Biosciences, UK).

2.12.1 *In Vitro* SUMOylation assay using peptide array

Despite being developed for use on target proteins within either endogenously expressing or overexpressing cell lysate, the *in vitro* SUMOylation kit (Enzo) was used to overlay a peptide array containing full length or truncated POPDC1 sequence. Membrane or glass slide peptide arrays were initially bathed in ethanol then washed in TBS-T three times to remove any residual alcohol traces. Arrays were blocked in 5% BSA for one hour at room temperature before the total SUMOylation kit was added. SUMOylation kit components sufficient for 20 reactions (one entire kit) were combined and diluted to 1 mL with 5% BSA in TBS-T. Arrays were incubated at 30°C for 1 hour with gentle agitation. Following incubation, arrays were washed three times in TBS-T for 10 minutes each wash and incubated in SUMO1 primary antibody initially then reprobed with SUMO2/3 primary antibody to detect any bound SUMO protein (Table 3). The membranes were washed again and incubated in an appropriate HRP-conjugated secondary antibody (Table 4) before membranes were visualised using ECL and were imaged using the Bio-Rad Universal hood II (Bio-Rad). Images developed by both methods were quantified using Quantity One software (Bio-Rad). Antibody only control assays were carried out to ensure there was no unspecific binding.

2.13 *In Vitro* Phosphorylation Assays

To determine whether there was a phosphorylation site on POPDC1 or an effect on the phosphorylation status of the two proteins when they were interacting, and various *in vitro* phosphorylation assay was performed.

2.13.1 *In vitro* Phosphorylation of POPDC1

A range of purified POPDC1-GST concentrations from 0.5 µg to 2 µg was incubated with or without 100U of the PKA catalytic subunit (Abcam) in PKA phosphorylation buffer (20 mM Tris; pH7.5, 150 mM NaCl, 0.5 mM $MgCl_2$, 5 % Phosphoblocker, 0.5 mM DTT) supplemented with adenosine-5'-triphosphate (ATP) for 30 minutes at 37 ºC with constant shaking. The sample was subjected to SDS-PAGE and western blotted with a PKA substrate antibody (Sigma-Aldrich) (Table 3). An appropriate secondary antibody was used, and membranes were visualised using the Odyssey Infrared Imaging System (LI-COR Biosciences, UK) for fluorescence detection of the secondary antibodies (Table 4). Fluorescence signal intensity is quantified using the Odyssey application software (LI-COR Biosciences, UK).

2.13.2 *In vitro* Phosphorylation of POPDC1 peptide array

To identify sites of phosphorylation, the *in vitro* assay was utilised alongside peptide array technology. Full length and truncated POPDC1 sequence covalently linked to nitrocellulose membranes were overlaid with the same PKA buffer with or without the PKA catalytic subunit. Initially arrays were blocked with 5% PhosphoBlock for 1 hour at room temperature. Components of the assay were added, and membrane were incubated at 37ºC for 1 hour with gentle agitation. Detection was performed using a PKA substrate antibody (Sigma-Aldrich) primary and a Rabbit-HRP secondary. Membranes were visualised using ECL and were imaged using the Bio-Rad Universal hood II (Bio-Rad). Images developed by both methods were quantified using Quantity One software (Bio-Rad).

2.13.3 *In vitro* Phosphorylation of POPDC1 and PDE4A in Complex

To investigate the change in phosphorylation 1 µg of POPDC1-GST and 1 µg PDE4A4-MBP were incubated for 1 hour at 4 ºC with end-over-end rotation in order to allow time for binding. Following incubation, the samples were treated following the protocol in section 2.13.1.

2.14 Acyl-Rac for Palmitoylation status of proteins

Acyl-rac to determine palmitoylation status of target protein was carried out as described in (Forrester et al., 2011). Following the harvesting and incubation of NRVM (2.3.3), cells were washed with PBS and collected in 300 – 500 µL blocking buffer (100 mM HEPES, 1.0 mM EDTA, 2.5% SDS, 0.1 % MMTS, pH7.5). Lysed cells were incubated at 40 ^{o}C for 4 hours with shaking at 12000 rpm. Ice cold acetone was added at three times the volume of blocking buffer used, tubes were inverted several times and samples were incubated at -20 ^{o}C for 20 minutes to allow for the precipitation of proteins in the sample. Tubes were subjected to centrifugation at 14,000 x G for 5 minutes. The supernatant was removed, and the pellet was washed extensively with 70% ethanol and allowed to air dry. The pellet was resuspended in binding buffer (100 mM HEPES, 1.0 mM EDTA, 1% SDS, pH 7.5) and incubated at 40 ^{o}C with agitation for 1-2 hours. During this incubation step, 2M Hydroxylamine (NH_2OH) at pH 7.5 was prepared. Thiopropyl sepharose beads (Sigma T8387) were washed and allowed to equilibrate using binding buffer. 50 µL of beads and either 2M NH_2OH or 2M NaCl were added to each sample. Binding reactions were carried out on a rotator at room temperature for 3 hours. Immediately after addition of all components, 25 µL of the sample was removed and 2 x SDS supplemented with 50 mM DDT was added, samples were then stored at -20 ^{o}C. This constitutes the total input sample (labelled unfractionated in figures). After incubation, tubes were centrifuged for 3 minutes at 14,000 x g and supernatant was aspirated. Five quick resin washes were carried out using binding buffer where the buffer was removed immediately, then four further washes with 2-3-minute incubations were performed. 50 µL of 2 x SDS sample buffer supplemented with 100 mM DTT was added to each tube to elute the protein from the beads. Prior to running on SDS-PAGE, samples were heated at 60^{o}C for 10 minutes. Samples were centrifuged at 14,000 x G to settle the beads before samples were run. Western blot analysis using POPDC1 specific antibody (Santa Cruz) as well as Caveolin3 (Abcam) as a positive control (Table 3). Membranes were visualised using the Odyssey Infrared Imaging System (LI-COR Biosciences, UK) for fluorescence detection of the secondary antibodies (Table 4). Fluorescence signal intensity is quantified using the Odyssey application software (LI-COR Biosciences, UK). Constitutively

palmitoylated proteins were seen to be 5x enriched in the hydroxylamine bead samples in comparison to the total input (unfractionated) samples.

2.15 Statistical Analysis

All values presented in this work are presented as mean ± SEM from at least three experimental replicated, unless stated otherwise. Statistical significance was determined using paired or unpaired t-tests or, if there were more than two conditions within the collected data, a one-way analysis of variance (ANOVA) was employed. In cases where ANOVA was used, Tukey's post-hoc analysis was carried out. This allows for the comparison between the mean values of each group to the mean of every other group and is considered to be the best method of examining confidence intervals or if the sample sizes within the experiment are not equal. A p-value of >0.5 (*) was considered the threshold for significance, with $p<0.01$ (**) representing high significance and $p<0.001$ (***) being very high significance. All graphical representation was produced using GraphPad Prism™ 6.

3 Confirming the interaction between POPDC1 and PDE4A

3.1 Introduction

The POPDC family have been identified as the most recent category of cAMP effector proteins (Froese et al., 2012). All other cAMP effector protein groups form signalling complexes with PDEs to create compartmentalised, cAMP-driven signalling nodes that are localised throughout the cell. Although the components of many cAMP effector complexes have been identified, there has been no evidence to suggest that POPDC1 forms interactions with PDEs. One family of PDEs that is particularly important within the cardiovascular system is PDE4, which has been extensively shown to be crucial in the control of localised signalling underpinning several cardiac functions.

PDE4 activity has been shown to localise with the ryanodine receptor and the voltage-gated potassium channels in the heart. This interaction allows the control of the activation of PKA and subsequently the phosphorylation of key proteins involved in excitation-contraction coupling (Dodge et al., 2001, Terrenoire et al., 2009). There are multiple PDE4 isoforms found within heart however their non-redundant nature has been extensively illustrated (Richter et al., 2008, De Arcangelis et al., 2009a). In addition, the unique N-terminal region of the isoforms can lead to different localisation of the PDE4. PDE4A4/5 have been shown to localise to the ruffles at the cell periphery suggesting proximity to POPDC1 at the cell membrane (Beard et al., 1999, McPhee et al., 1999, O'Connell et al., 1996).The interaction of PDE4A5 with the SH3 domains of the Src family protein kinases was originally thought to be the main membrane targeting component of this isoform (O'Connell et al., 1996). However, deletion of the SH3 interaction site did not confer a total loss of protein targeting to the cell membrane (Huston et al., 2000a). Progressive deletion of the N-terminal later identified multiple sites within the noncatalytic portion of PDE4A5 that contributed towards its membrane localisation (Beard et al., 2002). This information led us to hypothesis that PDE4A4/5 would be a likely candidate for an interaction with POPDC1.

In cardiac myocytes, cAMP levels increase following β-adrenergic stimulation leading to the activation of cAMP effector proteins such as PKA, EPAC and cyclic-nucleotide gated ion channels. The orchestration of this signalling is underpinned by PDEs, which generate discrete and distinct pockets of cAMP that breach the threshold of activation for the cAMP effectors.

POPDC1 is known to possess many interaction partners. One of particular interest is its interaction with TREK1, the two-pore potassium channel (Froese et al., 2012). As previously mentioned, this interaction is modulated by the cellular levels of cAMP. At low basal levels, the proteins interact within the plasma membrane but at heightened cAMP concentrations e.g. after ß-adrenergic stimulation, the TREK1-POPDC1 complex disassembles. Interaction with POPDC1 led to a two-fold increase in the channel's current which was lost upon loss of binding (Froese et al., 2012). As this interaction is modulated by cAMP levels, it would seem appropriate that the signalosome would also contain a PDE to ensure inappropriate modulation of the TREK1-POPDC complex under basal conditions

3.2 Hypothesis and aims

Considering the information above, my hypothesis is that POPDC1 forms a signalling complex with a PDE4 to provide control over POPDC1's cAMP binding. I hypothesise that the interaction with a PDE4 will serve to function as a modulator of POPDC's interactions with other proteins such as TREK1. Currently, there is no evidence to suggest that such a complex exists.

The aims of this chapter are as follows:

- To determine whether PDE4 and POPDC1 exist in a signalling complex.
- To characterise the interaction of POPDC1 and PDE4 using proximity ligations assays, co-immunoprecipitations and pure protein interaction analysis
- To fine map areas of POPDC1-PDE4 binding via peptide array technology.
- To confirm that the POPDC1-PDE4 complex can be inhibited using cell-penetrating disruptor peptides based on the information gleaned from peptide array mapping.

3.3 Results

3.3.1 Localisation of POPDC1 and PDE4A

It is known that POPDC1 is localised at the plasma membrane, t-tubules, intercalated discs, caveolae, lateral membranes and more recently, the nuclear envelope and nucleoplasm (Froese et al., 2012, Schindler et al., 2012b, Alcalay et al., 2013, Schindler et al., 2012a). As such, we sought to identify whether PDE4A4/5 was found in the same compartment. PDE4A4/5 has previously been shown to localise to membranes (Huston et al., 2000a, Beard et al., 2002) and interact with a number of membrane partners such as the SRC family kinases (McPhee et al., 1999) and p75-NTR (Sachs et al., 2007), hence we hypothesised that it was a reasonable candidate to test for POPDC1 interactions.

Firstly, a cellular fractionation was performed using the model cell-line HEK293 cells transiently transfected with Popdc1-myc and PDE4A5-VSV constructs. Cells were lysed and separated into cytoplasmic, membrane and nuclear compartments. These fractions, and a whole cell lysate sample were run on SDS-PAGE and subjected to western blotting to detect levels of POPDC1 and PDE4A5 in each fragment. Confirmation of the fraction's purity was performed using Na^+/K^+ ATPase for the membrane fraction.

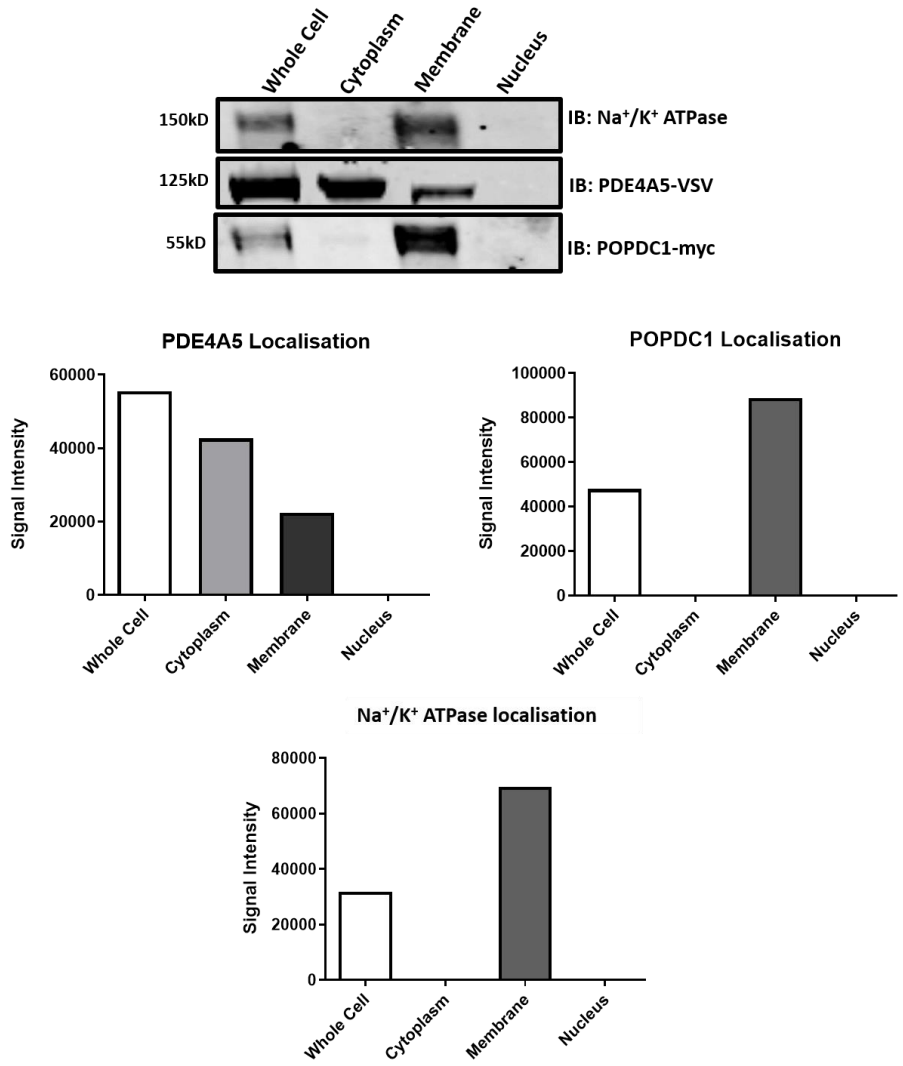

Figure 3.1 Subcellular fractionation of Popdc1 and PDE4A5 in transiently transfected HEK293 cells. HEK293 cells were transiently transfected with Popdc1-myc and PDE4A5-VSV before being subjected to subcellular fractionation outlined in Material and Methods. The resulting fractions were run using SDS-PAGE and blotted for MYC and VSV to determine the localisation of Popdc1 and PDE4A5 respectively. GAPDH was used to determine the purity of the cytoplasm fraction and Na^+/K^+ ATPase was used as a marker for the membrane fraction. Bands were quantified using ImageJ Studio and graphs produced in PRISM for comparison between fractions. Representative of an n=2.

As expected, the majority of Popdc1 was found in membrane fragment (Figure 3.1, upper panel and graph middle right). There was a larger proportion of PDE4A5 found in the cytoplasm compared to that of the membrane, however as previously published (Huston et al., 2000a, Beard et al., 2002), a "pool" of the phosphodiesterase was clearly visible in the membrane fraction (Figure 3.1, upper panel and graph middle left). The NA^+/K^+ ATPase is a solute pump that facilitates the transport of sodium out of the cell and potassium into the cell against a gradient concentration. It is found exclusively in the plasma membrane

(Matchkov and Krivoi, 2016). As such, it was used to confirm the validity of the fraction (Figure 3.1, upper panel and lower graph). The results indicate that transfected Popdc1 and PDE4A5 can both localise to membrane compartment providing evidence that the two may have the potential to interact at that location.

Furthermore, to examine whether endogenously expressed Popdc1 and PDE4A5, colocalise to the same compartment in a more physiologically relevant cell type, a further subcellular fractionation was carried out using neonatal rat ventricular myocytes (NRVM) (Figure 3.2).

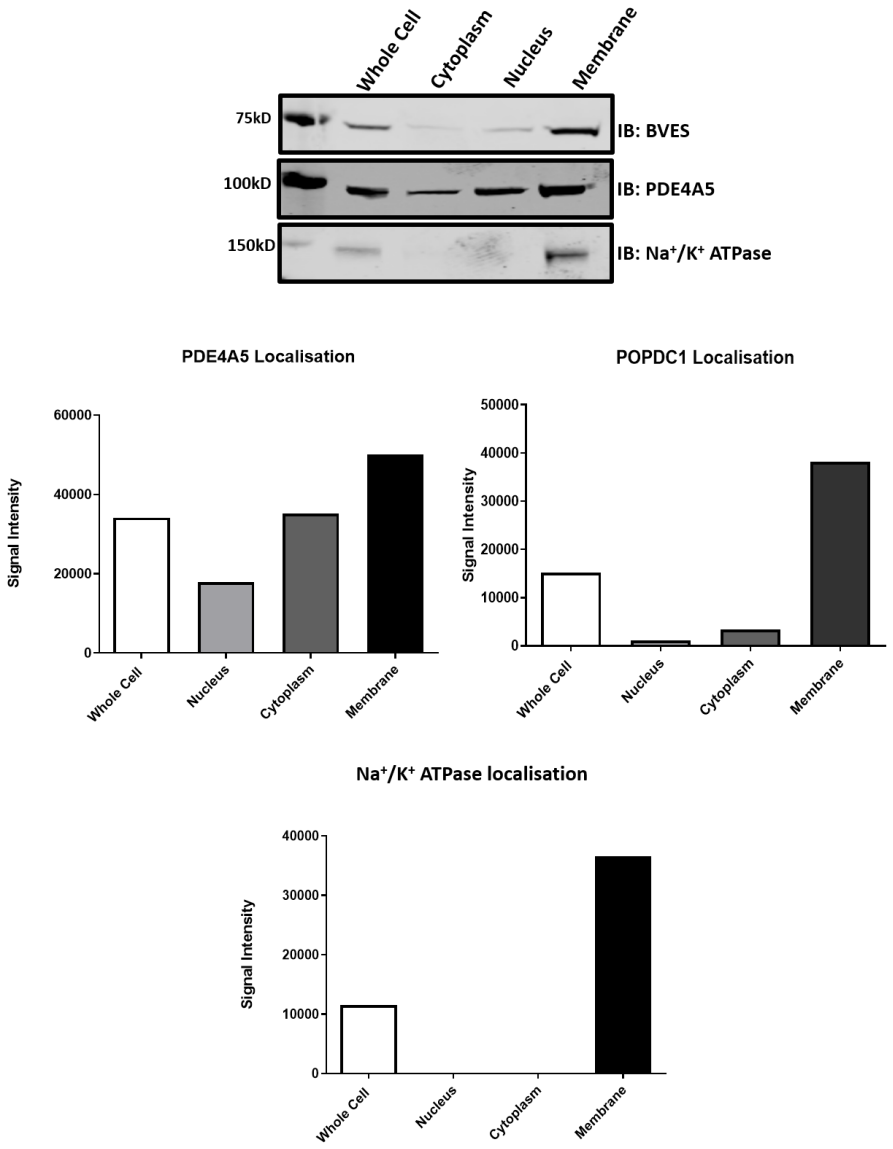

Figure 3.2: Subcellular Fractionation of Neonatal Rat Ventricular Myocytes. Neonatal rat ventricular myocytes were harvested after 2 hours incubation in M2 media. Samples were subjected to subcellular fractionation following the protocol outline in Material and Methods. Cells were fragmented to give cytoplasm, nucleus and membrane compartments. Samples were subjected to SDS-PAGE and Western blotted for Popdc1 and PDE4A5. To determine the purity of the fragment's Na^+/K^+ ATPase was used as a membrane marker. Quantification was performed using ImageJ and graphs were produced in Prism6 to allow for comparison. Representative of an n=2.

As in the transiently transfected HEK293 cells, Popdc1 was found to be predominantly at the membrane of the cell (Figure 3.2, upper panel and graph middle right). Small amounts of Popdc1 were found in both the cytoplasm and the nucleus, which supports the theory presented by Brand and colleagues that a small population of POPDC1 exists outside of the membrane e.g. in the nucleus (Schindler et al., 2012a). The Popdc1 distribution seen in Figure 3.2 may also be

due to carry over artefacts during the actual fractionation itself. PDE4A5 has a tighter membrane localisation in the ventricular myocytes than in the transfected cells (Figure 3.2, upper panel and graph middle left). Interestingly, a population of PDE4A5 was also found in the nucleus and this agrees with work that identifies the protein in the perinuclear space (Huston et al., 2000a). Once again, the fractionation protocol was validated by complete localisation of the Na^+/K^+ ATPase to the membrane fraction (Figure 3.2, upper panel and lower graph).

To support the data from produced by crude subcellular fractionation, immunofluorescence microscopy was undertaken in the same cells outlined above i.e. transiently transfected HEK293 cells and isolated NRVM. HEK293 cells were transfected with POPDC1-flag and PDE4A4-VSV constructs. After a 24hour transfection period, cells were subjected to the staining protocol outlined in the Material and methods section (2.3.5).

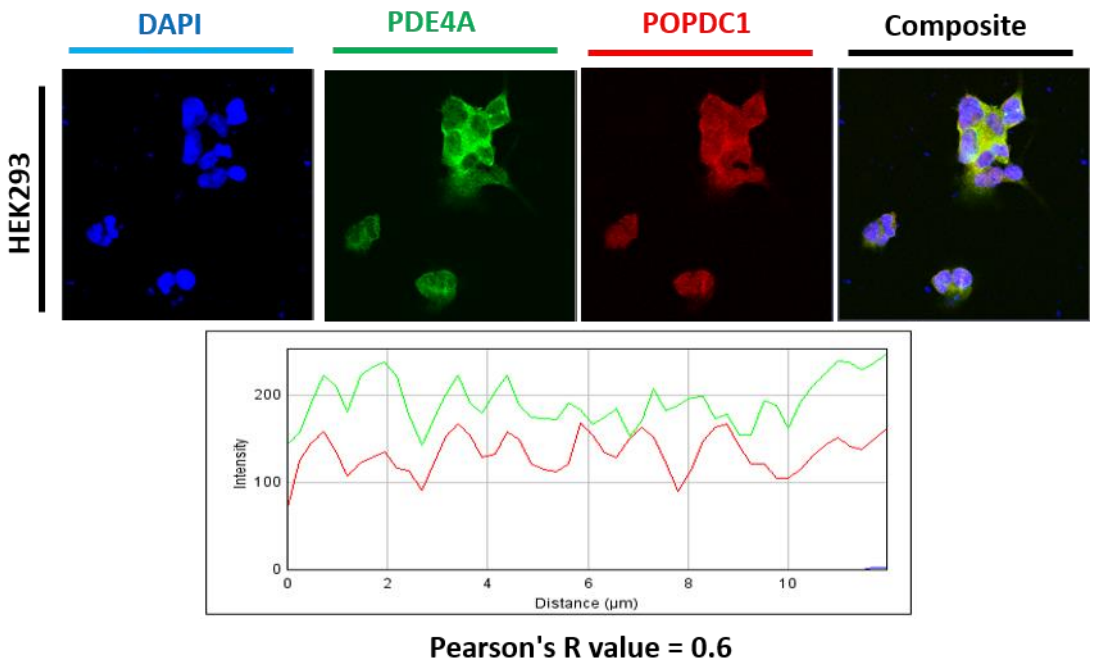

Figure 3.3: Immunofluorescence Microscopy using transfected HEK293 cells. HEK293 cells were transiently transfected with human POPDC1 tagged with FLAG and the human PDE4A4 isoform tagged with VSV. These transfected cells were incubated for 24 hours before being fixed and permeabilised allowing primary antibodies specific to the tag of the protein to be added. Samples were subjected to appropriate fluorescent secondary antibody. Cells were assayed for POPDC1 (red), PDE4A4 (green) and DAPI nuclear staining (blue). Images are representative of three different experiments. Images were taken using the Zeiss™ 5 LSM Confocal Microscope and analysed using Zeiss Image Studio including production of the intensity graph and Pearson's co-efficient. Experiment typical of n=15 cells.

From the images presented in Figure 3.3, POPDC1 seems to be localised to the plasma membrane and the cytoplasm (third upper panel). This is unsurprising as the protein is highly overexpressed and will fill unnatural positions. PDE4A4 appears to be localised mostly in the cytoplasm with some at the plasma membrane (second upper panel). As can be seen in the intensity plot (Figure 3.3, lower graph), POPDC1 (red) and PDE4A4 (green) follow similar peaks and patterns of intensity suggesting the possible co-localisation of the two proteins. Accompanied with a moderate Pearson's co-efficient of 0.60, the data indicates some co-localisation suggesting the possibility that POPDC1 and PDE4A4 interact.

Again, to determine if the same co-localisation was present in isolated primary heart cells, NRVMs were plated on coverslips before undergoing the same protocol as performed with transfected cells. Primary antibodies specific for Popdc1 and PDE4A5 were used with appropriate fluorescent secondary antibodies (Figure 3.4).

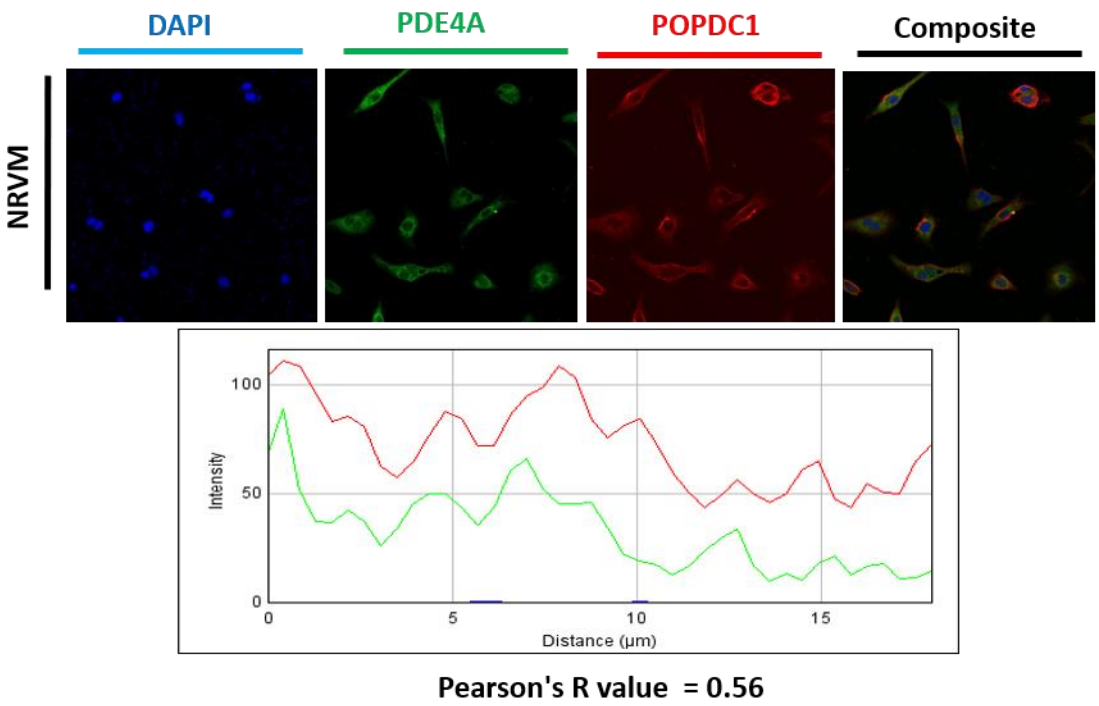

Figure 3.4: Immunofluorescent Microscopy using Rat Neonatal Ventricular Myocytes. Culture day 2 NRVM were blocked and permeabilised before staining with an isoform specific PDE4A5 antibody and a Popdc1 specific antibody. Appropriate immunofluorescent antibodies were used giving Popdc1 in the red channel and PDE4A5 in green with DAPI nuclear staining in blue. Images are representative of three different experiments. Images were taken using the Zeiss™ 5 LSM Confocal Microscope and analysed using Zeiss Image Studio including production of the intensity graph and Pearson's co-efficient. Images are representative of three different experiments. Experiment typical of n=15 cells.

As expected, the vast majority Popdc1 was found localised to the membrane of the cardiomyocytes (Figure 3.4, third upper panel) with PDE4A5 predominantly localised to the cytoplasm (Figure 3.4, second upper panel). The intensity plot (lower panel) shows that both POPDC1 and PDE4A5 follow the same intensity peaks and patterns in a similar fashion to the transfected proteins in Figure 3.3. This suggests that the two proteins, in their endogenous environment, could be co-localising. The Pearson's co-efficient is lower than produced by the overexpression confocal experiments. This was to be expected as both proteins are being overexpressed causing more localisation of the two. There is still a moderate Pearson's co-efficient value obtained again supporting the co-localisation of the Popdc1 and PDE4A5 and possible interaction.

3.3.2 Confirming the interaction between POPDC1 and PDE4A

As co-localisation studies suggest that pools of Popdc1 and PDE4A can exist in similar compartments, I undertook biochemical analysis to find out whether Popdc1 and PDE4A4/5 interact to form a signalling complex. Co-immunoprecipitations from lysate extracted from HEK293 cells overexpressing the putative partners were performed to see if an interaction could be detected. In the first instance, Popdc1 was immunoprecipitated using its myc tag via myc affinity resin. Control IPs were performed using Myc affinity resin and mock transfected HEK293 cells.

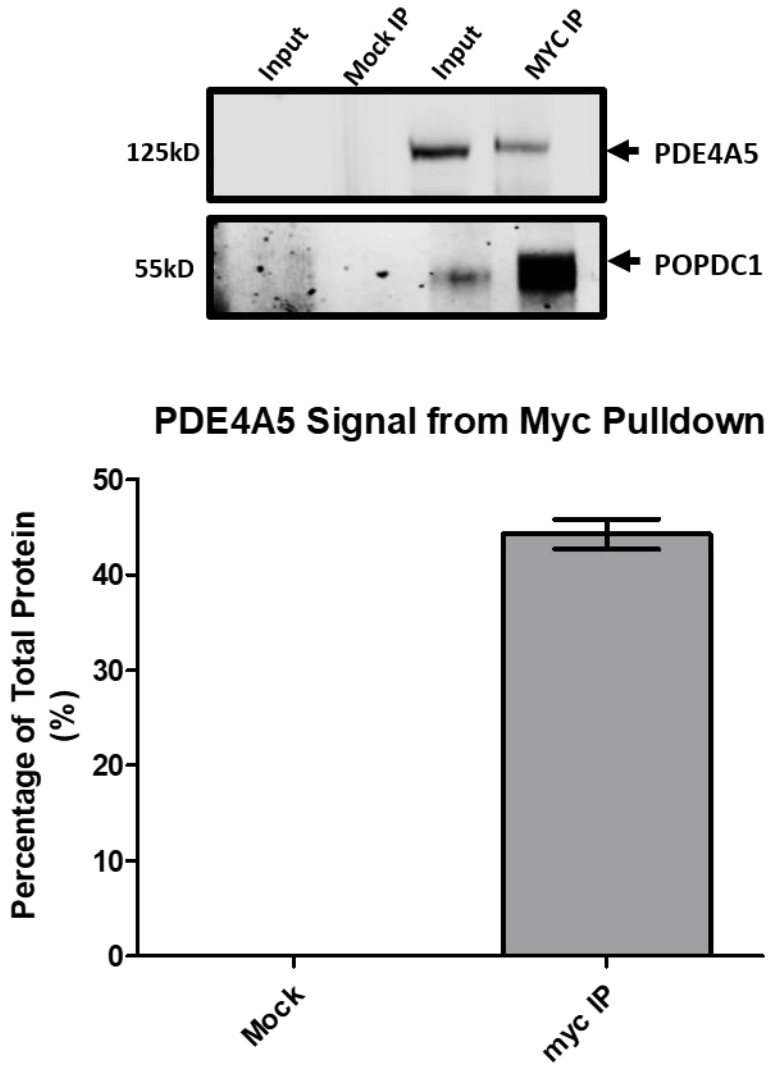

Figure 3.5: Co-Immunoprecipitation using co-transfected HEK293 cells. HEK293 cells co-expressing Popdc1 and PDE4A5 were set up for co-immunoprecipitation following the protocol outlined in the material and methods. Popdc1 was precipitated using myc affinity resin specific to the proteins tag. The samples were then western blotted for both myc to identify successful immunoprecipitation and VSV to identify PDE4A5. Image is a representative example from an n of 5 and presented as mean ± SEM. Intensities of bands were recorded using ImageJ and graphs were produced using GraphPad Prism 6.

Transfected PDE4A5-VSV was successfully co-immunoprecipitated with Popdc1s Myc tag pulldowns (Figure 3.5, upper panel, lane 4) suggesting existence of a Popdc1-PDE4A interaction. Control experiments were clear (Lanes 1 and 2 upper panel). The amounts of PDE4A5 being pulled down with Popdc1 seem low in comparison to the input levels (Figure 3.5, upper panel, lane 3 vs lane 4). This may provide evidence that the interaction between Popdc1 and PDE4A5 is a highly localised one that is small globally but is important locally at the membrane. To provide supporting evidence of this, reciprocal Co-IPs were performed using VSV antibody coupled to Protein G sepharose beads specifically

immunoprecipitating PDE4A5 by its tag (Figure 3.6). Again, HEK293 cells were transiently transfected with Popdc1-myc and PDE4A5-vsv constructs.

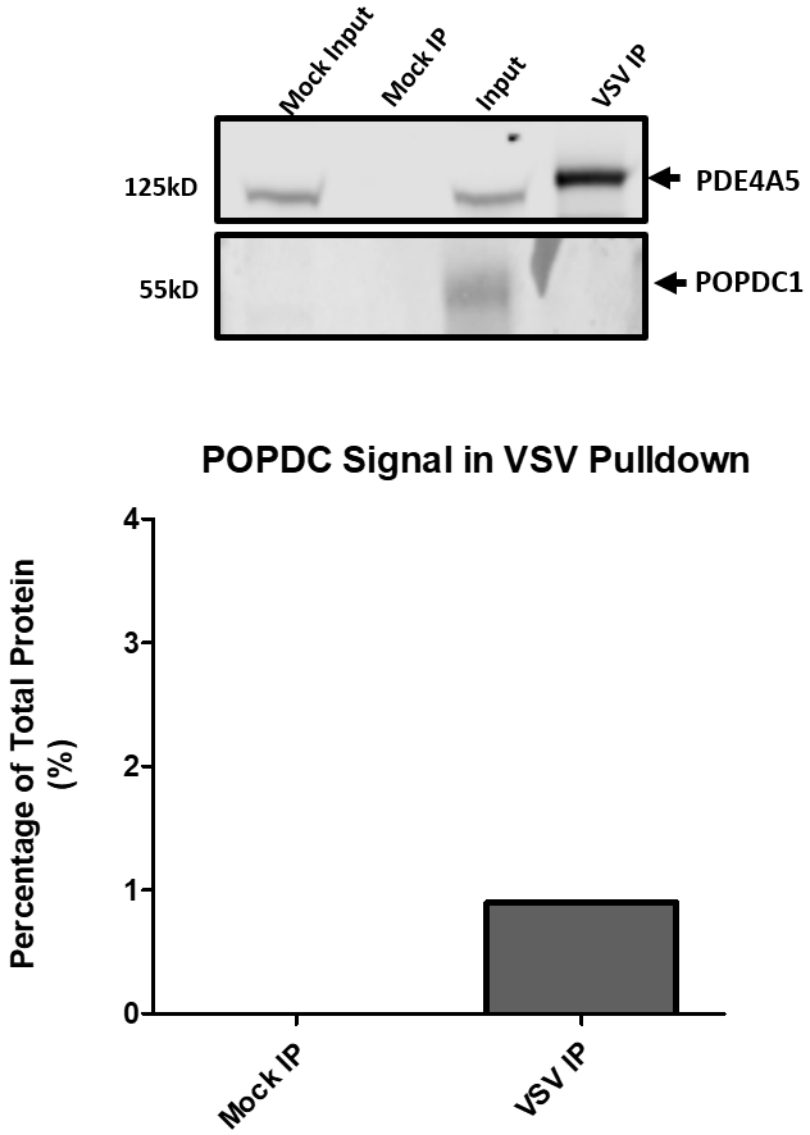

Figure 3.6 PDE4A5 Co-immunoprecipitations using transiently transfected HEK293 cells. HEK293 cells were transiently transfected with Popdc1-myc and PDE4A5-vsv for 24 hours before harvesting. PDE4A5 was precipitated using VSV antibody, specific to its tag, conjugated to Protein G sepharose beads. Samples were western blotted for myc corresponding to the tag on POPDC1 and VSV corresponding to the tag on PDE4A5.Graphs produced by GraphPad Prism 6^{TM}, mean ± SEM. Representative of n=3.

In contradiction to data shown in Figure 3.5, no Popdc1 pulled down with PDE4A5 (Figure 3.6, lower panel lane four). It is interesting that Popdc1 cannot be co-immunoprecipitated when precipitating PDE4A given the result of the opposing immunoprecipitation (Figure 3.5). This may be the result of several factors such as the tag of the PDE may be brought into a close proximity with

binding site of POPDC1 when the two proteins interact. Therefore, when the antibody specific to this tag is added there is a disruption of the interaction causing a loss of Popdc1 to be seen in the co-immunoprecipitation using PDE4A.

To determine whether the interaction of Popdc1 with a PDE4 was specific to PDE4A (Figure 3.5), isoform specific Co-IPs were carried out using two other long isoforms, PDE4B1 and PDE4D7 (Figure 3.7). These isoforms were selected as each contains both the UCR1 and UCR2 present in PDE4A5. Although the majority of the UCR domains sequence are conserved between the different isoforms there exists small distinct regions of differing amino acid residues. Transiently transfected HEK293 cells were incubated with G-sepharose beads and myc antibody as previously described.

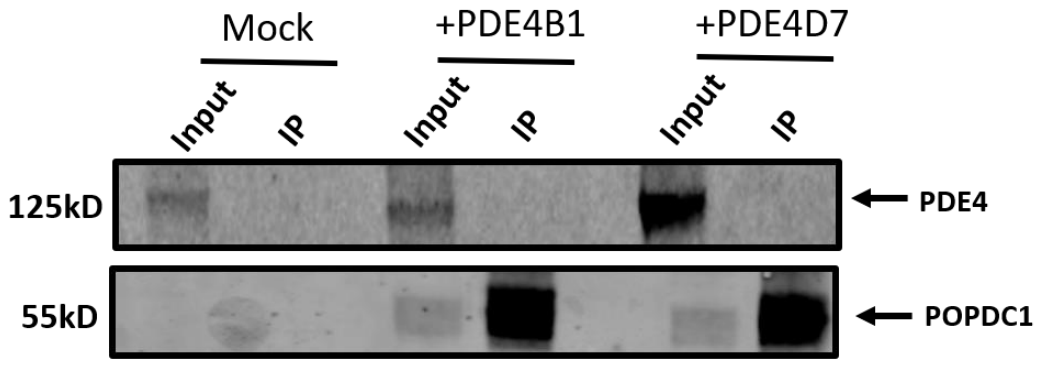

Figure 3.7: Co-Immunoprecipitations with long PDE4 isoforms to check for specificity. HEK293 cells were transfected with Popdc-myc accompanied by either PDE4B1-VSV and PDE4D7-VSV 24 hours prior to harvesting. Popdc1-myc was precipitated using myc antibody conjugated to Protein G Sepharose beads. Mock condition represents cells transfected with PDE4A5 with no Popdc1. Western blotting for VSV and Myc were used to identified presence of proteins in sample. Figures representative of an n=3.

Clear bands representing the protein at the correct molecular weight, 125kD, can be seen in the input lane showing that the proteins are being expressed in the lysate. When Popdc1 immunoprecipitates were blotted for VSV, allowing for the detection of the PDEs, there was no visible band at the relevant molecular weight (Figure 3.7, upper panel, lanes 4 and 6). Therefore, it was concluded that in transfected HEK293 cells Popdc1 interacts with PDE4A5 and not PDE4B1 and PDE4D7.

To recreate this finding in a more physiologically relevant cell type, co-immunoprecipitations were carried out in tandem with NRVM and adult rabbit septal cells (ARSM). In this case, POPDC1 (BVES) antibody-conjugated beads were used allow for the precipitation of the endogenous Popdc1. Popdc1 and PDE4A can be visualised in bands present at 100kD in the input lanes for both cell types (Figure 3.8A, lane one and B lane one). Clear immunopurification of Popdc1 was achieved from NRVMs (Figure 3.8A lane three) but this was not so clear in ARSM (Figure 3.8B, lane 3). Encouragingly, a clear co-immunopurification of Popdc1 and PDE4A could be detected from the NRVM lysate (Figure 3.8A, lane three). Conceptually, we envisage small amounts of the Popdc1-PDE4A complex that is highly localised in cells, so it was surprising to be able to detect this interaction using endogenously expressed proteins

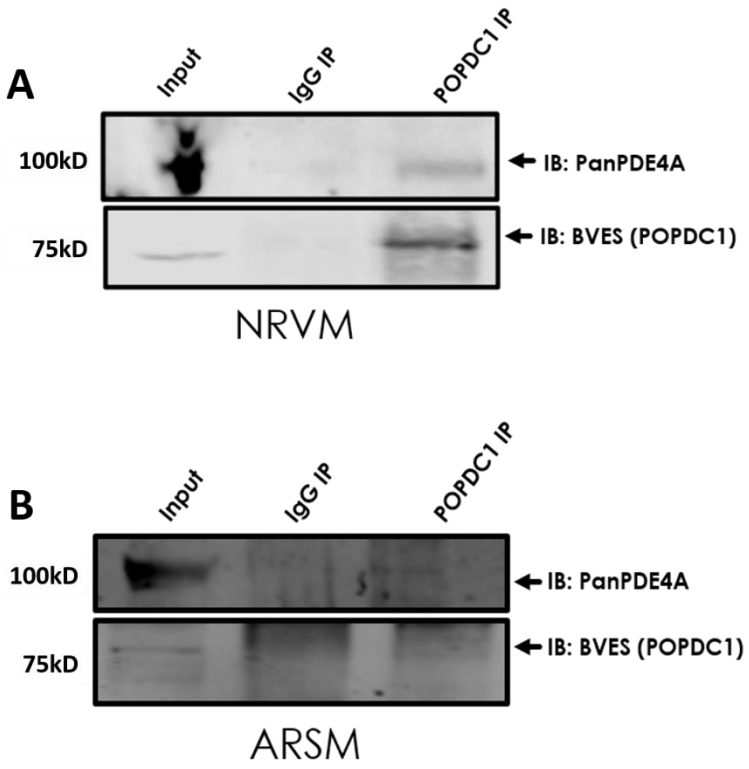

Figure 3.8: Endogenous Co-Immunoprecipitations in NRVM and ARSM. A NRVM were isolated from day 2 neonatal Sprague Dawley Rats. **B** ARSM were isolated from 12-week-old male New Zealand white rabbits. After culturing, cells were harvested and lysed using the protocol outlined in the material and methods. BVES-antibody conjugated to Protein G-sepharose beads were used to precipitate Popdc1 in both cases and the samples were western blotted for PDE4A using an isoform specific antibody. Control co-IPs were carried out using the same lysate sample with Protein G beads only. Arrows indicate the presence of Popdc1 and PDE4A. Image is a representative of an n of 3.

Following positive identification of the endogenous PDE4A-Popdc1 interaction, further biochemical and microscope-based assays were carried out to provide other forms of robust supporting evidence for the existence of signalosomes containing Popdc1 and PDE4A5. Proximity Ligation Assay (PLA) is a highly sensitive technique which can be used to detect protein-protein interactions *in situ* (Zatloukal et al., 2014). PLA was performed using ventricular myocytes from neonatal Sprague-Dawley rats (Figure 3.9). Briefly, ventricular myocytes were incubated with antibodies specific to Popdc1 and PDE4A5. Subsequently, cells were washed and incubated with appropriate PLA probes. If the proteins are within 40 nm of each other a rolling circle amplification occurs. This results in discrete red fluorescence signals when imaged (Söderberg et al., 2008, Bellucci et al., 2011). Wheat germ staining was performed to identify single cells through detection of the plasma membrane (Figure 3.9). Confocal microscopy was used to detect the fluorescent signal. This method is perfect to visualise the occurrence of Popdc1-PDE4A5 clusters via discrete fluorescent signal produced when the proteins interact (Figure 3.9).

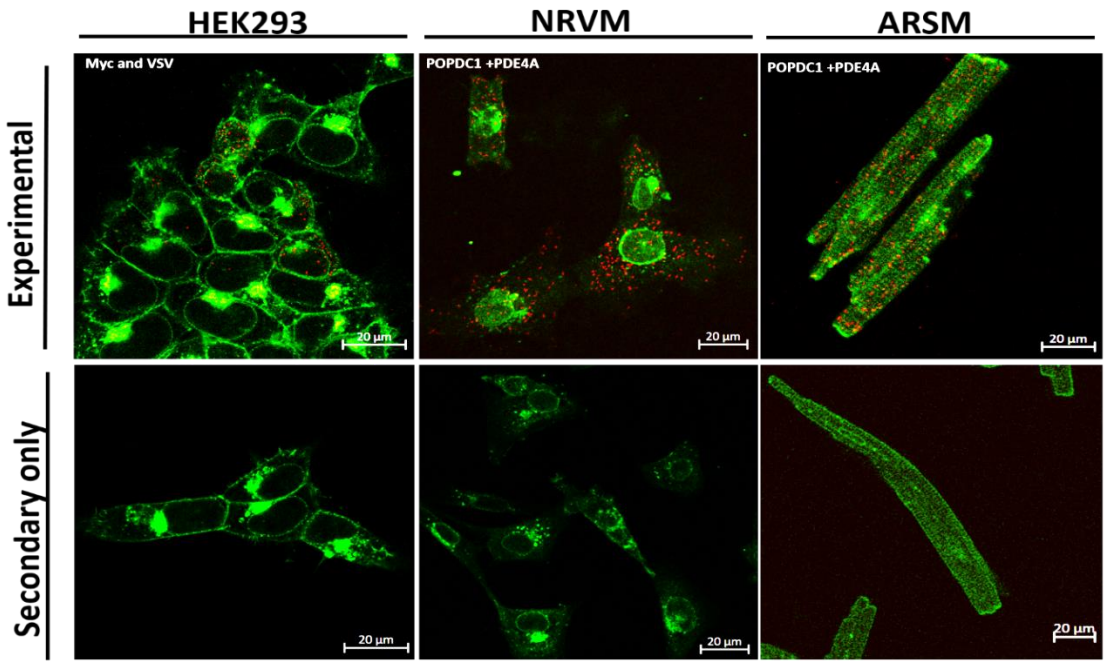

Figure 3.9: Proximity ligation assay using transfected HEK293, NRVM and ARSM. HEK293 cells were transfected with Popdc1 and PDE4A5 24 hours prior to fixing and PLA protocols being carried out. NRVM were fixed on day two after isolation and ARSM 4 hours after isolation. PLA in HEK293 cells was carried out using myc and VSV primary antibodies and using BVES (POPDC1) and PDE4A primary antibodies in NRVM and ARSM. Positive PLA signal is detected when the proteins tagged are less than 40nm apart. Negative controls were performed where the PLA kit was applied directly to the fixed cells to ensure no off-target staining. Cells were counterstained with wheat-germ agglutin (green) for membrane staining. Cells presented are representative of a n of 3 experiments. Scale bars shown represent 20µM.

Under basal conditions, as can be seen in Figure 3.9 (top three panels) Popdc1 and PDE4A form interactions (signified by red dots) in both transfected cells and isolated myocytes. Transfected HEK293 cells and endogenous NRVM seem to have PDE4A-Popdc1 interactions distributed throughout the cell whereas, in the ARSM there seems to be more localised signal to the membrane, t-tubules and intercalated discs. Such a result was expected as the intracellular structures of cardiomyocytes become more defined in adult cells. Samples of each cell type were incubated with secondary antibody to ensure no unspecific signals were being produced (Figure 3.9, lower panels). Results here have supported the notion that Popdc1-PDE4A interactions exist under basal conditions and these seem targeted to membrane structures in more mature myocytes.

As previously mentioned, multiple PDE isoforms contain the evolutionary conserved URC1 and UCR2 domains that are found in the PDE4A long isoform. To further determine that Popdc1 had specificity for PDE4A, PLA was carried out initially in HEK293 cells transfected with PDE4B1 and PDE4D7 as in Figure 3.7.

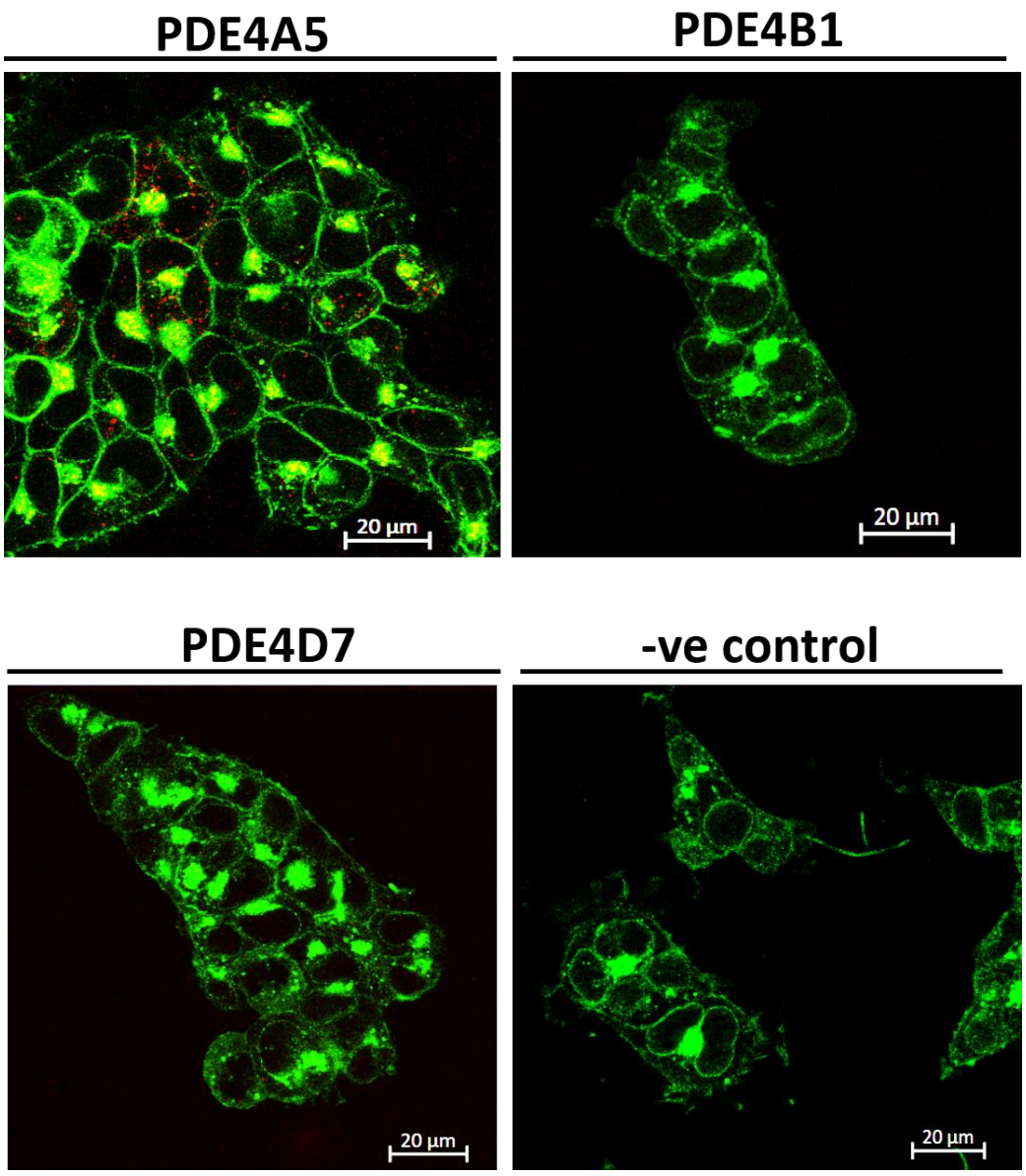

Figure 3.10: Analysing the PDE isoform specificity in transfected HEK293 cells. PLA was performed 24 hours post transfection. Myc primary antibody was used to detect Popdc1 and VSV primary antibody was used to detect all PDE4 isoforms. Positive PLA signal was identified by the presence of distinct and discrete red dots. PLA signal is only shown in cases where Popdc1 forms a complex with a PDE4. HEK293 were counterstained with wheat-germ agglutin (green) for membrane staining. Negative controls were performed where the PLA kit was applied directly to the fixed cells to ensure no off-target staining. Images represent and n=3 experiments containing at least 15 cells. Scale bars shown represent 20µM.

As can be seen in Figure 3.10, positive co-localisation can only be seen in cells transfected with Popdc1-myc and PDE4A5-VSV (Figure 3.10, left panel). Cells transfected with Popdc1 and either PDE4B1 (second panel) or PDE4D7 (third panel) showed no co-localisation. This data is in agreement with the specificity result seen in co-immunoprecipitations (Figure 3.7). Further confirmation that PDE4A is the preferred PDE4 partner for Popdc1 was obtained by evaluating the

possibility of endogenous interactions being formed between Popdc1 and PDE4A PDE4B and PDE4D in NRVMs. Again, red dots that signify Popdc1-PDE4 interactions were only observed in cells that were treated with Popdc1 and pan-PDE4A antibodies (Figure 3.11, left panel) whereas PanPDE4B and D primary antibodies (second and third panels) produced comparatively little signal (middle left and middle right panels).

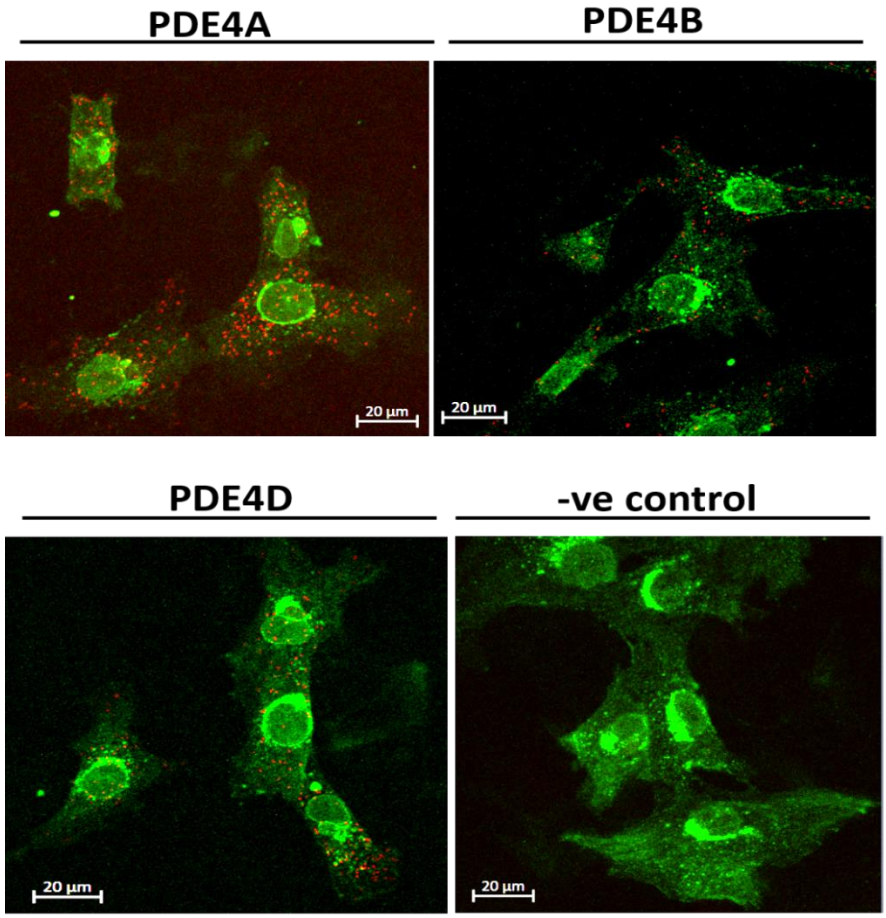

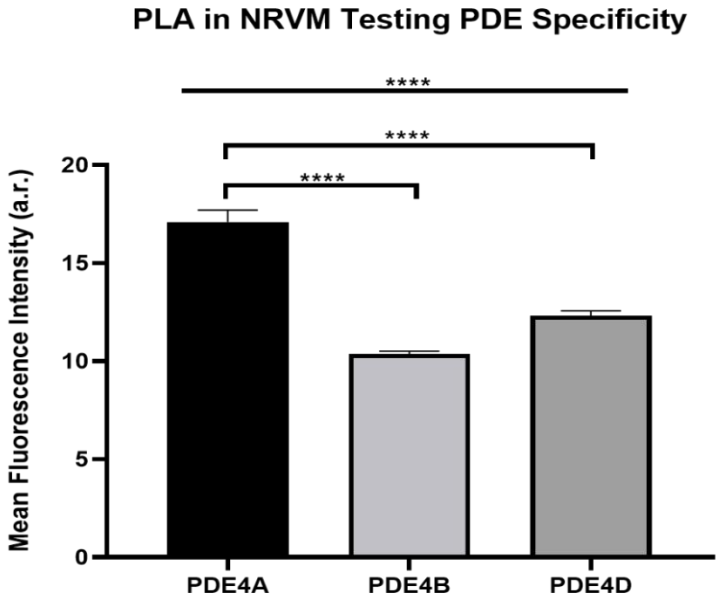

Figure 3.11: Analysis of the PDE isoform specificity in NRVM using PLA. NRVM were fixed two days after isolation. BVES (POPDC1) with either Pan PDE4A, PDE4B and PDE4D primary antibody were used in conjunction with the described PLA protocol. PLA signal (red) is only shown in cases where Popdc1 forms a complex with a PDE4. Cardiomyocytes were counterstained with wheat-germ agglutin (green) for membrane staining. Negative controls were performed where the PLA kit was applied directly to the fixed cells to ensure no off-target staining. One-way ANOVA statistics were performed using the intensity measurements taken from n=45 Popdc1 and PDE4A cells, n=27 Popdc1 and PDE4B cells, and n=40 Popdc1 and PDE4D cells. P<0.0001 value represented by ****. Scale bars shown represent 20µM.

From the experiments in Figure 3.11, the obviously strong and robust PLA signal between Popdc1 and PDE4A was expected, however the weaker signals between Popdc1 and PDE4B and PDE4D showed that the Popdc1 interaction may take place in regions that are common to all PDE4 long forms (Figure 3.11). To determine whether Popdc1 had a stronger binding to PDE4A in comparison to the others, a minimum of 27 cells were measured for intensity of PLA signal and a one-way ANOVA was performed (Figure 3.11, bar chart). This analysis revealed that Popdc1 did indeed have a more robust binding to PDE4A compared to the other two isoforms. The specificity for PDE4A, may in part be due to the membrane localisation of the PDE (Houslay, 1996) or differences in primary sequence.

3.3.3 Confirmation of the interaction using recombinant purified protein.

Co-immunoprecipitations using endogenous and overexpressing cell lysate provided support for the interaction between POPDC1 and PDE4A5. However, to determine if this interaction was direct or dependent upon other proteins, recombinant purified proteins were utilised for pull-down assays and far western techniques. Recombinant POPDC1 Popeye domain-HIS-GB1, kindly gifted by Professor Thomas Brand (Imperial College London, UK), was purified using the protocol outlined in (section 2.6.1). Briefly, the protein was purified using Ni-NTA resin. The resin bound protein was washed with buffer containing 10 mM imidazole. Elutions of the protein from the beads were performed using a linear gradient from 100 to 250 mM Imidazole. Two 500 µl fractions were collected from each imidazole concentration and analysed using western blotting or Coomassie staining (Figure 3.12). Successful purification of the Popeye domain-His-GB1 recombinant protein is seen by the band at 25kDa in the SDS-PAGE shown in Figure 3.12A and confirmed by immunoblotting targeting the His tag (Figure 3.12B).

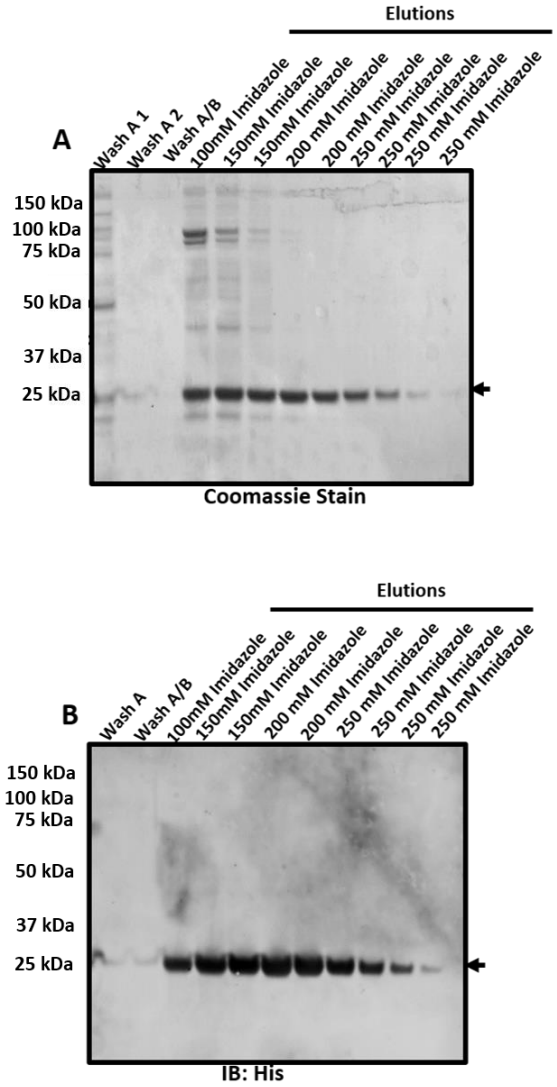

Figure 3.12: Recombinant Purified POPDC1 Popeye domain-His-GB1. Recombinant POPDC1 Popeye domain tagged with HIS and a solubility peptide GB1 was purified using the protocol outlined in the material and methods section. The protein was purified using Ni-NTA resin. The resin with bound protein was washed with buffer containing 10mM Imidazole and eluted in a linear gradient of 100mM to 25mM imidazole. Two 500 µl fractions were eluted using each concentration were collected. Eluted fractions were then analysed on 4-12 % SDS-PAGE gels and visualised using **A** Coomassie staining and **B** western blotted for HIS. The arrow indicated the successful purification of POPDC1-HIS-GB1.

To investigate whether POPDC1 was interacting with PDE4A4 directly, a co-immunoprecipitation was performed using purified recombinant POPDC1-HIS-GB1 and PDE4A4-MBP. Briefly, POPDC1-His-GB1 and PDE4A4-MBP were added in equal molar concentrations and incubated for 1 hour before the addition of Ni-NTA resin. After an hour incubation with the beads, samples were processed and run on SDS-PAGE prior to western blotting (Figure 3.13).

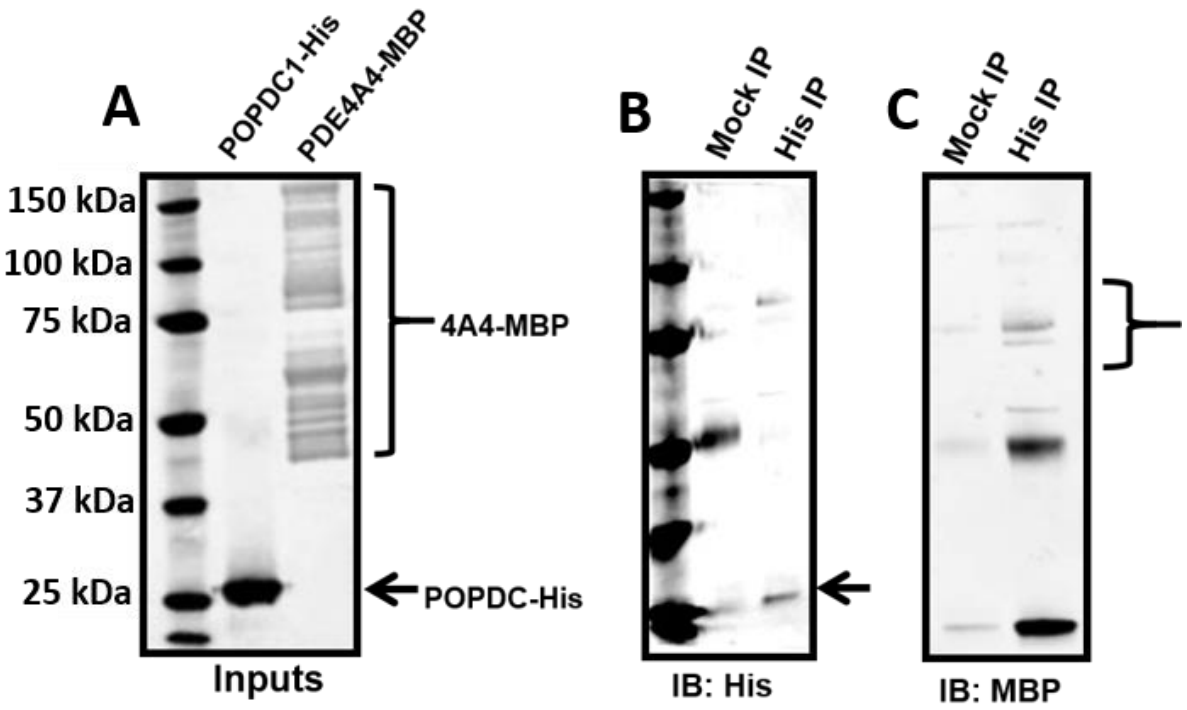

Figure 3.13: Recombinant protein co-immunoprecipitation. Recombinant purified Popeye domain from POPDC1-His and PDE4A4-MBP were incubated together. The Popeye domain of POPDC1 was used as bait to pull down PDE-4A4-MBP. Input samples for both proteins were run to confirm the protein was present in the sample (**A**). Samples were western blotted for both His to confirm pull down (**B**) and MBP to confirm interaction (**C**). Arrow indicated POPDC1 and bracket represents PDE4A4. Example is a representative example of an n of 3.

Purified Popeye domain of POPDC1-His was efficiently isolated (Figure 3.13, middle panel) and could directly pull down PDE4A4-MBP (see Figure 3.13, right panel) confirming direct interaction as well as indicating that the Popeye domain in POPDC1 is the region that binds to PDE4A. This data suggests that the two proteins may directly interact with each other *in vivo* and gives support to the hypothesis that PDE4A4 is responsible for shaping the cAMP gradient that the cAMP effector protein POPDC1 is exposed to.

Further biochemical assays were carried out to add supporting evidence to the notion that direct interaction between POPDC1 and PDE4A4 takes place. For these experiments the Popeye domain of POPDC1 Popeye domain tagged with GST was purified (Figure 3.14). Optimization of the induction process was carried out prior to large scale purification.

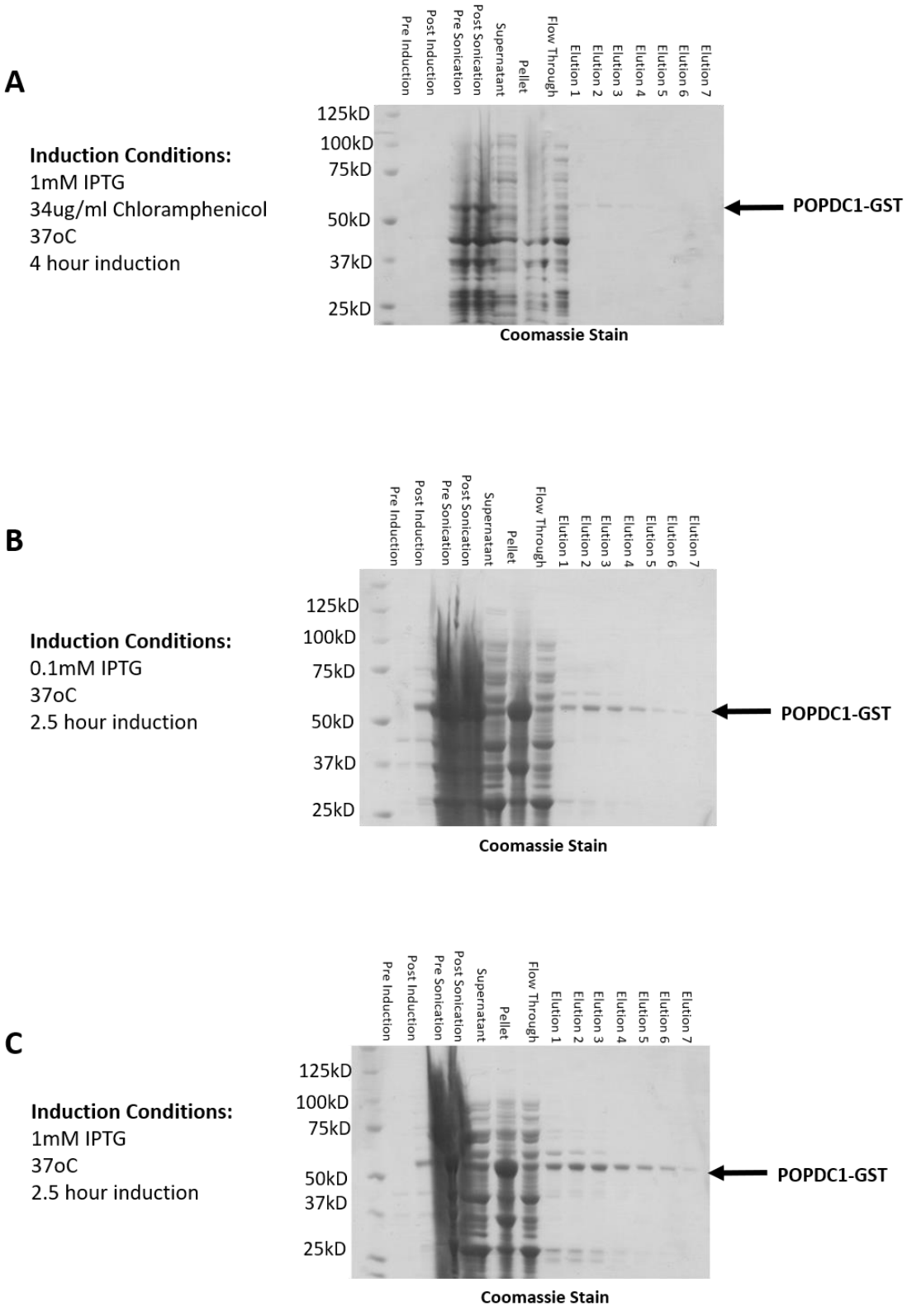

Figure 3.14: POPDC1 Popeye domain -GST optimised purification. To determine the optimal conditions for protein expression, a range of induction conditions were utilised using increasing concentrations of IPTG with or without chloramphenicol (conditions are noted next to each gel). Recombinant POPDC1 tagged with GST was purified using the protocol outlined in the material and methods section. Glutathione beads with affinity for the GST tag were used to capture POPDC1. POPDC1-GST was eluted from the beads using elution buffer containing reduced Glutathione. Arrow represents the correct molecular weight (55kD) therefore signalling expression of the protein.

As can be seen in Figure 3.14A-C (elution lanes 1-7), Popeye domain of POPDC1-GST was successfully purified in all growth conditions. However, optimal growth conditions were observed to be 1mM IPTG during a 2.5-hour incubation at 37 ºC given the presence of a stronger band at 55kD indicating purified POPDC1-GST (Figure 3.14C, elution lanes 1-7) in comparison to any of the other conditions. This information was used to produced recombinant purified POPDC1-GST required for further biochemical studies. To confirm the identity of POPDC1-GST, a western blot was performed immunoprobing for GST (Figure 3.15).

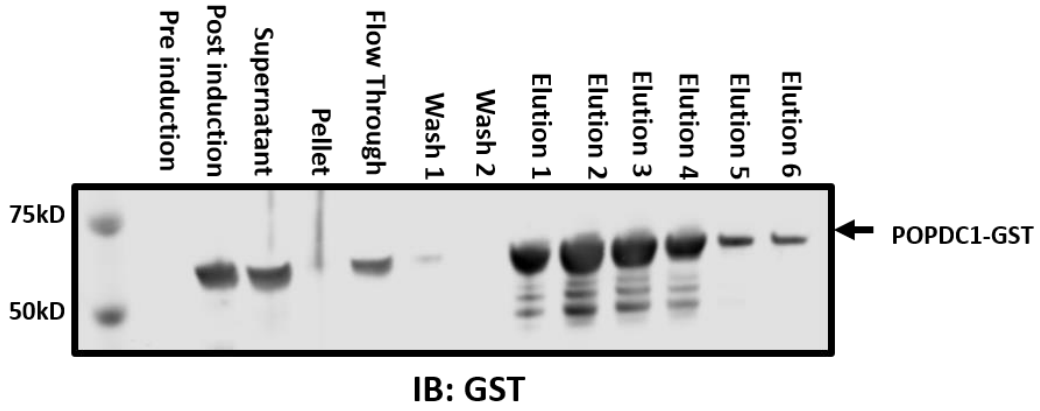

Figure 3.15: Purified Recombinant POPDC1 Popeye domain - GST conformation Western blot. Recombinant purified POPDC1 tagged with GST was run via SDS PAGE. Membranes were immunoblotted for GST corresponding to the tag on the recombinant POPDC1 Popeye domain. Arrow indicates the correct band seen at 55kDa.

Having correctly produced the POPDC1 Popeye domain tagged with GST, a far western was performed using the purified recombinant POPDC1 Popeye domain-GST and PDE4A4-MBP (Figure 3.16). POPDC1 Popeye domain-GST and positive control proteins, UBC9-GST (Houslay et al., 2017) and P75-Ntr-GST (Sachs et al., 2007) that have previous been shown to be PDE4A binders, were separated by SDS-PAGE before being western blotted for GST (Figure 3.16A, first panel), and MBP (Figure 3.16A, middle panel). These proteins are immobilised on nitrocellulose membranes and can act as bait for the PDE4A4 in a far western assay. As can be seen in Figure 3.16B, MBP-PDE4A4 binds directly to the immobilised bait proteins (POPDC1, UBC9 and P75-Ntr). Negative controls were carried out using RHE PfPdx1, a protein that can phosphorylate and active the Plasmodial PLP Synthase Complex (Figure 3.16 C and D). This was performed to ensure there was no unspecific binding of PDE4A4-MBP to proteins that were not

known to be interactors. As can be seen in Figure 3.16 D, there was no interaction between PDE4A4-MBP and RHE PfPdx1.

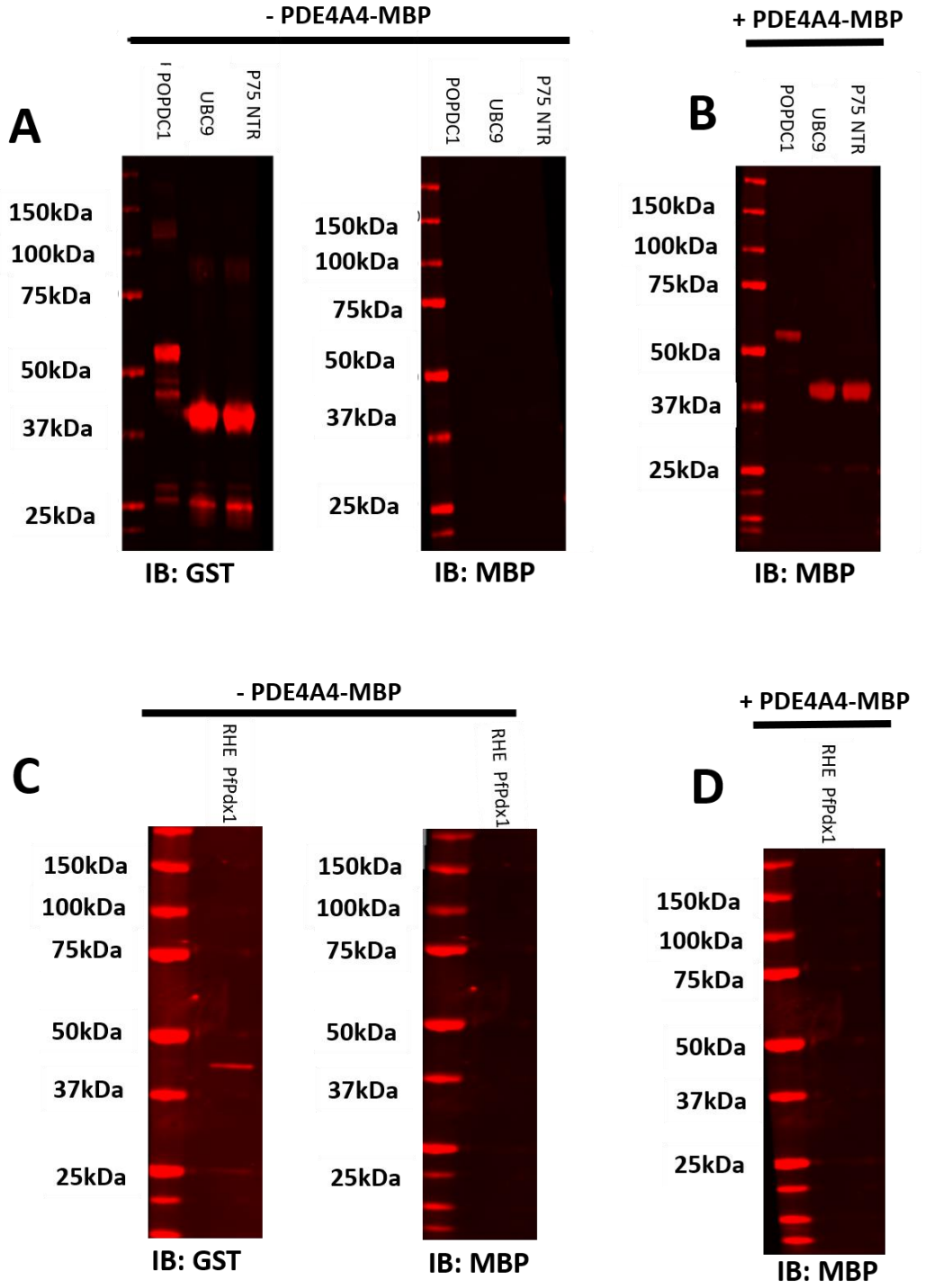

Figure 3.16: Far Western using Recombinant Purified Protein. A Purified Recombinant Popeye domain of POPDC1-GST, UBC9-GST and P75-Ntr -GST were separated by SDS-PAGE and western blotted for GST, to confirm successful transfer of the protein to the nitrocellulose membrane. Separate membranes were probed for MBP, the tag on the recombinant PDE4A4 protein. **B** This membrane was incubated with PDE4A4-MBP for 4 hours before being re-probed with MBP. **C** Negative controls were performed using RHE PfPdx1-GST. To confirm the presence of the protein on nitrocellulose membrane they were probed for GST, Separate membranes were probed for MBP to confirm there was no cross-reactivity. **D** This membrane was incubated with PDE4A4-MBP for 4 hours before immunoblotting for MBP.

Figure 3.16 shows the presence of bands at 55 kDa in the Popeye domain of POPDC1 lane and bands ~40 kDa in both the UBC9 and $P75^{NTR}$ lanes. This suggests that PDE4A4 is directly binding to these proteins without any other interacting proteins. P75 neurotrophin receptor ($P75^{NTR}$) belongs to the family of Tumour necrosis factor receptors (TNFR) and is a known interactor of PDE4A4 via binding to its unique C-terminal (Sachs et al., 2007).

Collectively the data presented so far in this chapter indicates that there is a robust, reproducible and novel interaction between POPDC1 and PDE4A4/5. This is a direct interaction that has been confirmed in binding experiments using overexpressed and endogenous proteins in cell lysates and with purified recombinant protein.

3.3.4 Mapping Binding Regions of PDE4A on POPDC1

In this chapter, POPDC1/Popdc1 has been shown to interact with PDE4A4/PDE4A5 in both HEK293 cells and NRVM (Figure 3.6 and Figure 3.8). A peptide array approach was employed to determine the essential residues for the interaction and effectively map binding sites on both proteins. A peptide library of POPDC1 sequence was synthesized onto cellulose membranes as described in section 2.9.2. Initially, overlapping 25mers covering the full POPDC1 sequence were synthesised. Arrays were incubated with cell lysate overexpressing PDE4A4-VSV, PDE4D9-VSV and an un-transfected lysate control prior to being probed with a VSV primary antibody (Figure 3.17). Chemiluminescence was used to identify sites of interaction. As this procedure is known to be semi-quantitative, intensity of the spot partially correlated to binding affinity, whereas no signal was detected when peptides were outside the binding motif. To ensure the detection was due to the binding of an interacting protein, an un-transfected cell lysate was used as a control. Representative regions of the full length POPDC1 arrays are shown that exhibited the greatest degree of interaction (Figure 3.17).

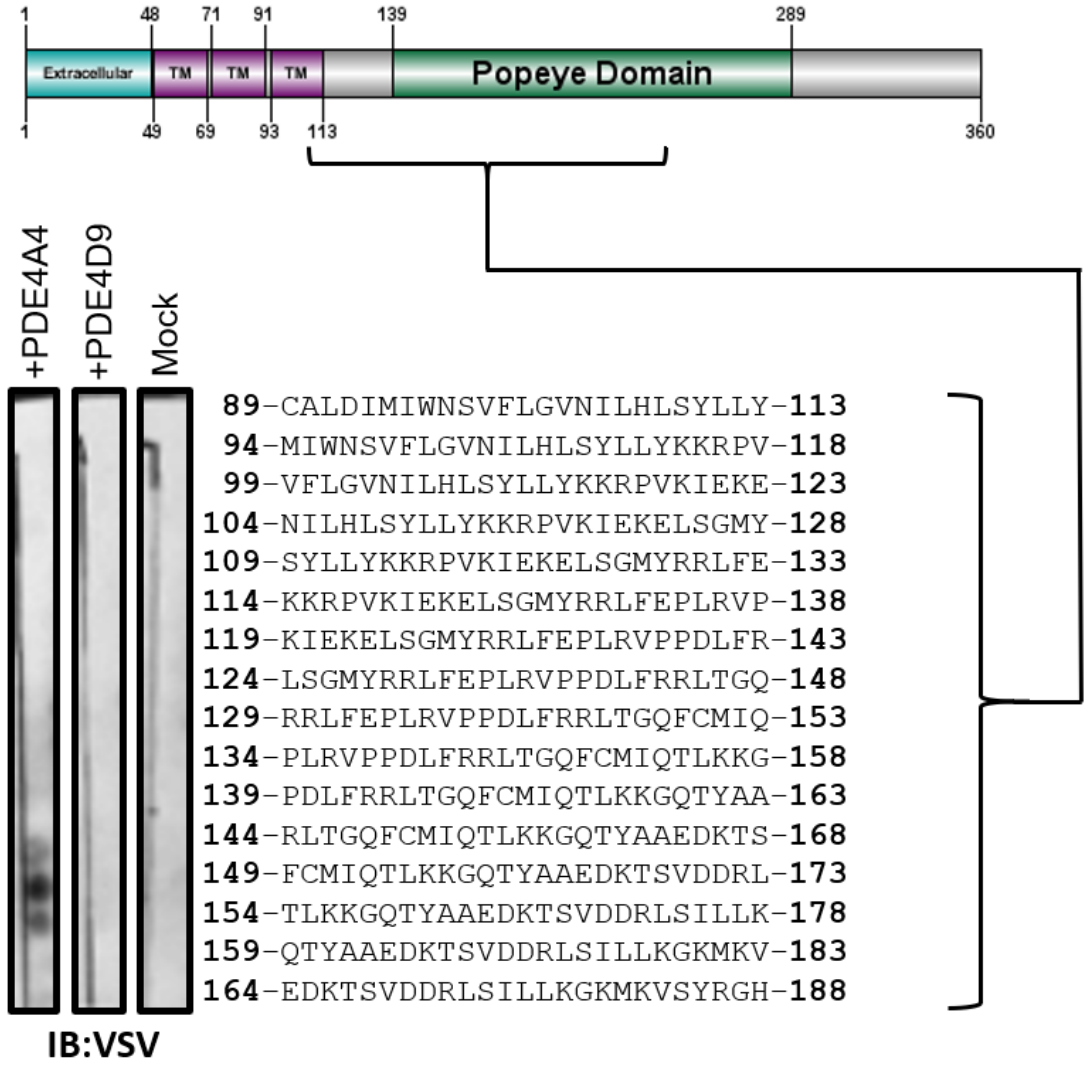

Figure 3.17: Peptide Array of Full Length POPDC1 overlaid with PDE4A4.
Overlapping 25mer peptides, offset by 5 amino acids, for the full-length sequence of POPDC1 were synthesised on cellulose membranes and probed with HEK293 lysate overexpressing VSV-tagged PDE4A4 (+PDE4A4, left panel), VSV-tagged PDE4D9 (+PDE4D9, middle panel) or untransfected HEK293 lysate (Mock, right panel). Binding of VSV-tagged protein to peptides was detected using anti-VSV antibody. The protein location and sequence of each peptide is shown to the right.

Binding of PDE4A (Figure 3.17, left panel) but not PDE4D9 (middle panel) to immobilised POPDC1 sequence was apparent and control experiments were clear (right panel). Interestingly, the binding site identified is housed within the Popeye domain of POPDC1 (see Figure 3.17). This site, according to predicted secondary structure, lies within two ß-sheets allowing it to be partially accessible to other proteins. To further narrow down the putative PDE4A4 binding site, a motif scan was carried out (Figure 3.18). Clearly, the motif RLSILLK (in red) is of relevance to the biding of PDE4A4 but not PDE4D9.

Within the sequence identified, lies a familial missense mutation, R172H, previously outlined by Professor Hendrik Milting's Lab in Bad Oyenhausen, Germany (Schindler, 2014). *POPDC1*^{R172H} is caused by a missense mutation leading to an arginine at position 172 being substituted for a histidine. Patients identified with this mutation present with dilative cardiomyopathy (DCM). *POPDC1*^{R172H} There was little to no difference found in the mutant POPDC1s affinity for cAMP or in its co-localisation with the potassium channel, TREK1 (Schindler, 2014). This may mean that the mutation leads to a decrease in PDE4A4s ability to bind to POPDC1 and therefore affects the controlled decrease of cAMP in the vicinity leading to aberrant interaction with TREK1.

Figure 3.18: Motif scan using peptide array of PDE4A4 binding site on POPDC1. 25mers containing the proposed binding site shifted by 5 amino residues at a time. Membranes were overlaid with HEK293 lysate overexpressing PDE4A4-VSV or PDE4D9-VSV. Mock transfected HEK293 lysate was used as a control. Red highlighted sequence identifies that of the familial mutation site and the crucial binding residues identified previously.

To elucidate crucial amino acid residues that were necessary for POPDC1 ability to bind to PDE4A4/5. A peptide array using alanine scanning of the identified binding site on POPDC1 was performed. Briefly, the 25mer sequence identified in Figure 3.17 was synthesized on cellulose membranes and sequentially each amino acid was substitute with alanine (A) (Figure 3.19A). Alanine possesses a chemically inert methyl side chain meaning that its substitution eliminated the endogenous residue while retaining much of the proteins structure. In the instance that alanine was the native amino acid in the sequence, aspartic acid (D) was used as substitution due to the residues negative charge. The membrane

was overlaid with PDE4A4-VSV overexpressing cell lysate following the protocol outlined in section 2.9.2.2.

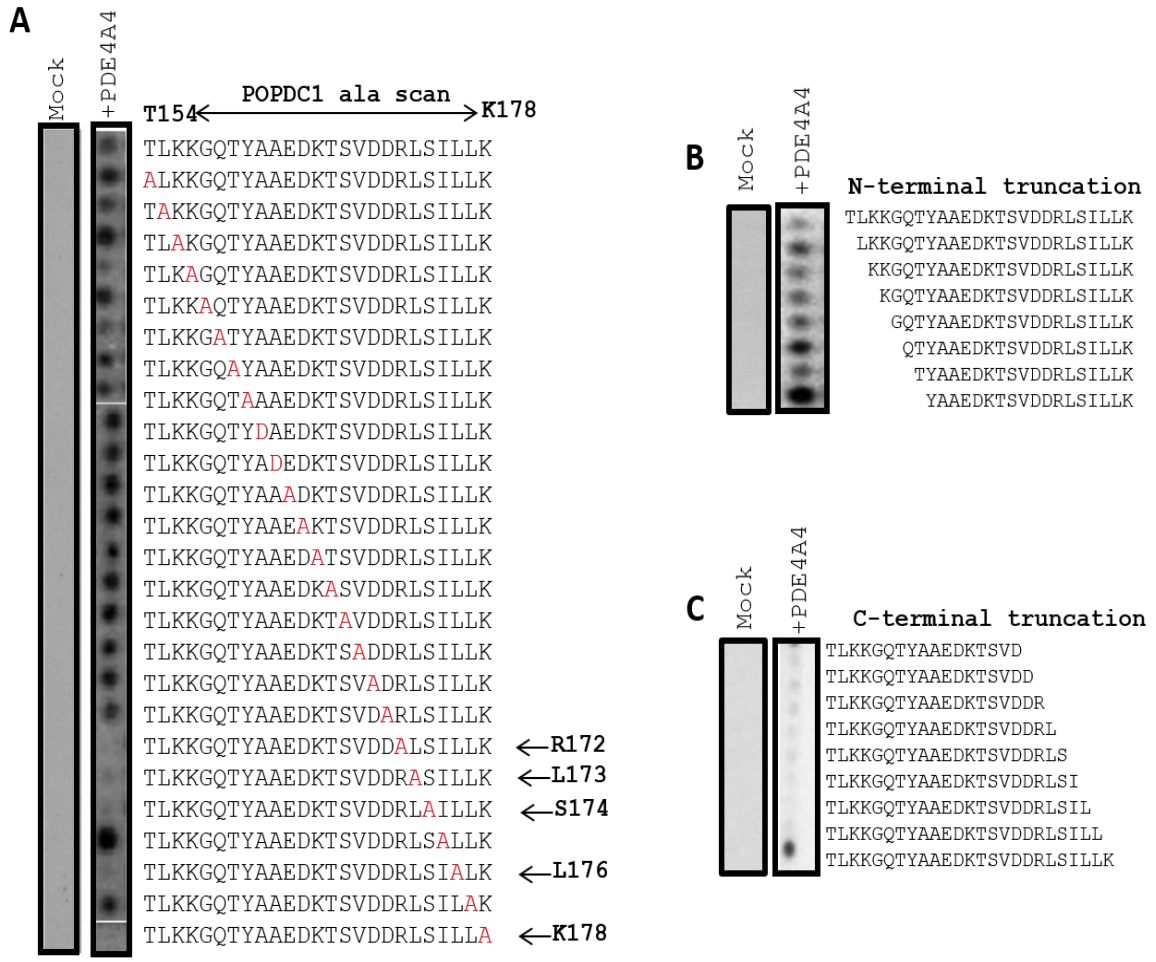

Figure 3.19: Peptide arrays showing alanine scans as well as N and C terminal truncations of identified binding site. A 25mer binding sequence previously identified was synthesized to cellulose membrane and walking alanine scans, where each residue was substituted an alanine, with shown in red. If alanine was in the original sequence the residue was substituted with aspartic acid (D), shown in red. Membranes were overlaid with PDE4A4-VSV overexpressing cell lysate before primary antibody incubation using a VSV antibody specific to the tag on PDE4A4. A lysate control was performed to ensure no unspecific binding. Imaging was performed using chemiluminescence. **B** is N-terminal truncations and B depicts C-terminal truncations. Control peptides were overlaid with un-transfected lysates. **C** C-terminal truncations. Control peptides were overlaid with un-transfected lysates and probed with the same VSV-antibody as used for the experimental membranes.

This technique identified five amino acid residues that are crucial to POPDC1s ability to bind PDE4A4/5 (Figure 3.19 **A**). In agreement with Figure 3.18, a crucial sequence, R-L-S-I-L-L-K is essential to the interaction of POPDC1 and PDE4A4/5. Interestingly, the residue involved in the human familial mutation is again highlighted, adding evidence to the hypothesis that arrythmias in

POPDC1^{R172H} patients may stem from lack of PDE4 binding to POPDC1, resulting in higher local cAMP concentration and consequently less TREK1 binding. To further validate these residues as important determinants for the interaction of POPDC1 and PDE4A4/5, N-terminal and C-terminal truncations of the binding region were generated (see Figure 3.19 **B** and **C**). As expected, sequential removal of these key residues (R-L-S-I-L-L-K) resulted in attenuation of the interaction between POPDC1 and PDE4A4/5 (Figure 3.19C). This data suggests that these five residues are required for the successful binding of PDE4A4/5 to POPDC1, including the mutated arginine at position 172. As expected, truncation of residues from the N-terminal of the original 25mer (T154 to K178) did not have any effect on binding (Figure 3.19B).

As mentioned, the PDE4A binding site on POPDC1 contains the identified POPDC1^{R172H} mutation site. To determine whether there was a potential change in PDE4A binding to this site when the mutation (R to H) was re-created by peptide array, sequences containing the R to H substitution were overlaid with purified recombinant PDE4A4 tagged with MBP (Figure 3.20).

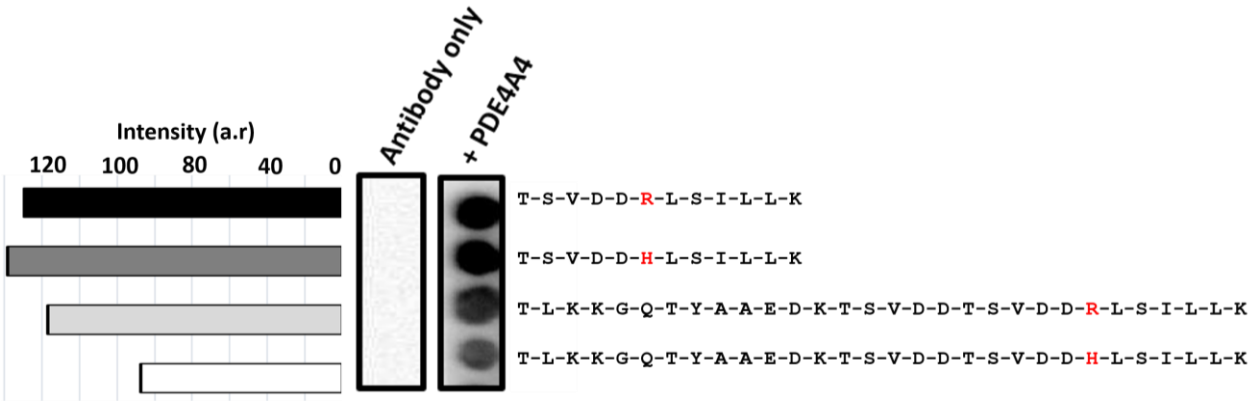

Figure 3.20: Peptide array of POPDC1 binding sequence with the R172H mutation change. Short 12mers and full 25mer binding site sequence were taken and the R172H mutation was added. These arrays were overlaid with purified recombinant PDE4A4 tagged with MBP before being probed with PDE4A4 specific antibody. An antibody only control membrane was also performed. Membranes were imaged using chemiluminescence. A graph was produced using intensity measurements taken of each spot using ImageJ.

Excitingly, a reduction in PDE4A binding was clear when the full 25mer sequence was recreated (Figure 3.20, comparing bottom two spots) suggesting that the familial mutation (R172 to H) phenotype may manifest by the inhibition of PDE4A

binding. In contrast, binding of PDE4A4 was not reduced in the shortened binding site sequence containing the mutant (Figure 3.20), comparing top two spots). This may be as a result of the short, linear nature of this peptide which may not have as much secondary structure as the 25mer.

3.3.5 Mapping the binding site of POPDC1 on PDE4A

In order to discover the POPDC1 binding site on PDE4A and potentially discover the nature of PDE4A specificity for the POPDC1 Interaction, I undertook the reciprocal experiment of that described above. The full length PDE4A4 sequence was encompassed by an array using 25mer peptide, shifted by five amino acid residues at a time. Once synthesized, membranes were overlaid with HEK293 lysate overexpressing POPDC1 tagged with the FLAG tag (Figure 3.21).

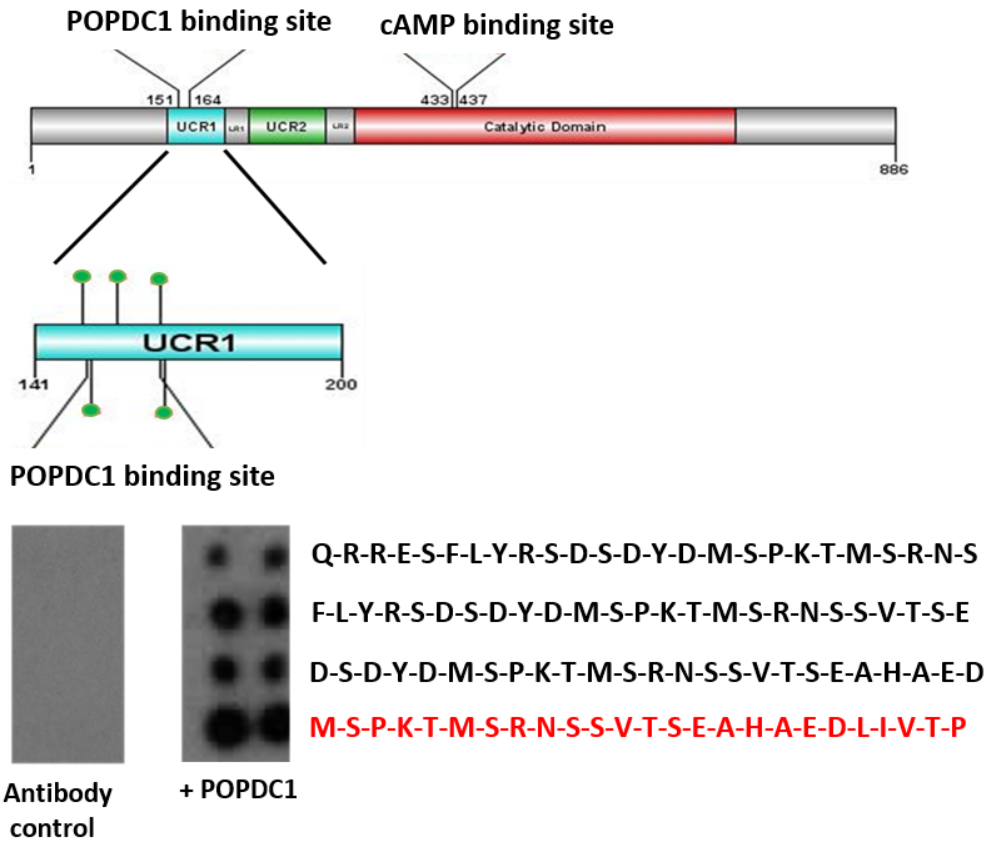

Figure 3.21: PDE4A4 peptide array identifying the binding site of POPDC1. 25mers of PDE4A4 covering the full length of the protein were overlaid with HEK293 lysate overexpressing POPDC1. HEK293 cells mock transfected were used as a control. Red highlighted sequence identified sites with strongest apparent binding. A schematic of PDE4A4 structure is shown depicting the POPDC1 binding site as well as highlight phosphoserines (represented by green circles).

A single binding region was identified for POPDC1 on PDE4A4. This region falls within the UCR1, specific to all PDE4 long isoforms. This region is highly conserved in all PDE4 subfamilies but does have small divergent areas, some of which feature in the POPDC1 binding site I have identified. Interestingly, just upstream of the POPDC1 binding site is a site that has previously been identified by our lab as a multifunctional docking site (Houslay et al., 2017) for a range of PDE4 interacting proteins. Known as the FLY domain (Phe141, Leu142, and Tyr143), this site lies within the UCR1 domain of PDE4 and allows for the binding of several proteins including mitogen-activated protein kinase-activated protein kinase 2 (MK2). Long forms of PDE4 can be phosphorylated by MK2 attenuating their activation by PKA phosphorylation (MacKenzie et al., 2011). This leads to an indirect modulation of PDE4s activity and hence disrupting cellular desensitization to cAMP and additionally for PDE4A this phosphorylation leads to

a conformational change reducing protein binding to the UCR2 domain (MacKenzie et al., 2011). In order for MK2 to phosphorylate PDE4 long forms effectively it has to interact at this docking site (Houslay et al., 2017). The interaction with POPDC1 may elicit a protective mechanism for PDE4A keeping it in its active form inhibiting the binding of MK2. Having identified a region of POPDC1 binding, alanine scans and C-terminal truncations were performed to isolate crucial amino acid residues essential to binding (Figure 3.22) and perhaps, PDE4A specificity.

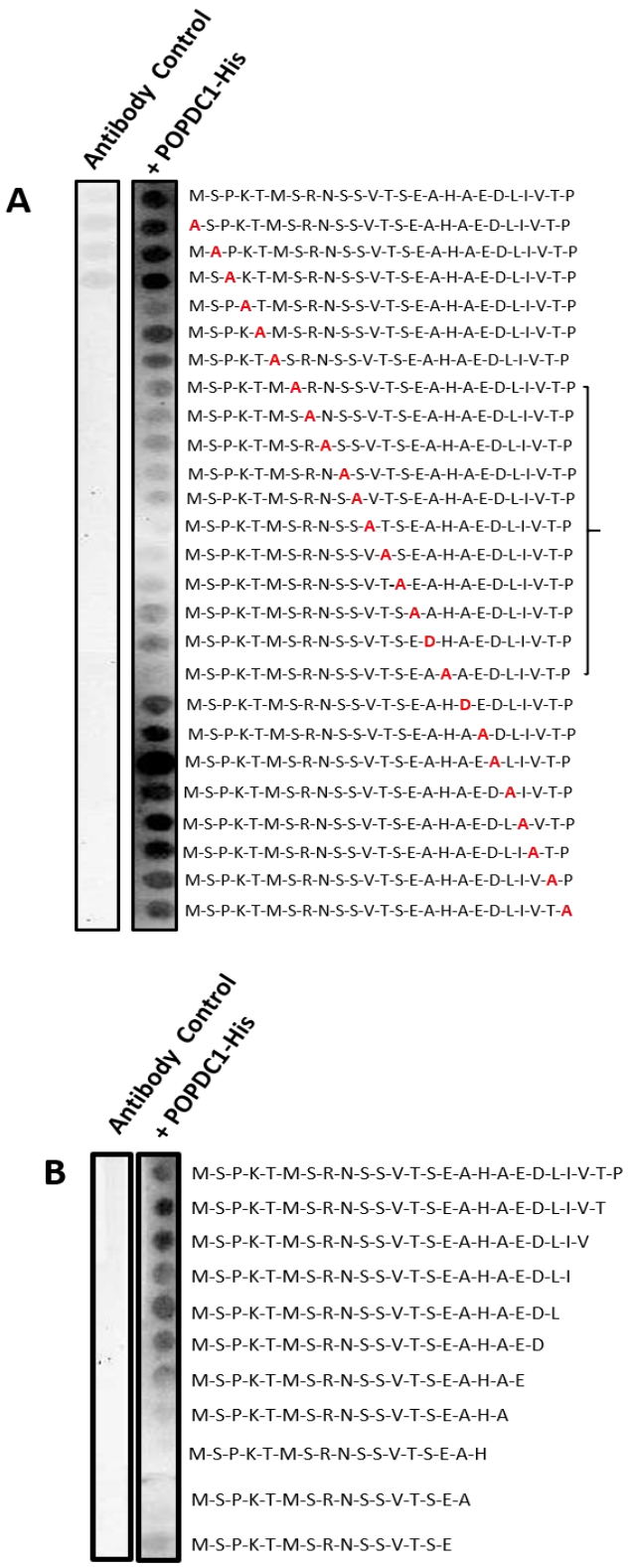

Figure 3.22: Alanine scan and C-terminal truncation of identified POPDC1 binding site on PDE4A4. **A** Walking alanine scans were performed on the identified binding site of POPDC1 on PDE4A4. Sequentially, each amino residue was substituted with an alanine or where the native residue was an alanine, an aspartic acid residue was used instead (shown in red). Residues crucial to binding have been highlighted in the bracket, Membranes were overlaid with POPDC1 Popeye domain tagged with His while control membranes were incubated in antibody only. **B** C-terminal truncations, removing one amino residue each spot was overlaid with POPDC1 Popeye domain tagged with His.

Alanine scanning was undertaken on the 25-mer that displayed the most robust binding of POPDC1 (Figure 3.21, last spot, sequence in red). Sequentially, each amino acid residue was substituted with an alanine, or where an alanine was present in the native sequence an aspartic acid. Membranes were overlaid with the POPDC1 Popeye domain tagged with His. Both the alanine scan (Figure 3.22A) and the C-terminal truncation (Figure 3.22B) identified a region containing 10 residues, (M-S-R-N-S-S-V-T-S-E-A-H-E-A-D; M161-D175 residues) that appeared to be critical to POPDC1 binding.

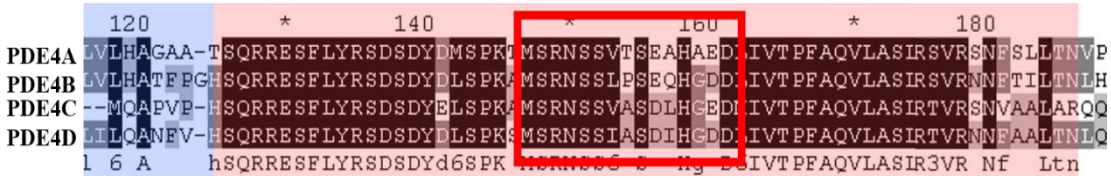

Figure 3.23: UCR1 sequence homology of long PDE4 isoforms. The UCR1 domain denoted in pink. Sequence homology between the PDE4 long isoforms is shown with a black background. The red box highlights the area of the sequence that was found to be crucial to the binding of POPDC1.

Interestingly, the residues that displayed the greatest loss of binding fall within one of the small variable regions of the UCR1 domain (Figure 3.23). As can be seen in Figure 3.23, when V-T-S-E-A-H-A-E-D (V167-D175 residues) sequence is disrupted, via alanine substitution or C-terminal truncation, there is a highly visible loss of the POPDC1 binding. This data not only identifies the putative POPDC1 binding site on PDE4 but also suggests a possible route by which POPDC1 specifically selects PDE4A (and not PDE4B, C or D).

3.4 Discussion

3.4.1 POPDC1 directly interacts with PDE4A

It is known that most proteins within the cell create a network of interactions with other proteins to create signalling cascades that are used to specifically activate physiological changes of cells in response to extra-cellular stimuli. Identifying a specific protein's 'interactome' allows for the function of said protein to be understood within one or more tissue/cell type. As discussed, the interaction of a cAMP effector protein with a PDE is crucial for the control and activation its function in response to Gs-coupled receptor activation and for its resistance to inappropriate activation under basal cAMP conditions (reviewed in (Baillie et al., 2003, Fertig and Baillie, 2018, Baillie, 2009)). PDEs are the critical component in regulating both spatial and temporal dynamics of cAMP leading to the creation of cAMP microdomains that allow for discrete and distinct signalling within the cell in response to single receptor types. This concept of cAMP compartmentalisation first devised by Larry Brunton and co-workers in the late 1970s has resulted in the identification of many localised cAMP "signalosomes" that contain a single cAMP effector and a PDE (Hayes et al., 1980, Beavo and Brunton, 2002, Hayes and Brunton, 1982, Maurice et al., 2014). With POPDC1 being a novel cAMP effector protein and it's interactome being interrogated, it was my hypothesis that a PDE would bind to a signalling complex containing POPDC1 and that the PDE activity associated would regulate POPDC1 function. The observations made in this chapter have shown, for the first time, that indeed POPDC1 interacts with a PDE4, having increased specificity for PDE4A. Other chapters in this thesis will attempt to decipher the exact role of the PDE4A pool associated with POPDC1

I have shown that an interaction between Popdc1 and PDE4A exists in both transfected HEK293 cells as well as in endogenously expressing NRVM and ARVM/ARSM (Figure 3.5, Figure 3.6, Figure 3.8, and Figure 3.9). Through the use of co-immunoprecipitations and PLA, Popdc1 was shown to bind PDE4A. In cardiomyocytes, the co-immunoprecipitations appeared to be less clear that those performed in overexpressing HEK293 cells (Figure 3.7 compared to Figure 3.8). A possible explanation for this is that the compartmentalisation of both Popdc1 and PDE4A means that there is only a discrete location where the two

proteins are found interacting. During co-IPs, the whole cell population is taken together meaning that the volume of lysate added to the reaction may only contain very small amount of the Popdc1-PDE4A interaction. An endogenous interaction was further supported through PLA, using antibodies detecting Popdc1 and PDE4 isoforms (Figure 3.9). This observation led to the first potential mechanism by which the activity of Popdc1 is controlled.

The formation of PDE signalling complexes in the heart have been extensively investigated. PDE4 family members have been shown to be vastly integrated into complexes containing numerous cardiac proteins, many of which are known to be involved in the excitation-contraction coupling as well as in calcium handling (Sin et al., 2011, Lehnart et al., 2005, Maurice et al., 2014, Bolger et al., 2003, Leroy et al., 2011, Beca et al., 2011, Terrenoire et al., 2009). One of the most well-defined signalling complexes, is that of PDE4D5 and ß-arrestin. When $ß_2$-adrenoreceptor is stimulated it leads to the production of cAMP through the activity of AC, and the surge in localised cAMP activates PKA. The desensitisation of this adrenergic signalling occurs through a negative feedback loop initiated when the receptor itself is phosphorylated by PKA. This switches the receptors signalling to an inhibitory one type, suppressing AC activity and other pathways such as ERK1/2 signalling (Daaka et al., 1997). The phosphorylation of the receptor by G-protein coupled receptor kinases leads to the recruitment of ß-arrestin further desensitising the receptor through preventing access to the G-protein (Krupnick and Benovic, 1998). Along with the recruitment of ß-arrestin there is an increase in localised cAMP degradation. Baillie and colleagues identified that this decrease was due to the activity of PDE4D5 recruited to the $ß_2$-adrenoreceptor by ß-arrestin (Baillie et al., 2003). PDE4D5 is not the only PDE isoform to interact with ß-arrestin, in fact all PDE4 isoforms can interact due to a conserved binding site in the catalytic region of the protein (Perry et al., 2002). However, PDE4D5 possesses a unique binding site for ß-arrestin in the N-terminal region giving it higher affinity for binding (Bolger et al., 2003). The interaction between PDE4D5 and ß-arrestin also functions to regulate the activity of a localised pool of PKA by tethering the PDE to a complex containing AKAP79 and $ß_2$-arrestin (Lynch et al., 2005). The formation of a complex containing a cAMP effector protein such as PKA, with a PDE allows for it to be hypothesised that the interaction between POPDC1 and

PDE4A may represent a novel control mechanism in cardiac signalling functioning to modulate the local cAMP levels.

Peptide arrays were utilised to fine map the binding sites involved in the interaction between POPDC1 and PDE4A (Figure 3.17, Figure 3.18, Figure 3.19, Figure 3.20, Figure 3.21, and Figure 3.22). Examining the interaction motif for PDE4A on POPDC1 identified a region (R-L-S-I-L-L-K) within the evolutionarily conserved Popeye domain (Figure 3.17). Based on predicted secondary structure, a proportion of these amino residues are buried within a ß-sheet making them inaccessible to interacting proteins. Given the close proximity of this site to the cAMP binding motifs (DSPE and FQVT motifs) (Froese et al., 2012), it could be hypothesised that the binding of cAMP confers a conformational change making the binding region accessible. Small molecule binding inducing a structural change has previously been shown to create more accessible binding regions. An example of this is found with TnI, the actomyosin ATPase inhibitory subunit which elicits its inhibitory effect upon the binding of Ca^{2+} to TnC, another subunit of troponin (Tobacman, 1996, Zhang et al., 2011). The presence of Ca^{2+} causes the increased binding of TnI to tropomyosin due to a regulated conformational change in the C-terminal end of TnI. This conformationally controlled interaction is thought to restrict tropomyosin movement at resting conditions when calcium levels are low, therefore, inhibiting actomyosin ATPase and muscle relaxation (Zhang et al., 2011). In addition, given that the structure of POPDC1 is only predicted based on sequence homology it may also be the case that the amino residues identified are far more exposed than initially anticipated.

Interestingly, the identified binding site of PDE4A on POPDC1 contains the disease related familial mutation, R172H. A German lab group headed by Professor Hendrik Milting, initially identified the missense mutation in *POPDC1* in a patient presenting with dilative cardiomyopathy (DCM) (Schindler, 2014). The mutation results in the change of an arginine to histidine at position 172 (R172H). Interestingly, further analysis of 200 other known candidate genes for this disease identified a mutation in the Laminin A/C gene meaning the two may be contributing to the disease phenotype (Schindler, 2014). Investigations into the effects of the mutation on the function of POPDC1 were carried out using

recombinant POPDC1[R172H]. cAMP binding affinity was tested and showed no significant differences in comparison to their WT counterparts. There were also no changes in the subcellular localisation of the protein or in POPDC1s ability to interact with TREK1 (Schindler, 2014). I hypothesise that this mutation lessens PDE4A binding affinity (Figure 3.20) and this may be due to the fact that arginine is typically found on the outside domains of proteins where it's hydrophilic group can interact with the polar environment, meaning it is usually found at the interface of interacting proteins. As it is positively charged it contributes to a wide range alterations in both nucleic acid and protein interactions (reviewed in (Bayer et al., 2005)). Methylation of arginine residues allows for weakening of the bonds between interacting protein allowing for a reversible binding. It has been shown in several disease-causing mutations that the change from an arginine (Arg) to a histidine (His) can result in in drastic conformational changes. Arg>His mutations have become of more importance in recent years as work on the molecular mechanisms of His switches in pH sensors, or proteins with pH sensitive functions and activities (White et al., 2017, Schönichen et al., 2013). Arginine is known to have a pK_a (where K_a is the acid dissociation constant) of around 12 whereas histidine with a pK_a of 6.5 can then titrate with the narrow pH range and shows a shift in population from protonated to neutral species at a higher pH. This creates the pH of the protein to increase which can change both the activity and interactions of a protein. For example, in some cancers an Arg-to-His mutation in the growth factor EGFR has been suggested to stabilise the kinase through a conformational change to an constitutively active state when there is a high cellular pH (White et al., 2017). Therefore, the subtle change from Arg>His could result in drastic changes in protein-protein interactions and stability (White et al., 2017). In the context of POPDC1/PDE4A complex the change from Arg>His in POPDC1 could have numerous implications. For example, this could result in a conformational change which may create either weak or dysregulated binding of PDE4A *in vivo*. Lack of cAMP regulation around POPDC1 would affect its subsequent interactions with other proteins such as TREK1. As TREK1 and POPDC1 interact under basal cAMP conditions the dysregulated rise in cAMP would dissociate the two leading to aberrant TREK1 current (Froese et al., 2012). This, in part, may answer the question of how the mutation in POPDC1 contributes to cardiac arrythmia.

Furthermore, a single point mutation in proteins has frequently been shown to have major contributions to disease either by interrupting protein complexes, by affecting the functionality of that protein, or by impacting on the control of cAMP signalling (Studer et al., 2013). An example of this is the point mutation identified in the cAMP/cGMP degrading PDE10A found in patients suffering from Childhood-Onset Chorea with Bilateral Striatal Lesions (Mencacci et al., 2016). Chorea is a hyperkinetic disorder that results from the dysfunction of the striatal medium spiny neurons (MSNs) (Hermann and Walker, 2015). The substitution of phenylalanine to a leucine at position 300 or 334 in the highly conserved GAF-B domain leads to a dramatic reduction in the activity of PDE10A after stimulation. This was shown to be due to the altered residues being located within the cAMP binding pocket (Mencacci et al., 2016). Studies have shown that PDE10A has two states, active and super-active therefore, when cAMP intracellular levels are high the PDE is switched to the super-active state. Given that the regulation of MSN activity is largely due to the regulation of cAMP, the loss of PDE10A activity and subsequently disrupted localised cAMP signalling drives the progression of this disease (Threlfell and West, 2013, Mencacci et al., 2016). In addition, six identified separate missense mutations in PDE3A have been linked to the development of hypertension and brachydactyly type E (HTNB) (Maass et al., 2015). The mutations increased the PKA-mediated phosphorylation of PDE3A resulting in increased cAMP-hydrolytic activity. cAMP inhibits myosin light chain kinase (MLCK) through PKA causing vascular smooth muscle cell (VSMC) relaxation. Increasing the activity of PDE3A was predicted to be contributing to the progression of disease by lowering the cAMP concentration in VSMC thereby promoting peripheral vascular constriction (Maass et al., 2015). Such data suggests that the disruption of localised cAMP dynamics as a consequence of point mutations can contribute toward disease. This provides precedent for the point mutation in POPDC1^{R172H} leading to a reduction in PDE4A binding (Figure 3.20) that could contribute towards the onset of conditions such as DCM.

Of note, is the data gained in this chapter that suggests POPDC1 has the capability to bind to PDE4 long isoforms but with a higher affinity for PDE4A that leads to a degree of specificity. Previously in the PDE field, dogma has dictated that the unique N-terminal directs binding, but it is becoming more apparent that other interaction sites on PDE4 contribute to specificity (Murdoch et al.,

2007, Richter et al., 2008). As the site identified here found in the evolutionary conserved UCR1 domain, it is of no surprise that this would allow for the binding of other isoforms containing this domain. Multiple isoform binding is not uncommon either, for example the Disrupted-in-schizophrenia (DISC1) protein has been shown to interact with isoforms from PDE4A, PDE4B and PDE4D however but possesses higher affinity for PDE4B (Murdoch et al., 2007). Likewise, beta-arrestin recruits PDE4 to Gs-coupled receptors as part of the desensitisation mechanism but has a preference for PDE4D5 via an extra binding site (Baillie et al., 2003, Baillie et al., 2007, Bolger et al., 2003). We have shown here that POPDC1 interacts with PDE4 isoforms endogenously much like DISC1 however has a preference for PDE4A. Evidence for this is displayed in Figure 3.10 and Figure 3.11 through preferential PDE4A association observed in the PLA experiments carried out in NRVM and HEK293. The PDE4A isoform specific sequences found in the UCR1 domain could be crucial binding specificity residues for POPDC1 association. In addition, the localisation of PDE4A long isoforms may in part be the contributing factor to their preferred binding. PDE4A4/5 are known to be associated with ruffles at the cell periphery via a highly proline-rich region which allows for its binding to SH3 domains found in various Src family tyrosyl protein kinases (Beard et al., 1999, McPhee et al., 1999, O'Connell et al., 1996). With POPDC1 known to be predominantly membrane-bound but able to localise to multiple locations within the cell under different conditions (Schindler et al., 2012a, Alcalay et al., 2013, Swan et al., 2019), we can hypothesize that it can form interactions with other PDE4 isoforms when there is little to no PDE4A present in the vicinity. At the membrane, one of POPDC's most important interactions is that of TREK1 and I have not looked at whether the PDE4A interaction interferes with the TREK1 interaction.

The POPDC1/PDE4A interaction may be present in other tissues given that both proteins are expressed throughout the body (protein expression analysis (Lindskog, 2016). As such, this signalling complex may harbour different functions and interactions dependent on its localisation. Detailed analysis must be done to identify whether this interaction is present within any other tissue type using the same methods outlined in this work. Given that both POPDC1 and PDE4A are known to be expressed within the brain, it may be hypothesised that this complex would be present in distinct brain regions with functional signalling

implications (Hager and Bader, 2009, McCarthy, 2006, Pérez-Torres et al., 2000, McPhee et al., 1995, Lakics et al., 2010). Dysregulated cAMP dynamics have been shown to correlate to the progression of disease pathology for example the PDE4D orchestration of cAMP response element binding (CREB) in Alzheimer's disease (AD) (reviewed in (Tibbo et al., 2019)). In the mammalian brain, cAMP signalling has been implicated in many critical neural functions including synaptic plasticity, cellular excitation, pain and motor function, and facilitating learning and memory (Pierre et al., 2009, Bollen and Prickaerts, 2012, Kandel, 2012, Brady, 2011). Increases in cerebral cAMP activates PKA that is associated with CREB which is vital for synaptic plasticity, formation of long-term memory, and cognition (Frey et al., 1993, Bailey et al., 1996, Gilleen et al., 2018, Blokland et al., 2019, Takeo et al., 2003, Averaimo and Nicol, 2014, Tibbo et al., 2019). Errors in this signal transduction driven by anomalous PDE activity result in cAMP dysregulated responses in key areas of the brain that affect memory formation and Aß production driving the Alzheimer's Disease symptoms (Ricciarelli and Fedele, 2018). The formation of a POPDC1/PDE4A complex in the brain may correlate with distinct regulation of localised cAMP dynamics and as such contribute to normal cAMP signalling. This novel POPDC1/PDE4A complex may have implications in many tissues and its dysregulation could contribute to tissue specific disease pathology.

3.4.2 Methodological considerations and future directions

Although we have provided strong evidence for a novel interaction between POPDC1 and PDE4A, with the benefit of hindsight, there are a number of aspects of this project that require further investigation to provide further corroboration of these results.

The ability to both extract Popdc1 from endogenously expressing cells and to precipitate it using commercially available POPDC1 antibodies proved to be problematic. Due to its membrane localisation, the extraction protocol developed is harsh as extensive sonication cycles are required to fragment the cell membrane allowing for isolation of Popdc1; this means there may be collateral damage to other proteins such as PDEs reducing their binding ability in

co-IPs. In addition to this, the commercially available antibodies for POPDC1 have been shown by Dr Roland Schindler (thesis submission at Imperial College London, 2012) to be inefficient in detecting the protein via western blotting. This in part, could have led to the lack of clear Co-IPs in cardiac myocytes from both rabbits and rat. Currently, there are new antibodies being produced as interest in POPDC1 has grown, meaning that the endogenous Co-IPs should be performed again with the new batches. Furthermore, the increased ability to isolate POPDC1 via the new antibodies, would allow for a mass spectroscopy screen of endogenous binding partners to be undertaken. This would support our case if PDE4A was specifically identified as a POPDC1 binder. The interaction in this thesis relied heavily upon HEK293 cells overexpressing POPDC1. The PLA experiments demonstrated that Popdc1 was able to bind to PDE4A and to a lesser extent PDE4B and PDE4D in NRVM. Due to the time constraints of this project, the specificity of the interaction was not investigated in adult cardiac myocytes. Immature cardiomyocytes are known to lack the mature phenotype of adult cardiomyocytes (reviewed in (Peter et al., 2016)). Due to the lack of structure, POPDC1 may therefore encounter the other PDE4 isoforms that possess a cytoplasmic localisation. The analysis of the interaction in adult cells would determine whether the maturity of the cells influences the specificity for PDE4A.

In addition, as POPDC1 is part of a three-member family that all share conserved regions, one of which is the area identified as a binding site for PDE4A, it is possible that all POPDC proteins bind PDE4A. Each POPDC isoform possesses its own interaction partners controlled, in part, by cAMP binding (Schindler et al., 2012b). The need for control of cAMP levels is as equally important with these isoforms as it is for POPDC1 so it could therefore be hypothesized that they too would interact with a PDE. In order to gain a full picture of how POPDC proteins function it would be necessary to determine whether other PDE isoforms are involved in the formation of signalling complexes. Peptide arrays containing sequences from both POPDC2 and POPDC3 overlaid with PDE4 isoforms as well as PLA in endogenous cells and overexpressing cell lines such as carried out in this chapter, would allow for the confirmation of any interaction. This information would provide a detailed signalling pathway that would elucidate how POPDC proteins drive the development of disease pathology which currently is unclear.

3.4.3 Chapter summary

In conclusion, the data provided in this chapter suggests a novel interaction between POPDC1 and PDE4A exists that likely controls localised cAMP dynamics in the vicinity of POPDC1. This is consistent with our hypothesis, which was developed with the prior information that all other known cAMP effector proteins are found to form signalling complexes containing PDEs. Future investigations should focus on determining the specificity of the interaction between Popdc1 and PDE4A in adult cardiac myocytes as well as identifying whether the other POPDC isoforms create interactions such as this. In doing so, an in-depth mechanism by which POPDC proteins contribute to normal cellular function and disease pathology could be identified. Compartmentalized signalling is an important facet in controlling cellular function and as such, this finding is of significance.

4 Functional implications of the POPDC1-PDE4 complex

4.1 Introduction

It is hypothesised that cAMP binding to the Popeye domain drives a conformational change that results in modulation of binding sites for specific POPDC interacting proteins (Schindler and Brand, 2016). This increases the diversity and number of proteins that can interact with POPDC1 under different physiological conditions. The previous chapter provided robust evidence that a complex of POPDC1 and PDE4 exists, so I sought to determine what the role of the complex is and tried also to gain insight into the mechanism that underpins the function. Signalling complexes that contain PDEs are known to have a wide range of cellular functions in the heart. Often the interaction with a PDE regulates the activity of the bound protein by modulating the local cAMP concentration. The L-type calcium channel (LTCC) is a protein involved in the excitation-contraction coupling whose function is closely modified by its interaction with PDE4B (Leroy et al., 2011). LTCC then functions to allow calcium influx through the cardiomyocyte membrane triggering the release of calcium from intracellular stores by the RyR. Increased calcium presence in the cytoplasm leads to a positive inotropic effect (Bers, 2002). Under ß-adrenergic stimulation, PKA phosphorylates the pore forming sub-units of LTCC increasing the activity of the channel (Fuller et al., 2010, Bünemann et al., 1999) . PDE4B$^{-/-}$ mice displayed a markedly increased calcium current through the LTCC increasing contractibility of myocytes (Leroy et al., 2011). The interaction with PDE4B therefore serves to modulate the activity levels of the LTCC in the heart to maintain normal pace making function. The POPDC1/PDE4 complex may operate in a similar fashion with PDE4A controlling the activity and interactions of POPDC1 through the modulation of localised cAMP dynamics.

4.1.1 POPDC1 in cardiac disorders

POPDC1 is strongly expressed in the heart and this expression pattern has been observed in all of the animal models studied including Xenopous, mouse and zebrafish (Wu et al., 2012b, Ripley et al., 2006, Smith and Bader, 2006). In the adult heart, POPDC1 is highly expressed in the atria, ventricles, atrioventricular

node (AVN), sinoatrial node (SAN) as well as the His bundle and Purkinje fibres (Froese et al., 2012). Analysis of POPDC1 function has pointed to a role in the control of precise electrical conductance in the heart (Han et al., 2019). *POPDC1*$^{-/-}$ mutant mice developed stress-induced sinus bradycardia following exposure to physical exercise, mental stress or injection of isoproterenol suggesting that the mice could possibly not regulate a change in heart rate or action potential (Froese et al., 2012). Changes in heart rate of POPDC1$^{-/-}$ mice were also accompanied by an altered SAN pacemaker pause (Froese et al., 2012). An interesting point is that the presentation of these changes was not seen in young mice however at 5-8 months, the severe stress-induced bradycardia with sinus node dysfunction manifested (Froese et al., 2012). This phenotype is reminiscent of sick-sinus-syndrome (SSS), which is the most frequent cause of pace making device implantation in elderly individuals with no prior heart disease issues (Han et al., 2019). The dysregulation of POPDC1 expression and/or changes to its function have been speculated to be the cause of this disease pathophysiology.

During a myocardial ischemia/reperfusion (I/R) event, there are numerous damaging changes made to the myocardial ultra-structure, cardiac function and electrophysiology (Ferdinandy et al., 2007). It has been demonstrated that POPDC1 protein and mRNA are decreased during I/R and that POPDC1$^{-/-}$ mutants had a lower functional recovery compared to their WT counterparts (Alcalay et al., 2013). In addition, Schindler *et al.*, forced expression of POPDC1^{S201F}, a cAMP binding domain mutant, in murine cardiac cells and increased the hyperpolarisation and upstroke velocity of the action potential (Schindler et al., 2016b). Furthermore, the expression of the homologous POPDC1^{S191F} in zebrafish displayed the same heart and skeletal muscle phenotypes, including cardiac arrythmia and limb-girdle muscular dystrophy, seen in patients harbouring POPDC1 mutations (Schindler et al., 2012b). These concepts and how they relate to my data will be discussed more in depth later.

4.1.2 Excitation-contraction coupling

As discussed in section 1.1, the propagation of electrical activation throughout the myocardium is carried by the action potential. The shape and duration of the potential is variable across the atrium and ventricles. For a coordinated

muscular contraction resulting in the efficient expulsion of blood, the electrical activation throughout the heart muscle must be coordinated spatially and temporally (Bers, 2002). Activation is initiated in the SAN from specialised pacemaker cells and is propagated through the atrial tissue. The signal reaches the AVN which in turn passes the impulse through the His-Purkinje fibres in the septum of the heart. The atrium and ventricles are electrically separated from each other in order to ensure that the atrium contracts prior to the ventricles. The endocardium (inward facing surface) of the ventricles become activated and propagates the signal through gap junctions to the epicardium (outward facing surface) resulting in the coordinated contraction of the ventricles (systole). This electrical activity can be observed externally using an electrocardiogram. On an ECG trace Figure 4.1, the P-wave is caused by the depolarisation of the atria which is followed closely by the QRS complex (Hadjem and Naït-Abdesselam, 2015). This complex represents the ventricular depolarisation. The T-wave represents repolarisation of the ventricles which is driven by the efflux of K^+ and the unbinding of calcium from troponin leading to the relaxation of the muscle (diastole) (reviewed in (Bers, 2002)). The QT-interval duration is a marker of normal ventricular function. A change in QT interval duration can indicate an altered ventricular electrical function often caused by a deleterious change in protein regulation and /or ion channel transport (Bartos et al., 2015). I will use these principals later in this chapter to determine whether treatment of heart tissue with the POPDC1-PDE4 disruptor peptide elicits a change in action potential.

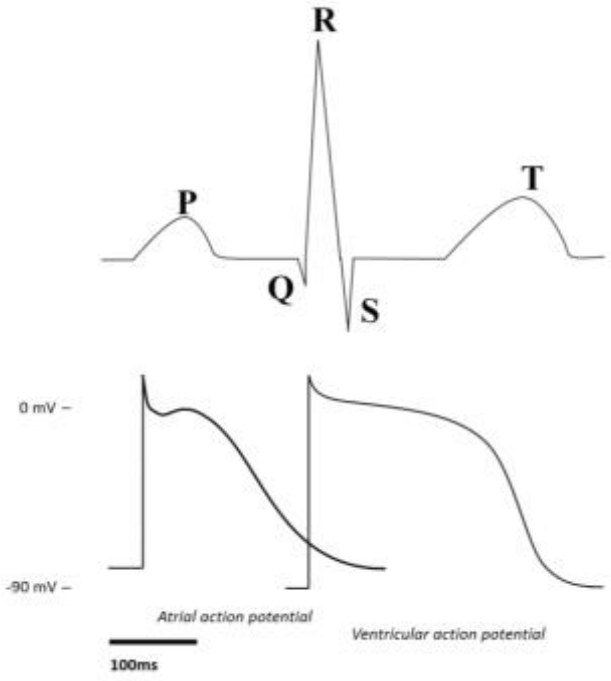

Figure 4.1 Cardiac electrocardiogram (ECG) trace. Diagrammatic representation of the depicting the respective influence of atrial and ventricular action potentials to the P-wave, QRS complex and T-wave respectively. Ventricular action potential was utilised in CellOptiq experiments. The electrical signal of a heartbeat begins at the sinoatrial node and travels to the atria causing them to contract pushing blood to the ventricles, this signal is recorded as the P wave. The PR interval is the time from the beginning of the wave to the beginning of the QRS complex. As the signal passes to the ventricles through the atrioventricular node (AV), it slows allowing blood to fill the ventricles. This decreased signal appears as a flat line between the P wave and the start of the Q wave. The signal progresses from the AV node through the bindle of His into the left and right bindles. Electrical signals can then pass across the ventricles causing the muscle to contract and pump blood to lungs and rest of body. This signal is recorded by the QRS complex given that these waves occur in rapid succession. The ventricles can recover to their normal resting state, shown by the T wave. The ST segment is the flat, isoelectric section representing the interval between ventricle depolarisation and repolarisation. The distinct ECG pattern for atria and ventricles are shown in an overlapping manner depicting the signal transmission through the main heart tissues.

4.1.3 The ventricular action potential

The ventricular action potential comprises of five major phases (0-4) with each phase being the result of a balance of ionic currents driven by ion channels controlling the dynamic membrane potential (E_m) of the cell. The duration of the action potential depends on the movement of ionic currents in and out of the cell.

The mediation of phase 0 is under the control of the voltage-gated Na^+ channel through its rapid activation and deactivation (Figure 4.2). Phase 1 represents the

opening of the K^+ channel, whose transient outward current ($I_{to,\,f,}$ fast and $I_{to,s}$, slow components) mediates the rapid repolarisation of the cell. Both phase 2 and phase 3 are the product of direct competition between the inwards currents of the voltage-gated L-type calcium channels and the Na^+/Ca^{2+} exchanger (NCX), and the voltage-gated delay rectifier K^+ channels outward current (Carmeliet, 1999). Finally, phase 4 occurs when the myocyte is at rest, known as diastole. In non-pacemaker cells the voltage during this rest state is kept constant at around -90 mV (Bers, 2002).

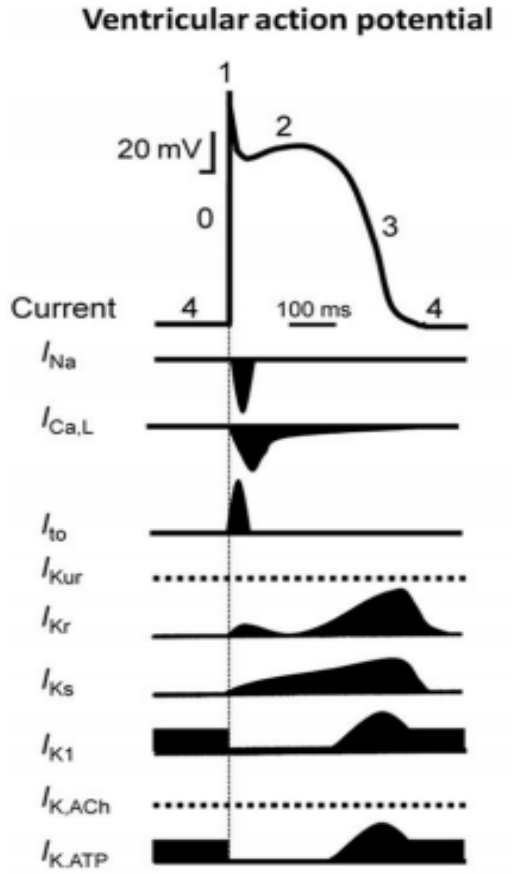

Figure 4.2: Trace of the ventricular action potential. Phases of typical ventricular action potential (AP). The upper panel depicts the ventricular action potential and the numbers noted on the traces correspond to the 5 phases of the action potential. Activation and deactivation of associated inward (Na^+, Ca^+) and outward (K^+) currents throughout the course of the action potential are shown in the lower panel. (Image taken from (Jost, 2009**)).**

4.1.4 Permeation and gating of TREK1 channels

In this thesis, the potassium channel, TREK1, has been used to detect functional changes following modulation of the POPDC1/PDE4A complex. TREK1 is the most studied background K_{2P} channel with its primary role being to control excitability

and maintain the membrane potential below the threshold of depolarisation (Djillani et al., 2019). Interestingly, the dimeric structural arrangement of these channels is in stark contrast to that of voltage-gated and inward rectifier channels (Patel and Honoré, 2001). The arrangement of these two-pore channels appears to underlie 'background' K^+ (K_B) conductance in cardiac myocytes (Backx and Marban, 1993, Kim and Clapham, 1989, Yue and Marban, 1988). K_B conductance channels have been hard to characterise in native cells as they are often insensitive to conventional K^+ channel inhibitors as well as lacking defining features of a conventional channel such as a strong-voltage dependence (Goonetilleke and Quayle, 2012).

TREK1 channels are known to be active over a wide range of membrane voltages which are found physiologically. Therefore, they are able to contribute to the membrane potential at both rest and excitation, for example during the repolarisation of an action potential (Goonetilleke and Quayle, 2012). Interestingly, the outward current of TREK1 is larger than its inward current for a given driving voltage. This is a phenomenon known as outward rectification (Patel et al., 1998, Dedman et al., 2009). In a physiological K^+ gradient, creation of a positive charge results in the instantaneous increase in outward K^+ current due to an increased driving force in K^+ ions. However, K^+ current continues to increase over time which is indicative of voltage-gating. K_{2P} channels such as TREK1 lack a voltage-sensor, which is present in other K^+ channels. Deletion of the C-terminal of TREK1 has, however, been shown to remove its voltage-dependant gating (Maingret et al., 2002). It has also been suggested that phosphorylation of the channel at serine 133 (S133) may have an inhibitory effect on TREK1's voltage-dependant gating properties (Dedman et al., 2009, Patel et al., 1998).

4.1.5 TREK1 channel regulation

TREK1 channels have been shown to have relatively low activity under basal conditions (Honoré, 2007, Patel et al., 1998). This activity is increased by numerous influencing factors such as membrane stretch and intracellular acidification (Patel et al., 1998, Honoré, 2007). For example, TREK1 channels are activated by the mechanical deformation of the cell membrane as well as chemical stimuli (Honoré, 2007, Patel and Honoré, 2001). An additional feature

of TREK1 channels is that they are sensitive to lipids e.g. polyunsaturated fatty acids (PUFAs), such as arachidonic acid, and phosphatidyl inositol 4,5 bisphosphate (PIP_2) in the lipid bilayer (Patel and Honoré, 2001, Chemin et al., 2005, Lopes et al., 2005). Inhibition of TREK1 signalling, on the other hand, can be triggered by ligands that are coupled to the G_s and G_q signalling pathways (Patel et al., 1998). Importantly for this work, the inhibitory effects of G_q signalling pathway is most likely due to phosphorylation by PKA (Patel et al., 1998). G_q signalling pathway inhibition is routed via PKC phosphorylation or lack of activating PIP_2 at the membrane (Murbartián et al., 2005, Lopes et al., 2005). Collectively, it has been suggested that TREK1 activity is tightly controlled by several cross-talking signalling pathways.

4.2 Hypothesis and aims

As discussed, POPDC1's functions are modulated by cAMP binding and I hypothesise that PDE4A forms a complex with POPDC1 to regulate its exposure to cAMP under basal conditions. To test this hypothesis, I had the following aims:

- To determine if PDE4A activity and its ability to be phosphorylated by PKA is altered by direct association with POPDC1.

- To develop and test a cell-penetrating peptide that can disrupt the interaction between POPDC1 and PDE4A

- To use such a POPDC1-PDE4 disruptor to investigate whether PDE4 activity regulates Popdc1 binding to TREK1 and whether this in turn affects contractility and formation of action potentials in ARVMs.

4.3 Method

4.3.1 Preparation of ARVM for CellOPTIQ

Left-ventricular (LV) cardiomyocytes were isolated from 12-week-old New Zealand White Rabbits and used in experiments detailed here. To investigate contractility and relaxation, adult rabbit ventricular myocytes were plated on glass bottom microwell dishes (35mm petri dish, 14mm Microwell; MatTek®) and allowed to settle for 2 hours prior to each experiment. Cells were treated with 10μM disruptor peptide or 10μM scrambled peptide for 2 hours at 37ºC prior to measurements being carried out. Images were taken in the 35mm microwell dishes at room temperature.

4.3.2 Action potential imaging

CellOPTIQ® (Clyde Bioscience Ltd; Glasgow, UK) software was used in the collection of high-speed images of contracting single ARVM. This high-powered *in vitro* system allows for the simultaneous measurements of contractility, voltage and calcium in live cells. For this set of experiments, all three parameters were evaluated. Cells were paced with electrodes at 40mV with 20ms duration at a frequency of 1Hz. For each cell a 30 second recording was taken recording at 100 frames per second using a 60x objective lens.

4.3.3 Contractility measurements using ImageJ

Contraction measurements in cardiomyocytes were achieved using measurements of sarcomere length. High-speed (100 frames per second) and high resolution (2048x2048 pixels) video was recorded. Image sampling duration allowed for a minimum of 5 beats to be recorded and subsequently averaged for analysis. Contraction duration (CD_{50}) was recorded, considering both contraction and relaxation. CD_{50} represents the time from 50% contraction to 50% relaxation of the myocyte.

For measurement analysis, the macro programme SarcomereLength created in ImageJ by Dr Francis Burton (University of Glasgow), was utilised. Each stack of images was analysed by manually positioning a linear selection perpendicular to the cell allowing for the capture of isotropic contractions. The line length was

dependent upon cell size and width was kept constant at 50 pixels to reduce any pixel noise.

4.3.4 Fluorescent signal analysis of voltage and calcium

Trace analysis was carried out using CellOPTIQ software. The unfiltered trace was baseline-subtracted, filtered using 3-point, 15 pass filter. The upstroke and repolarisation phases were filtered adaptively to target smoothness and measured by number of curve inflections. Values used in analysis were T_{rise} (upstroke 10%-90% depolarisation) and action potential duration (APD) $_{30,50,75,90}$ values, representing time (ms) from upstroke to various degrees of repolarisation. For example, APD_{50} represents the time from 50% contraction to 50% relaxation. These were plotted to allow visualisation of phase 3 (repolarisation phase).

4.3.5 Analysis

As described in 4.3.3images of contracting ARVM were converted into contraction traces using ImageJ software whereas trace analysis for action potential investigation was conducted using CellOPTIQ software. The measurement of movement and voltage was taken as a trace of contraction or repolarisation (a.u.) over time. Measurements at each interval were presented as a scatter plot with bar.

4.4 Results

4.4.1 Examining PDE4 activity in the presence of POPDC1.

I have provided robust data (Chapter 3) showing a novel interaction between POPDC1 and PDE4A4/5. The next logical step was to investigate the functional role of this novel signalling complex. I attempted this by first looking to see whether the direct interaction of POPDC1 with PDE4A affected the enzyme's PDE activity and regulation. Secondly, I determined whether PDE4 activity controls TREK1 binding to POPDC and thirdly, using a novel POPDC1-PDE4A disruptor peptide, I sought to see what physiological consequences were changed when PDE4A in the vicinity of POPDC1 was displaced.

4.4.1.1 POPDC1 does not alter PDE4As PKA phosphorylation status

PDE4 activity is known to be regulated by phosphorylation in the UCR1 by PKA (Ekholm et al., 1997, Laliberté et al., 2002, Richter and Conti, 2002). Such phosphorylation events in long isoforms, such as PDE4A4, cause their activation through the proposed disruption of the UCR1-UCR2 interaction and the subsequent interaction of UCR2 with the catalytic domain (Richter and Conti, 2002, Laliberté et al., 2002). PKA phosphorylation of PDE4 long forms constitutes a feedback control mechanism that shapes the temporal nature of cAMP responses. To assess whether the interaction with POPDC1 affected the potential of PDE4A4/5 to become phosphorylated by PKA an *in vitro* PKA assay was performed. For the assay, 2µg of PDE4A4-MBP combined with either 2µg of the Popeye domain of POPDC1-GST or GST control were incubated with or without 25 units of active catalytic PKA subunit in phosphor-buffer containing Mg^{2+} and ATP. As mentioned, it is known that the phosphorylation of PDE4A4 by the PKA catalytic subunit causes the activation of the enzyme through increasing its sensitivity to the Mg^{2+} cofactor (Laliberté et al., 2002). Proteins were then tested for phosphorylation status by SDS-PAGE and western blot analysis (Figure 4.3). Probing of blots with a specific phosphoserine antibody that identified the phospho-motif in UCR1 domain of PDE4A4 was undertaken (Figure 4.3 B and C). Additionally, a 'pan' PKA substrate antibody (R-X-X-pS/T) allowed for the effect of POPDC1s presence on PDE4A phosphorylation to be analysed (Figure 4.3 B and C).

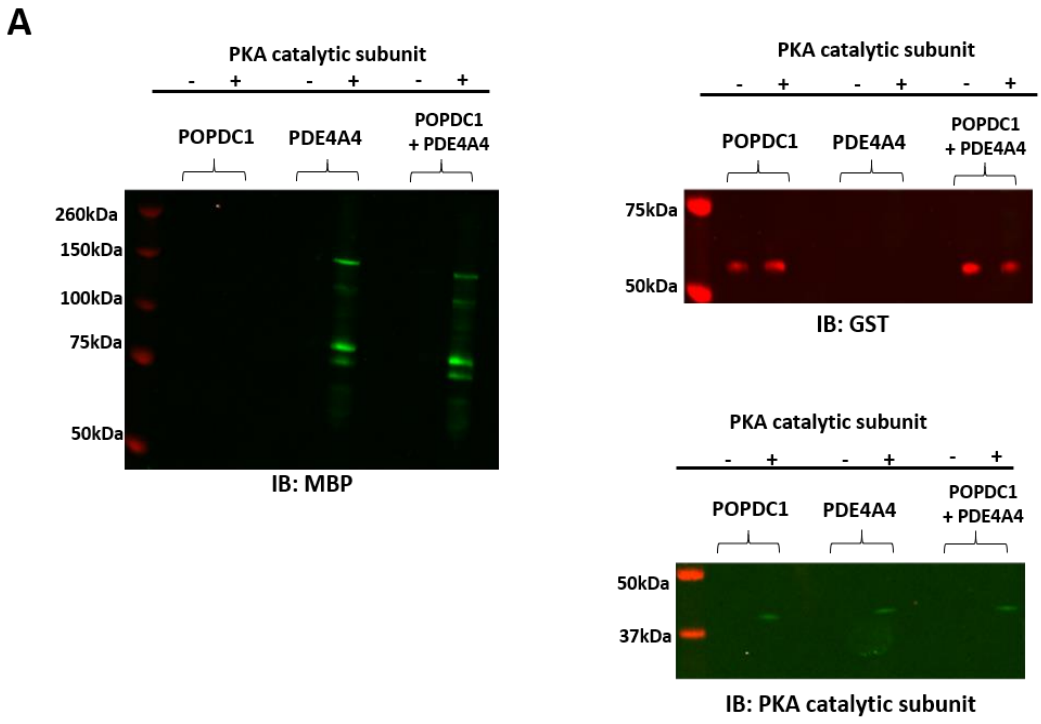
A
PKA catalytic subunit
- + - + - +
POPDC1
PDE4A4
POPDC1 + PDE4A4
260kDa
150kDa
100kDa
75kDa
50kDa
IB: MBP
PKA catalytic subunit
- + - + - +
POPDC1
PDE4A4
POPDC1 + PDE4A4
75kDa
50kDa
IB: GST
PKA catalytic subunit
- + - + - +
POPDC1
PDE4A4
POPDC1 + PDE4A4
50kDa
37kDa
IB: PKA catalytic subunit

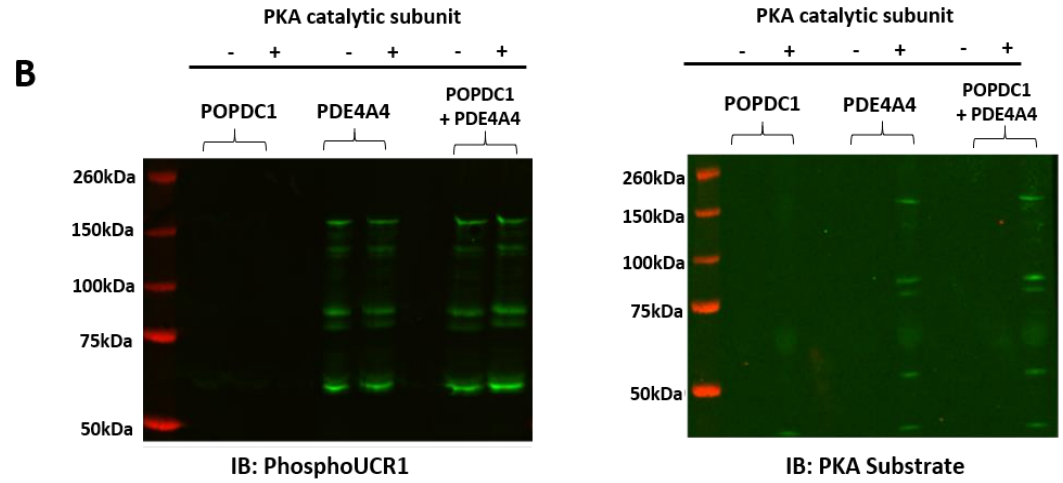
B
PKA catalytic subunit
- + - + - +
POPDC1
PDE4A4
POPDC1 + PDE4A4
260kDa
150kDa
100kDa
75kDa
50kDa
IB: PhosphoUCR1
PKA catalytic subunit
- + - + - +
POPDC1
PDE4A4
POPDC1 + PDE4A4
260kDa
150kDa
100kDa
75kDa
50kDa
IB: PKA Substrate

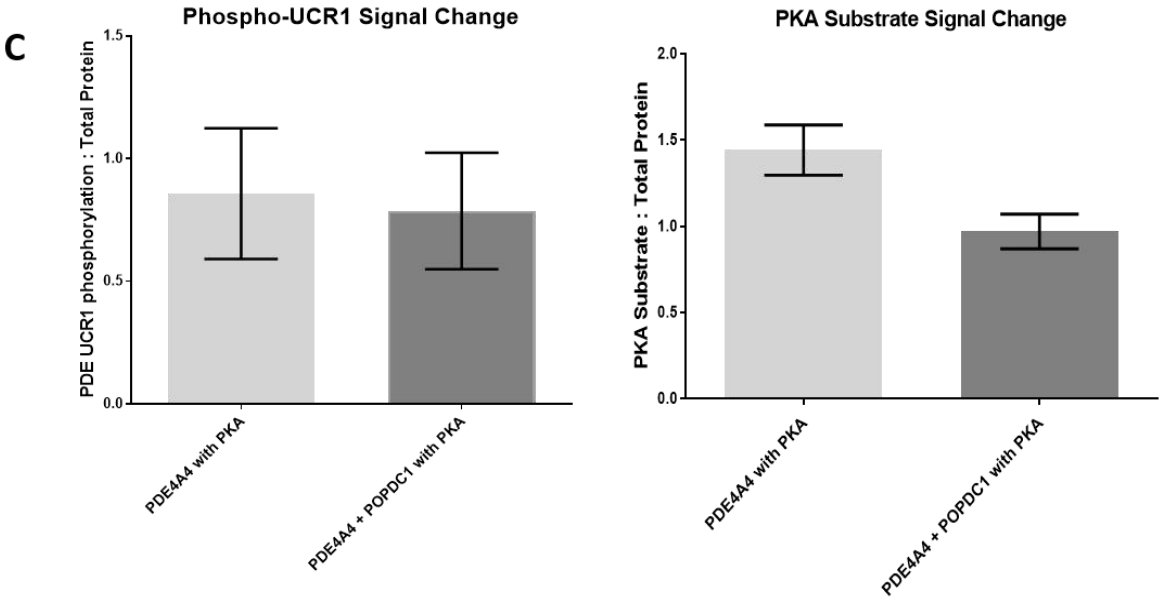
C
Phospho-UCR1 Signal Change
PDE UCR1 phosphorylation : Total Protein
1.5
1.0
0.5
0.0
PDE4A4 with PKA
PDE4A4 + POPDC1 with PKA
PKA Substrate Signal Change
PKA Substrate : Total Protein
2.0
1.5
1.0
0.5
0.0
PDE4A4 with PKA
PDE4A4 + POPDC1 with PKA

Figure 4.3 *In Vitro* PKA Phosphorylation Assay using Recombinant Purified Popeye domain of POPDC1-GST and PDE4A4-MBP. Equal molar concentrations of POPDC1-GST and PDE4A4-MBP were incubated with PKA catalytic subunit. **A** Samples were separated by SDS-PAGE and probed via Western-blotting. Control assays were run without the presence of PKA catalytic subunit. Control blots for MBP (top left), GST (top right) and PKA catalytic subunit (right second panel) were performed to confirm the presence of POPDC1 and PDE4A4. **B** PKA substrate and a specific PDE phospho-UCR1 antibodies were used to detect changes in the level of PDE phosphorylation. **A** and **B** Intensities were calculated using ImageJ and normalised to controls. **C** shows graphs generated using GraphPad Prism presented representing an n of 3, mean ± SEM.

Initially, the identity of each purified protein was checked by immunoblotting for the tag on the recombinant protein. Figure 4.3A (2 gels on top panel) clearly shows the presence of both PDE4A4-MBP and POPDC1-GST. In addition, the amount of active PKA catalytic subunit was evaluated to ensure that all experimental samples contained an equal concentration of active kinase (Figure 4.3, second panel on right). Samples were further probed for phospho-UCR1 (PKA site) (Figure 4.3, left) and pan PKA phospho-substrate antibody to allow observation of the effect of POPDC1 on PDE4A phosphorylation by PKA (Figure 4.3B, right). The top band on each gel, representing PDE4A, were normalised to control blots (GST and MBP). A multitude of bands can be seen in the PDE4A lane as the protein has started to degrade. Changes in the phosphor-UCR1 signal are displayed in the graph on the left in panel C of Figure 4.3 and on the right-hand side the changes identified in pan-PKA substrate signal are depicted. My data clearly suggests that the interaction of PDE4A with POPDC1 does not appear to impact the ability of the enzyme to become phosphorylated by PKA (Figure 4.3C).

4.4.1.2 POPDC1 does not impede the catalytic ability of PDE4A

Given that the presence of POPDC1 does not cause any modulation in the activation of PDE4A through PKA dependent phosphorylation of UCR1, I sought to discover whether there was any impact on its intrinsic catalytic ability. Although PDE4 long forms are activated by PKA phosphorylation, the basal activity of these enzymes is high without modification by PKA. As outlined in the previous chapter, the binding site of POPDC1 is found within UCR1 of PDE4A4 and conversely, the PDE4A binding site in POPDC1 lies in the Popeye domain. This conformation means that the two proteins may cover a large fraction of the other's catalytic domain. To check whether POPDC1's interaction affects PDE4 activity, a PDE assay utilising the chemical shift from the hydrolysis of

radiolabelled 8-[^{3}H]-cAMP to [^{3}H]-5'-AMP to [^{3}H]-adenosine was performed (Marchmont and Houslay, 1980).

To determine the optimum concentration of recombinant purified PDE4A4-MBP to be used in the PDE assay, increasing amounts of PDE4A4-MBP (from 0µg to 10µg) was used in a pilot study. 10ug was selected as the concentration as counts produced were high enough to detect and in the linear range of the assay (Figure 4.4A). Furthermore, to ensure the identity of the purified PDE4, it was necessary to ensure that the PDE4A4-MBP was susceptible to rolipram. As shown in Figure 4.4B, there is almost complete inhibition of PDE4A4s ability to hydrolyse cAMP in the presence of 10mM rolipram confirming the purified protein's identity.

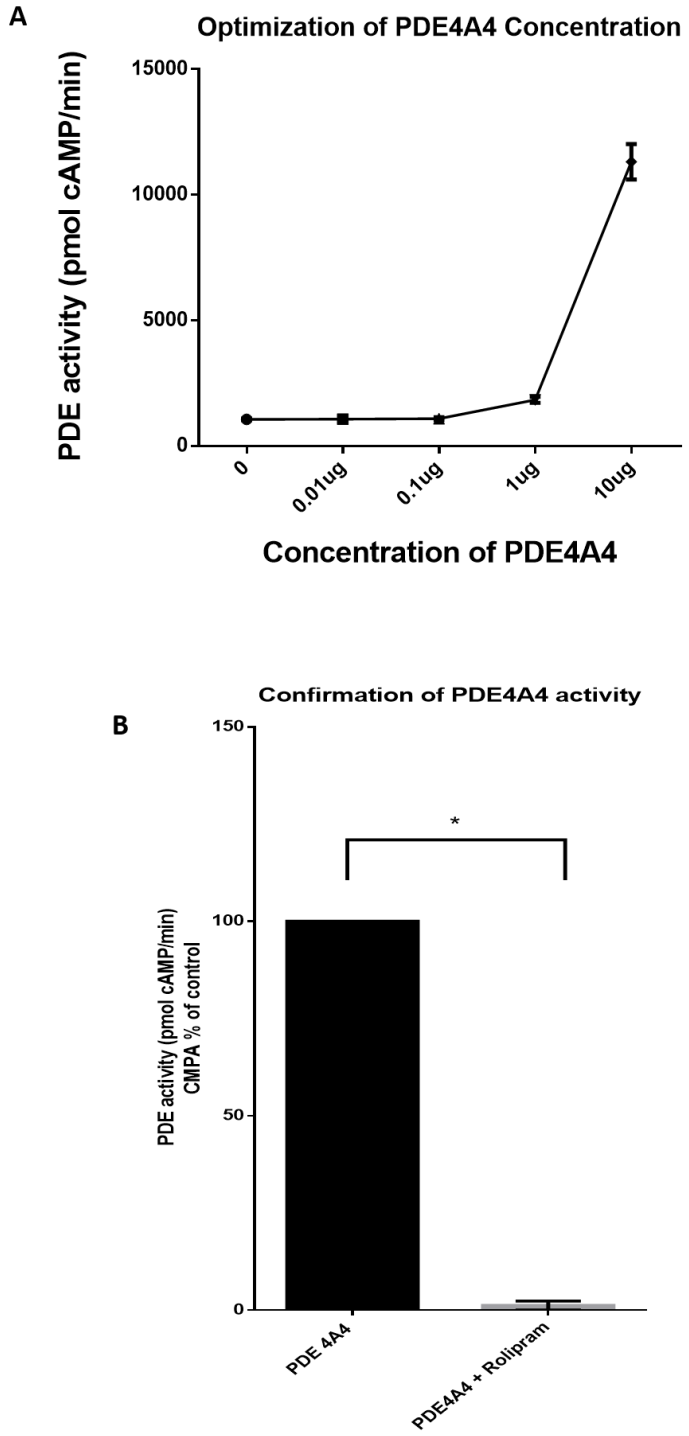

Figure 4.4: PDE4A4-MBP concentration optimization for use in PDE Assay and conformation of PDE4A4-MBP activity. A- Increasing concentrations of PDE4A4-MBP were used in a PDE activity assay to determine a concentration to be used in the experimental assay. **B-** An optimized concentration of PDE4A4-MBP, 10 µg, were used in both the control and experimental PDE activity assays. To confirm the activity of PDE4A4-MBP, samples were exposed to 10 mM Rolipram prior to the PDE activity assay. The hydrolysis of radiolabelled 8-[^{3}H]-cAMP to [^{3}H]-5'-AMP to [^{3}H]-adenosine was measured using a Tri-Carb 2900TR Liquid Scintillation Analyser and results are displayed in pmol cAMP/ min. Graph represents mean ±SEM taken from an n=3.

Using the predetermined concentration of PDE4A4-MBP, a further PDE assay was carried out in the presence of a range of Popeye domain of POPDC1-GST concentrations from 0µg to 40µg. POPDC1 did not appear to have a significant impact on the basal catalytic ability of PDE4A4 at any of the concentrations tested (Figure 4.5). The lack of change in the levels of cAMP hydrolysed by PDE4A provides further support that POPDC1 does not function to modulate the activity of the PDE4 enzyme by inhibition or allosteric activation.

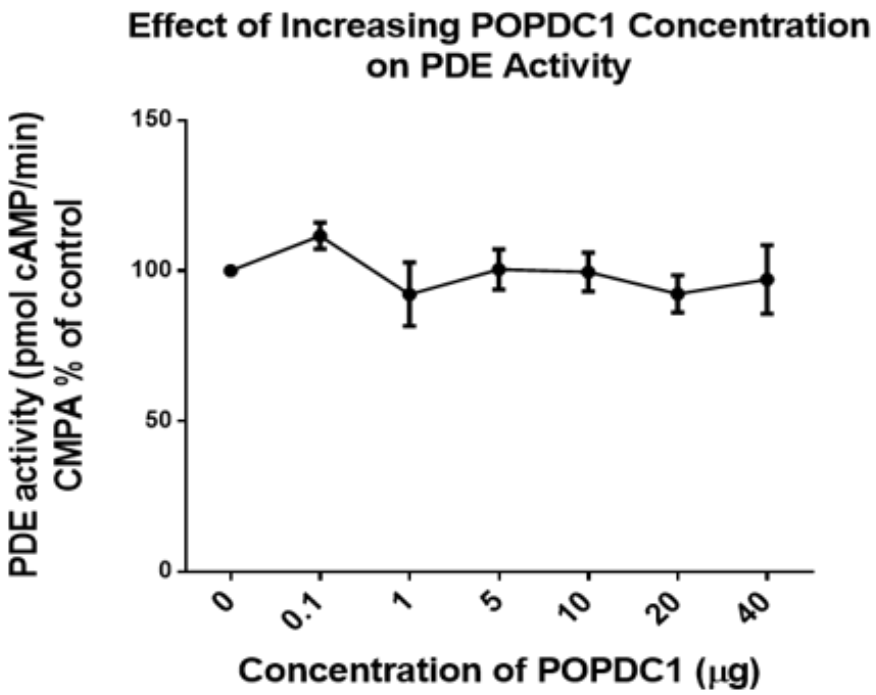

Figure 4.5: Radiolabelled PDE Assay using increasing concentrations of POPDC1. Purified recombinant POPDC1-GST and PDE4A4-MBP were incubated together and subjected to PDE assay. The activity of PDE4A4 was analysed by hydrolysis of an 8-[^{3}H]-labelled cAMP substrate as described in material and methods section 2.10.3. Graphs were determined using GraphPad Prism 6^{TM}. Results are displayed in pmol cAMP/ min and are represented as a mean ±SEM, n=3.

The last caveat investigated was whether the interaction with POPDC1 conveyed any protection to the PDE4 from inhibition by rolipram. Rolipram was among the first generation of selective PDE4 inhibitors and was initially produced as a putative antidepressant agent (Wachtel, 1983). The compound is directed against the active site of the PDE, actively competing with cAMP, and exhibits a 100-fold selectivity for PDE4 over the other isoforms. It is known that nearly all PDE4s exist in two conformations; a high-affinity rolipram binding domain and a

low-affinity rolipram binding domain (Souness et al., 2000). As such, equal concentrations of both recombinant POPDC1-GST and PDE4A4-MBP proteins or PDE4A4-MBP and GST alone, which functioned as a control assay, were exposed to increasing concentrations rolipram. No significant differences between the GST control assay and the experimental POPDC1 were identified (Figure 4.6). POPDC1 did not confer any protection against rolipram's inhibitory actions at any concentration. This data suggests that there are no deleterious conformational changes that occur in PDE4A when it binds directly to POPDC1. All the data thus far in this chapter supports the concept that it is PDE4 activity that will likely alter POPDC1 function and not *vice versa*.

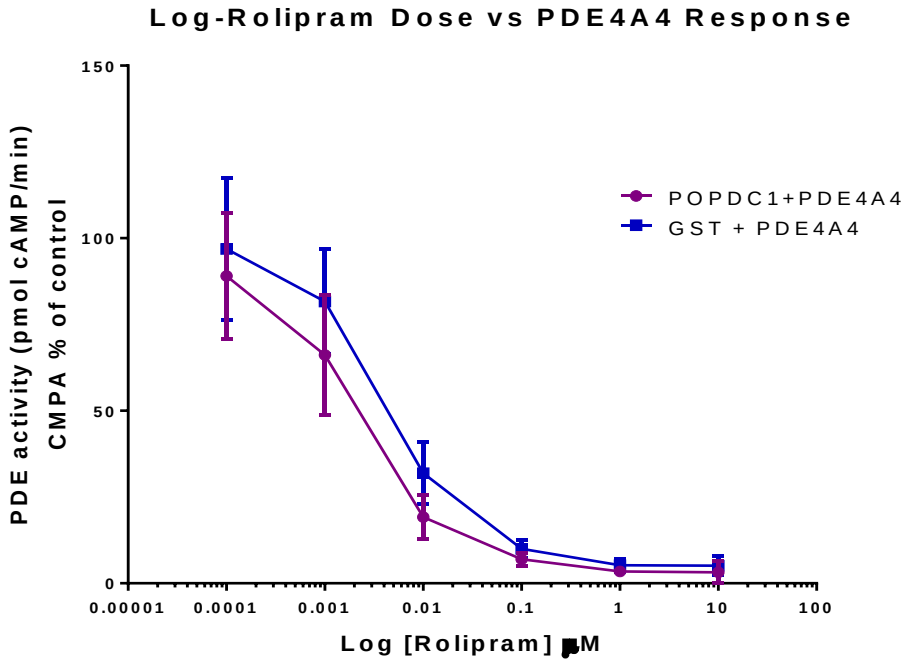

Figure 4.6: Dose response curve for radiolabelled PDE Assay using increasing concentrations of Rolipram. Purified recombinant POPDC1-GST and PDE4A4-MBP were incubated with increasing concentrations of Rolipram (blue). An identical assay was carried out for the control with POPDC1-GST substituted for GST alone (purple). The activity of PDE4A4 was analysed by the hydrolysis of an 8-[^{3}H]-labelled cAMP substrate as described in material and methods section 2.10. Graphs were determined using GraphPad Prism 6^{TM}. Results are represented as a mean ±SEM, n=3.

4.4.2 Development of a disruptor peptide

Peptide array data from the last chapter determined the identity of a 25mer POPDC1 sequence to which PDE4A bound. This information influenced the development and production of a cell-penetrating disruptor peptide that could possibly disturb PDE4A from the vicinity of POPDC1. Conceptually, displacement of the small "pool" of PDE4A that localises with POPDC1 should leave global PDE4 activity unchanged but should have a large and measurable effect on POPDC1 function. Perhaps cAMP in the vicinity of POPDC1 would rise following disruptor peptide treatment leading to the dissociation of POPDC1 from TREK1 (Froese et al., 2012). As the same PDE isoform may possess many interaction partners and function at other microdomains within the cell, the disruptor peptide would only target the specific microdomain where that interaction occurred (reviewed in (Omori and Kotera, 2007)). The use of a peptide such as this adds a layer of specificity beyond the use of any dominant negative PDE4A construct or siRNA as both techniques target the whole population of a single isoform in all its locations. The cell permeable disruptor peptide was based on the 25mer sequence identified from POPDC1 peptide arrays and contained the sequence: TLKKGQTYAAEDKTSVDDRLSILLK. A scrambled peptide was also produced as a control, containing the same amino-acid residues in a random order: TTLYTDSSVLKGKRLQDKEKALADI. This sequence was checked by BLAST to ensure it was not present in another protein. Both peptides had stearate group conjugated at the N-terminal to allow cell penetration. This technique has been used successfully with other peptides that target specific PDE4 pools (reviewed in (Wills et al., 2017)). To determine whether the disruptor peptide was active in hampering the interaction between POPDC1 and PDE4A, co-IPs experiments were carried out. HEK293 cells transfected with POPDC1-myc and PDE4A5-VSV were treated with either 10μM disruptor peptide (fifth and sixth lane of Figure 4.7) or scrambled peptide (last two lanes of Figure 4.7) for 2 hours prior to harvesting. Co-immunoprecipitations were performed from cellular lysates using myc conjugated Protein G beads to precipitate POPDC1. Control experiments were carried out using a 'mock' transfected lysate, which contained no transfected POPDC1-myc or PDE4A4-VSV (first and second lane of Figure 4.7) as well as transfected HEK293 cells treated with DMSO vehicle control instead of peptide (third and fourth lane of Figure 4.7).

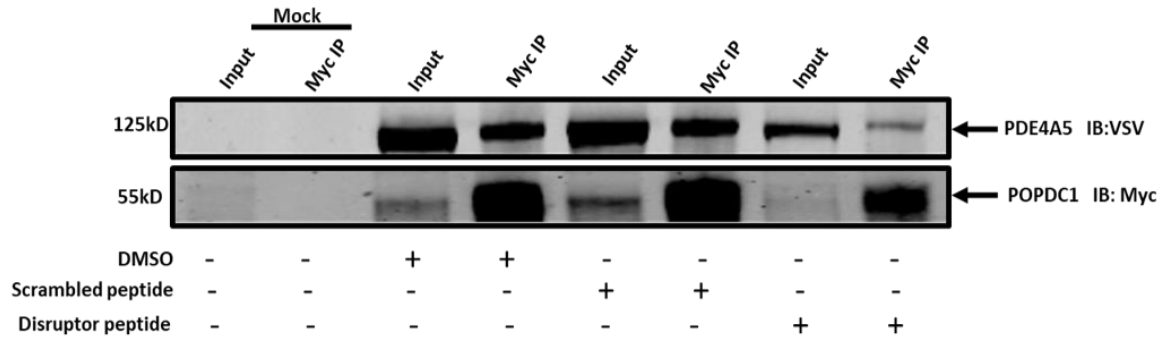

Figure 4.7: Disruptor Peptide Treatment Co-immunoprecipitations. HEK293 cells were transiently transfected with Popdc1-myc and PDE4A5-VSV for 24 hours prior to a two-hour treatment with 20 µM Disruptor peptide. The disruptor peptide was designed to be targeted to novel binding site. Western blot analysis was performed using VSV and myc antibodies that are specific for the tag on both proteins. The presence of DMSO, scrambled peptide or disruptor peptide is noted by + for present or - for not present noted below the gel. Figure displayed is representative of an n=3.

As depicted in lane 5 and 6 of Figure 4.7, the scrambled peptide does not change in the level of PDE4A5 that is precipitated with Popdc1. However, treatment with the disruptor peptide (lanes 7 and 8 of Figure 4.7) clearly shows the reduced PDE4A5 levels that co-immunoprecipitated with Popdc1 confirming the activity of the cell penetrating peptide in disrupting the Popdc1-PDE4A5 complex. The disassembly of the Popdc1-PDE4A5 interaction was further validated using PLA in transiently transfected HEK293 cells. Cells remained untreated (Figure 4.8 panel B), treated with 10µM scrambled peptide for two hours (Figure 4.8 panel C), or 10µM disruptor peptide for two hours (Figure 4.8 panel D) prior to the PLA protocol being carried out. Mean fluorescent intensities were calculated using ImageJ and displayed on the graph in Figure 4.8 alongside the results of a one-way ANOVA. Results show no reduction in the PLA signal in (E) in the scrambled peptide group when compared to untreated cells. A one-way ANOVA identified the significant difference in PLA signal between the untreated group and scrambled peptide group compared with the disruptor peptide treated group (one-way ANOVA; $p<0.0001$). This dramatic reduction in PLA signal agrees with the results seen in co-immunoprecipitation experiments and provided conformation that the disruptor peptide was able to attenuate formation of the Popdc1-PDE4A interaction.

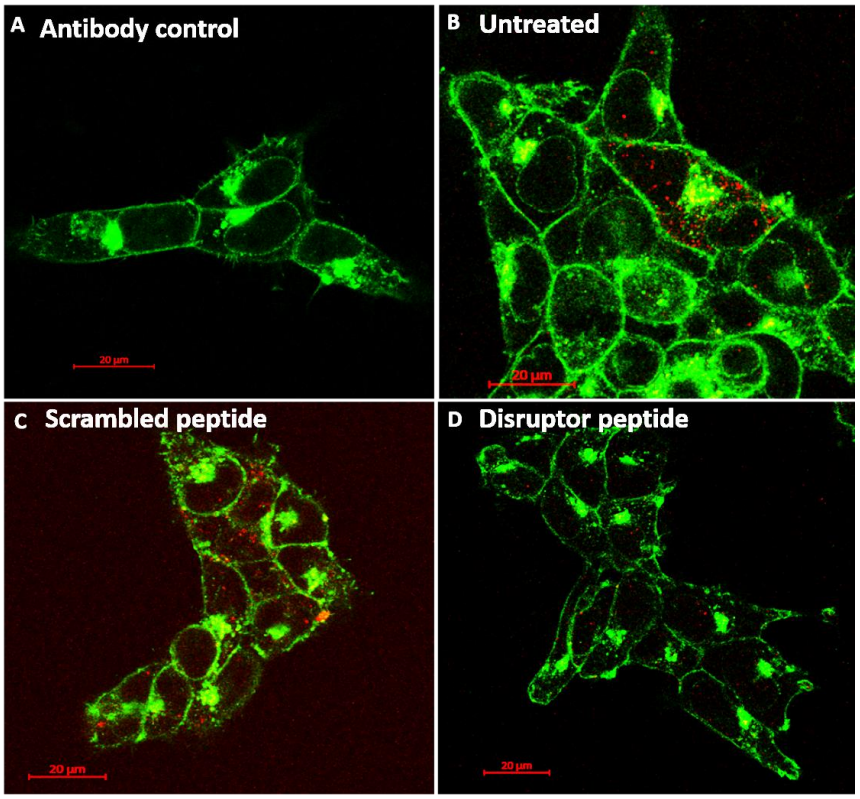

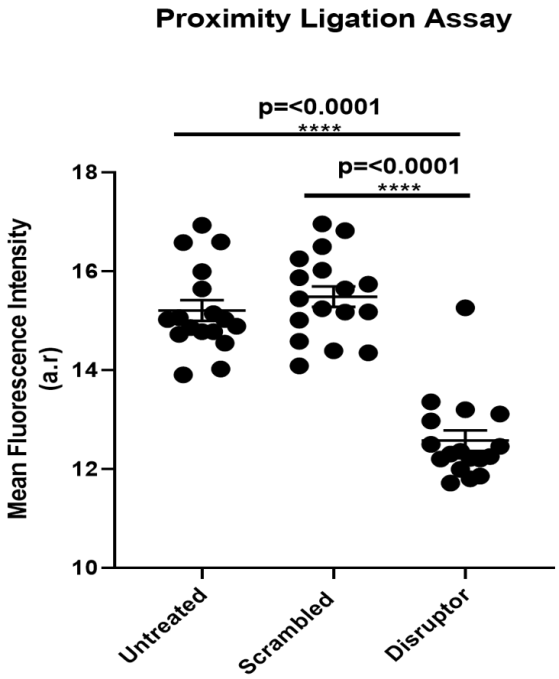

Figure 4.8: Disruptor peptide treatment of transiently transfected HEK293 cells analysed using Proximity Ligation Assay. HEK293 cells were transiently transfected with Popdc1-myc and PDE4A5-VSV. As a control, HEK293 cells were left untreated prior to fixing, representative example in panel. For all conditions, myc and VSV antibodies were used to detect Popdc1 and PDE4A5 respectively. **B.** Panel **C** depicts the 10µM scramble peptide treated cells where panel **D** are cells treated with 10µM disruptor peptide. Positive PLA signal is detected when the proteins tagged are less than 40nm apart. Negative controls were performed where the PLA kit was applied directly to the fixed cells to ensure no off-target staining, panel **A**. Scale bars shown represent 20µM. Mean immunofluorescence intensity were calculated from n=3 with 17 cells counted per experiment per condition using ImageJ and significance was calculated using a one-way ANOVA with Tukey's post-hoc analysis, displayed using GraphPad. P values given on graph.

Further confirmation of the efficacy of the disruptor peptide was sought against endogenous Popdc1-PDE4A interactions in NVRM. The same conditions used for the model cell line HEK293 were utilised for NRVM. Secondary only controls (Figure 4.9, panel A) provided evidence that no background staining could be detected. Much as in HEK293 cells, NRVM treated with the disruptor peptide displayed significantly reduced PLA signal (Figure 4.9, panel D) in comparison to untreated cells (Figure 4.9, panel B; one-way ANOVA, $p<0.0001$) and to the scrambled peptide condition (Figure 4.9, panel C; one-way ANOVA, $p<0.0001$). The confirmation of the disruption of the endogenous Popdc1-PDE4A interactions has further confirmed the binding site identified in the previous chapter and is supports the notion that the disruptor peptide can be used in physiological experiments in NRVMs.

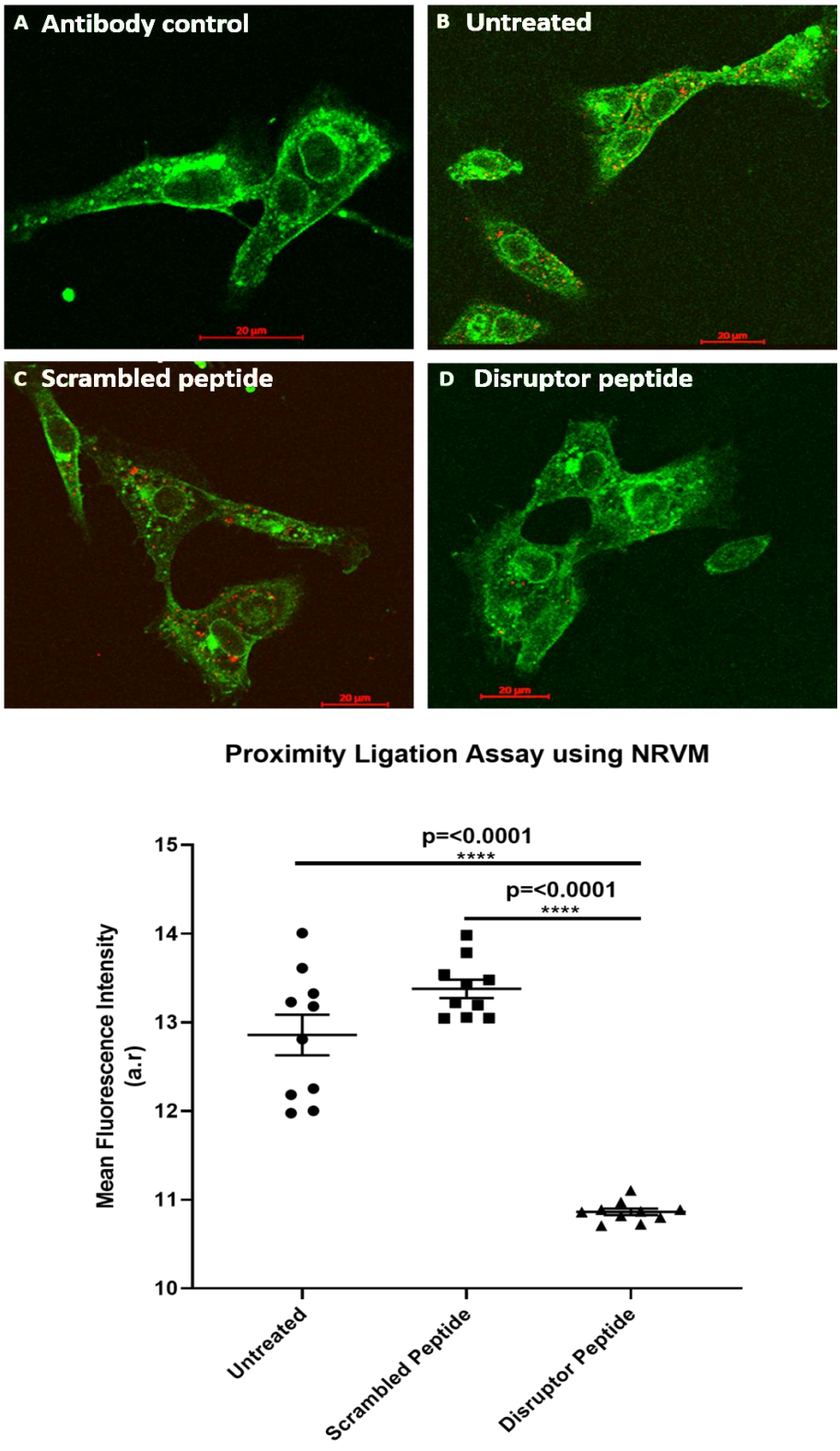

Figure 4.9: Disruptor peptide treatment of NRVM cells analysed using Proximity Ligation Assay. As a control, HEK293 cells were left untreated prior to fixing, representative example in panel. BVES (POPDC1) and Pan4A antibodies were used to detect Popdc1 and PDE4A respectively. **B.** Panel **C** depicts the 10µM scramble peptide treated cells where panel **D** are cells treated with 10µM disruptor peptide. Positive PLA signal is detected when the proteins tagged are less than 40nm apart. Negative controls were performed where the PLA kit was applied directly to the fixed cells to ensure no off-target staining, panel **A**. Cells presented are representative of a n=10 experiments. Scale bars shown represent 20µM. Mean immunofluorescence intensity were calculated using ImageJ and significance was calculated using a one-way ANOVA with Tukeys post hoc analysis, displayed using GraphPad. P values given on graph.

4.4.3 Disrupting the interaction between POPDC1 and PDE4A modulated the POPDC-TREK1 interaction

Froese and colleagues provided evidence to suggest that the interaction between POPDC1 and the two-pore potassium channel TREK1 is modulated by cAMP (Froese et al., 2012). Using a bimolecular FRET sensor that consists of POPDC1-CFP and TREK-1-YFP it was revealed that under conditions of high cAMP the proteins disassociated as a result of the direct allosteric effect of cAMP binding to POPDC1. Addition of either isoproterenol or forskolin to generate an increase in cellular cAMP resulted in a rapid recline in the YFP/CFP ratio. To confirm that this was in fact due to the ability of POPDC1 to bind cAMP, a cAMP binding deficient POPDC1^{D200A} mutant protein was used in conjunction with isoproterenol treatment. Results gained from these FRET experiments showed that the interaction between the two proteins is not lost if POPDC1 is unable to bind to cAMP. It can be therefore be hypothesised that the binding of cAMP to POPDC1 results in a conformational change lessening its interaction with TREK1. We sought to determine whether PDE4A had an indirect role in regulating this interaction via its local control of cAMP levels in the vicinity of POPDC1. HEK293 cells stably expressing PDE4A4 were transfected with the two described bimolecular FRET probes. The cells were left untreated (Figure 4.10, top two panels), treated with 25μM forskolin (Figure 4.10 middle two panels) or treated with 10μM of the PDE4 specific inhibitor, rolipram, (Figure 4.10 last panel). As expected, treatment with a saturating dose of the AC activator (forskolin, 25μM) lead to a significant reduction in the FRET ratio (Figure 4.10 graph; student's t-test, p=0.0151)(Froese et al., 2012). This reduction represents the dissociation between POPDC1 and TREK1. To determine whether this effect could be produced by the inhibition of PDE4 directly, cells were treated with rolipram (10μM). Interestingly, there was an even greater reduction in the FRET ratio after rolipram compared to that of forskolin (Figure 4.10 graph; student's t-test, p=0.0083) suggesting that the PDE4A tethered to POPDC1 had a greater influence on POPDC1 activity than a large increase in cAMP produced by forskolin. Identifying that the direct inhibition of PDE4 could result in the modulation of POPDC1-TREK1 complex is the first indication of a molecular regulation of POPDC1 by a PDE.

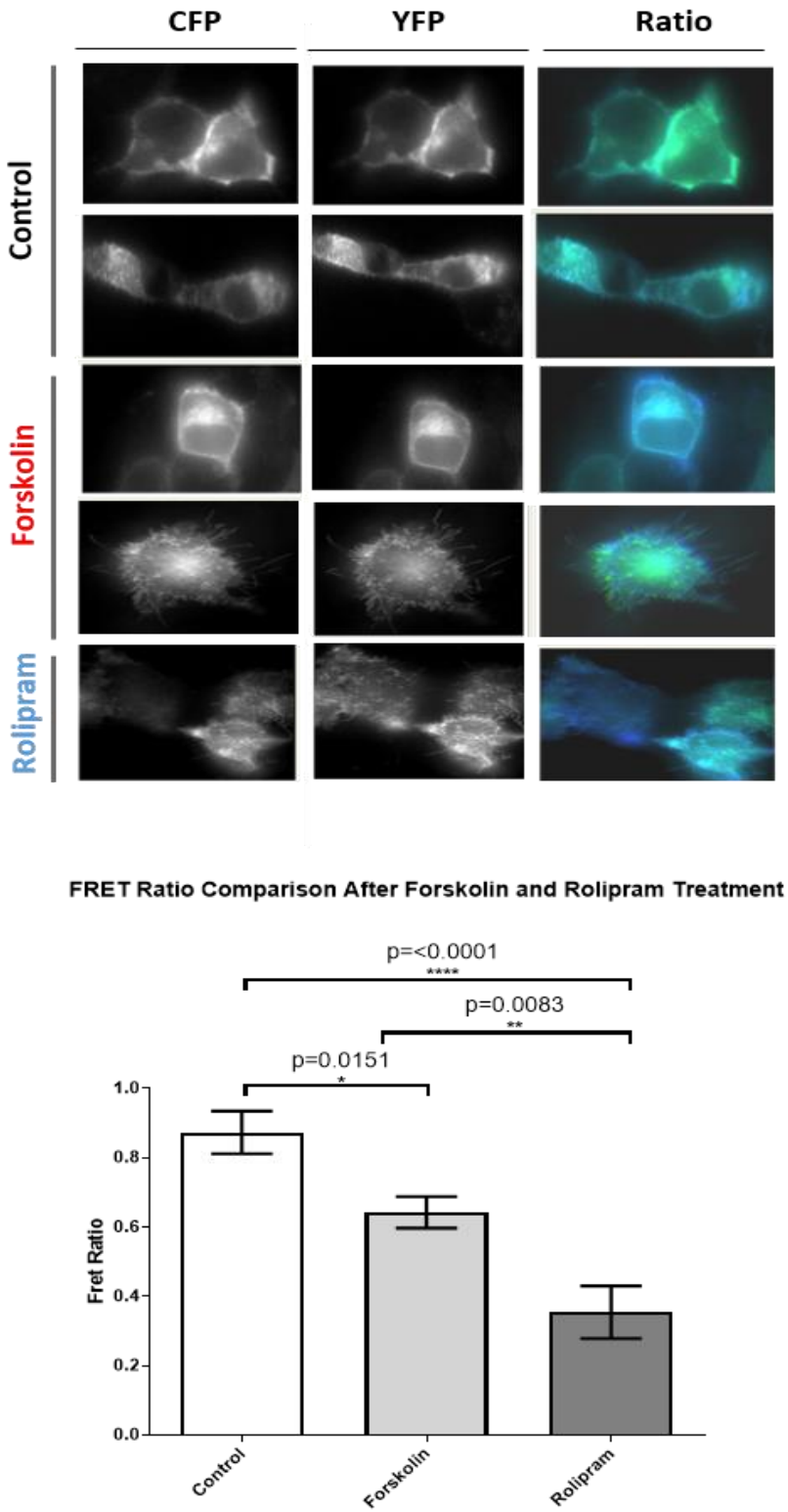

Figure 4.10 Fluorescence Resonance Energy Transfer (FRET) Microscopy using HEK293 PDE4A4 stable cells transiently transfected with POPDC1-CFP and TREK1-YFP. Static measurements were taken from cells prior to the addition of either forskolin or rolipram. Measurements were collected every 5 seconds for a total of 300 seconds per condition. Quantification of the mean FRET ratio change in control, 25 µM forskolin and 10 µM rolipram treated cells. The CFP column represents the POPDC1-CFP signal, the YFP column represents the TREK1-YFP signal while the final column shows the ratio between the two fluorphores. Results represented as mean ± SEM, control n=9, forskolin n=15, rolipram n=15 per experiment (n=3). Significance was evaluated using a one-way ANOVA with Tukeys post-hoc analysis, ** p=<0.005, ***p=0.001, compared to control.

Through the direct inhibition of PDE4, the interaction between POPDC1 and TREK1 was reduced dramatically, however, rolipram is a panPDE4 inhibitor and cannot selectively inhibit PDE4A compared with other sub-families (PDE4 B,C,D) (Bolger et al., 1993, Cheng et al., 1995, Müller et al., 1996). Therefore, to confirm that the disruption of the POPDC1-TREK1 complex was specifically due cAMP microdomains controlled by localised PDE4A activity, further FRET experiments were carried out using HEK293 PDE4A4 stably expressing cells treated with the cell penetrating disruptor peptide (used in Figure 4.7 and Figure 4.8). Static measurements were collected at 5 second intervals for 300 seconds. Background fluorescence was subtracted from the CFP and YFP intensities and mean subtracted intensities calculated for POPDC1-CFP and TREK1-YFP probes. Both the untreated group (Figure 4.11, graph A) and scrambled peptide group (Figure 4.11, graph B) show no significant deviation in the CFP and YFP intensities confirming that POPDC1 and TREK1 are interacting as expected. In the disruptor peptide group (Figure 4.11, graph C), there is a distinct change in the CFP and YFP intensities shown on the graph. This separation of the two probes correlates to the distance between the two proteins in the cell meaning that the addition of the peptide has broken the POPDC1-TREK1 interaction or has prevented it from forming. When the FRET ratio of the three conditions were analysed using a one-way ANOVA (Figure 4.11, panel D), a significant reduction can be observed in the disruptor peptide group compared to the other two conditions (one-way ANOVA with multiple comparisons $p=0.001$). Given the difference found, post-hoc analysis was used to identify that there was a significant change between the scrambled peptide and the disruptor peptide group (post-hoc analysis between scrambled and disruptor peptide groups $p=0.024$) (Figure 4.11, panel D).

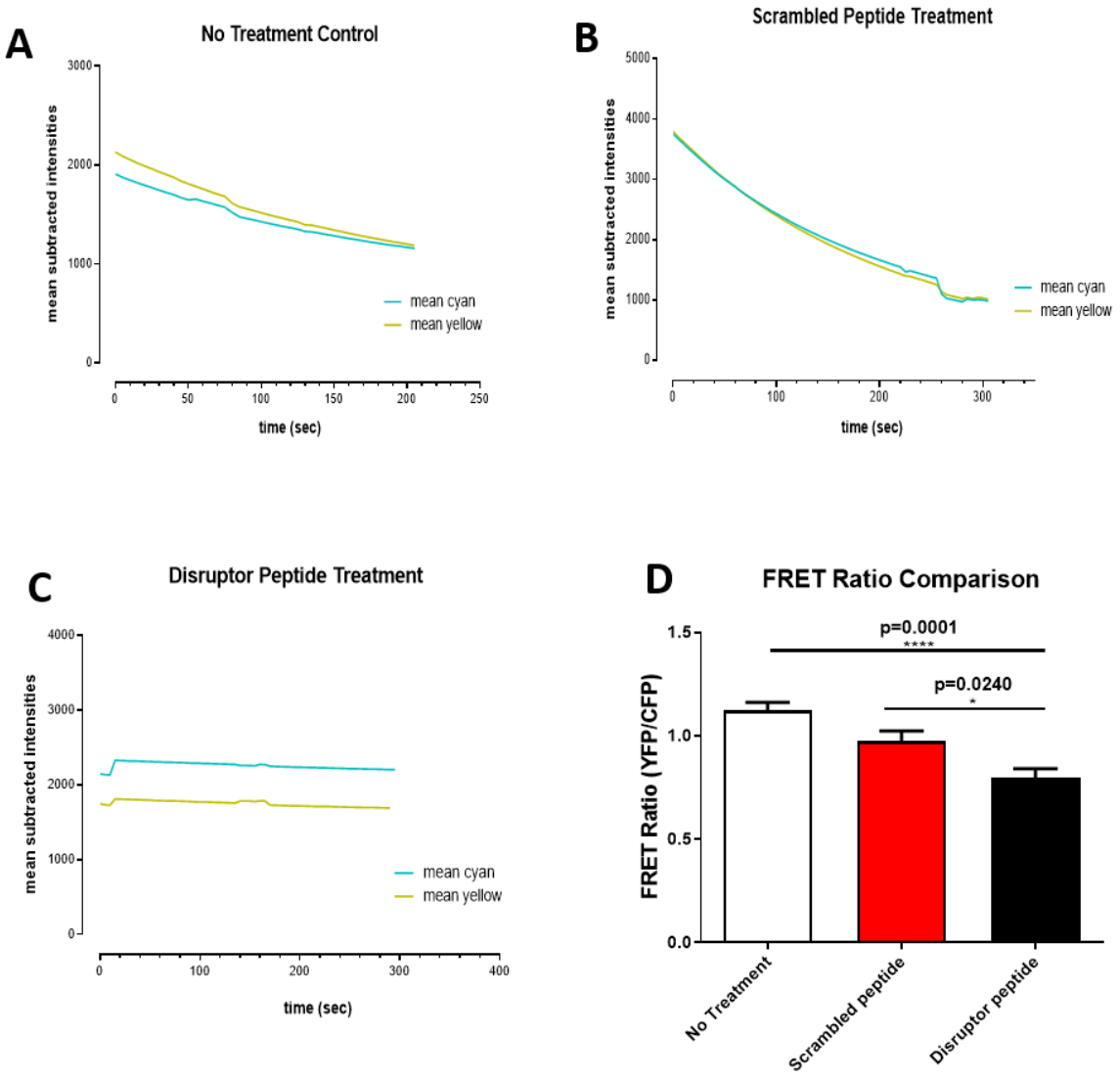

Figure 4.11: Fluorescence Resonance Energy Transfer (FRET) Microscopy using HEK293 PDE4A4 stable cells transiently transfected with POPDC1-CFP and TREK1-YFP treated with disruptor peptide. Quantification of the mean FRET ratio change in control (panel A), 25 µM forskolin (panel B) and 10 µM rolipram (panel C) treated cells. Measurements were collected every 5 seconds for a total of 300 seconds per condition. Background fluorescence was subtracted from mean intensities and is plotted as mean subtracted intensities. Results represented as mean ± SEM, untreated n=11, scrambled peptide n=11, disruptor peptide n=20 per experiment (n=3). A one-way ANOVA with Tukey's post-hoc was carried out and p values are presented on the graphs.

4.4.4 Disrupting the Popdc1-PDE4A complex changes action potential of cardiac myocytes but not contraction.

Having shown that the disruptor peptide prevents the formation of both the Popdc1-TREK1 interaction and the Popdc1-PDE4A interaction, the next rational step was to investigate the changes in functional output in endogenous cells. Utilising CellOptiq® (Clyde Biosciences ltd; Glasgow, UK) the changes in action potential formation in adult rabbit ventricular myocytes following treatment with the scrambled or disruptor peptide were measured. Subsequent evaluation of action potential parameters would allow for evaluation of the functional effects of the PDE4A pool that associates with Popdc1. These experiments were carried out in cells which were paced at 1Hz at baseline conditions, as well as under conditions of 10μM scrambled or 10μM disruptor peptide treatment. Measurements at four points were collected at a percentage of repolarisation (Figure 4.12) and compared (Figure 4.13)

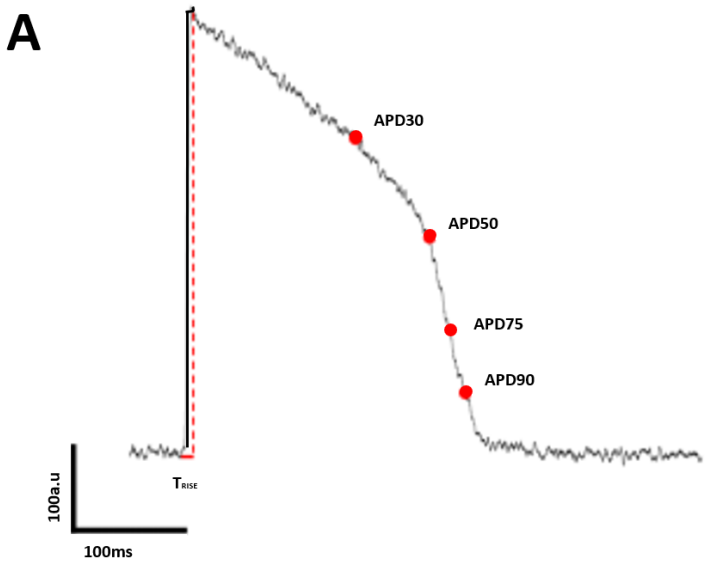

Figure 4.12 Trace of an action potential with noted measurement points. The measurements are plotted as a trace of repolarisation (a.u) over time (ms). The APD measurements were taken throughout the repolarization phase at 30%, 50%, 75% and 90% repolarisation. (Image taken from (Lachaud, 2019)).

No time extensions were seen at any percentage of repolarisation for the scrambled peptide in comparison to the untreated group (Figure 4.13). However,

there is a significant elongation of the repolarisation phase at APD_{30} (Figure 4.13, panel A), APD_{50} (Figure 4.13, panel B), APD_{75} (Figure 4.13, panel C), and APD_{90} (Figure 4.13, panel D) in the disruptor peptide treated cardiomyocytes in comparison to both control groups (one-way ANOVA, post-hoc: Tukey's multiple comparison $p<0.0001$). The differences in the four action potential parameters indicates that the action of the disruptor peptide may be due to the alteration of the repolarising current of a K^+ channel, potentially TREK1.

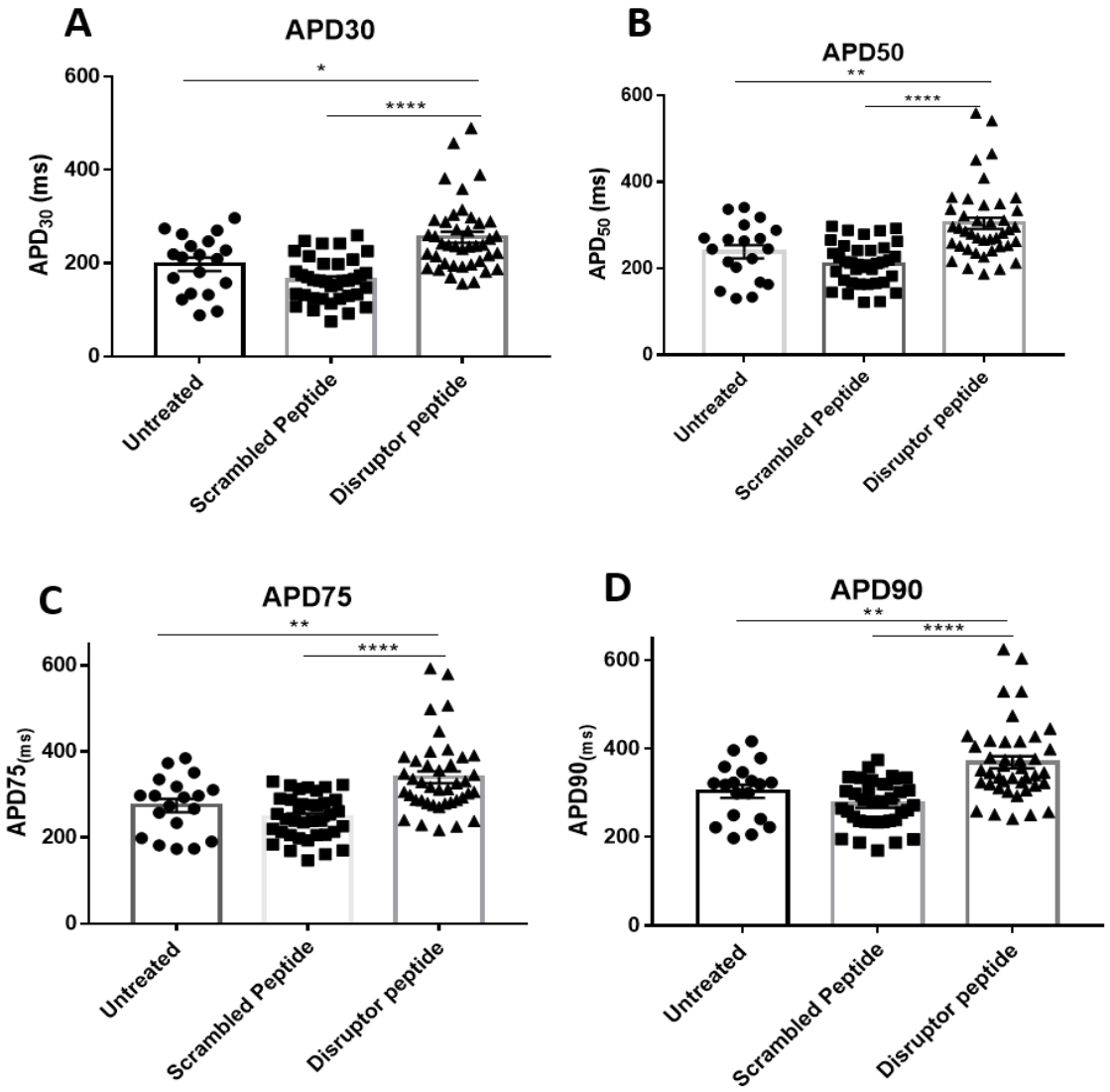

Figure 4.13: CellOptiq measurements of action potential depolarisation in ARVM. Measurements were collected from 4 points during the repolarisation phase: (**A**) APD_{30}, (**B**) APD_{50}, (**C**) APD_{75}, and (**D**) APD_{90} for each cell and displayed on scatter plot graphs with bars ± SEM. Three conditions were used; untreated, 10µM scrambled peptide, or 10µM Disruptor peptide. Untreated cells, n=19, scrambled peptide n=37 and disruptor peptide n=42 cells. One-way ANOVA with Tukey's post-hoc analysis, performed using GraphPad Prism ™. ****$p<0.0001$, **$p<0.01$. (Experiments carried out with the help of Ms Sara Dobi, University of Glasgow).

Frequently, changes in action potential are met with changes in contraction profiles (Pinnell et al., 2007). As such, we sought to determine whether the changes in action potential correlated with a change in contractility of the cardiomyocytes. Using the parameter, contraction duration 50 (CD_{50}), the time between 50% upstroke and 50% downstroke is determined, meaning that both contraction and relaxation are considered (Figure 4.14).

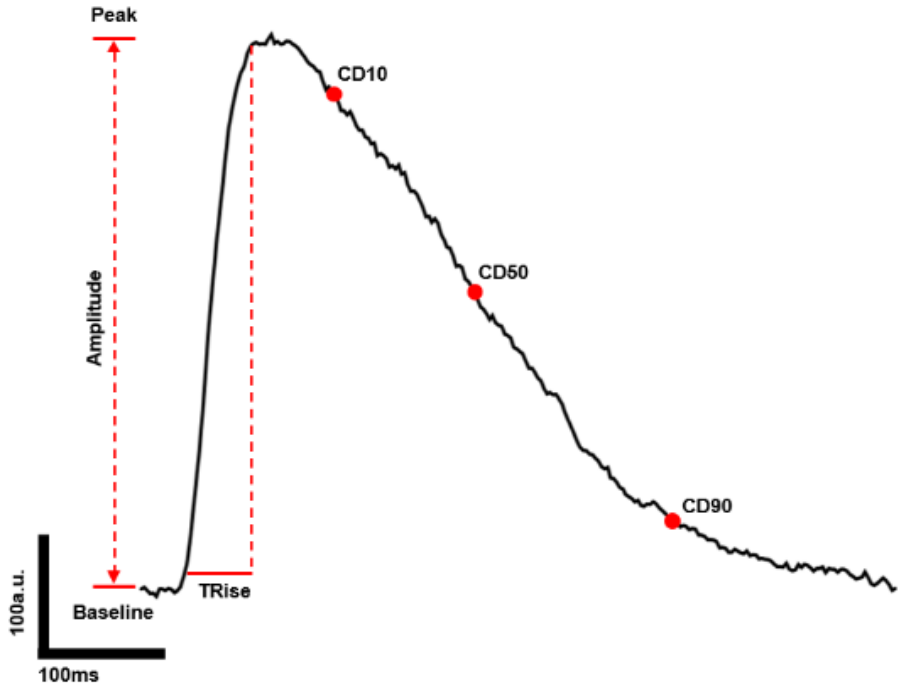

Figure 4.14 Example calcium transient recorded parameters from CellOptiq. Baseline shows the resting diastolic Ca^{2+} with the peak depicting the maximum fluorescent value i.e. the systolic calcium peak. The TRise is the time (ms) from baseline to the maximal calcium peak. The decay of this peak was measured at only CD_{50} which is represent the time take from 50% upstroke to 50% downstroke. (Image take from (Lachaud, 2019)).

In the same trend as APD measurements, there was no alteration between the CD_{50} of the scrambled peptide cells in comparison to the untreated control cells (Figure 4.15). However, treatment with the disruptor peptide also resulted in no significant changes in CD_{50} time compared to the two control conditions (Figure 4.15). So, although action potentials are elongated, this did not manifest as an observable change in myocyte contractility.

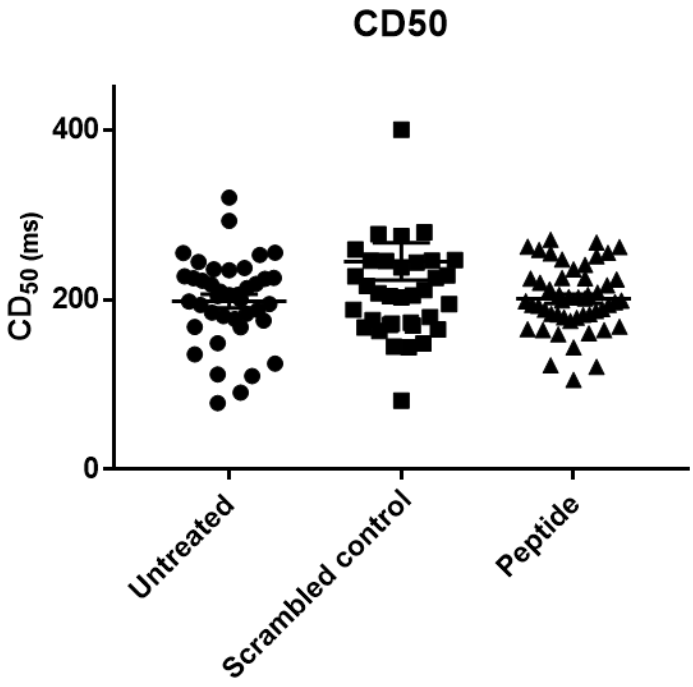

Figure 4.15 Contraction duration at 50% contraction and 50% relaxation measurements. CD50 is the time (ms) from 50% upstroke to 50% downstroke, taking into account both contraction and relaxation. Adult rabbit ventricular myocytes were treated with 10µM scrambled peptide or 10µM disruptor peptide and incubated for 2 hours prior to imaging. Each point represents the mean value from one cell. Untreated cells, n=19, scrambled peptide n=37 and disruptor peptide n=42 cells. One-way ANOVA with Tukey's post-hoc analysis, performed using GraphPad Prism ™. (Experiments carried out with the help of Ms Sara Dobi, University of Glasgow).

4.5 Discussion

4.5.1 POPDC1 does not impede the function of PDE4A

In this chapter, I have shown that POPDC1 does not have an impact on the function of PDE4A either through its activation by PKA (Figure 4.3) or its hydrolytic activity (Figure 4.5). This is not surprising as with all other cAMP effector proteins that interact with PDEs (apart from itself in a dimer), the only one to have an effect on the activity of PDEs is PKA (Moorthy et al., 2011). Upon the activation of PKA by elevated cAMP levels, the binding of the PKA Riα subunit to the PDE causes its catalytic activation (Moorthy et al., 2011). The PKA catalytic subunit also phosphorylates PDE4 long forms in the UCR1 region promoting activation (MacKenzie et al., 2002, Byrne et al., 2015, Houslay and Adams, 2010). As such, it is hypothesised that PDE4A modulates POPDC1 by altering the cAMP gradient in its vicinity. As previously mentioned, POPDC1 is a known cAMP effector protein that undergoes a proposed conformational change when it is bound to cAMP (Froese et al., 2012). The formation of the POPDC1/PDE4A complex may control POPDC1's function by various means and this may be considered alongside the literature available at present which proposes models by which POPDC1 may function. Currently, there are four proposed working models for the role of POPDC1 in cAMP pathways (Figure 4.16). The first working model which has been proposed is the 'cargo model' (Figure 4.16A) which postulates that cAMP influences POPDC1's role in modulating membrane expression of interaction partners. The means by which POPDC1 modulates vesicle trafficking and membrane trafficking of proteins, such as cav3, is not fully understood but it can be hypothesised that PDE4A would control this process through the shaping of the localised cAMP gradient (Benesh et al., 2013, Hager et al., 2010, Alcalay et al., 2013, Smith et al., 2008). The 'switch model' (Figure 4.16B) shows the binding of cAMP to POPDC1 leads to a direct change in the activity of an interacting protein such as TREK1. As mentioned, under conditions of high cAMP, the TREK1/POPDC1 complex is reduced (Froese et al., 2012). Therefore, association with PDE4A would reduce the elevated cAMP to basal levels in the POPDC1 microdomain allowing for the POPDC1/TREK1 complex to reform. The third mode to be offered is the 'shield model' (Figure 4.16C). This model further builds on the switch model and hypothesises that cAMP binding to the Popeye domain may drive indirect

downstream effects (Brand and Schindler, 2017). In its unbound state POPDC1 would function as a shield to block other proteins from being accessed by kinases and this protection would be lost with cAMP binding to the Popeye domain. How this model would result in the modulation of downstream processes remains unclear however, in this scenario PDE4 could be proposed to function in order to return that protection by removing bound cAMP. Lastly, the 'sponge model' (Figure 4.16D) hypothesises that POPDC1 binds cAMP in order to reduce the local activation of other proteins in the cAMP pathway, such as PKA. This takes into account the abundant levels of POPDC1 in cardiac and skeletal muscle (Brand and Schindler, 2017). A lowering of *POPDC1* expression, such as in patients with missense mutations, would result in an increase in free cAMP and therefore lead to a sustained activation of other cAMP effector proteins (Schindler et al., 2016b). In this scenario PDE4A would function to prevent cAMP from binding POPDC1 resulting in a greater reduction in cAMP effector protein activation.

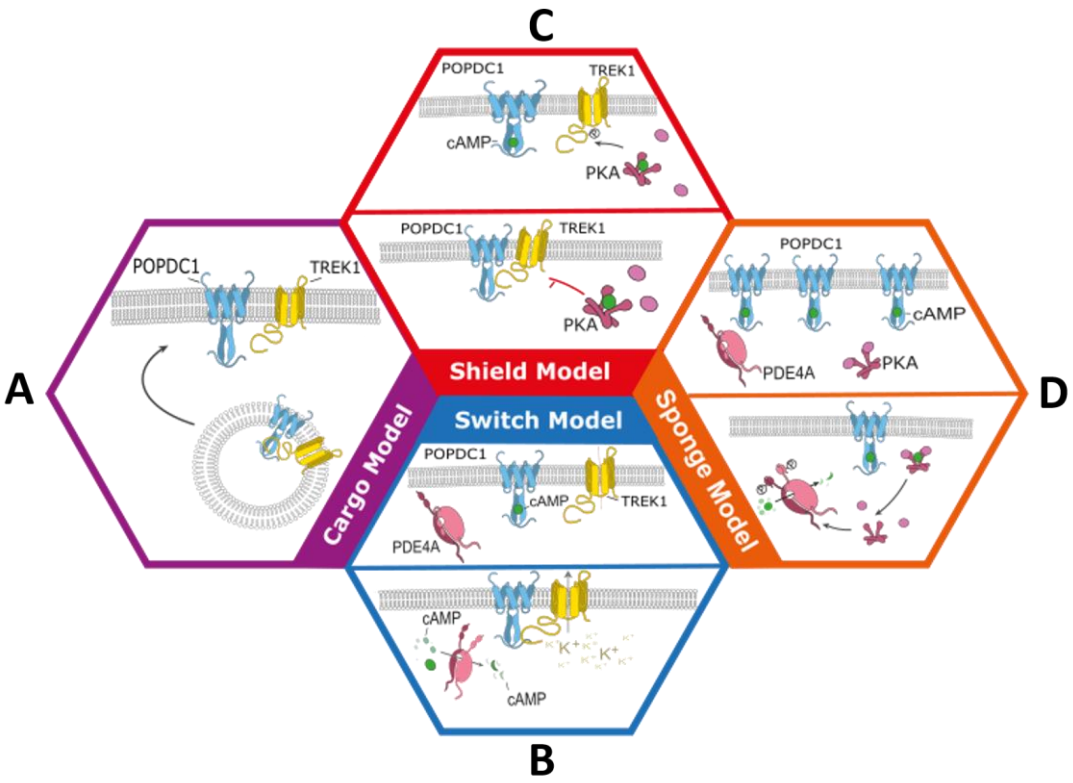

Figure 4.16 Proposed working models of POPDC1. A The cargo model depicts POPDC1 modulating the localisation of interacting proteins dependent upon whether cAMP is bound to the Popeye domain. For example, this model would explain how POPDC1 is directly involved in the membrane association of interacting proteins such as TREK1 and Cav3. B The switch model. cAMP bound to POPDC1 causes a direct change in the activity of an interacting protein. POPDC1s interaction with TREK1 is known to form under basal cAMP levels. This complex is broken when cAMP levels are high which could be due to cAMP being directly bound to POPDC1. C. The shield model. POPDC1 blocks interaction partners from cellular kinases in low cAMP levels. This protection is lost when the Popeye domain bind cAMP. TREK1 is phosphorylated by PKA, it could be hypothesised that POPDC1 would block the access of PKA under lower cAMP levels. When cAMP binds to POPDC1 this shield is lost and TREK1 is subjected to PKA phosphorylation. D The sponge model depicting POPDC1 sequestering cAMP in order to lower cAMP available to other effector proteins. Figure adapted from (Swan et al., 2019).

I have provided evidence suggesting that POPDC1 was not modulating the activity of PDE4A in a negative manner. It is interesting to note that the binding site of POPDC1 on PDE4A that was identified in the previous chapter lies within the dimerization motif of PDE4 (Bolger et al., 2015). The monomeric PDE4 long form is more catalytically active due to the lack of ‘trans-capping’ by the other monomeric subunit in the dimer (Burgin et al., 2010). It is unclear if the POPDC1 is binding a monomer or dimer of PDE4A4 , however if it was the former, by binding a more catalytically active PDE4A it may be that elevated cAMP concentrations are rapidly brought back down to basal levels allowing for the interaction of other partners, such as TREK1, to occur. Although no increase in

catalytic activity was identified in the PDE activity assay (Figure 4.5), the purified-recombinant PDE4A4-MBP may be in a monomeric state due to its exogenous environment, meaning a dramatic change would not be seen in the presence of POPDC1-GST. This regulation would have great importance in the heart, as POPDC1 interaction with TREK1 increases the outward current of K^+ ions driving action potential repolarisation (Schindler et al., 2012b).

4.5.2 PDE4 modulates POPDC1 interactions creating output changes

One of the most important findings from this chapter is the development of a cell-penetrating peptide that is able to block the interaction between POPDC1/Popdc1 and PDE4A (Figure 4.7, Figure 4.8, Figure 4.9, Figure 4.11). This allowed for the physiological investigation of the functional role of the POPDC1/PDE4A interaction.

FRET experiments carried out in this chapter have shown that the POPDC1/TREK1 complex can be modulated through increased cAMP levels initiated by the pharmacological inhibition of PDE4 generally (Figure 4.10) or the specific inhibition of POPDC1-PDE4A binding (Figure 4.11). This information coupled with the changes found in the repolarisation of the action potential (Figure 4.13), suggests that the blocking of the interaction between TREK1/Popdc1 and Popdc1/PDE4A has a role in the control of beating of cardiac myocytes and proposes a role for the POPDC1-PDE4 complex in cardiac tissue. Current literature has shown that the co-expression of POPDC1 and WT TREK1 leads to a 40% increased current amplitude through TREK1 (Schindler et al., 2016b). $POPDC1^{S201F}$, which is unable to bind cAMP due to a mutated DSPE motif, enhanced the outward K^+ current by 90% presumably leading to an increased conductivity through TREK1 channels in complex with this mutant POPDC1 (Schindler et al., 2016b). The effects of WT POPDC1 on the TREK1 channel current was removed post-treatment with 8-Br-cAMP whereas this loss was not seen when $POPDC1^{S201F}$ was transfected with TREK1 suggesting that the inability to bind to cAMP leads to a shortened action potential repolarisation due to the increase outward K^+ current (Schindler et al., 2016b). It must be noted that this study was performed using spontaneously beating HL-1 cells, a cardiac muscle cell line, whereas CellOPTIQ in this chapter utilised ventricular myocytes that

beat upon stimulation. Although not carried out in the same cell type, the combined information from this chapter and the paper by Schindler and colleagues can be useful in giving some indication of the role of POPDC1 in the sinoatrial node (Schindler et al., 2016b).

Thinking of the action potential as a balance between the influx of sodium and calcium along with the efflux of potassium allows us to hypothesis what may be happening to create an elongated action potential seen with disruptor peptide treatment. The fight for control by the three channel groups correlates to the stages of action potential (Pinnell et al., 2007). The initial T_{RISE} phase, which is the upstroke time (ms) from 10% to 90% depolarisation, is driven by the activation of voltage-gated sodium channels altering the membrane potential and allowing for the Ca^{2+} channels to take control (Pinnell et al., 2007). The K^+ channels reach their activation threshold and begin the repolarisation phase of the action potential. TREK1 functions as a K_B channel which controls the resting membrane potential and acts as a 'break' for K^+ control (Backx and Marban, 1993, Kim and Clapham, 1989, Yue and Marban, 1988, Goonetilleke and Quayle, 2012, Osterrieder, 1988). The result of reducing the current through the TREK1 channel results in a lower total K^+ efflux therefore creating a longer repolarisation phase, such as seen with the disruptor peptide treated CellOptiq data (Figure 4.13). It could be hypothesized that in the presence of the disruptor peptide POPDC1 cannot bind PDE4A therefore, cAMP levels remain high which results in an extended period of dissociation between POPDC1 and TREK1 and, as such a lowering the K^+ efflux.

The issue with targeting this interaction is that creating an elongated repolarisation by blocking a K^+ channel can have a lethal impact. The potassium channel hERG (human-ether-a-go-go-related gene), for example, is an essential channel for normal electrical activity in the heart (Sanguinetti and Tristani-Firouzi, 2006, Curran et al., 1995). Known inherited mutations in the *HERG* gene have been shown to cause long QT syndrome, a cardiac repolarisation disorder that often a predisposition to life threatening arrythmias. A similar disorder to this could in fact be triggered by the prescription of hERG-blockers such as quinidine which were designed as anti-arrythmia treatment (Sanguinetti and Tristani-Firouzi, 2006). In addition, the use of common non-cardiac medications

such as antihistamines can also trigger ventricular arrythmia and sudden death through blocking of the hERG channel. As such, pharmaceutical companies removed such blockers from production and many new compounds are screened against the hERG-channel activity in the early stages of drug discovery.

It remains to be determined whether there are any off-target effects with the disruptor peptide that could potentially block other potassium channels such as hERG creating a lethal phenotype. In addition, as the cell penetrating disruptor peptide would unbiasedly inhibit the interaction between POPDC1 and PDE4A in any compartment in the heart this could lead to a worsened phenotype.

Although we have shown that blocking the Popdc1-PDE4A4 interaction has created an elongated AP (Figure 4.13), this did not appear to have an impact on the contractibility of the cardiomyocytes (Figure 4.15). POPDC1 mutations have previously been described to drive an arrhythmic phenotype (Froese et al., 2012). There are several reasons that may explain why we have not seen changes in CD_{50} in this chapter. Firstly, the beginning of the contractile cycle is not linked to the end of the AP cycle (Pinnell et al., 2007). Given the short experimental time, it may be possible that the contraction changes have not yet been propagated. In order to change the contraction of the cardiomyocyte, there is often the culmination of the three channels that creates the dysregulation in signalling driving the altered contraction (Faber and Rudy, 2000). A longer incubation time with the disruptor peptide may have triggered these changes. Secondly, in patients with the POPDC1 mutations, it is possible that the change in the control of multiple interaction partners is how POPDC1 contributes to the development of disease phenotype. At present we do not have the capability to investigate any other interaction partners due to limitations in physiology-based techniques. For this project, I only had the means to functionally investigate TREK1 due to the availability of FRET-probes and conduct potassium measurements in CellOptiq, I had access to no such technique to look at other interaction partners. Finally, it may be that we cannot see the change in contraction in a single cell since the change in response is extremely small in the ventricles given the lower expression levels of POPDC1. In the SA and AV node POPDC1 expression is at its highest therefore a more prominent change in contraction (Froese et al., 2012). This could be combated using a

whole heart system. Previous studies from the Baillie lab have shown that the cell penetrating disruptor peptide can be injected into the heart and measurements on contractibility and electrical signalling can be taken (Martin et al., 2014, Sin et al., 2015). Performing this study may allow us to determine whether the disruption of POPDC1/PDE4A complex is contributing to the development of cardiac arrythmia and AV block, a condition impairing the propagation of electrical signalling throughout heart, as seen in familial mutations of POPDC1 and Popdc1 knock-out models (Froese et al., 2012, Kirchmaier et al., 2012, Schindler and Brand, 2016).

POPDC1 has been shown to interact with caveolin 3, a protein responsible for stabilising caveolae which are the specialised membrane invaginations, through a consensus sequence found at the distal end of the Popeye domain (Vaidyanathan et al., 2018, Alcalay et al., 2013). Caveolae are proposed to be important for the compartmentalisation of the sarcolemma and β-AR, AC, numerous protein pumps and exchangers for example, NCX, and ion channels (inward rectifier potassium, sodium and L-type calcium channels) have all been shown to exist in caveolae (Swan et al., 2019, Vaidyanathan et al., 2018). In *Popdc1* null mutants cardiomyocytes displayed a dramatic reduction in the number of caveolae while their size increased (Alcalay et al., 2013). In addition, these mutant hearts showed an impaired calcium transient, and an increase in oxidative stress sensitivity as well as an increased susceptibility to ischemia/reperfusion (I/R) injury (Alcalay et al., 2013). Also noted was a larger infarct size when POPDC1 is not present (Alcalay et al., 2013). Mentioned previously in this discussion, investigations into other POPDC1 interactors (other that PDE4 and TREK1) was out with the scope of my thesis even although these may be contributing to the arrythmia and cardiac disease phenotype displayed in mutated models and patients. We have only investigated modulation of the POPDC1/TREK1 complex but, it may be the cumulative changes in POPDC1 interactions that drives disease phenotype. As such, blocking the PDE4A interaction with POPDC1 may have numerous unknown consequences, such as loss of caveolae stability, that would need to be investigated to gain a full picture of POPDC1s function.

Providing evidence that my cell-penetrating peptide disruptor of Popdc1-PDE4 can create a measurable functional change has set the precedent for potentially looking at function changes of the POPDC1/PDE4A interaction in other locations. As described in the discussion of the previous chapter, POPDC1 is known to have high expression in muscle cells and heart cells but it is also widely expressed throughout the body including the brain (Figure 4.17).

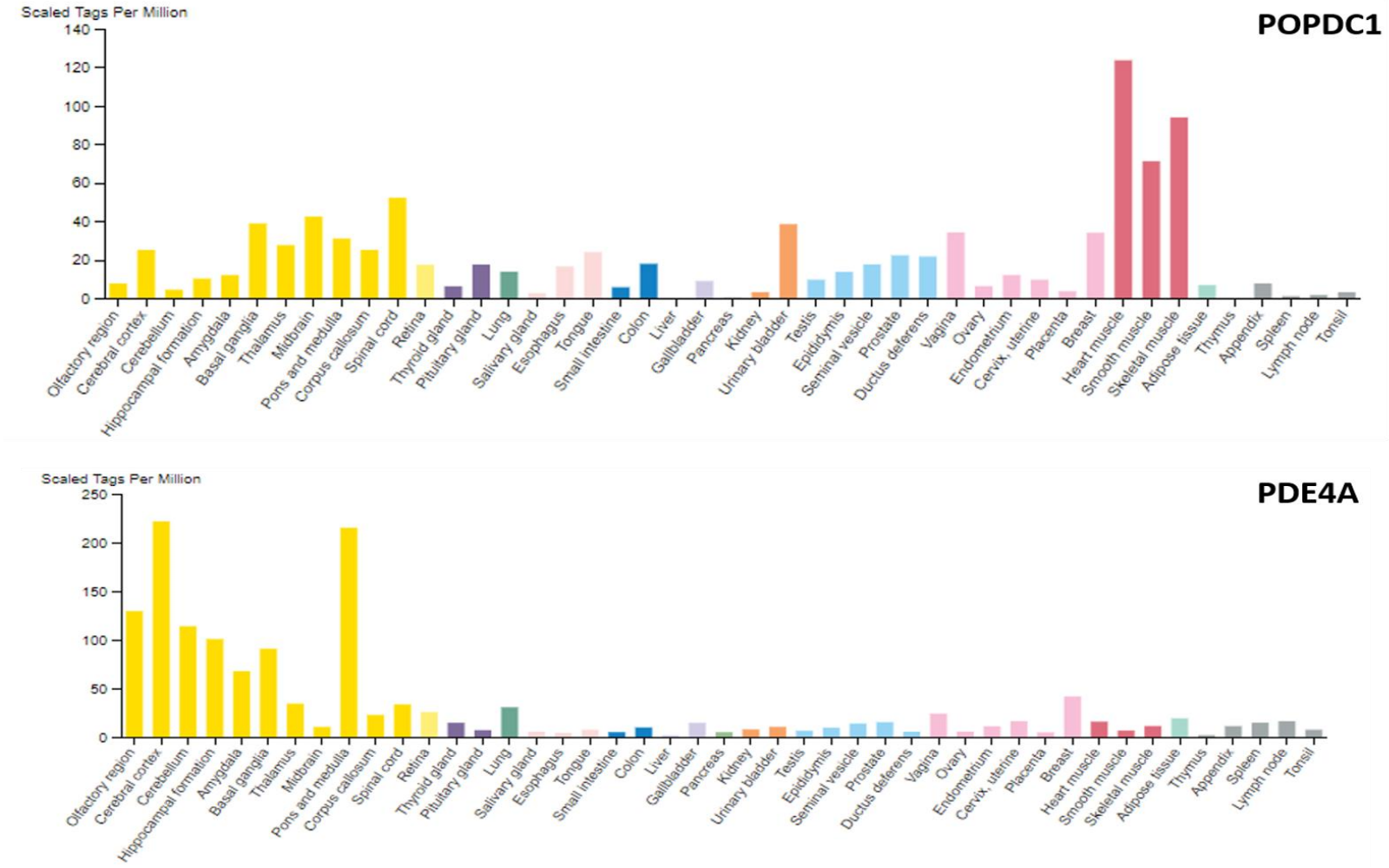

Figure 4.17 Expression of POPDC1 and PDE4A gene in the human body. RNA sequencing data of POPDC1 and PDE4A in human tissue elucidated the tissue expression patterns. RNA expression is shown as reads per kilogram per million mapped reads (RPKM). Data was collected from the Human Protein Atlas project (Lindskog, 2016). (Figure taken from The Human Protein Atlas).

As can be seen in Figure 4.17, the expression of PDE4A in the heart is very low in comparison to other regions. Interestingly, both POPDC1 and PDE4A have high levels of expression in regions of the brain (McCarthy, 2006, Hager and Bader, 2009, Pérez-Torres et al., 2000). This means that the formation of the POPDC1/PDE4A complex may have functional outcomes that could be interrupted in brain disease pathophysiology. Furthermore, TREK1 is mainly expressed in the brain with secondary levels being found in heart and smooth muscle cells (Djillani et al., 2019). In addition, TREK1 has been described to have cytoprotective effects after ischemic injury in the brain (Heurteaux et al., 2004). Ion channels are responsible for the regulation of processes including neuronal excitability, plasticity and neurotransmitter release and as such TREK1's regulation is crucial (Benatar, 2000).

This poses an interesting question as to how the change from POPDC1/TREK1 complex to POPDC1/PDE4A interaction alters from what we have seen in a cardiac environment. For example, TREK1 is involved in the perception of pain due to its localisation in the small dorsal root ganglion (DRG) neurons and in central hypothalamic neurons (Maingret et al., 2000). The TREK-1 channel is inhibited by cAMP which is mediated by PKA phosphorylation on its C-terminal at serine233 (Maingret et al., 2000). It could be hypothesised that POPDC1 'shields' TREK1 from phosphorylation increasing its outward current under basal conditions, as described previously, then as cAMP levels rise, the dissociation of POPDC1 allows for TREK1 phosphorylation and subsequent inhibition. POPDC1 forms a complex with PDE4A in order to reduce the local cAMP levels allowing the POPDC1/TREK1 complex to reform. This, of course, is speculation as more detailed studies of the POPDC1/PDE4A complex needs to be completed to confirm both its existence in other tissues as well as any potential function.

4.5.3 Methodological changes and future directions

There are several avenues that must still be investigated to create a full picture of the physiological pathways that POPDC1/PDE4A interaction is involved in. One point that needs to be addressed is that the human POPDC1 sequence, which binds PDE4A and is utilised in development of disruptor peptide is slightly

different from rodent isoforms. It is also intended to use this disruptor peptide in experiments in model organisms such as xenopus and zebrafish due to the availability of Popdc1 mutants from Professor Thomas Brand (ICTEM, Imperial College London).

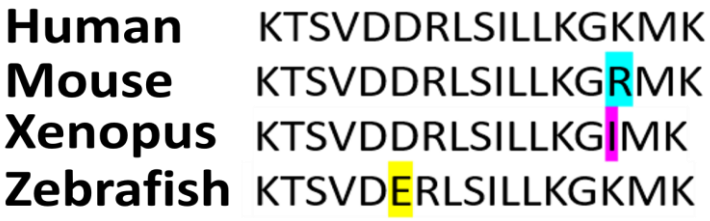

Figure 4.18 Protein sequence alignment of the binding site of PDE4A on POPDC1 identified in the 4 discussed models. The crucial amino resides identified in the peptide array that was used to generate the disruptor peptide. The changed amino residues between the species are highlighted.

However, it can be seen in Figure 4.18, that the sequence of the PDE4A binding site in POPDC1 is highly conserved throughout these species with only one amino residue change. In addition, the amino acid residue change is found out with the crucial binding motif (R-L-S-I-L-L-K). With the data described in this chapter, I would suggest that the disruptor peptide is able to function in all these organisms despite the small sequence differences.

Our analysis of changes in Popdc1s interactions initiated by the presence of the cell-penetrating disruptor peptide (Figure 4.11) must be repeated in a more relevant physiological setting, for example by using NRVM and ARVM. This was attempted during this project in NRVM, however the transfection of both POPDC1-CFP and TREK1-YFP reduced the viability of the myocytes leading to a poor FRET signal being produced (data not shown). The inability to examine the FRET dynamics in a more endogenous cell type limits the scope of the information that can be taken from POPDC1/PDE4A/TREK1 dynamics.

Primary studies using CellOPTIQ (Figure 4.13) need to be repeated with a prolonged incubation period with the peptide in order to investigate cell contraction and calcium signalling to determine whether the change in AP corresponds to a change in beating frequency. The temporal pattern of

ventricular repolarisation is known to be of critical importance in arrhythmogenesis (Porter et al., 2018). As such any factor or small molecule that can modulate or destabilize this repolarisation is of great importance in investigating the onset and development of arrythmias (Porter et al., 2018). In addition, the use of a specific TREK1 inhibitor compound such as Spadin (Djillani et al., 2017) in CellOptiq experiments would mean it could be confirmed that the changes in AP noted with disruptor peptide were due to loss of TREK1 current.

One other caveat that must be addressed is the cell type in which these experiments were carried out. Initial studies to examine Popdc1's role in maintaining a steady beating frequency were carried out using the spontaneously beating HL-1 cell line (Schindler et al., 2016b). There are key physiological differences between these cells and the ventricular myocytes that the experiments in this chapter utilised. Much like the HL-1 cell line, cells within the SA node are characterised as having no true resting potential but generate spontaneous and regular action potentials. In addition to a lack of resting potential, one stark difference is that at the end of the repolarisation phase the membrane potential is very negative (~ -60mV) known as afterhyperpolarisation phase (Grant, 2009). During POPDC1 forced expression in HL-1 cells there was a more pronounced afterhyperpolarisation (Schindler et al., 2016b). More importantly, expression of POPDC1^{S201F} resulted in a more efficient raising K^+ conductance resulting in an increased hyperpolarised membrane potential. This may explain the presentation of an AV block observed in patients and mutant zebrafish (Schindler et al., 2016b).This effect cannot be seen in the ventricular myocytes that were used in this set of experiments. As such, these experiments should be carried out on isolated SA node cells to give a more pronounced picture of how the disruption of POPDC1/PDE4A interaction may contribute to arrythmia by altering AP in these pacemaker cells. As mentioned previously, conducting contraction and action potential experiments such as Langendorff perfused whole heart assay after treatment with the disruptor peptide would provide information on the effects of a lost Popdc1/PDE4A interaction on a whole heart system.

Along with the need for more data to be generated using more physiologically relevant cells or whole organ, a method targeting the peptide to specific domains within the heart needs to be addressed. POPDC1 is expressed throughout the atria, ventricles and more importantly the SA and AV node, and inhibiting the interaction between POPDC1 and PDE4A may have alternative effects depending on localisation. In fact, prolonged treatment with the peptide could contribute to a pronounced arrhythmic phenotype given the inability to target the peptide only to SA and AV node only. Viral targeting or genetic manipulation may work to target the disruption of the POPDC1/PDE4A interaction.

4.5.4 Conclusion

In this chapter I have provided evidence that the function of the PDE4A tethered to POPDC1 is to modulate the local cAMP gradient in the vicinity of POPDC1 and hence modulate the interaction of POPDC1 with TREK1. Specifically blocking the interaction between Popdc1 and PDE4 led to noted physiological change, i.e. the elongated repolarisation of ARVM, that can be explained by reference to the function of TREK1. Additional work is required to confirm and expand on these findings as well as investigate the interaction in a different tissue where both PDE4A and POPDC1 are highly expressed.

5 Analysis of POPDC1 in heart failure

5.1 Introduction

5.1.1 Dilative Cardiomyopathy

Cardiomyopathies are a group of clinical disorders involving the cardiac muscle that result in mechanical and electrical dysfunction leading to dilated, hypertrophic or restrictive pathophysiology (Hershberger et al., 2010). Dilative cardiomyopathy (DCM) is characterized by left ventricular or biventricular dilation and impaired contraction that cannot be explained by numerous abnormal loading conditions such as hypertension or by coronary artery disease. In its late DCM stages, tissue damage accompanied by collagen accumulation in the ventricle wall is present however, the severity of myocardial scarring is only part of the contributing factors leading to the expansion in the ventricle chamber volume (Tanaka et al., 1987, Roberts et al., 1987, Schwarz et al., 1983). One of the major contributing drivers of ventricular dilation is myocyte elongation through the addition of newly formed sarcomeres (Beltrami et al., 1995). There is also an increase in myocyte diameter, although this expansion is moderate and inadequate to preserve the thickness of the chamber wall. As a consequence there is decompensated eccentric hypertrophy which characterizes the development of dilated cardiomyopathy in humans (Anversa et al., 1993). In animal models, rapid ventricular pacing leads to a cardiac myopathy and these animals display an increase in ventricle chamber diameter, mural thinning, alterations in coronary blood flow and ventricular wall stress which is consistent with human disease (Shannon et al., 1991, Spinale et al., 1991).

There have been numerous genetic mutations that have been linked to DCM that are commonly separated into two categories: defects in force generation and defects in force transmission. Defects in generating force are usually due to a loss of integrity within the sarcomere. Mutations in cardiac myosin heavy chain have been found to cause disruption at either the site of actin-myosin binding or at the site of flexible joints of the myosin protein that are responsible for its mobility during the contraction event (Rayment et al., 1993). In addition, mutations in TnC disrupt its calcium dependent interactions which are important for the generation of ATP to drive the actin-myosin contraction (Kamisago et al.,

2000). Once the actin-myosin contraction is complete, the force is transferred to the extracellular matrix from the sarcomere. This is driven by interactions between the actin subunit and specific cytoskeletal units (Olson et al., 1998). Two mutations coding for regions on the surface of α-tropomyosin have been identified in an area that is proposed to be responsible for tropomyosin-actin interactions (Olson et al., 1998). Mutations in dystrophin, desmin and sarcoglycan have also been shown to diminish the transmission of force (Muntoni et al., 1993, Li et al., 1999, Tsubata et al., 2000).

Regardless of the cause of the DCM, as the disease progresses and the cardiac muscle of the ventricle becomes weaker, the heart becomes less able to pump blood through the body and maintain a normal electric rhythm. This eventually can progress to heart failure or severe cardiac arrythmias (Luk et al., 2009).

5.1.2 Human heart failure

Heart failure (HF) is defined as a clinical syndrome that is caused by structural and functional defects in the myocardium. This results in an impairment in the filling of the ventricles or the subsequent ejection of blood (Inamdar and Inamdar, 2016). The onset of HF may also be caused by damage from numerous cardiac injuries including myocardial infarction. Myocardial infarction occurs when there is improper blood flow to part of the heart leading to the heart muscle being injured during the lack of oxygen (Lu et al., 2015). This obstruction of blood flow is usually caused by the narrowing and blocking of the coronary arteries with plaques, cholesterol and fat deposits (Lu et al., 2015). Often this prolonged lack of oxygen causes ischemia and ischemic HF.

The progression of HF is caused by reduced function in the left ventricular myocardium through altered cell metabolism and morphology however, dysfunction in the endocardium, myocardium, heart valves and pericardium can drive the progression of HF (Inamdar and Inamdar, 2016). Under normal conditions the heart derives most of its energy from free fatty acids (FFA)and glucose oxidation (Neely et al., 1972, Lopaschuk et al., 2010). There is a switch between oxidation of FFA and glucose called the Randle cycle, which is disrupted during heart disease. In progressive heart failure there is an imbalance between the requirement and the available oxygen and metabolic supplies.

Cardiac cells display a decrease in glucose uptake that drives production of lactate increasing cellular acidosis (Fragasso, 2016). The culmination of these changes results in the modulation in ultrastructural properties of the ventricles leading to their remodelling. This remodelling describes the morphological changes in; heart wall thickness and shape, mass of the heart (hypertrophy and atrophy), and increases in area of scarring after MI (Azevedo et al., 2016). Remodelling initially overcomes the deleterious changes in cellular metabolism and morphology however over time this becomes less efficient and subsequently results in the progression to heart failure (Delgado and Willerson, 1999).

5.1.3 Alterations in the biology of cardiac myocytes

In animal models of heart disease and human heart failure samples, it is has been shown that the initiation of cardiac remodelling starts with changes in cardiac myocytes (Dash et al., 2001, Mann and Bristow, 2005). There have been numerous studies that have suggested that failing human cardiac myocytes undergo changes that drive the loss of contraction, loss of myofilaments, alterations in cytoskeletal proteins, alterations in excitation-contraction coupling and desensitisation of ß-adrenergic signalling (Schaper et al., 1991, Beuckelmann et al., 1992, Bristow et al., 1982). Many of these changes are thought to protect the failing cardiomyocytes against the deleterious effects of excessive activation of proteins such as norepinephrine, angiotensin II, endothelin, aldosterone, and TNF (Mann and Bristow, 2005). For example, the over production of angiotensin II, a smooth muscle constrictor and hypertrophic agent, can contribute to many of the deleterious effects. Angiotensin II acts mainly through two receptors angiotensin II type 1 (AT_1) and AT_2, each of which has distinct downstream targets that counteract each other to elicit opposing effects (Booz and Baker, 1996, Ferrari et al., 2002). AT_1 receptors are known to cause vasoconstriction, cell growth, positive inotropism, and aldosterone and catecholamine release (Booz and Baker, 1996). Conversely, the AT_2 receptors are involved in the mediation of vasodilation, inhibition of cell growth, apoptosis, negative inotropism, and natriuresis (Booz and Baker, 1996). The two receptors also share common downstream targets such as arachidonic acid and nuclear factor-κB (NF-κB) (Patterson et al., 1999, Booz and Baker, 1996). Two main actions of angiotensin II are thought to be part of the damaging effect on vascular cells that contribute towards vascular remodelling. Firstly, angiotensin

II can stimulate reactive oxygen species (ROS) in the vascular wall leading to a smooth muscle growth thus contributing to remodelling (Wang et al., 2001, Dzau, 1993). Secondly, it has been shown that angiotensin II in smooth muscle can activate NFκB which in turn regulates several inflammatory cytokines, such as tumour necrosis factor α (TNFα), chemokines and cell adhesion molecules (Ferrari et al., 2002). Together these inflammatory molecules contribute toward the development of atherosclerosis and cardiac remodelling by driving inflammation, smooth muscle cell proliferation and apoptosis (Dichtl et al., 1999, Selzman et al., 1999, Erl et al., 1999). Protein expression and activity changes cumulatively lead to a pronounced defect in the contractile ability of the myocyte as well as a loss of responsiveness to adrenergic control mechanisms (Bristow et al., 1982, Beuckelmann et al., 1992, Schaper et al., 1991). These are the hallmarks of the failing myocardium (Mann and Bristow, 2005). In fact, isolated failing myocytes were shown to have a ~50% reduction in contraction in comparison to their healthy counterparts (Davies et al., 1995). In addition, there is extensive remodelling of the t-tubule network, manifesting in abnormal calcium handling, and of the caveolae, resulting in disorganisation of the components held within signalling complexes (Davies et al., 1995, Galbiati et al., 2001, Fridolfsson and Patel, 2013). As mentioned, lack of POPDC1 has been shown to lead to structural rearrangements in the phenotype of cardiomyocytes, suggesting a reduction or dysfunction of POPDC1 may facilitate progression to cardiac failure (Schindler et al., 2016b).

5.1.4 Cardiac Fibroblasts

Although cardiac myocytes are extremely important in the remodelling events during heart disease, there exists another group of cells that have an important role in the remodelling process. It has been proposed that the adult heart consists of around 30% myocytes and 70% non-myocytes (Zak, 1974, Nag, 1980). Cardiac fibroblasts are one of the non-myocyte cellular components of the heart and are widely distributed connective tissue cells. Within the heart fibroblasts possess numerous important roles in cardiac development, defining cardiac structure, maintenance of proper cardiac function and remodelling during disease (reviewed in (Souders et al., 2009)). In addition, cardiac fibroblasts represent both sources and targets of different stimuli which aid in the coordination of chemical, mechanical and electrical signals between the cellular

and acellular components of the heart. Following initial cardiac injury, fibroblasts respond to these factors causing a change in the fibroblast gene expression and their migration toward the injured region of the heart to promote wound healing and scar formation. As the heart undergoes remodelling associated with the transition to heart failure there is an increased in cytokine and growth factor secretion which leads to the proliferation and the migration of fibroblast allowing for the remodelling of the cardiac interstitium (Brown et al., 2005, Weber, 2004).

5.1.5 POPDC1 in heart failure

The progression to heart failure is known to be associated with expression changes in multiple myocardial genes (Andrée et al., 2000). However, the exact role played by these proteins is still not fully understood. It remains unclear as to how novel myocardial genes, such as the POPDC family of proteins are contributing to heart failure (Gingold-Belfer et al., 2011). Previous studies have mentioned POPDC1's role in the pathophysiology of both cardiac and skeletal muscle (Andrée et al., 2002a). Observations from transgenic mice lacking Popdc1 suggest they had impaired recovery from ischemia/reperfusion injury (Gingold-Belfer et al., 2011). Current evidence describing POPDC1 being intrinsically involved in cellular signalling drives the hypothesis that its expression is important in normal heart function (Gingold-Belfer et al., 2011, Alcalay et al., 2013, Froese et al., 2012, Schindler et al., 2012b). Furthermore, POPDC1 is found in intercalated discs, the facilitator of electrical signal propagation between myocytes, and this observation adds more support to the notion that the POPDC family's role revolves around maintaining proper cardiac function (Noorman et al., 2009, Gingold-Belfer et al., 2011). Often, heart failure is associated with disarray of myocytes, accompanied by alterations in the expression and distribution of many proteins which contributes towards the impairment of myocardial mechanical and electrical function seen with this condition (Hein et al., 1994, Arai et al., 1993, Kostin et al., 2003). Connexin43 (Cx43) expression is known to be reduced in end stage heart failure with its localisation being redistributed to the lateral sarcolemma from the intercalated discs (Kostin et al., 2003). A primary look at POPDC1 levels in failing hearts provided evidence of a reduction in both mRNA and protein levels (Gingold-Belfer et al., 2011). Alcalay and colleagues provided further support of this

hypothesis by showing that levels of POPDC1 protein and mRNA were downregulated in I/R (Alcalay et al., 2013). Further research found that POPDC1 is also crucial for the structural maintenance of caveolae via its interaction with Cav3 which, as described in the introduction, is essential for ion channel function in cardiac contraction (Alcalay et al., 2013). This combined evidence suggests that POPDC1 is functionally relevant to the maintenance of cardiac health and that it is altered within disease progression.

5.2 Hypothesis and Aims

As described, POPDC1 has been shown to interact with several proteins involved in various cellular functions such as ion channel conductance and cell adhesion. These interactions and their alteration during heart disease have been suggested to have an impact on the loss of function in the heart (Alcalay et al., 2013, Kliminski et al., 2017, Osler et al., 2005). With only minimal data on the changes in POPDC1 levels in failing hearts, we sought to further investigate expression in both human heart and porcine heart. Using tissue kindly donated from Dr Rodger Hajjar (New York, USA) and Dr Kenneth Campbell (University Kentucky, USA) and processed by Dr Gillian Borland (University of Glasgow), POPDC1 expression levels were compared in heart failure to healthy counterparts.

As such, the specific aims of this chapter are as follows:

- To determine whether POPDC1 expression is altered in a porcine model of MI.

- To investigate if these changes are pheno-copied in human heart failure samples

5.3 Methods

5.3.1 Porcine tissue samples

Samples were kindly gifted by Dr Roger Hajjar (New York, USA). Prior to samples being sent, male Yorkshire pigs (also known as English Large White pigs) were subjected to left anterior descending (LAD) cardiac artery balloon occlusion, which is commonly used as a model of MI, for a period of 2 hours (day 0). This involves the insertion of a balloon into the LAD artery preventing blood flow to the left ventricle, subsequently resulting in an infarction (Koudstaal et al., 2014). Sham animals underwent surgery (day 0) and recovery in the same time frame as experimental animals. Tissue samples were collected from the left ventricle and snap frozen at -80^{o}C prior to being shipped on dry ice. Samples were then processed for Western blotting. All porcine work was carried in accordance with ARRIVE (Animal Research: Reporting In Vivo Experiments) guidelines.

50 mg of tissue was placed in a 2 ml RNase free tube along with 5 mm stainless steel beads. 700 µl of RIPA buffer substituted with protease cocktail inhibitors (Roche, West Sussex, UK), phosphor-stop tablets (Roche, West Sussex, UK) and 25mM N-ethylmaleimide (Sigma-Aldrich Dorset, UK). The samples were then homogenized to lyse the tissue. Tubes for pulsed for 45 seconds with a 3-minute incubation on ice to prevent sample overheating, this cycle was repeated three times. Samples were centrifuged for 10 minutes at 13,000 rpm at 4^{o}C and the supernatant was collected in a fresh tube. The supernatant was subjected to Bradford assay and Western blotting through the protocols described in sections 2.4.2, 2.8.1 and 2.8.3.

5.4 Results

5.4.1 Results Porcine heart tissue comparison

Levels of POPDC1 were investigated using samples kindly donated by Dr Roger Hajjar (New York, USA). Porcine hearts have often been used as a model to study heart disease due to the comparable anatomical structure to human hearts. This makes pig HF models more apt than many rodent model systems. (Lelovas et al., 2014). Using samples from this model, I observed that there was a slight increase in POPDC1 levels immediately after onset of an MI with the highest levels after 2 weeks, with levels returning to that of sham at the 3 month stage (Figure 5.1). Power calculations using the data and trends collected from my experiment (n of 3 for each experimental time point), identified that an n of 23 would be needed to accurately identify a statistically significant difference in POPDC1 expression in a similar sample set.

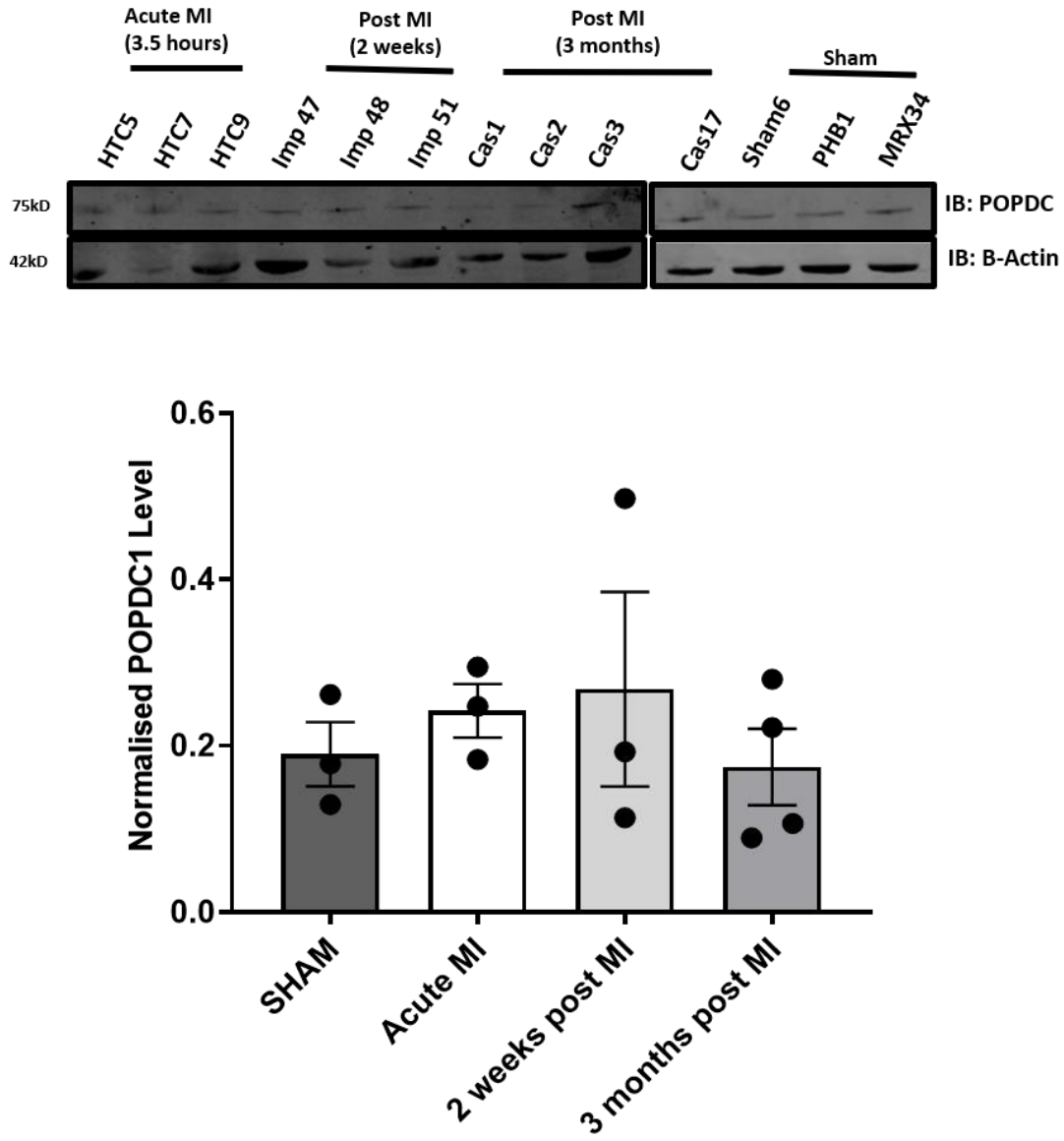

Figure 5.1 POPDC1 expression in porcine models for MI. Tissue taken from pigs subjected to LAD balloon artery occlusion to induce MI were western blotted for POPDC1. The labels given to each of the 3 animals in a group represent the code name of that animal throughout the study. Four times points after myocardial infarction (MI) were examined; acute MI (3.5 hours after MI) (first three lanes), 2 weeks post MI (three lanes) and 3 months MI (third set of three lanes). Control pig tissue (last three lanes) that had not been subjected to the LAD balloon were used to determine baseline levels of each protein. Samples were separated via SDS-PAGE and subjected to western blotting. Immunoblotting for POPDC1 was undertaken to compare expression levels of the protein at each time point. B-actin was used as a loading control allowing samples to be normalised for comparison, ImageJ was used to quantify band intensities for each protein. Values were normalised to β-actin and graphs were produced using GraphPad Prism. Graphical results represented as mean ± SEM, n=3 for each experimental time point. Statistical analysis was performed using a one-way ANOVA.

Having identified a potential trend of POPDC1 upregulation, PDE4A levels were examined. As with POPDC1, there was a trend toward an increase in PDE4A levels immediately after MI with levels decreasing soon after. Residual PDE4A levels (following decrease) were higher in comparison to sham after 3 months (Figure 5.2). Once again, a power calculation identified that an n=15 would be required to produce significant differences between the MI samples and sham based on the n of 3 represented here.

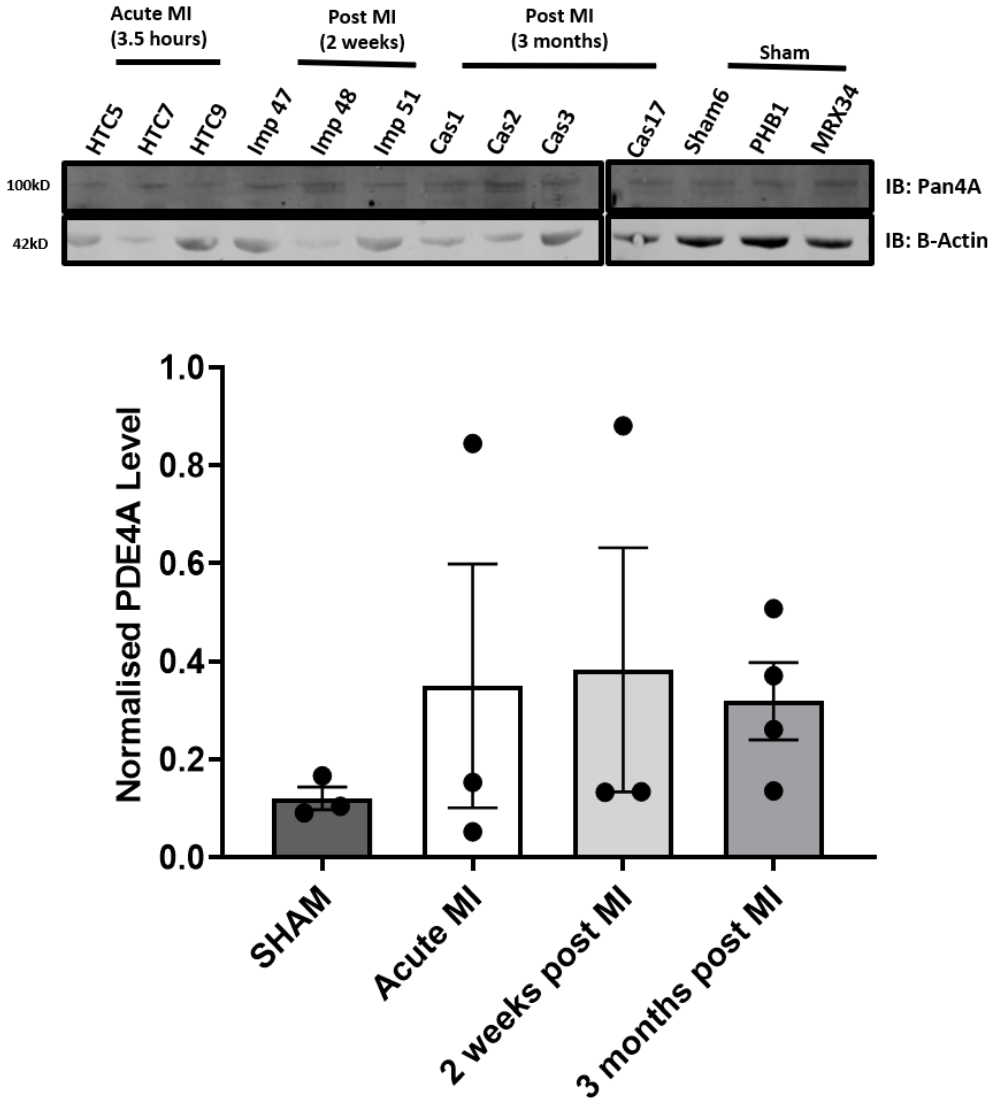

Figure 5.2 Expression levels of PDE4A in porcine models of MI. The Pig MI samples previously used to examine POPDC1 levels were western blotted for PDE4A and compared to basal levels using sham as a control. The labels given to each of the 3 animals in a group represent the code name of that animal throughout the study. B-actin was immunoblotted for to provide a loading control. Band intensities were calculated using ImageJ and PDE4A values were normalised to β-actin values. GraphPad was used to produce a graphical representation of the results. Results represented as mean ± SEM, n=3 for each time point. Statistical analysis was performed using a one-way ANOVA. There is a trend showing the increase of PDE4A at all stages after MI.

5.4.2 Total expression levels of POPDC1, PDE4A and Cav3 remain unchanged in Heart Disease.

Having observed upward trends in POPDC1 and PDE4A expression immediately after an MI, with a reduction to near basal levels after prolonged recovery, I sought to identify whether there was any change in protein expression during end stage heart failure. MI remains the most common cause of heart failure worldwide (Cahill and Kharbanda, 2017, Roger, 2013). Heart failure as mentioned, is defined as the syndrome resulting from cardiac injury or structural changes that leads to the impairment of the ventricle to either fill or eject blood (Yancy et al., 2013). In this instance, ischemic heart failure can be caused as a secondary outcome of MI. Due to the occlusion of the vessel during MI, there is tissue death which in turn leads to a lack of blood flow to that area in the aftermath. Ischemic heart failure patient samples and healthy donors, kindly gifted by Dr Kenneth Campbell (University of Kentucky), were analysed via western blotting for POPDC1, PDE4A and another POPDC1 interacting protein, caveolin 3.

Table 5: Characteristics of human heart samples.

Sample No.	Case Type	Sex	Age (yrs)	Race	BMI	Smoker	Heart Failure	Primary Diagnosis	Region
1	Organ donor	Male	26.5	White	24.46	Smoked in past			Epicardium
2	Organ donor	Male	50	White	29.4	Smoked in past			Epicardium
3	Organ donor	Female	41.6	White	unknown	unknown			Epicardium
4	Organ donor	Male	32.5	White	40.4	Smoker			Endocardium
5	Organ donor	Male	51.6	White	31.2	Smoker			Epicardium
6	Organ donor	Male	37.4	White	34.2	Smoker			Endocardium
7	Organ donor	Male	38.6	White	24.1	Smoker			Epicardium
8	Heart transplant	Male	55.8	White	34.2	Smoked in past	Ischaemic	Ischaemic cardiomyopathy	Epicardium
9	Heart transplant	Male	66	White	29.4	Smoked in past	Ischaemic	Ischaemic cardiomyopathy	Epicardium
10	Organ donor	Male	22.2	White	Unknown	Unknown			Endocardium
11	Heart transplant	Female	51.3	White	30.6	Smoked in past	Ischaemic	Ischaemic cardiomyopathy	Epicardium
12	Heart transplant	Female	59.4	White	24.1	Never smoked	Ischaemic	Ischaemic cardiomyopathy	Not specified
13	Organ donor	Male	32.5	White	40.4	Smoker			Epicardium
14	Heart transplant	Female	49	White	22.9	Smoked in past	Ischaemic	Ischaemic cardiomyopathy	Epicardium

15	Heart transplant	Male	75.5	White	32.8	Never smoked	Ischaemic	Chronic systolic heart failure	Endocardium
16	Heart transplant	Male	66	White	29.4	Smoked in past	Ischaemic	Ischaemic cardiomyopathy	Endocardium
17	Organ donor		26.5	White	24.46	Smoked in past			Endocardium
18	Organ donor		38.6	White	24.1	Smoker			Endocardium
19	Heart transplant		65.2	White	37.3	Never smoked	Ischaemic	Ischaemic cardiomyopathy	Epicardium
20	Heart transplant		49	White	22.9	Smoked in past	Ischaemic	Ischaemic cardiomyopathy	Endocardium
21	Organ donor		51.6	White	31.2	Smoker			Endocardium
22	Organ donor		35.7	White	22.2	Unknown			Epicardium
23	Heart transplant		65.2	White	37.3	Never smoked	Ischaemic	Ischaemic cardiomyopathy	Endocardium
24	Heart transplant		58.3	White	24.1	Never smoked	Ischaemic	Ischaemic heart failure and post-MI pericarditis	Endocardium
25	Heart transplant		50.5	Black or Asian	22.3	Smoked in past	Ischaemic	Ischaemic heart failure	Epicardium
26	Organ donor		37.4	White	34.2	Smoker			Epicardium
27	Heart transplant		33.5	White	37	Never Smoked	Ischaemic	Ischaemic cardiomyopathy	Epicardium
28	Heart transplant		59.4	White	24.1	Never smoked	Ischaemic	Ischaemic cardiomyopathy	Not specified
29	Organ donor		23.3	White	20.45	Never smoked			Epicardium

30	Heart transplant	33.5	White	37	Never Smoked	Ischaemic	Ischaemic cardiomyopathy	Endocardium
31	Heart transplant	55.8	White	34.2	Smoked in past	Ischaemic	Ischaemic cardiomyopathy	Endocardium
32	Heart transplant	37.8	White	25.9	Never smoked	Ischaemic	Ischaemic cardiomyopathy	Not specified
33	Organ donor	22.2	White	Unknown	Unknown			Epicardium
34	Heart transplant	75.5	White	32.8	Never smoked	Ischaemic	Chronic systolic heart failure	Epicardium
35	Organ donor	23.3	White	20.45	Never smoked			Endocardium
36	Heart transplant	51.3	White	30.6	Smoked in past	Ischaemic	Ischaemic cardiomyopathy	Endocardium
37	Organ donor	35.7	White	22.2	Unknown			Endocardium
38	Heart transplant	48.8	White	24.2	Smoked in past	Ischaemic	Ischaemic heart failure	Endocardium
39	Organ donor	41.6	White	Unknown	Unknown			Endocardium
40	Heart transplant	56.5	White	30.2	Smoked in past	Ischaemic	Ischaemic heart failure	Not specified
41	Organ donor	50	White	29.4	Smoked in past			Endocardium

Human heart failure samples are detailed in Table 5. As mentioned, POPDC1 was shown by Gingold-Belfer and colleagues as well as Alcalay and colleagues to be down-regulated in end stage heart failure (Gingold-Belfer et al., 2011, Alcalay et al., 2013).Using the above samples, I could detect a robust signal for POPDC1 in healthy and disease patient tissue (Figure 5.3, panel A-C). However, there was no significant diminution of POPDC1 levels in patients with ischemic heart compared to their healthy counterparts (Figure 5.3, panel D).

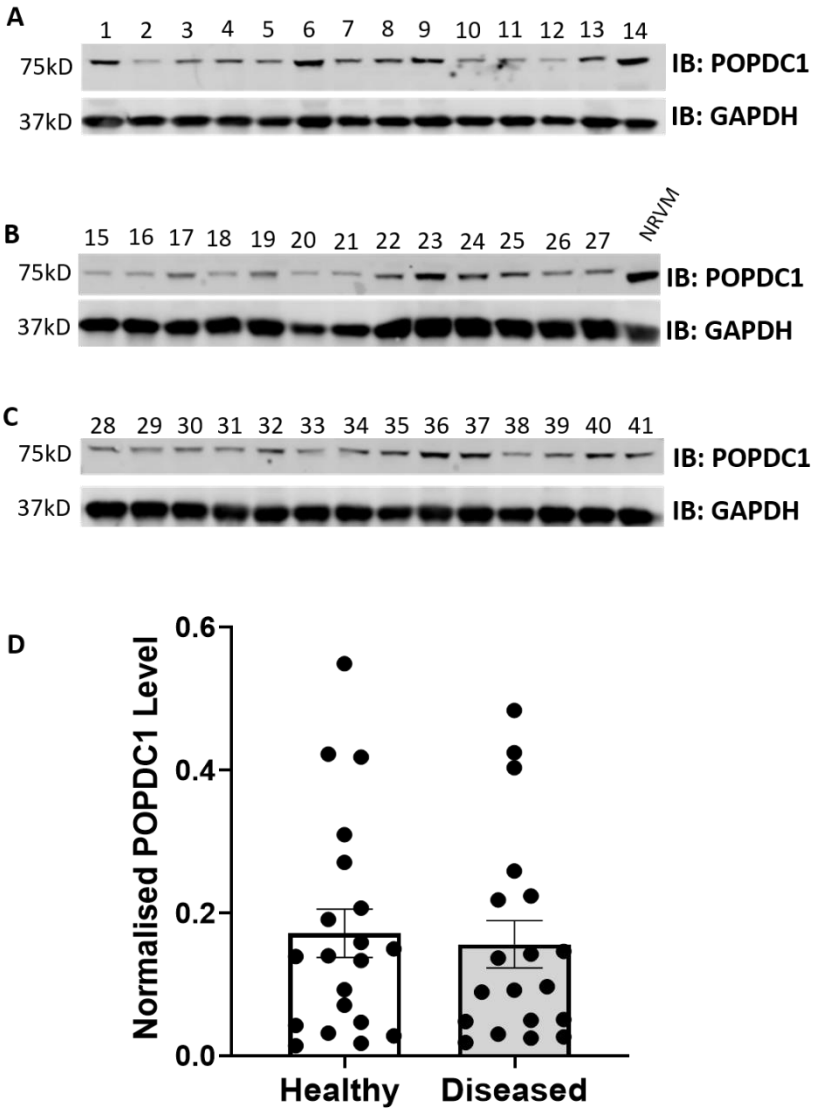

Figure 5.3 POPDC1 expression and comparison analysis in human heart samples from organ donor control patients and transplant patients suffering from heart failure. Human heart tissue samples were blotted for POPDC1 and GAPDH as a loading control. NRVM lysate was run as a positive control to ensure POPDC1 was present. Blots for samples 1-14, 15-27 and 28-41 are shown in A.B and C respectively. Samples from NRVM were run as a control for POPDC1 expression. D, graph shows mean ± SEM for n=20 for healthy and n=21 for diseased samples which were normalised to the respective GAPDH value. Students t-test was performed.

As no change in POPDC1 levels were identified, the next step was to determine if the levels of the novel interactor, PDE4A, was altered in the end-stage of ischemic heart failure. Samples were probed for PDE4A using a panPDE4A antibody. The presence of a band at ~100kD identified PDE4A long isoform in human heart (Figure 5.4, panel A-C). Once again, there was no significant change in total expression level of PDE4A between healthy and diseased human hearts (Figure 5.4).

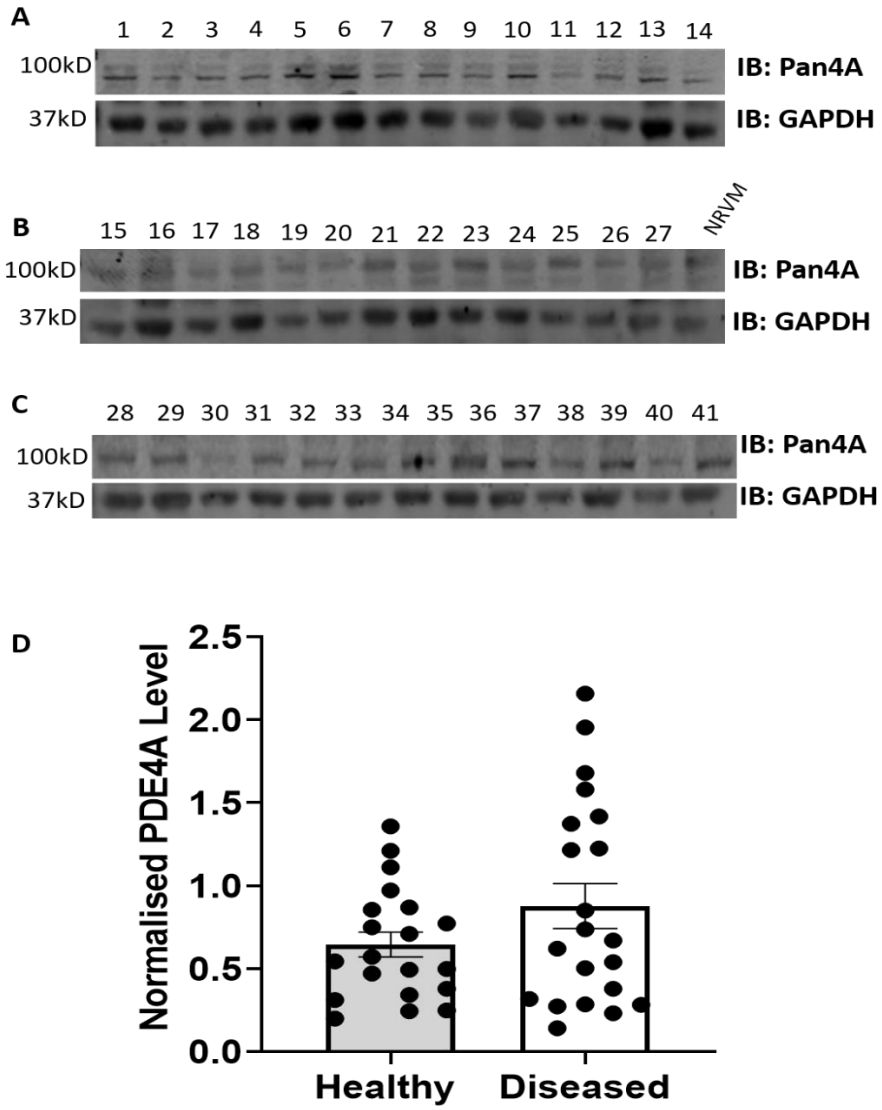

Figure 5.4 PDE4A expression in human heart failure samples from organ donor control patients and ischemic heart failure patients. Human heart tissue samples were blotted for PDE4A and GAPDH as a loading control. NRVM lysate was run as a positive control to ensure PDE4A was present. Blots for samples 1-14, 15-27 and 28-41 are shown in A.B and C respectively. Samples from NRVM were run as a control for PDE4A expression. D, Graphical results show mean ± SEM for n=20 for healthy and n=21 for diseased samples which were normalised to the respective GAPDH value. Students t-test was performed.

Finally, I evaluated the expression of Cav3 in the human heart samples. Due to the known interaction between POPDC1 and evidence from Alcalay and colleagues that the POPDC1-Cav3 interaction was decreased in end-stage heart failure, I examined whether the expression levels of Cav3 were altered in comparison to healthy patients (Gingold-Belfer et al., 2011, Alcalay et al., 2013). Cav3 is highly expressed in human heart (Figure 5.5, panel A-C) and I could easily detect Cav3 protein. Similar to POPDC1 and PDE4A, Cav3 protein expression was not significantly altered between healthy and diseased patient heart tissue (Figure 5.5, panel D).

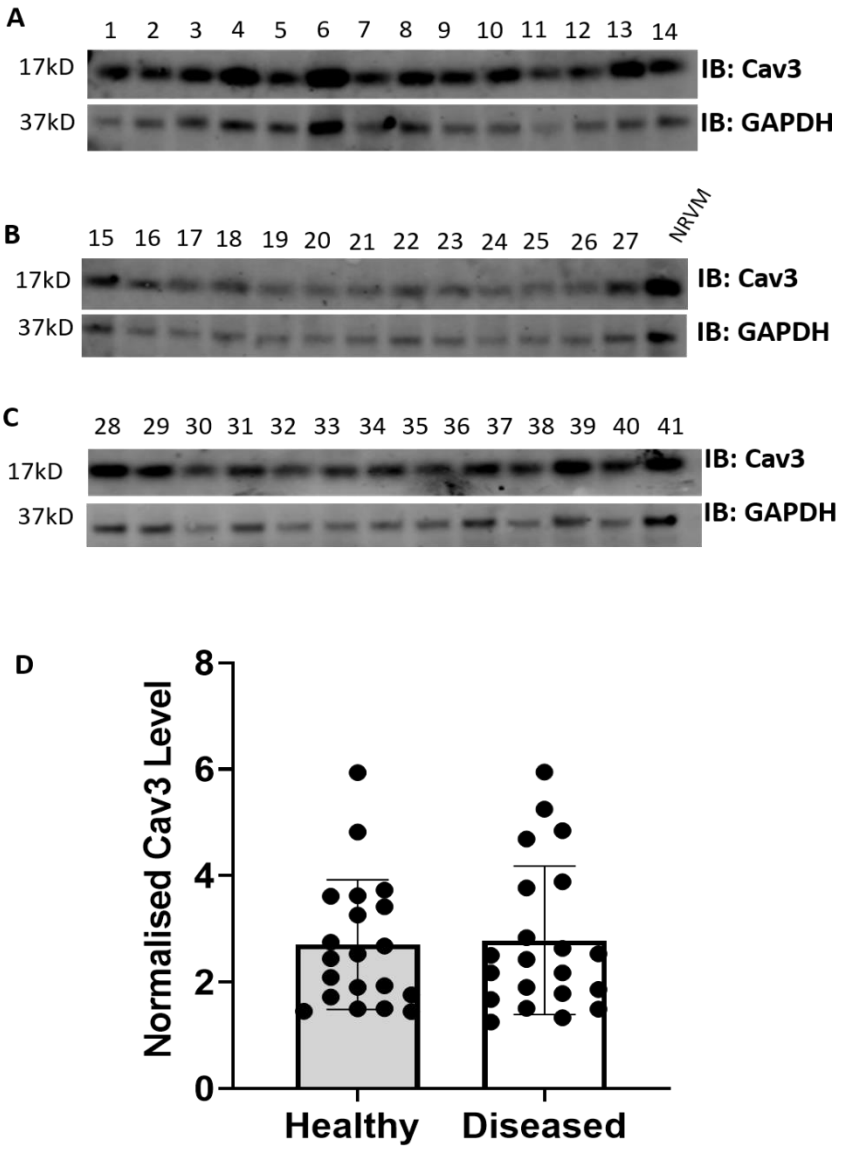

Figure 5.5 Cav3 expression in human heart failure samples from organ donor control patients and ischemic heart failure patients. Human heart tissue samples were blotted for Cav3 and GAPDH as a loading control. NRVM lysate was run as a positive control to ensure Cav3 was present. Blots for samples 1-14, 15-27 and 28-41 are shown in A.B and C respectively. Samples from NRVM were run as a control for Cav3 expression. D, ImageJ was used to determine the

intensities of the bands on the gel. Graph shows quantitative normalised to GAPDH mean ± SEM for n=20 for healthy and n=21 for diseased samples. Students t-test was performed.

Collectively, no significant changes in protein expression levels were seen in total heart tissue between healthy and disease groups of either POPDC1, PDE4A or Cav3.

5.4.3 Comparison between endocardium and epicardium

Despite the lack of alterations in the expression level of any of the three proteins of interest, we sought to determine if there was a change in the expression levels of any of the proteins present in the epicardium in comparison to the endocardium. Samples from healthy organ donors and ischemic heart failure patients were segregated on whether they were harvested from the epicardium or the endocardium of the heart. On comparison, there appeared to be a trend towards more POPDC1 being expressed in the endocardium of the diseased patients in comparison to healthy donors (Figure 5.6, panel A) although the changes were not significant ($p>0.05$). Such a trend was not seen in the epicardium samples (Figure 5.6, panel B). Although only a trend, this does allow for some speculation that although the total level of POPDC1 might not be altered compartmentalised changes may occur.

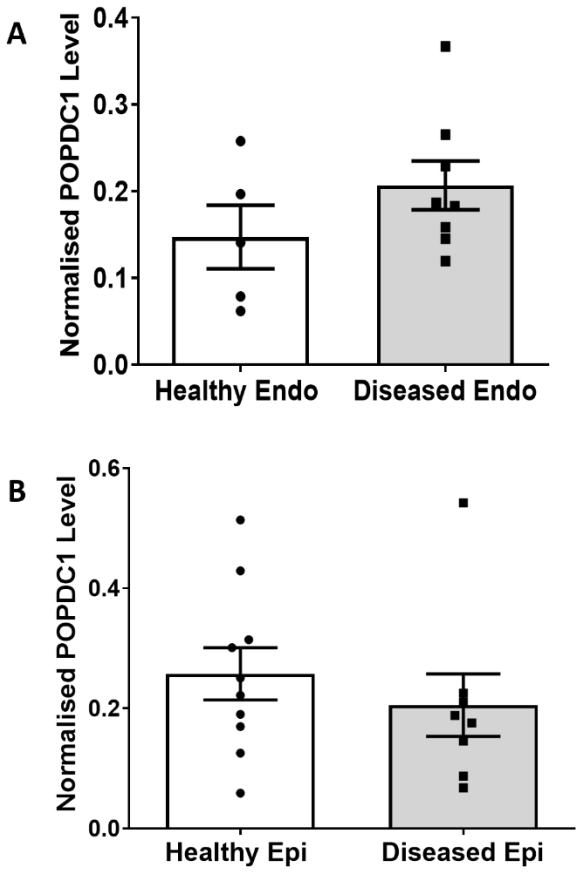

Figure 5.6 Comparison of POPDC1 compartment expression levels in Epicardium and Endocardium of healthy and diseased hearts. Graphical results shown were produced using the values obtained from the blots from Figure 5.3. A denotes the changes in endocardium expression of POPDC1 diseased and healthy samples. B, comparison of diseased and heathy epicardium POPDC1 levels. Both graphs show normalised mean ± SEM for n=20 for healthy and n=21 for diseased samples. Students t-test was performed.

A similar comparison of the evaluation of PDE4A levels in epicardium vs endocardium produced a borderline significant increase in the expression levels found in the diseased epicardium in comparison to healthy samples (Figure 5.7Figure 5.6, panel B). This follows the same trend as found in the pig MI model samples as the levels of PDE4A were still elevated 3-months post MI (Figure 5.2). In contrast, PDE4A expression level within the diseased endocardium remained unaltered when examined next to the healthy endocardium (Figure 5.7, panel A). This poses an interesting question about the possible compartment specific changes in PDE4A profile that may underpin the pathology.

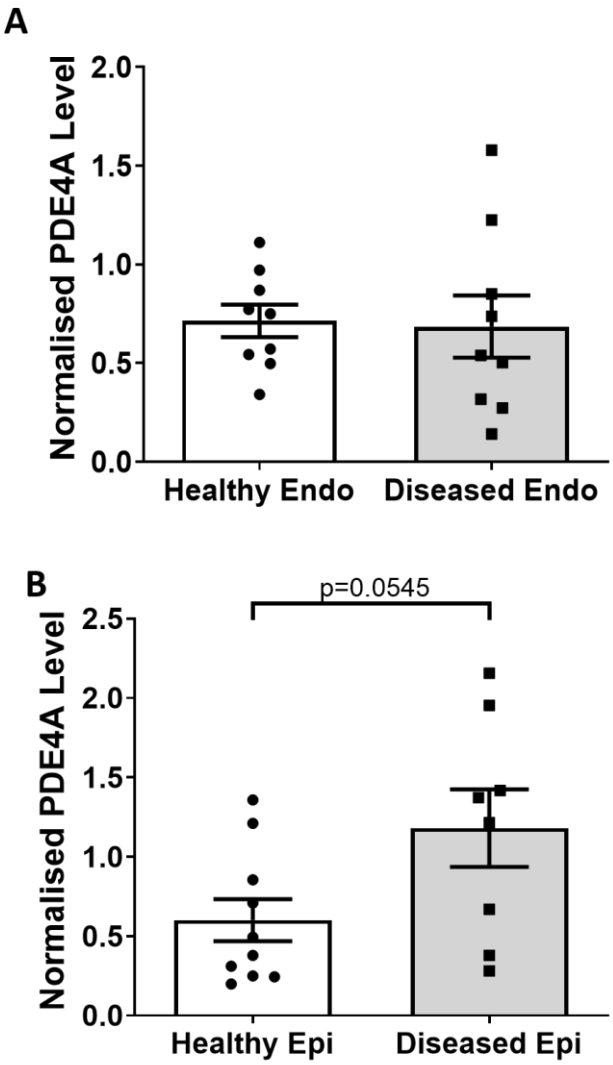

Figure 5.7 PDE4A expression levels in the endocardium and epicardium compartments. Graphical results shown were produced using the values obtained from the blots from Figure 5.4. A denotes the changes in endocardium expression of PDE4A diseased and healthy samples. B, comparison of diseased and heathy epicardium PDE4A levels. A p value of 0.0545 was found using a student's t-test showing a borderline significant change. Both graphs show normalised mean ± SEM for n=20 for healthy and n=21 for diseased samples. Students t-test was performed.

Finally, Cav3 levels were further examined to determine whether there were compartmental changes in expression. There appeared to be no change in Cav3 levels in either the endocardium or the epicardium of diseased hearts in comparison to healthy donors (Figure 5.8A and B, respectively). This is interesting, as it has been established that there is the dysregulation of caveolae within diseased myocytes meaning these results do not correlate with previously published data (Bryant et al., 2014, Bryant et al., 2018, Feiner et al., 2011).

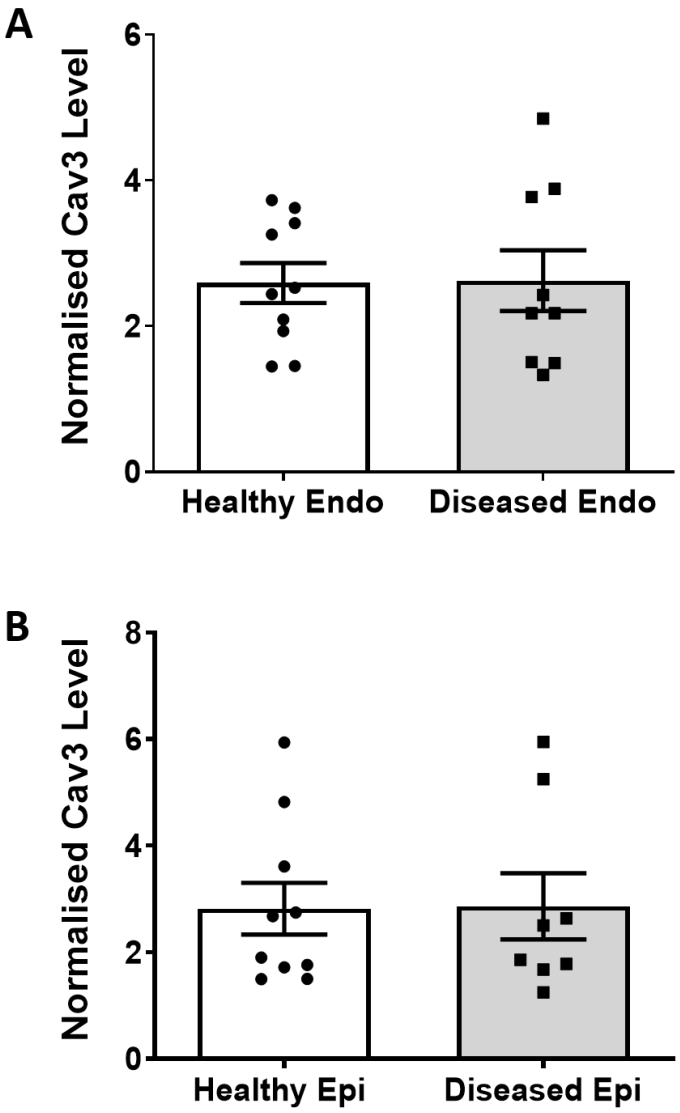

Figure 5.8 Cav3 expression levels and comparison in the endocardium and epicardium compartments. Graphical results shown were produced using the values obtained from the blots from Figure 5.5. A denotes the changes in endocardium expression of Cav3 diseased and healthy samples. B, comparison of diseased and heathy epicardium Cav3 levels. Both graphs show normalised mean ± SEM for n=20 for healthy and n=21 for diseased samples. Students t-test was performed. No significant changes were identified in either compartment.

5.5 Discussion

5.5.1 POPDC1 expression does not appear to be downregulated in ischemic heart failure

Previous studies have characterised a role for POPDC1 in the structural maintenance of cardiac and skeletal muscle (Andrée et al., 2002a). Gingold-Belfer and colleagues noted that transgenic mice lacking *Popdc1* expression displayed impaired recovery from ischemic injury (Gingold-Belfer et al., 2011). In addition, in failing human hearts, a reduction in POPDC1 mRNA expression was observed following myocardial I/R injury, which could be correlated to POPDC1 protein levels (Alcalay et al., 2013). I have shown here that in the immediate aftermath of MI in porcine models, there is a trend towards an increased level of POPDC1 in tissue isolated from whole hearts (Figure 5.1). It should be noted that although there appeared to be an increase in the level of POPDC1 immediately after MI, this was not significant and could be explained by the natural variability between samples. This was also true for PDE4A (Figure 5.2). The low n number does not allow for a conclusion to be made about how POPDC1 and PDE4A expression changes as part of the response to MI or heart failure. However, based off the slight increases in expression identified some hypothesis about the roles of the proteins in disease could be made.

POPDC1, through its interaction with Cav3, has been postulated to have a role in the protection of cardiac muscle. As previously mentioned, POPDC1 is a known interactor of Cav3 and has been shown to be important for the maintenance of caveolae numbers, as well as their size and structure (Alcalay et al., 2013). It has been previously established that the muscle specific Cav3 plays a critical role in cardiac protection, in ischemic preconditioning as well as in calcium handling during excitation-contraction coupling (Patel et al., 2008, Calaghan and White, 2006, Löhn et al., 2000). In addition, recovery from I/R and preconditioning were hindered when POPDC1 was lacking in hearts or cardiomyocytes (Alcalay et al., 2013). It may stand to reason that while there is increase of the expression of POPDC1 in the area where damage is immediate, there is a compensatory increase in the other unaffected cardiac tissue to maintain normal cardiac function.

In this light, a potential increase POPDC1 expression in the aftermath of an MI injury (Figure 5.1), if confirmed, could pose an interesting mechanism of how the heart creates protection from disease. Current published data has not clearly identified how POPDC1 either contributes towards cardiovascular disease or offers a protective function. Langendorff-perfused hearts from Popdc1-null mice were subjected to an I/R protocol of 30-minute normoxic stabilization, 30-minute global ischemia and 90 min reperfusion prior to analysis. These hearts exhibited larger infarct sizes as well as a decrease in their ability to recovery post injury (Alcalay et al., 2013). In addition, Popdc1-null cardiomyocytes displayed impaired $[Ca^{2+}]_I$ transients leading to augmented sensitivity to oxidative stress (Alcalay et al., 2013). Using this information, an explanation for the initial increase in POPDC1 could be that there is increased expression to aid in the recovery of the affected tissue. POPDC1, as mentioned in section 1.3.3, has several roles including in cell-cell junctions, in formation and maintenance of caveolae where many cardiac signalling molecules exist, in controlling the ion channel TREK1 and other functions that are needed to maintain normal cellular homeostasis (Schindler et al., 2012b, Amunjela and Tucker, 2017a, Froese et al., 2012, Kliminski et al., 2017, Han et al., 2019). I hypothesise that the increase in POPDC1 protein seen here is an attempt to maintain POPDC1 function in cells that are undergoing drastic morphology and signalling changes.

To illustrate this concept one can consider the example where contractile function is improved in response to pathological and physiological changes such as in MI, where there is hypertrophic growth without myocyte proliferation (Maillet et al., 2009). The small GTPase Cdc42 activated by GEFT was identified to be a signalling intermediate that could restrict cardiac growth in response to said physiological changes. Cdc42 is specifically activated in the heart after there is pressure overload. Maillet and colleagues identified that the loss of Cdc42 renders the heart more able to drive hypertrophic growth, post pressure overload, therefore suggesting that the usual function of Cdc42 is to antagonize cardiac growth (Maillet et al., 2009). This is in stark comparison to the other Rho GTPases such as Ras, Rac1 and RhoA, which have all been shown to drive hypertrophy (Zheng et al., 2004, Sussman et al., 2000, Satoh et al., 2006).

It has been postulated that POPDC1 interaction would act as a negative regulator of GEFT activity meaning it would be subsequently be important in the control of Cdc42 signalling. To support this, downregulation of POPDC1 resulted in randomised cell movements and changes possibility due to the perturbation of Cdc42/Rac1 signalling (Smith et al., 2008). Similarly, previous work has shown knockdown of POPDC1 expression, in cultured corneal epithelial cells, resulted in a disruption of epithelial integrity as well as delayed healing of epithelial sheets after wounding (Fenteany et al., 2000, Kofron et al., 2002, Nobes, 2000). This data further supports the function for Cdc42/Rac1 in wound healing and in maintaining epithelial sheet integrity. As POPDC1, when lost, was found to cause increased activation of Cdc42 it could be hypothesised that POPDC1 would function to control activation of GEFT by correctly localising it and as such control the function of Cdc42, thus stopping cellular hypertrophy and growth (Smith et al., 2008, Hager and Bader, 2009). As Cdc42 is highest at the leading edge of the cell it would be appropriate to suggest that the interaction of POPDC1 with GEFT would lead to a complex at the membrane allowing for the GEFT-activation of Cdc42 (Etienne-Manneville and Hall, 2002).

I speculate that POPDC1 expression changes in the aftermath of an MI may function to increase the onset of hypertrophy to protect the remaining cardiac tissue. The increase in Cdc42 drives the hypertrophy phenotype of undamaged cardiomyocytes in order to compensate for damage to the heart tissue after MI and to preserve cardiac function (Rubin et al., 1983, Beeri et al., 2008, Assayag et al., 1997). The trend in increasing POPDC1 was only found to exist in the time frame of two weeks post MI after which it is lost (Figure 5.1). Previously it has been shown that the hypertrophic response is often accompanied by improved function in cardiomyocytes (Mørk et al., 2007). This remodelling process has been labelled maladaptive due to late stage hypertrophy often leading to a reduction in contractibility and altered Ca^{2+} signalling which culminate in the deterioration of cardiac function (Mørk et al., 2007). In the case of POPDC1 signalling, the initial increase in expression would correlate to and facilitate the onset of hypertrophy by increasing activation of Cdc42 as an acute response by the heart. The damage and stress on the heart tissue is either resolved and POPDC1 signalling returns to basal, or the hypertrophy does not elicit its protective effects and the starved tissue develops into ischemic heart failure

(Cahill and Kharbanda, 2017). This pattern of increased protein expression in the acute aftermath of an MI, which is lost after period of time is not uncommon. For example, in the first 20 minutes after an MI there is a significant increase in the levels of Hypoxia inducible factor-1 alpha (HIF-1α) which dissipates after 1 hour (Al-Salam and Hashmi, 2014). This in turn drives the increase in Galectin-1 (GAL-1) within 4 hours post insult, which is then lost after 7 days (Al-Salam and Hashmi, 2014, Seropian et al., 2013). Gal-1 Is an evolutionarily conserved ß-galactosidase-binding lectin which plays an essential role in the control of inflammation and neovascularisation (Camby et al., 2006, Liu and Rabinovich, 2010). As such, it was proposed that GAL-1 functions to protect normal cardiac homeostasis as well as in post-infarction cardiac remodelling by blocking cardiac inflammation (Seropian et al., 2013). Therefore, the initial change in expression of HIF-1α followed quickly by its return to normal levels (yet the prolonged levels of GAL-1) sets precedent a for what I have described with POPDC1.

There are many more interaction partners of POPDC1 which all may in turn elicit changes that lead to the a cardioprotective effect in response to acute MI injury. These interactions may also contribute to end stage heart failure when the cardioprotective efforts are lost.

Another interesting observation from this chapter is that I have identified a trend toward an increase in PDE4A expression that begins in the acute phase after MI (Figure 5.2) and remains higher in the epicardium of heart failure patients (p=0.0545) (Figure 5.7, panel B). It has previously been reported that PDE4A expression is reduced in hypertrophic cardiomyocytes and in non-ischemic heart failure hearts in comparison to healthy hearts (Abi-Gerges et al., 2009, Richter et al., 2011, Kittleson et al., 2005). The identified decline was hypothesised to be in response to a deficit in cAMP synthesis but, this change in PDE signalling may be maladaptive as it could lead to a loss of compartmentalised cAMP signalling (Fischmeister et al., 2006, Rochais et al., 2004). Local loss of PDE4A in certain cAMP micro-domains, may lead to unrestricted diffusion of cAMP and the subsequent pan-activation of cAMP effector proteins and uncontrolled downstream signalling. Data from the initial reports from Abi-Gerges and colleagues (Abi-Gerges et al., 2009), were collected from isolated rat cardiomyocytes, whereas I used whole heart tissue from pig

and human subjects which may have different adaptive systems compared with rodents.

On the other hand, there is also evidence for the specific increase of PDE4A5, the rodent orthologue of PDE4A4, to protect fibroblasts from apoptosis (Huston et al., 2000b). This may correlate with the increase identified in this study as the increased PDE4A4 would function to protect the fibroblasts in the heart after MI. Also of note is the fact that PDE4A4 has been shown to be increased in macrophages during chronic obstructive pulmonary disease (COPD) as part of the inflammatory response (Barber et al., 2004). Macrophages have been shown to have key functions in the promotion of infarct healing and myocyte protection and increase vascularisation in ischemic tissue as well as its regeneration (Herold et al., 2004, Dewald et al., 2005, Minatoguchi et al., 2004, Trial et al., 2004, Chazaud et al., 2003, Eisenberg et al., 2003). The role of macrophages in this process is complex but it is believed that, like many acute responses to MI, although beneficial in the acute phase it becomes deleterious in the late phase of remodelling (Leor et al., 2006). Increasing macrophages infiltration in response to injury may be responsible for the PDE4A seen in the whole heart tissue samples used here.

Finally, I also investigated Cav3 expression in this chapter due to the prior knowledge that hypertrophy and heart failure are associated with a decrease in its expression(Bryant et al., 2014). Western blot analysis showed no changes in the Cav3 expression in heart failure in comparison to healthy counterparts (Figure 5.5). However, overexpression of Cav3 was shown by Kong and colleagues to be cardioprotective by reducing the phenotypic and functional changes brought on by pressure overload (Kong et al., 2019). As such, the lack of change in Cav3 expression may be due to protective effects returning to basal after acute injury.

5.5.2 Methodological considerations and future directions

Several considerations must be taken into account when examining the results presented in this chapter. Although, I have identified a trend that hints toward an increased expression in both POPDC1 and PDE4A in the acute stages post MI in pig, it should be noted that the study is underpowered with only an n of 3 hearts

per condition. Therefore, the addition of more replicates would make any conclusions more solid.

In addition, using data produced to formulate a pathway of POPDC1 expression and potential function using human and porcine tissue may result in discrepancies due to the mixed model experiments. There are in fact major anatomical differences between pig and human hearts that could also result in a differing response to injury (Crick et al., 1998). One example is that the Purkinje fibres in pig possess large subendocardial fibres which provide the animal with a more neuro-stimulated myogenic contraction system than humans (Ibrahim et al., 2006). In addition, their vascular resistances are more than 2-fold higher than that in humans therefore, they may be able to compensate with the damage of an MI better (Thein and Hammer, 2004). It also must be considered that there is intrinsic variability between individual human and porcine subjects that cannot be resolved with such a small sample size.

It is always important to discuss the difference between statistical significance and biological relevance (Page, 2014). Small changes that appear to not be statistically significant may result in a large, biologically significant, physiological change. For example, the reduction in expression of Small-Conductance Ca^{2+}-Activated K^{+} (SK3) channels which modulate arterial tone and blood pressure, was shown to elicit a significant biological impact on arterial tone contributing to attenuated vasoconstriction responses (Taylor et al., 2003). This could allow us to hypothesize that the anything outside of basal levels of POPDC1 or PDE4A could have a biological impact, even with minute changes.

One final point that must be addressed is that the samples collected from patients of heart failure and organ donors represent a snapshot in time. The levels of natural variations in protein expression, in stages of heart failure, age of patient or smoking status may mask any potentially significant changes that would have been identified by Western blotting (Egerstedt et al., 2019, Volkova et al., 2005, Rababa'h et al., 2019, Vileigas et al., 2019). The patients possessed a wide range of health and lifestyle backgrounds (data not shown) that all may generate variations in protein expression levels. In addition, the lack of subtle changes seen could also be attributed to the process of normalising protein concentration for Western blotting. Band intensities of the protein of interest

e.g. POPDC1 calculated using ImageJ software were normalised to the band intensities of the loading control protein e.g. GAPDH. This process allows for samples on different blots to be compared. The intensity measurements are an estimation of how much protein is in a sample therefore, it is possible that subtle changes are not detected using this method.

5.5.3 Conclusion

In conclusion, we have identified that there is a trend toward an increase in POPDC1 and PDE4A levels post-MI, which is not in-line with published data. In samples of human heart failure there appeared to be a shift in POPDC1 expression between the epi-and endocardium, which saw more POPDC1 being present in the epicardium of diseased hearts and lower levels in epicardium compared to healthy samples. For PDE4A, there was a borderline significant increase in PDE4A levels in the epicardium of diseased hearts. Collectively, this evidence allows for speculation that there may be alterations in the compartmentalisation of the POPDC1/PDE4A complex during heart failure that may contribute to disease pathology by virtue of alterations in regulation of the POPDC1 interactome rather than a lack of POPDC1 expression *per se*.

6 Investigating the SUMOylation, Phosphorylation and Palmitoylation of POPDC1

6.1 Introduction

The number of human-protein coding genes is around 20,700 however the actual proteome includes hundreds of thousands of functionally different proteins (ENCODE-Project-Consortium, 2012, Schlüter et al., 2009) due to mRNA splicing, promoter diversity and post-translational modification . Post-translational modifications (PTMs) are a set of chemical changes that a protein can undergo after translation that can influence the protein's function, stability and location. More than 200 diverse types of PTMs are currently known to exist which elicit a wide variety of functional effects on their target proteins (Duan and Walther, 2015). Within this chapter three PTMs will be examined; phosphorylation, SUMOylation and palmitoylation (Figure 6.1).

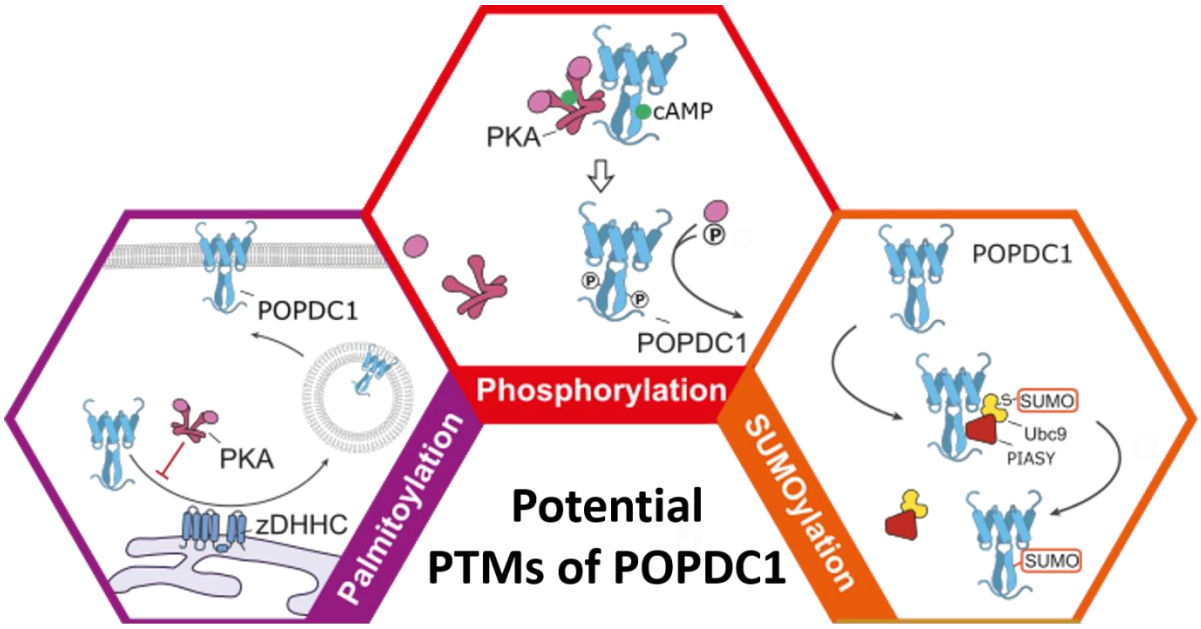

Figure 6.1 Some of the potential PTMs of POPDC1. The palmitoylation (purple panel) of proteins has been extensively investigated due to its membrane targeting function. One mechanism by which POPDC1 may achieve its desired localisation is through palmitoylation of the protein after synthesis in the Golgi body, as shown here. Other functions for palmitoylation are known such as inferring membrane stability. Phosphorylation (red panel) of proteins is a very common mechanism used to control their activity. Given the importance of cAMP dynamics in the interactions of POPDC1, it may be the case that POPDC1 is subjected to phosphorylation by protein kinase A (PKA). When PKA (pink) is activated in the cell the catalytic subunits can function, adding a phosphate (P) group onto its target substrate. This may have numerous functional consequences including conformational changes that could expose new binding regions. In the same thread as phosphorylation, the PTM of SUMOylation (orange panel) can result in the creation of new binding regions or in contrast, target a protein towards a degradation pathway. SUMOylation occurs through the collaborative effort of SUMO E1, E2 (Ubc9) and E3 (e.g. PIASY) ligases attaching a SUMO group to the target protein. Upon attachment of the SUMO modification the SUMO E1-3 enzymes are released.

6.1.1 PKA phosphorylation

Protein phosphorylation is a major mechanism by which protein function can be regulated in response to both intracellular and extracellular stimuli (Ardito et al., 2017). This reversible modification occurs through protein kinases, such as PKA, which link a phosphate group (PO_4) to the polar group R of various amino acids (Ardito et al., 2017) and phosphatases, which do the opposite. The addition of a negatively charged phosphate group modifies the protein from hydrophobic polar to hydrophilic polar resulting in a change in protein conformation that can influence interaction with other proteins or molecules. Not only can phosphorylated proteins bind and form complexes but they can consequently allow for the detachment of protein complexes (Alberts et al.,

2002). Phosphoproteins primarily rely on the ATP as the phosphate group donor (Ardito et al., 2017).

6.1.1.1 Kinases

In more recent years kinases have been considered to hold a crucial role not only in signalling but it the transduction of that signal (Hornberg et al., 2005, Heinrich et al., 2002). Most protein-phosphorylation events occur on a serine (S or Ser), a threonine (T or Thr), or a tyrosine (Y or Try) residue (Roskoski, 2012). Less common is the phosphorylation of a histidine (H or His) or an aspartate (D or Asp) residues but, these are less stable phosphorylation events (Ardito et al., 2017). The superfamily of protein kinases is responsible for all protein phosphorylation. Most kinases can also be phosphorylated as part of the activation mechanism and this promotes a cascade of signalling events culminating in the phosphorylation of the terminal protein substrate that impinges on the physiological function of the cell (Alberts et al., 2002). The activation or deactivation of kinases can occur through; *cis*-phosphorylation/autophosphorylation, by binding an activator or inhibitor or by changes in their subcellular localisation in relation to their target substrate (Roskoski, 2012).

The catalytic domain of the protein kinase contains two sub-domains, N and C terminal (Schwartz and Murray, 2011). The two subunits are connected by a peptidic strand that forms an active site containing both a front and back pocket (Ardito et al., 2017). The activation of this catalytic domain is caused by the phosphorylation of the activation loop or alternatively through an allosteric mechanism (Schwartz and Murray, 2011). Kinases also possess a non-catalytic domain which allows for the attachment of substrates and the recruitment of other signalling proteins (Nishi et al., 2014).

There are currently 218 human protein kinases which have been identified and they are classified according to the amino acid residue they phosphorylate. Most of the known kinases can phosphorylate both Serine and Threonine residues (serine/ threonine kinases -STKs), others act on Tyrosine (Tyrosine kinases -TKs), while others act on all three (dual-specificity kinases – DSKs) (Miller et al., 2008, Hunter, 2009).

6.1.1.2 Protein Kinase A

One serine/threonine kinase is the cAMP dependent protein kinase A (PKA). The activity of its two catalytic (C) subunit is regulated by the two regulatory (R) subunit isoforms, (Taylor et al., 2004). In addition to the R units, substrate specificity is governed via attachment to scaffold proteins called A kinase anchoring proteins (AKAPs). AKAPS have the ability to target PKA through its R subunits to different sites within the cell bringing them into close proximity with PKA substrates (Gold et al., 2006).

During its activation, the C-subunit is initially phosphorylated by phosphoinositide-dependent protein kinase at T197 (Cheng et al., 1998, Cauthron et al., 1998). The phosphorylation of T197 in the activation loop is necessary for the activity of PKA and once this has been phosphorylated it is not turned over readily (Steinberg et al., 1993, Adams et al., 1995, Taylor et al., 1990, Shoji et al., 1979). The C-subunit is regulated through the interaction with the inhibitory R-subunit which sequesters the C-subunit in an inactive heterodimeric holoenzyme. Upon the binding of 2 cAMP molecules to each R-subunit, there is a conformational change whereby there is the dissociation of the holoenzyme realising the C-subunit (Taylor et al., 1990). The free C-subunit can then go on to phosphorylate a wide range of cytoplasmic and nuclear protein substrates (Moore et al., 2003). For example, S54 of the cAMP-specific PDE4D3 is known to be a PKA phosphorylation site that is crucial for activation of the enzyme (Sette and Conti, 1996).

6.1.2 SUMOylation

6.1.2.1 The SUMO family

The post translational modification of SUMOylation, is based on the covalent attachment of small ubiquitin-like modifier (SUMO) protein to a substrate (Hannoun et al., 2010). However, the name SUMO is misleading as sequence homology has shown that there is only ~18% similarity with ubiquitin (Müller et al., 2001). This modification is highly conserved in a wide range of species and displays a wide range of functional effects such as regulation of the cell cycle and transcription, to the targeted subcellular localisation of proteins and their

degradation (Müller et al., 2001, Seeler and Dejean, 2003, Verger et al., 2003, Hannoun et al., 2010).

There are three SUMO homologues that have been identified in humans: SUMO-1, SUMO-2 and SUMO-3 (Johnson, 2004). SUMO-2 and SUMO-3 have a 95% sequence homology with each other but only share 50% sequence homology with SUMO-1 (Johnson, 2004). SUMO proteins are able to covalently bind to lysine residues in the target substrate, which are mostly contained within the SUMO consensus sequence, ΨKxD/E, where Ψ corresponds to a large hydrophobic amino acid, K is a lysine residue, x is any amino acid and D/E is an aspartic acid or a glutamic acid residue (Hannoun et al., 2010). It has been noted however, that proteins can be SUMOylated out with this consensus motif and currently ~40% of known SUMOylated proteins do not possess this consensus sequence (Hannoun et al., 2010, Ulrich, 2009). Binding occurs through the formation of an isopeptide bond between the C-terminal carboxy group of the SUMO protein and the ε-amino group of the lysine residue of the substrate protein (Hannoun et al., 2010). A unique property of SUMO-2 and SUMO-3 is the ability to form polySUMO chains that are covalently linked to each other through the lysine residue at the N-terminus of their consensus sequence (Hannoun et al., 2010). SUMO-1 does not contain this consensus site and as such is not able to form polySUMO chains therefore it can act as a chain terminator (Ulrich, 2009, Kurepa et al., 2003, Kroetz, 2005).

6.1.2.2 SUMOylation cascade

The enzymatic process of adding a SUMO protein to the target substrate is largely similar to that of its cousin, the ubiquitination pathway. Both of these pathways utilise three enzymes: the activating enzyme, E1; the conjugating enzyme, E2; and the ligase enzyme, E3 (Takahashi et al., 2001, Gareau and Lima, 2010, Hannoun et al., 2010) (Figure 6.2). Like ubiquitin, SUMOs are initially synthesised as propeptides that require cleavage (Mukhopadhyay and Dasso, 2007). Cleavage reveals a C-terminal di-glycine motif and which must occur in order to allow conjugation to a substrate (Mukhopadhyay and Dasso, 2007). The next step involves the SUMO E1 activating enzyme, which interacts with the SUMO protein creating an energetic thioester bond. The heterodimer E1 enzyme contains two subunits known as Aos1 (SAE1) and Uba2 (SAE2) (Figure 6.2)

(Han et al., 2018). Formation of the thioester bond by E1 is required for the conjugation E2 enzyme to interact with SUMO. So far there has only been one identified E2 enzyme, Ubc9, which can be located at the nuclear pore complex (NPC) or at the nucleoplasm side of the NPC (Han et al., 2018). The activated SUMO protein is transferred to a cysteine residue at position 93 in the active site of Ubc9 through a transesterification reaction leading to the formation of an E2-SUMO thioester compound. Unlike SUMO-E2, multiple SUMO-E3 proteins have been identified, each of which has substrate specificity for numerous SUMO target proteins with little redundancy (Ulrich, 2009, Han et al., 2018). The most prominent group of E3 ligases in humans is the protein inhibitor of activated STAT (PIAS) family which consists of 5 proteins made up of 4 human PIAS genes; PIAS1, PIAS3, PIASxα and PIASγ (Palvimo, 2007, Liu and Shuai, 2008, Liu et al., 1998). The PIAS family of proteins contain SP-RING domains, which bind to Ubc9, and SUMO interacting motifs (SIMs), which can bind to SUMO directly promoting SUMOylation of substrates (Hochstrasser, 2001). SUMOylation, just like phosphorylation is a reversible process that is under the control of a family of cysteine proteases called sentrin-specific proteases (SENPs) (Figure 6.2) (Mukhopadhyay and Dasso, 2007). These proteases are able to deSUMOylate proteins by simply removing SUMO from its substrate. There are seven known SENP family members which possess a level of substrate specificity (Mukhopadhyay and Dasso, 2007, Ulrich, 2009).

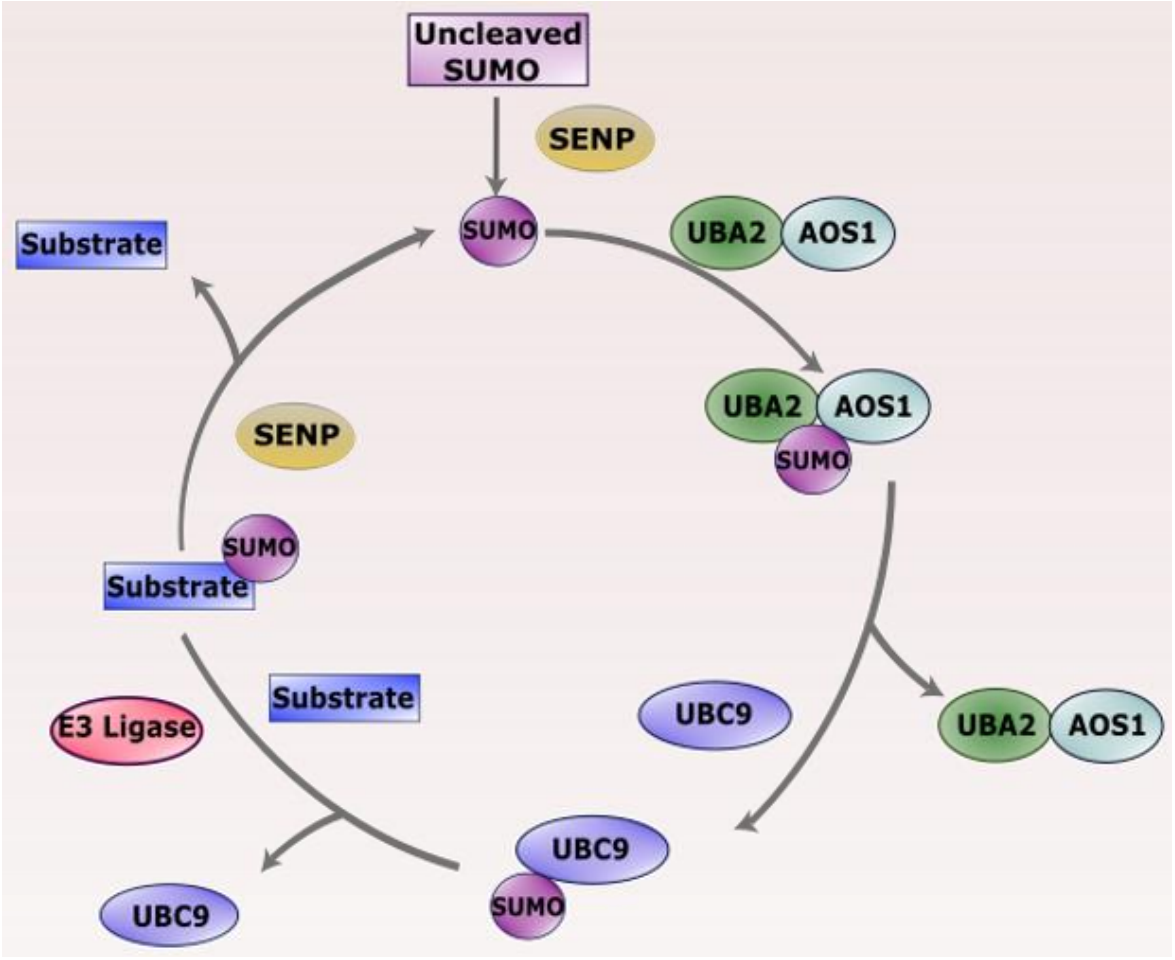

Figure 6.2 SUMOylation Cascade. The SUMOylation cascade begins with the cleavage of the C-terminal portion of the pro-form of SUMO. This process is carried out by sentrin-specific proteases (SENP). SUMO protein is then bound to the E1 protein, which exists as complex containing UBA2 and AOS1. This interaction is dependent upon ATP-Mg^{2+}. Next, SUMO is transferred to the catalytic cysteine of the E2 conjugating enzyme UBC9. An E3 ligase then catalyses the removal of SUMO from UBC9 and facilitates the conjugation of SUMO to the target protein. SENP's can remove added SUMO from a substrate to create a dynamic and reversible pathway. (Figure adapted from (Hannoun et al., 2010)).

6.1.2.3 Functional effects of SUMO

The SUMO system is essential in almost all organisms (Ulrich, 2009). There is however, no single defined effect of SUMOylation on a target protein and investigations have shown that a wide range of functional outcomes are possible (reviewed in (Ulrich, 2009)).

Firstly, SUMOylation of a target protein can alter its interactions with other proteins (Ulrich, 2009). The conjugation of the SUMO protein can allow for the creation of an additional binding site altering its interaction with other proteins or allowing the substrate to be targeted to a specific subcellular location. Some

proteins interact with SUMO covalently using a C-terminal di-glycine motif and others can interact in a non-covalent manner due to the presence of SIMs. An example of a SIM binding protein is p73, a member of the p53 tumour suppressor family, which has been shown to only interact with certain proteins after it has been SUMOylated (Minty et al., 2000). SUMOylation can also result in the blocking of an interaction site therefore preventing protein-protein interaction formation (Ulrich, 2009). It has also been shown that SUMOylation has the ability to modify the conformation of substrate proteins affecting the way substrates interact with other proteins (Steinacher and Schär, 2005). Additionally, some SUMOylation sites can only be utilised if they are adjacent to an already phosphorylated phospho-site (Hietakangas et al., 2006). A phosphorylation-dependant SUMOylation motif, ψKxExxSP, where P represents a proline, has previously been identified in a number of transcription factors (Hietakangas et al., 2006). This contains the classical SUMO interaction motif two amino residues upstream of a phosphorylation site. For example, PDE4D5 is known to be phosphorylated by PKA in order to elicit its activation (Lynch et al., 2007). SUMOylation of PDE4D5 at a phosphorylation-dependant SUMOylation motif next to the PKA phosphorylation site results in its locking into a hyperactive state (Li et al., 2010). In addition, the SUMO modification of PDE4D5 can also acts as a shield, blocking inhibitory phosphorylation by ERK (Li et al., 2010). Finally, SUMO and ubiquitin can function cooperatively, for example a protein can be SUMOylated after which it is targeted to the nucleus leading to its ubiquitination and degradation (Huang et al., 2003, Ulrich, 2009). Conversely, SUMOylation of a protein can block ubiquitination at the same lysine residue (Liebelt and Vertegaal, 2016).

Many of SUMO targets are nuclear proteins that are involved in the regulation of transcriptional activity, however, there is an emerging field of study characterising a role for the SUMOylation of cytosolic proteins that elicit a wide range of functional effects (Yang et al., 2017). In summation, SUMO conjugation can trigger a variety of outcomes for a target substrate such as; modulating the protein's interactions with other proteins, its subcellular localisation, and its stability (Ulrich, 2009).

6.1.3 Palmitoylation

The lipid modification known as palmitoylation is a reversible and regulated modification that has numerous cellular functions (reviewed in (Charollais and Van Der Goot, 2009)). The process of palmitoylation generally consists of the addition of C16 carbon saturated fatty acyl chain to a cysteine residue on a cytoplasmic region of the protein (known as S-palmitoylation) via the formation of a thioester linkage (Zhang and Hang, 2017). It is this high-energy thioester bond that underpins S-palmitoylation's reversible state. The primary function of S-palmitoylation is to target proteins to specific membrane compartments or microdomains (Levental et al., 2010, Rocks et al., 2005, Kanaani et al., 2008, Schroeder et al., 1997). In influencing the localisation of proteins and their trafficking, palmitoylation can have critical consequences for protein function. Interestingly, 40% of the membrane proteome has been estimated to be S-palmitoylated (Roth et al., 2006, Hemsley et al., 2013, Kang et al., 2008).

6.1.3.1 S-palmitoylation pathway

Palmitoylation is known to occur at a wide variety of sequence motifs within both soluble and transmembrane proteins, which has made identification of a consensus sequence difficult. The diversity in substrates is accommodated by a large array of enzymes known as the DHHC protein acyl-transferases (PATs) family (Fukata et al., 2004, Huang et al., 2004, Lobo et al., 2002, Roth et al., 2002, Roth et al., 2006). There are 23 distinct mammalian DHHC PATs, which together carry out most of the palmitoylation events within the cell (Putilina et al., 1999, Ohno et al., 2006). The DHHC PATs are multi-pass transmembrane proteins that are mainly localised to the intracellular compartments of the membrane but are also found at the plasma membrane (Ohno et al., 2006). DHHC proteins palmitoylate substrates by a twostep process: firstly the enzyme is auto-acylated and then it transfers its attached palmitoyl-residue to the target protein (Jennings and Linder, 2012, Mitchell et al., 2010). The process of depalmitoylation is tightly regulated and is carried out by the cytoplasmic enzymes acyl-protein thioesterases 1 and 2 (APT1 and APT2) (Bachovchin et al., 2010).

6.1.3.2 Regulatory effects of palmitoylation

Palmitoylation is normally found coupled with either N- myristoylation or prenylation (Shahinian and Silvius, 1995). N- myristoylation is the addition of myristic acid (C14) to a glycine residue with an exposed NH_2 group in the target protein (Zha et al., 2000) whereas prenylation results in the attachment of farnesyl or geranylgeranyl isoprenoids to a C-terminal cysteine residue within its consensus sequence (Wright and Philips, 2006). These groups collectively can regulate membrane interactions with soluble cytosolic proteins. Single chains of either myristoyl or prenyl chains allow for transient membrane association allowing DHHC proteins to carry out palmitoylation and stabilise membrane binding (Shahinian and Silvius, 1995). In this way, palmitoylation is crucial for the stability of some membrane proteins. An example of this is found in the $G\alpha$ subunits of G proteins which are myristoylated and palmitoylated to increase stability in the membrane (Linder et al., 1993). In contrast to many other static lipid modifications, the reversibility of palmitoylation allows for dynamic regulation of protein localisation such as seen in the Ras protein family (Rocks et al., 2005, Roy et al., 2005, Goodwin et al., 2005). For example, without palmitoylation, H-Ras and N-Ras display weak membrane affinity and lower trafficking to the membrane. Palmitoylation promotes Ras trafficking from the Golgi to the plasma membrane and stabilises its membrane interaction. Subsequent depalmitoylation causes Ras to disassociate with membrane and the process can begin again (Goodwin et al., 2005, Rocks et al., 2005).

6.2 Hypothesis and Aims

There is currently little data on the extent and identity of POPDC1 PTMs and such modifications could be important for POPDC1 function. The possibility that POPDC1 could be modified by three of the most common PTMs was examined. Firstly, prediction software was used to determine that POPDC1 contained possible sites of phosphorylation, SUMOylation and palmitoylation. The main aim of this chapter was to determine whether these modifications could be detected using a variety of assays. More specifically, the aims were as follow:

- To identify and confirm a phosphorylation site in POPDC1 using peptide array

- To examine whether POPDC1 contains a motif for SUMOylation and determine if SUMOylation can occur in endogenous NRVM

- To investigate if POPDC1 can be palmitoylated in endogenous NRVM

6.3 Results

6.3.1 POPDC1 contains a site for PKA phosphorylation in the Popeye domain

The lack of knowledge surrounding control of POPDC1 by PTM led to the hypothesis that it may be a target of phosphorylation. As POPDC1 is a newly discovered cAMP effector I was intrigued by the possibility that POPDC1 could be a substrate for PKA. Via phospho-site prediction software (GPS 5.0) I highlighted 11 possible serine and threonine residues that could be sites of PKA phosphorylation (Table 6). This Group based prediction software makes a computational prediction of phosphorylation sites along with their cognate protein kinase through a novel algorithm. The algorithm uses motif recognition parameters to score the site giving insight as to the probability of its existence. Given that these residues were widespread throughout the entire POPDC1 sequence, it was determined that the initial screen would encompass the full POPDC1 sequence on a peptide array membrane.

Position	Code	Kinase	Peptide	Score
12	S	AGC/PKA/PRKACB	ESSPLRESTAIGFTP	1.266/21.95/4.204
13	T	AGC/PKA/PKACA	SSPLRESTAIGFTPE	0.599/1.713/3.637
125	S	AGC/PKA/PRKACB	VKIEKELSGMYRRLF	3.59
146	T	AGC/PKA/PKACA	PDLFRRLTGQFCMIQ	2.426/3.304
174	S	AGC/PKA	TSVDDRLSILLKGKM	22.36/1.857
236	T	AGC/PKA/PKACA	CWSRERLTYFLESEP	2.39
258	T	AGC/PKA/PRKACB	YLIGKDITNKLYSLN	2.851
263	S	AGC/PKA/PRKACB	DITNKLYSLNDPTLN	2.075
295	S	AGC/PKA/PKACA	SMLEMRNSIASSDS	0.485/22.403/1.951
314	S	AGC/PKA/PKACA	HQFLRGTSSMSSLHV	1.227/22.222/2.58
329	S	AGC	SSPHQRASAKMKPIE	0.851

Table 6 Prediction of PKA motifs in POPDC1 using GPS 5.0 kinase prediction software. Full length human POPDC1 human sequence was run through the CUCKOO Workgroups Group-based Prediction system (GPS) to highlight predicted phosphorylation motifs within the protein (Xue et al., 2010). The table notes the residue position of the phosphorylated serine (S) or threonine (T) as well as the sequence in which the site is found. Also, notes the confidence score of each site. The higher this score the higher the probability that it exists biologically.

Initially the full length POPDC1 sequence, presented in 25mers on a peptide array, each spot sequentially shifted by 5 amino residues (described in 2.9.2), was overlaid with purified, active PKA catalytic subunit in a kinase assay mix to identify any PKA phosphorylation sites (Figure 6.3). Using a PKA phospho-substrate antibody, only one site was identified for PKA phosphorylation on a threonine residue at position 236 (Figure 6.3, denoted in red). This residue lies in the middle of the Popeye domain around 50 amino residues downstream of the identified PDE4A binding site and of the predicted TREK1 binding site (described in section 3.3.4). T236 was one of the sites predicted through the phospho-site virtual screen adding some validity to the result. There was no unspecific binding of the PKA substrate antibody in the control array that was not overlaid with PKA cat subunit (Figure 6.3).

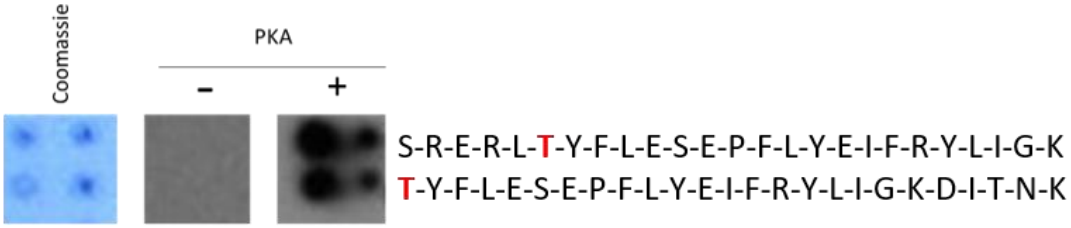

Figure 6.3 *In* vitro PKA assay using full length POPDC1 peptide array. To identify any PKA phosphorylation sites, POPDC1 full length was spotted on cellulose in 25mer peptides that were shifted by 5 amino residues each time. The peptide array was overlaid with PKA catalytic subunit (denoted with + above). Peptide arrays were stained with Coomassie or incubated with antibody only as controls (denoted with – above). Arrays were imaged using Xomat® (Kodak). Red letters indicate the threonine that is the potential site of phosphorylation.

To confirm that it was the threonine residue that was being phosphorylated by PKA, walking alanine scans were carried out on the identified 25mer (Figure 6.4). Sequentially each amino residue was substituted with an alanine and the peptide array was overlaid with the PKA catalytic subunit in the kinase assay mix. Ablation of the threonine residue led to a complete loss of phosphorylation (Figure 6.4). Interestingly, the change in the amino residues R232 and R-L-T (residues 234-236) collectively, resulted in a loss of PKA phosphorylation.

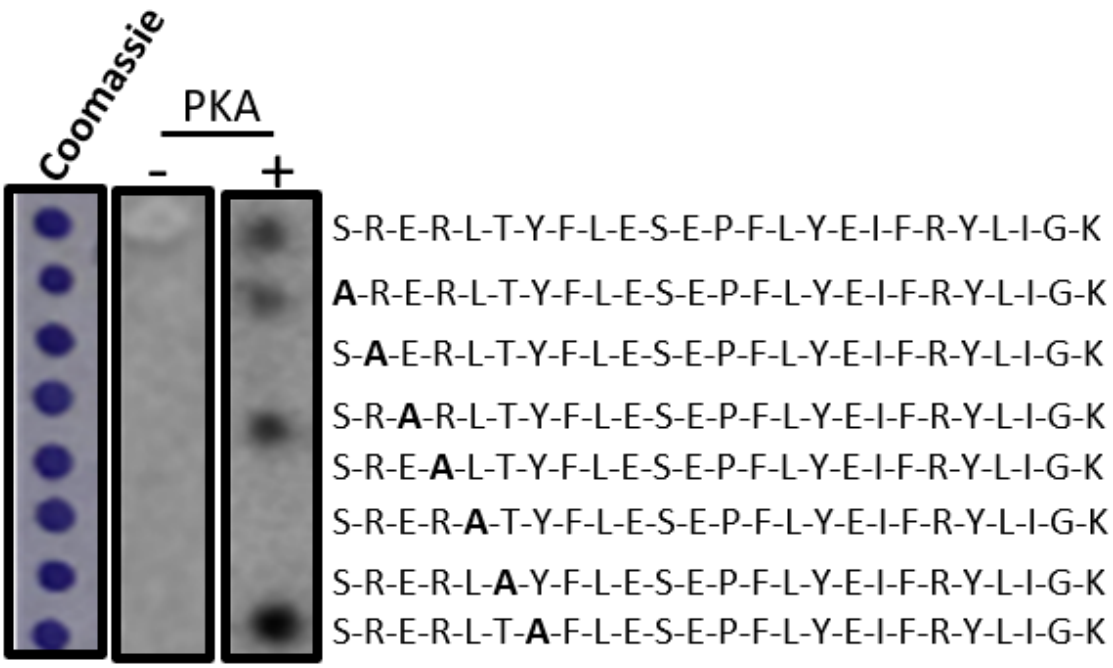

Figure 6.4 Walking Alanine scan of PKA site. Sequentially, 25mer amino acid sequence, surrounding and including the PKA site on POPDC1, were substituted with alanine (shown in bold). Arrays were subjected in vitro PKA assay before being immunoblotted for PKA substrate. Control slides were not subjected to *in vitro* PKA assay only probed with primary and secondary antibody. An untreated array was Coomassie stained as a protein concentration control.

A secondary alanine scan peptide array, that substituted two residues, at a time was carried out to examine if the sequence immediately prior to the T236 was crucial to POPDC1s ability to be phosphorylated by PKA (Figure 6.5). Interruption of the S-R-E-R-L-T (residues S231-T236) sequence resulted in the complete loss of phosphorylation, identifying that this site was critical to the addition of the phosphate group of T236.

Collectively this evidence provides the first conformation of a possible PKA-dependent phosphorylation site on POPDC1.

Figure 6.5 Double Alanine Substitutions of PKA site. In each instance two amino residues surrounding and including the PKA site were substituted with alanine. Arrays were subjected to *in vitro* PKA assay before being immunoblotted for PKA substrate (denoted with +). Control slides were not subjected to *in vitro* PKA assay only probed with primary and secondary antibody (denoted with -). An untreated array was Coomassie stained as a protein concentration control.

6.3.2 POPDC1 contains a SUMO site that can be SUMOlyated *in vitro*

As mentioned, SUMOylation of protein substrates can have a wide range of effects from increasing or decreasing their stability to modulating their interactions with other proteins (Ulrich, 2009). The next step in examining the potential post-translational modifications of POPDC1 was to investigate whether it could be modified by SUMO. SUMOylation of a target proteins occurs through the conjugation of a SUMO protein to a lysine situated in the consensus sequence ΨKxD/E, where Ψ represents a large hydrophobic residue, K a lysine residue, x is any amino acid and D/E is an aspartic acid or glutamic acid respectively (Hannoun et al., 2010).

As there has been no previous work carried out on SUMOylation of POPDC1, SUMOplot™ prediction software was utilised to identify any potential sites of SUMOylation (Figure 6.6A). The software identifies possible SUMOylation sites and gives the probability of the lysine contained within this site being SUMOylated based on the classical consensus motif. Not only does it identify

classical motifs, but also close consensus motif matches that share a similar hydrophobicity pattern (Abgent, SUMOplot™ Analysis Program). One SUMO consensus site that was identified in this scan, lysine at position 119 (K119), can be seen to reside immediately upstream of the Popeye domain (Figure 6.6B). In addition, two SIMs were predicted to exist, one in the extracellular N-terminus and the other at the end of the Popeye domain.

A

Position	Peptide	Score	P-value	Type
24-28	FTPELESIIPVPSNKTTCE	35.392	0.14	SUMO Interaction
119	LYKKRPVKIRKRLSG	16.642	0.004	Sumoylation consensus
217-221	HKGEKFQVTIIADDNCRFL	35.197	0.132	SUMO interaction

B

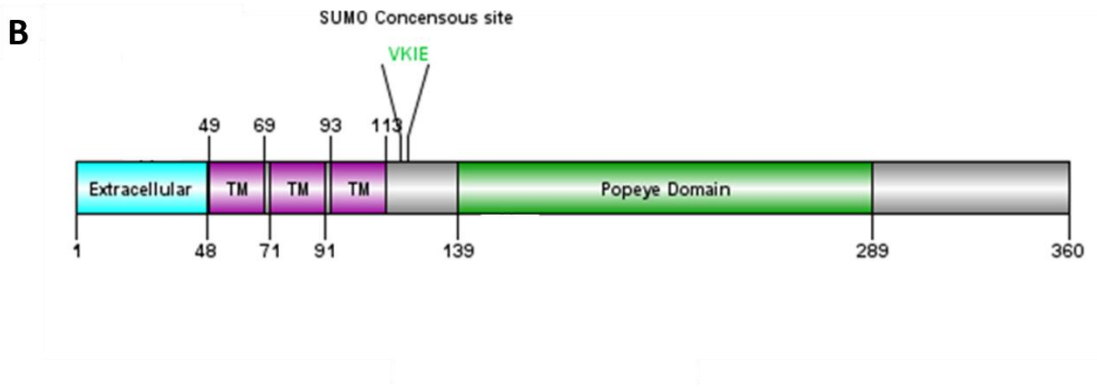

Figure 6.6 Sumo site scan and schematic of POPDC1 with sites. A SUMOplot ® was used to identify potential SUMOylation sites and SUMO interacting motifs (SIMs) in POPDC1. Sequence of SUMOylation binding or SIM are highlighted in red text. The confidence score of each site is given alongside its position in the POPDC1 protein. The higher the score the higher the probability that this is a biologically found SUMOylation site. **B,** A schematic representation of POPDC1 protein showing SUMO consensus sequence and its position on the protein.

To confirm whether this predicted site was SUMOylated, peptide arrays containing the full-length sequence of POPDC1 (25mers shifted by 5 a.a.) were exposed to an *in vitro* SUMO assay kit (Enzo). Using a SUMO2/3 specific primary antibody it was shown that the predicted consensus site was able to be modified by SUMO (Figure 6.7). Furthermore, there was no evidence of non-specific binding in the antibody only control. SUMOylation of the P-V-K-I-E motif was lost in the 5mer shifts that did not contain said motif (Figure 6.7 lowest spot) or where the motif was close to the point of immobilisation at the N-terminal of peptide (Figure 6.7, 2nd lowest spot).

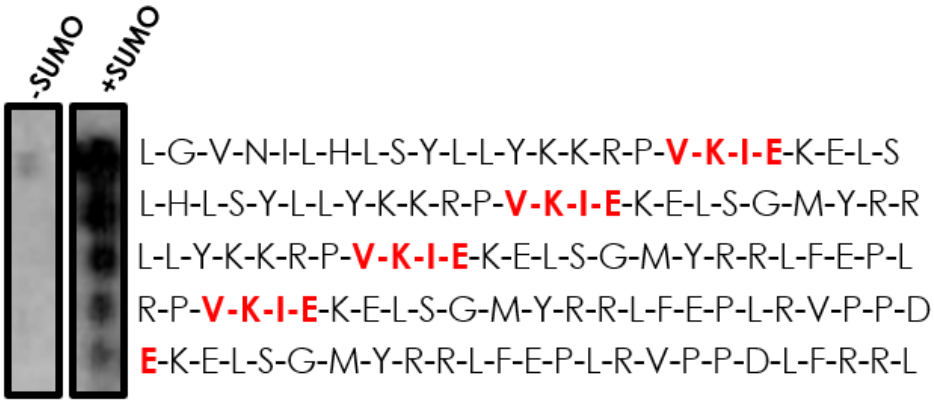

Figure 6.7 *In* vitro SUMO assay using full length POPDC1 peptide array confirmed SUMO motif. Full length POPDC1 sequence covered in 25mer spots on peptide arrays were used in an *in vitro* SUMO assay. 25mers were shifted by 5 amino residues each spot to allow full coverage of the protein. After 1-hour incubation at 37ºC in the presence of the SUMO kit, membranes were blocked in 5% BSA and incubated in SUMO2/3 primary antibody. Control membranes were not exposed to the SUMO kit. The consensus sequence identified is noted in red. POPDC1 can be SUMOylated on the VKIE motif at position (V118-E121).

Although peptide arrays have confirmed that the V-K-I-E (V118-E121) motif is a conjugation point for SUMO, peptide arrays are limited by the fact that they are immobilised peptides that are used in cell-free systems. This means that data from peptide array studies do not necessarily reflect the situation in the cell as short peptides cannot replicate tertiary structure of the proteins of interest. Therefore, the next step was to determine whether the POPDC1 protein could be SUMOylated in its natural conformation. To do this, NRVM lysates were subjected to an *in vitro* SUMOylation assay (Enzo) carried out according to manufacturers protocol. To determine whether SUMOylation of Popdc1 had occurred, the resulting assays were Western blotted for the target protein and the presence of a bandshift indicated the presence of SUMOylation. As a negative control, assays were performed without MgATP, a co-factor that is essential for SUMO E1 ligase activity. When NRVM lysates were subjected to the SUMO assay and immunoblotted for Popdc1 there was a distinct bandshift indicating that Popdc1 had been SUMOylated (Figure 6.8). This band was more intense than those in the control lanes but, a student's t-test did not show any statistical significance between samples with MgATP present and those without. The data presented here (Figure 6.8) suggests that endogenous Popdc1 from NRVM may be

SUMOylated *in vitro*, although further repeats of this experiment would be needed to confirm this PTM.

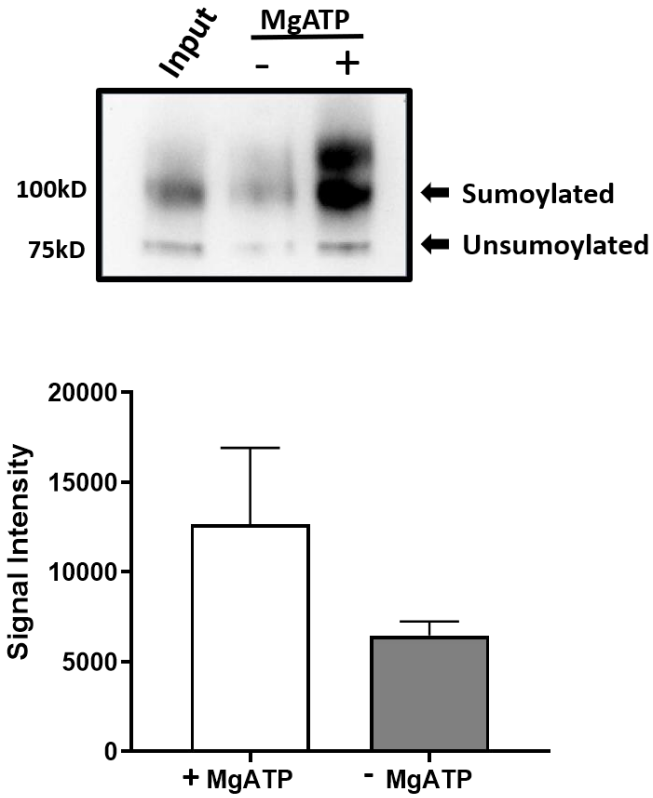

Figure 6.8 *In vitro* SUMO assay using NRVM lysate. NRVM was subjected to *in vitro* SUMOylation using a SUMO assay kit (Enzo). BVES (POPDC1) antibody was used to detect both SUMOylated and unSUMOylated Popdc1. A band shift of ~20kDa was present in the sample containing all assay components including MgATP. Control assays were run without the addition of MgATP, the crucial co-factor for the E1 enzyme meaning no SUMOylation can occur. The intensities of the lower unSUMOylated Popdc1 band and the upper SUMOylated Popdc1 band were measured using ImageJ studio and compared using GraphPad Prism ™. A student's t-test was carried out (p=0.33). Results represented as mean ± SEM, n=3.

6.3.3 Popdc1 is not palmitoylated in NRVM

Palmitoylation is a group of lipid modifications that are a common feature of many eukaryotic proteins. Unlike many other PTMs, there has been no strict consensus sequence identified, but the modification occurs on cysteine residues and these possess similarities in local amino acid sequences. They are usually: surrounded by basic or hydrophobic amino residues, adjacent to myristoylation and prenylation sites and they are frequently found in the cytoplasmic regions that flank transmembrane domains (Salaun et al., 2010). Using NetWheel,

protein helical and charge prediction software, a cysteine residue at position 89 in the POPDC1 sequence was identified to be a possible site of palmitoylation (NetWheel data not shown) (Figure 6.9). C89 is surround by a cluster of hydrophilic residues on one side with hydrophobic residues on the other. This could allow the residue C89 in Popdc1 to interact with the membrane in order for the palmitoyl to be conjugated to it through a DHHC PAT protein. Interestingly, this cysteine residue is conserved between Popdc1 and Popdc2 (Figure 6.9), supporting my hypothesis that it may provide some crucial function.

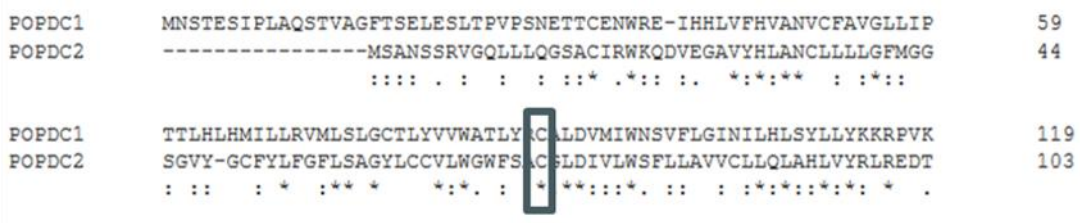

Figure 6.9 Identification of cysteine residue for possible palmitoylation in Popdc1. A cysteine residue identified through the NetWheel algorithm resides in the cytoplasmic region immediately following a transmembrane domain and was found to be conserved in Popdc2 (shown in grey box).

To confirm whether this site was able to become palmitoylated, a protocol for the identification of S-acylated species using resin-assisted capture (acyl-RAC) was utilised. After the blocking of free thiols with S-methyl methanethiosulfonate (MMTS), palmitoylated proteins were captured on thiopropyl sepharose beads (GE life sciences) in the presence of 200mM hydroxylamine (HA) (Forrester et al., 2011, Howie et al., 2014). Treatment with HA will block any newly free thiols from becoming exposed meaning that only the cysteine residues that have been palmitoylated will be precipitated with the thiopropyl sepharose beads. The beads contain thiol groups that are able bind to the free, palmitoylateable cysteine residues via the formation of mixed disulphide bonds. The level of palmitoylation was assessed by quantifying the band present in the HA lane, which captures cysteine residues where disulphide bonds that attach a C16 carbon saturated fatty acyl chain have formed, compared to the total protein in the unfractionated (UF) lane (Figure 6.10). As a negative control, NaCl was used in place of HA and this control showed no non-specific binding of either Popdc1 or Cav3 (Figure 6.10). It can be seen that no Popdc1 was palmitoylated in either of the two representative examples (Figure 6.10). Cav3 is known to be palmitoylated at multiple cysteine residues and was

therefore used as a positive control (Dietzen et al., 1995). The Cav3 band in HA lanes signals that the assay is functioning correctly (Figure 6.10).

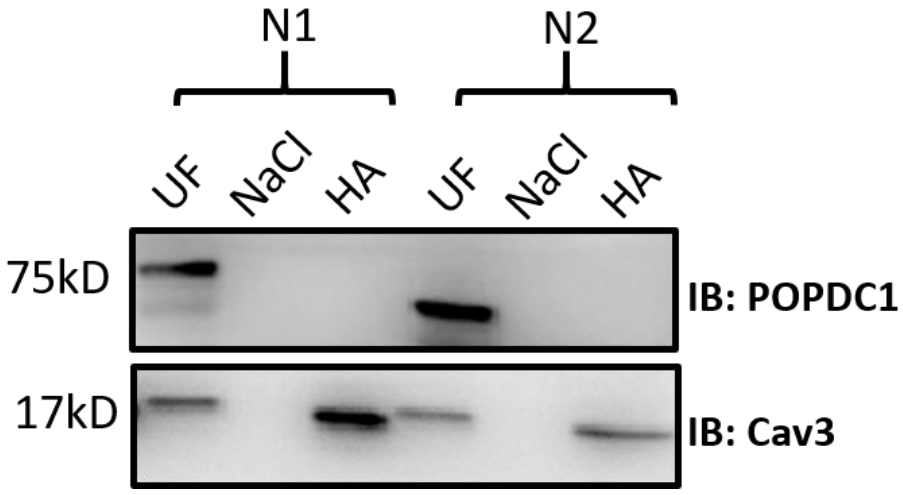

Figure 6.10 *In Vitro* Palmitoylation assay using NRVM lysate. NRVM lysate was harvested in blocking buffer (100M HEPES; 1mM EDTA; 2.5% SDS, 1% MMTS; pH7.5) prior to the acyl-RAC assay being carried out. Samples were either treated with hydroxylamine (represented in the HA lane) or NaCl as a negative control. Thiopropyl sepharose beads (GE Life Sciences) were used to capture free cysteine residues that had been palmitoylated during assay. The presence and level of palmitoylation was compared to the target protein abundance in the starting cell lysate (UF). The resin-captured fraction is reduced fivefold in volume in comparison to the to the unfractionated sample therefore the palmitoylated samples are fivefold enriched. Cav3 was used as it is a known positive control for palmitoylation. Figures are representative an n=2 of a total n=5. (Experiments carried out with help of Ms Alice Main, University of Glasgow).

Despite there being a correctly positioned cysteine residue, Popdc1 was found to not be palmitoylated in any of the replicates of this assay that were carried out.

6.4 Discussion

6.4.1 POPDC1 contains a site for PKA phosphorylation

Phosphorylation acts a major mechanism of control in regulating the contractile state of the heart via the modulation of numerous proteins. PKA phosphorylation is known to affect a variety of proteins that play a significant role in regulating cardiac contractility and performance of the heart, such as PLB, RyR2, and cardiac myosin binding protein-C (cMyBP-C) (Barefield and Sadayappan, 2010, Baryshnikova et al., 2008, Jones et al., 2008, Li et al., 2004, Wolff et al., 1996). For example, cMyBP-C phosphorylation results in force generation by affecting the interaction between the thick and thin filaments of actin (Barefield and Sadayappan, 2010, Tong et al., 2008). In addition, the PKA-dependent phosphorylation of the SR Ca^{2+} pump (also known as sarco-/endoplasmic reticulum Ca^{2+}-ATPase, SERCA) was shown to increase the Ca^{2+} affinity of the pump and increase calcium current I_{Ca}-triggered Ca^{2+}-release from the SR stores (Phrommintikul and Chattipakorn, 2006, Mattiazzi et al., 1994, Sichelschmidt et al., 2003). With phosphorylation playing such a crucial role in maintenance of cardiac function, the possibility that POPDC1 could be subjected to the same PTM was exciting as it could represent another regulatory mechanism of POPDC1 function and interactions. In this chapter evidence has been provided for the existence of a PKA phosphorylation site in the catalytic domain Popeye domain of POPDC1 (Table 6, Figure 6.3, Figure 6.4, and Figure 6.5). Given the close proximity of this putative phospho-site to the DSPE and FQVT cAMP binding motif it is obvious to suggest that phosphorylation may regulate cAMP binding in a similar way to PKA (Das et al., 2007). It could be suggested that the phosphorylation of the Popeye domain coupled with the binding of cAMP would lead to a conformational change leading to the gain or loss of binding to its interaction partners. This conformational change itself may serve as a means of regulating POPDC1's protein-protein interactions: for example, it has been discussed that POPDC1 interacts with TREK1 under basal cAMP levels but dissociates under high cellular cAMP. High levels of cAMP also lead to the activation of PKA, therefore upon POPDC1 binding to cAMP concomitant phosphorylation by PKA may induce a conformational change in the structure of POPDC1, dissociating it from TREK1. Phosphorylation dependant conformational changes have been reported in number of proteins, for example, the FXYD

proteins, which are the family of regulatory subunits of the Na^+, K^+-ATPase (NKA) ion pump. Phosphorylation of NKA at S936 modulates pumping activity by changing the accessibility to the ion-binding site (Poulsen et al., 2012). This gives support to my hypothesis that POPDC1 conformational change may be triggered, in part, by PKA phosphorylation in the Popeye domain. In addition, it has been postulated that the binding of POPDC1 to TREK1 indirectly prevents the channels activation by blocking its phosphorylation by PKA. It therefore may be that the phosphorylation of POPDC1 is due to this shield mechanism (Patel et al., 1998, Terrenoire et al., 2001).

Interestingly, the phosphorylation motif found in POPDC1 is unlike any canonical PKA motif. However, there is a high similarity between the motif in POPDC1, R-X-R-X-T, and the canonical protein kinase B (PKB) motif, R-X-R-X-T-S-hyd-R (Obata et al., 2000). PKB comprises of a NH_2-terminal Akt homology (AH) domain tethered to a catalytic domain (that shows high sequence homology with PKA and protein kinase C (PKC) and a short C-terminal domain. The activity of PKB can be initiated by numerous cellular stimuli including insulin, hyperosmolarity stress and increased cAMP (Cross et al., 1995, Burgering and Coffer, 1995, Andjelković et al., 1996, Filippa et al., 1999). POPDC1 may be phosphorylated by PKB rather than PKA. Given that the catalytic domain shares high sequence homology to PKA (Alessi et al., 1996) it may be that the forced phosphorylation assay carried out in this chapter that uses the catalytic domain of PKA has identified a PKB site. This would need to be confirmed through *in vivo* assays such as inhibition of either PKA or PKB and subsequent analysis of POPDC1 phosphorylation to confirm which kinase is interacting with POPDC1.

Despite the speculation about the functional outcome of POPDC1 PKA-dependent phosphorylation, the event itself needs to be confirmed *in vivo*. There are limitations with the use of peptide arrays as mentioned previously. Given that it the peptide array uses linearized peptides, the threonine we have shown to be able to be phosphorylated may not be exposed in the proteins native state. Based on Jpred4™ secondary structure prediction software, T236 lies within an α-helix in the heart of the Popeye domain therefore may not be accessible in basal conditions. cAMP binding to the Popeye domain may occur prior to PKA-phosphorylation allowing for a conformational change exposing the threonine to

be phosphorylated. Further research with a custom-made phosphor-site specific antibody against the region containing T236 would confirm the existence of this modification in cells and tissue. If true, this would represent the first instance of PKA regulation of another cAMP effector protein and would provide a new level of crosstalk within the cAMP signalling system.

6.4.2 POPDC1 is SUMOylated

This study presents the first evidence that POPDC1 can be SUMOylated at K119 within the consensus motif VKIE 118-121 (Figure 6.6 and Figure 6.7). Although in a cell-free system, SUMOylation using the *in vitro* assay, allowed for the putative site to be identified using peptide array method (Figure 6.7). The data suggests that all four amino acid residues in the consensus sequence are important for SUMOylation of POPDC1, as the removal of this sequence results in the loss of SUMOylation (Figure 6.7). This SUMOylation assay was also utilised to confirm the same result as the peptide array in NRVM lysate showing that Popdc1 can be SUMOylated in a biological environment. As time constraints did not allow further validation of this Popdc1 modification, other experiments that would have added extra evidence to the theory that POPDC1 gets SUMOylated would be to pull-down POPDC1 with SUMO agarose (agarose conjugated to SUMO specific antibodies), proteomics studies that not only confirm the existence of SUMO-POPDC1 but also identify possible sites at which this takes place, cloning of unSUMOylateable (K119 to R119) POPDC1 mutants that could be used in the cell free SUMO assay and finally proximity ligation techniques that show intimate co-localisation of antibodies directed against both SUMO and POPDC1.

SUMOylation of cardiac proteins has been well defined. One such protein is SERCA2a, an ATPase responsible for Ca^{2+} re-uptake in the excitation-contraction coupling. SERCA2a has been shown to be SUMOylated at lysine 480 and 585 and that this SUMOylation is critical to the activity and stability of the protein (Kho et al., 2011). In failing human hearts, the SUMOylation of SERCA2a is markedly reduced (Kho et al., 2011). The addition of SUMO by adeno-associated virus-mediated gene therapy in HF mice resulted in the stabilisation of SERCA2a by reducing its degradation which significantly improved cardiac function. Overexpression of SUMO1 by gene transfer rescued pressure overload-induced dysfunction concomitantly with a marked increase in the function of SERCA2a in

mouse and porcine (Kho et al., 2011, Lee et al., 2014, Tilemann et al., 2013). Given that increasing SUMOylation results in a protective outcome, a small molecule screen resulted in the identifying of *N*-(4-methoxybenzo[d]thiazol-2-yl)-5-(4-methoxyphenyl)-1,3,4-oxadiazol-2-amine (N106) that can drive *in vivo* and *in vitro* SUMOylation of SUMOs target substrates (Kho et al., 2015). N106 docks to a putative site of E1 ligase and confers its activity. The ability to therapeutically target the SUMOylation of SERCA2a presents as a novel approach to the treatment of HF. Using this novel N106 compound the SUMOylation of POPDC1 and the functional implications could be further deciphered using techniques outline previously.

Although K119 conforms to the classical SUMOylation motif, ΨKxD/E, there are additional factor that must be contemplated. For example, studies into the ETS-like protein, ELK-1, identified an extended SUMOylation motif in which the amino acid residues immediately downstream of the target K residue are negatively charged. Termed a negatively charged amino-acid dependent SUMOylation motif (NDSM), the extended site allows for upregulation of SUMOylation on that site (Yang et al., 2006). The identified POPDC1 site contains glutamic acid (E) residues at position 121 and 123, which are 2 and 4 amino acids downstream K119. Future studies should focus on determining whether these residues play a role in the ability of POPDC1 to become SUMOylated. POPDC1 conforms to the NDSM extended motif, but not to others known extended motifs known as phosphorylation-dependent SUMOylation motif (PDSM) and the hydrophobic cluster-dependent SUMOylation motif (HCSM). All three of these extended motifs are believed to upregulate SUMOylation of a target protein by increasing the SUMO pathways enzymatic substrate specificity (Hietakangas et al., 2006, Yang et al., 2006).

Given the evidence I have presented suggesting that POPDC1 is SUMOylated at the start of the cytoplasmic region, out with the Popeye domain, there are several hypotheses that can be made about the function of this SUMOylation. Firstly, SUMOylation may act to stabilize the protein, a phenomenon seen with IκBα (Ulrich, 2012). IκBα, is responsible for the inhibition of NFκB during the activation of inflammatory responses and it is stabilised by SUMOylation (Ulrich, 2012). Secondly, POPDC1 has also been shown to be localised to the nucleus and

it is not understood how this occurs. It is possible that the act of SUMOylation allows for the nuclear localisation of the protein, seen for example with NEMO proteins that require SUMOylation to be translocated to and retained in the nucleus (Huang et al., 2003, Liebelt and Vertegaal, 2016). Lastly, although the site we identified was not predicted to be a site for ubiquitination (scan performed using UbPred software – a predictor of protein ubiquitination sites) (data not shown), it may be possible that this SUMOylation site is incorrect. There is an accumulation of evidence that suggests that SUMOylation serves as a prerequisite for ubiquitination and thereby inducing protein degradation (reviewed in (Wei and Lin, 2012). It is possible that a further SUMOylation site exists that also contains the site for ubiquitination targeting POPDC1 for degradation by the proteasome. This is turn would provide a turnover mechanism for POPDC1. Further investigation such as proteomics, should be conducted to confirm the site identified is correct and that no other exists. For example a novel proteomics approach was undertaken through the stable expression of different SUMO paralogs in HEK293 cells, each of which contained a His_6 tag and a tryptic cleavage site at the C-terminus allowing for recovery and identification of SUMOylated peptides by mass spectrometry (Galisson et al., 2011). Using this method Galisson and colleagues identified 205 unique protein substrates with 17 SUMOylation sites that were present in 12 SUMO conjugates using HEK293 cells, with 3 of these sites being found in the promyelocytic leukaemia (PLM) protein (Galisson et al., 2011). This same method could be adopted to study POPDC1 SUMOylation status in healthy and disease states.

6.4.3 POPDC1 does not undergo Palmitoylation

The large majority of membrane proteins are incorporated into the membrane of the endoplasmic reticulum (ER). Protein folding then occurs within the ER at the three different topological environments that membrane bound proteins encompass, i.e. the cytoplasm, membrane and the lumen (Braakman and Hebert, 2013). Upon proper folding and assembly, the protein is transported from the Golgi and routed towards its final localisation. When the protein's lifespan has come to an end, it is usually targeted by lysosomes or autophagy for their degradation (Anelli and Sitia, 2008). As mentioned in section 6.1.3, most DHHC PATs are localised to a specific organelle; mainly to the plasma membrane, Golgi and endosomes. These transmembrane DHHC proteins can

palmitoylate a protein on cysteine residues located either inside or close to the membrane (Bijlmakers and Marsh, 2003). We initially identified a cysteine residue (C89) in POPDC1 that sits close to the membrane that fits with the conditions need for palmitoylation (explained in 6.3.3). Despite this initial step, after multiple attempts at an acyl-RAC using endogenous NRVM found no evidence that Popdc1 was palmitoylated (Figure 6.10). Given that palmitoylation is an important PTM crucial to the ability of some proteins membrane targeting, the lack of this PTM means membrane localisation of POPDC1 remains unclear (Bijlmakers and Marsh, 2003, Goodwin et al., 2005, Rocks et al., 2005). There are, however, numerous other membrane-targeting signals that may function to direct POPDC1 localisation to the membrane. Alongside palmitoylation, N-myristylation and S-prenylation are other lipid based PTMs that could be responsible for membrane localisation in this instance (Resh, 1999, Resh, 2006). In addition, structural domains within the protein itself; including C1,C2, PH, FYVE, PX and FERM domains, that can trigger the membrane localisation of a protein (reviewed in (Bhardwaj et al., 2006, Cho, 2001, Yang and Kazanietz, 2003, Nalefski and Falke, 1996, Rizo and Südhof, 1998, Ferguson et al., 2000, Lemmon and Ferguson, 2000, Stenmark et al., 2002, Bretscher et al., 2002). Therefore, it could be speculated that any of these other PTMs and/or structural domains are responsible for targeting POPDC1 to the membrane.

Further studies are required to create a clearer picture of how POPDC1s cellular localisation is controlled. The membrane targeting of the cAMP specific PDE4A1 was mapped by through the use of truncated protein constructs. Truncation of the N-terminal region produced a highly cytosolic protein as well as identifying an eleven residue helical module through ^{1}H-NMR structural analysis (Shakur et al., 1993, Shakur et al., 1995, Smith et al., 2007, Baillie et al., 2002). This module contains a core bilayer insertion unit comprised of two tryptophan residues known as the TAPAS-1 (tryptophan anchoring phosphatidic acid selective-binding domain 1) (Baillie et al., 2002). Replacement of this domain with a hydrophobic cassette comprising seven alanine residues also abolished membrane localisation indicating that trafficking and imbedding in the phospholipid bilayer was by the virtue of hydrophobic interactions (Smith et al., 2007). Confirmation of this site was undertaken using mutagenesis of the TAPAS-1 domain which resulted in a lack of PDE4A1 associated with the membrane in

COS1 cells (Baillie et al., 2002). Using a path of experiments such as this may help to identify regions of POPDC1 that contribute to the membrane association of the protein.

6.4.4 Methodological considerations and future direction

A large amount of work needs to be done to fully characterise PTMs that are important to POPDC1 and my work described here provides exciting but preliminary evidence to suggest that both SUMO and PKA phosphorylation might be altering POPDC1.

Although we have identified a site for phosphorylation it remains to be confirmed that POPDC1 can be phosphorylated *in vivo*. The limitations of peptide array technology have been covered in this thesis (section 3.4.1) therefore these results need further validation. Using the PKA assay utilised in peptide array experiments, forced phosphorylation of endogenous POPDC1 in NRVM could be examined. NRVM lysate would be exposed to the catalytic PKA subunit in PKA assay buffer as outline in section 2.13.3, allowing for the forced phosphorylation of PKA targets. This would confirm whether this was a PKA dependent phosphorylation as with other methods of activating intracellular kinase through increase in cAMP might result in POPDC1's phosphorylation by another source. The generation of a phospho-specific POPDC1 primary antibody using the PKA-phosphorylation site fine mapped using peptide array would allow for immunoprecipitation experiments to be carried out. Using NRVM lysate that was either treated with forskolin to increase PKA activity or with a PKA inhibitor such as H89, analysis of POPDC1 could be undertaken using the phospho-specific POPDC1 antibody to immunoprecipitate any PKA-dependent phosphorylated POPDC1. Confirming the phosphorylation of POPDC1 would assist in narrowing down how POPDC1 functions in terms of its interaction with TREK1. The shield model proposed that POPDC1 prevents PKA-dependent phosphorylation. As such, the phosphorylation of POPDC1 may result in a conformational change allowing PKA access to TREK1. A POPDC1 phospho-site mutant protein could be produced with a fluorophore tag to be used in FRET experiments. It was previously shown that treatment with forskolin to increase cAMP leads to a reduction in the

interaction between POPDC1 and TREK1 (Froese et al., 2012). The same protocol could be undertaken with cells transfected with the phospho-mutant or treated with a PKA inhibitor such as H89. A lack of FRET ratio changes in cells expressing a phospho-mutant construct treated with forskolin would signify blocking of PKA-dependent phosphorylation of POPDC1 is necessary to dissociate the POPDC1/TREK1 interaction. This result could then be compared to results from FRET experiments using cells transfected with WT-POPDC1 FRET construct and treated with PKA inhibitors. Completion of this set of experiments would elucidate how POPDC1 phosphorylation is involved in the modulation of POPDC1's interactions.

In this chapter, evidence was provided for POPDC1 SUMOylation. However, further investigation is required to fully confirm this modification. For a target protein to become SUMOylated, it must directly interact with UBC9 the only known SUMO E2 ligase (Knipscheer et al., 2008). A peptide array consisting of full length POPDC1 could be overlaid with UBC9 to produce a binding site. With this information a fusion protein could be created between POPDC1 and UBC9 (Kim et al., 2009, Jakobs et al., 2007, Weber et al., 2014) . Transfection into HEK293 cells would increase intracellular SUMOylation providing support for the notion that this is a PTM POPDC1 is subjected to. In addition, the creation of a SUMOylated-POPDC1 antibody that have previously been developed in our lab for SUMOylated TnI and B_2AR would allow for the endogenous detection of a SUMOylated Popdc1 (Wills, 2017, Fertig, 2019). Such evidence is crucial to validate this PTM of POPDC1.

It was previously stated that there is usually extensive cross talk between SUMOylation and ubiquitination. Given that a ubiquitin scan (data not shown) did not identify this motif as a site for the PTM it does not mean that POPDC1 is not SUMOylated. Given that the event of SUMOylation is thought of as pre-priming a protein for ubiquitination it may be that POPDC1 undergoes SUMOylation but not at the site identified (reviewed in (Wei and Lin, 2012)). In addition, given that the canonical SUMO motif is found in over a third of proteins, false positives are likely to exist. The SUMOylation kit contains all the enzymatic components and SUMO proteins in non-physiological, high concentration in order to allow target proteins to reach a detectable level.

Although no evidence of palmitoylation of POPDC1 was found in these experiments, it could be argued that membrane localisation of POPDC1 is the function of one of the previously mentioned membrane-localisation domains or other lipid modifications. As such, proteomic scans of POPDC1 could be undertaken to identify if such protein targeting domains exist. In addition, mass spectrometry of POPDC1 to identify further modifications could be done which may elucidate pathways for future investigations.

A final point to be noted is that neither the SUMOylation of the PKA-phosphorylation site are conserved in either of the other POPDC members (Figure 6.11). Many of the consensus motifs that have been identified for PTMs such as phosphorylation are weakly constrained and are often not conserved (Beltrao et al., 2013). The functional relevance of the identified PTMs of POPDC1 will have to be examined. Conservation domains within protein families usually identify regulatory hotspots that overlap functionally important regions (Beltrao et al., 2012). For example, 313 phosphorylation sites were identified in HSP70 proteins but only 2 were determined to be significant hotspots (Beltrao et al., 2012). More detailed analysis of the POPDC1 phosphorylation and SUMOylation status is required to determine whether these PTMs identified have any functional relevance.

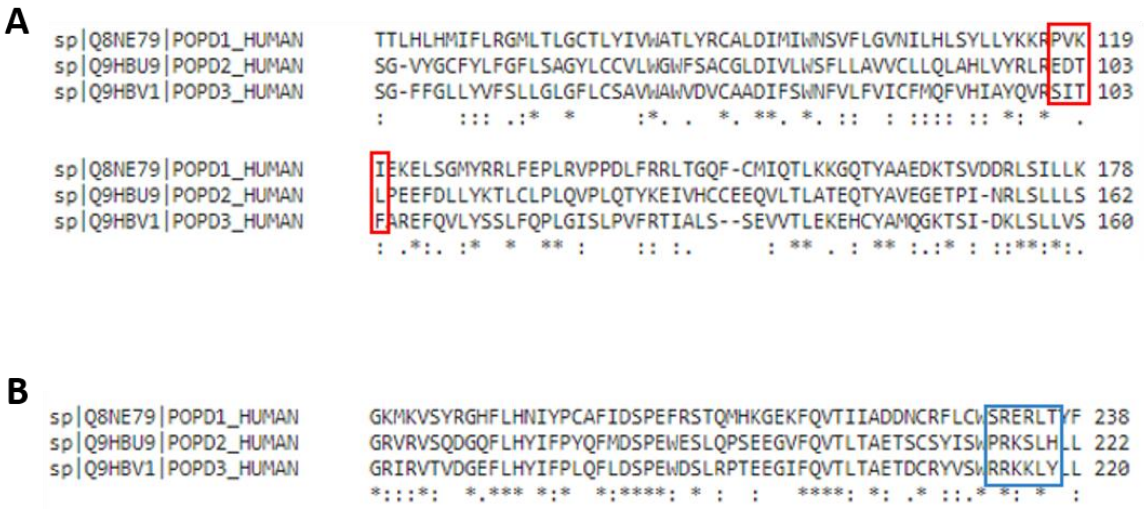

Figure 6.11 Clustal Omega alignment of POPDC1-3. Identified PTM sites were examined for conservation between the three POPDC family members. **A** the SUMOylation motif of POPDC1 (red) was not conserved in any of the other isoforms. **B** PKA-phosphorylation site, T236, or the surrounding amino residues (blue) are not present in POPDC2 or POPDC3.

6.4.5 Conclusion

In conclusion, in this chapter I have provided evidence that POPDC1 is subjected to phosphorylation and SUMOylation but not palmitoylation (Figure 6.3, Figure 6.8, Figure 6.10). These PTMs may serve as controls of POPDC1s function, localisation or that of its interaction partners. Given the wide range of possible modifications that can be made to a protein, the data here only provides a preliminary look at those affecting POPDC1. As such, there are numerous avenues that must be explored to fully understand how POPDC1 is controlled, modulated, stabilised and degraded in the cell. Now, with the successful identification of posttranslational modification sites on POPDC1, future work can focus on both; confirmation of the sites through the techniques outlined above and investigation of functional outcomes.

7 Structural analysis of POPDC1

7.1 Introduction

The question of what a protein does within a cell is a challenging one to answer. Even when you have information about some of the protein's biochemical characteristics, defining its exact biological role is difficult to do accurately. As protein structure and function are inextricably linked, solving foster understanding of function.

Currently, little is known about the structure of the POPDC protein family other than what has been deduced from structural homology modelling. POPDC proteins possess a short (27-39 amino residue) extracellular N-terminal domain that are subjected to N-linked glycosylation at two asparagine (Asn) residues (Asn^{20} and Asn^{27}) (Amunjela and Tucker, 2016b, Han et al., 2019). Predictions such as this is followed by three transmembrane domains linking to the intracellular portion of the protein. Following on from these transmembrane domains is the Popeye domain which houses the non-canonical phosphate binding cassette (PBC). The PBC, also known as a cyclic nucleotide binding domain (CNBD) consists of two conserved motifs, DSPE and FQVT, which are responsible for the binding of cAMP (Froese et al., 2012). The C-terminus contains the largest proportion of sequence variability between the isoforms and its function is unknown (Andrée et al., 2000).

Given the lack of known structure either for the full-length protein or the CNBD itself the mode by which POPDC proteins bind cAMP has been predicted through modelling studies. Problematically, there is a lack of sequence homology to classical cAMP effector proteins that have had their structures determined with cAMP bound. The closest sequence similarity was found in the bacterial catabolite activator (CAP) or the cAMP response proteins (CRP), where 20% similarity has been identified. As such the secondary predictions were built using the CNBD structure of *Streptomyces coelicolor* (PDB:2PQQ) as an initial template and the CNBD of PKA RII (PDB: ICX4) was used for refinement (Figure 7.1) (Amunjela et al., 2019) .

Figure 7.1 Homology model of the Popeye domain of POPDC. A homology model of the CNBD of POPDC3 was by Amunjela and colleagues created using *Phyre2* algorithm. The pink represents the FQVT and DSPE motif that are crucial to the proteins ability to bind to cAMP, which can be seen bound in the figure by the black arrow. The position of cAMP binding was predicted using the 3DLigandSite predictor (Kelley et al., 2015, Wass et al., 2010). As the closest homology to the CNBD of POPDC1 was found in the cAMP response (CRP) protein and bacterial catabolite activator (CAP), the CNBD of *Streptomyces coelicolor* was used as a template with PKA RII CNBD used to refine the structural prediction. (Adapted from (Amunjela et al., 2019)).

The POPDCs PBC is highly divergent from any of the known canonical CNBDs. In addition, the uncertainty surrounding the mode by which POPDC1 binds cAMP and the functional changes that occur makes it challenging to identify possible implications of mutations within the domain. Thus, determining POPDC's structure will be a crucial step in developing our understanding of its role in the cell.

7.2 Hypothesis and Aims

Structural analysis of POPDC1 has been under investigation for years with little success. Despite the slow progress it is clear that the information that can be gained from solving the structure of the first POPDC family member would allow for a more complete analysis of the protein's functions and interactions. Determining the structure could contribute to a better means of investigating how the modulation of the protein occurs under various cellular conditions such as high cAMP. Clarity on this point would contribute greatly to POPDC characterisation. Having POPDC1 coordinates would also be useful for confirming previously identified protein partner binding sites, for example the site of PDE4A interaction, and for insight into why familial mutations in POPDC are so devastating. As such, the aims of the work presented in this chapter are as follows:

- Create constructs expressing portions of the POPDC1 protein for structural analysis

- Determine expression conditions for the constructs that maximise the solubility of the protein by varying the induction conditions

- Isolate recombinant protein on a large scale with sufficient purity for structural analysis

- Confirm the functionality of purified recombinant proteins

7.3 Results

The isolation of a protein of interest can be a complex process that does not necessarily produce purified protein at the required yield or purity. Production of recombinant protein is often favoured as it can allow for high quantities of protein to be expressed at a relatively low economic cost. Many recombinant expression systems have been trialled and developed over the years, tailored to individual research needs. These are categorised based on the cell type used: prokaryotic cells such as *Escherichia coli (E.coli)*; eukaryotic cells such as insect cells, mammalian cells, yeast cells; and finally cell-free systems (Baneyx, 1999, Jarvis, 2009, Jarvis, 2014, Mattanovich et al., 2012, Carlson et al., 2012). Important factors must be considered in determining which expression system to choose including cost-effectiveness, source organism of the protein and scalability of expression.

The most commonly used system is *E.coli* due to numerous advantageous properties including high growth rates, high expression yields, cheapness of cell strains and growth media as well as a good understanding of protein expression machinery. There are, however, several disadvantages to the use of *E.coli* such as the lack of eukaryotic expression and folding machinery. In this study I took steps to ensure the highest yield, including the removal of rare codons, and the production of correctly folded protein (reviewed in (Rosano and Ceccarelli, 2014)).

7.3.1 Design of constructs

Eukaryotic genes often contain codons that are rarely used in highly expressed genes in *E.Coli*. A high frequency or the consecutive appearance of these rare codons can result in stalled translation, truncation or failed expression of the protein (Wada et al., 2001). As such, the *POPDC1* sequence was examined for the presence of these rare codons. There were 238 instances of rare codons were identified with many of these being found consecutively (Figure 7.2). In addition, the optimisation of the POPDC1 gene included the avoidance of RNA secondary structures that could stall translation. Therefore, a synthetic POPDC1 gene was produced, by Genewiz (UK), to create the optimal chance of protein expression for these experiments.

Amino Acid	Rare Codon	Frequency of Occurrence
Arginine	CGA	7
	CGG	18
	AGG	49
	AGA	37
Glycine	GGA	29
	GGG	22
Isoleucine	AUA	47
Leucine	CUA	18
Proline	CCC	45
Threonine	ACG	6

Figure 7.2: Identification of rare codons within POPDC1. The sequence of *POPDC1* was scanned for rare codons that would potentially affect its expression in *E.Coli*. Three proline residues and a threonine were identified to contain rare codons, with a proline and the threonine residue being found consecutively (Rare Codon Caltor programmed by Edmund Ng).

The yield and solubility of a recombinant protein has been shown to depend on the predicted domain boundaries in the protein that have been expressed (Edavettal et al., 2012). Polymerase chain reactions (PCR) were carried out with the synthetic POPDC1 being used as the template and primers designed to contain specific regions of the protein. The fragments all contained the Popeye domain flanked by different domains of POPDC1. The primer sequences for domain parameters were based on the JPRED prediction of where the regular secondary structure elements would end and then adjusted to incorporate a number of predicted disordered, hydrophilic residues (Kelley et al., 2015). The primers were designed to allow for the easy incorporation of the fragments into the pNIC28-Bsa4 backbone by ligation independent cloning. Using a combination of 5' and 3' primers, a total of ten constructs were designed to express different lengths of the POPDC1 protein (constructs used in this chapter are shown in Table 6). To create these fragments of POPDC1, PCRs were carried out using the conditions noted in Material and Methods section 2.7.

Table 6: List of constructs developed with fragment size in base pairs and primers used.

Residues	*Fragment*	*Size*	*Primers*
1-279	N-terminal + Popeye domain	837bp	Full length 5' and Popeye domain 3'
1-360	Full POPDC1	1080bp	Full length 5' and Full length 3'
111-279	Popeye domain	504bp	Popeye domain 5' and Popeye domain 3'
111-360	Popeye domain + C-terminal	750bp	Popeye domain 5' and Full length 3'

The products of the PCR reactions were analysed using gel electrophoresis (Figure 7.3) and the reactions were judged successful by the presence of bands at the appropriate base pair size (noted in Table). The absence of a band in the negative control lane provided further support that the PCR products were specific to the primers and POPDC1 template DNA.

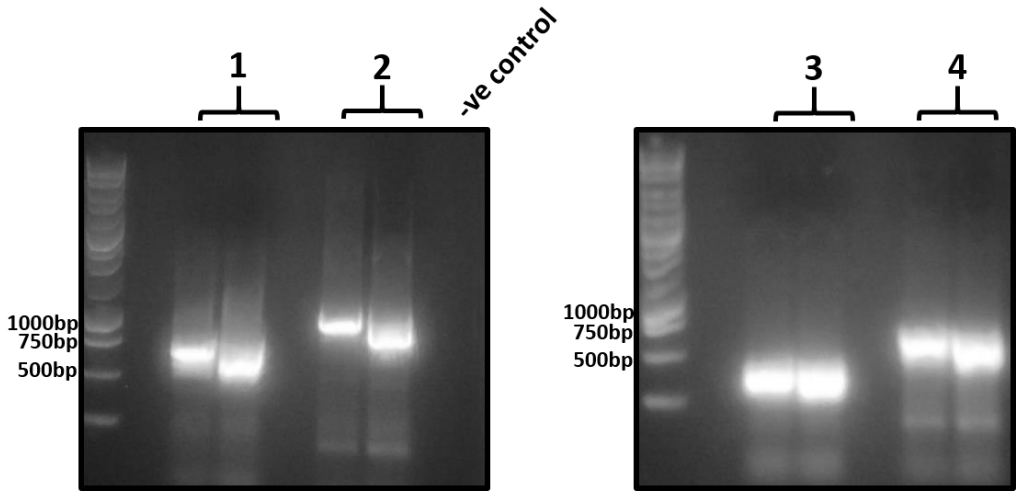

Figure 7.3 Gel electrophoresis confirmation of PCR products for development of POPDC1 constructs. PCR products from the 4 reactions noted above were examined via 1.5% agarose gel electrophoresis. Reaction 1 products contain the N-terminal – Popeye domain construct created using Full length 5' and Popeye domain 3' primers. Reaction 2 are the products containing the full POPDC1 protein created using the Full length 5' and Full length 3' primers. Reaction 3 products contain the Popeye domain created using the Popeye 5' and Popeye 5' primers. Reaction 4 products contain the Popeye domain – C-terminal fragment created using the Popeye 5' and the Full length 3' primers. A negative control was used by carrying out a similar PCR however, the primers were excluded. The lack of a band in this lane confirms that there was no unspecific amplification or contamination in the samples. (Work carried out with the help of Mr Donald Campbell, University of Glasgow).

Upon the confirmation that the fragment was the correct size, the bands were excised and extracted from the gel using a Monarch® DNA Gel Extraction Kit (New England Biolabs, US).

7.3.2 Subcloning

Subcloning is the process of transferring desired genes to a desired vector, in this case pNIC28-Bsa4. The pNIC28-Bsa4 backbone was used to allow for the expression of the protein with a TEV cleavable N-terminal hexa-histidine (His_6) tag. PCR fragments containing various regions of POPDC1 were cloned into the BsaI linearized and gel purified pNIC28-Bsa4 vector using the NEBuilder® HiFi DNA Assembly Cloning Kit following manufacturers protocol. An exonuclease within the kit digest the 5' ends of the double stranded DNA fragments creating long 3' overhangs, which can subsequently anneal strongly and specifically enough that the appropriately designed inserts are incorporated into the circularised vector. With this kit, the process is further enhanced by the action of DNA polymerase that fills any single stranded gaps and a ligase that ligates the resulting nicked ends in the reconstituted plasmid. Plasmids were

transformed into DH5α competent cells and allowed to grow on LB agar plates. Between four and five colonies were picked from each transformation and a colony PCR was carried out using the corresponding primers (Figure 7.4 A-D). Initially, the only fragment that was successfully transformed contained the Popeye domain only identified by bands of around 500bp in size (Figure 7.4 A). To address the lack of transformation of two of the constructs, the transformation was reattempted using an increased concentration of fragment insert (see section 2.7.2). The presence of bands in the full-length construct transformation (Figure 7.4 B) at around 1000bp and in the constructs containing the Popeye domain flanked by the C-terminal at 750bp (Figure 7.4 C) confirmed their successful transformation into competent cells. Furthermore, Figure 7.4D shows that one colony contained the transformed plasmid containing the Popeye domain alongside the N-terminal domain (band at ~830bp). In addition to colony PCR, each of the samples from each successful transformation was sent for DNA sequencing. Those colonies that contained the correct sequence were taken onto further testing.

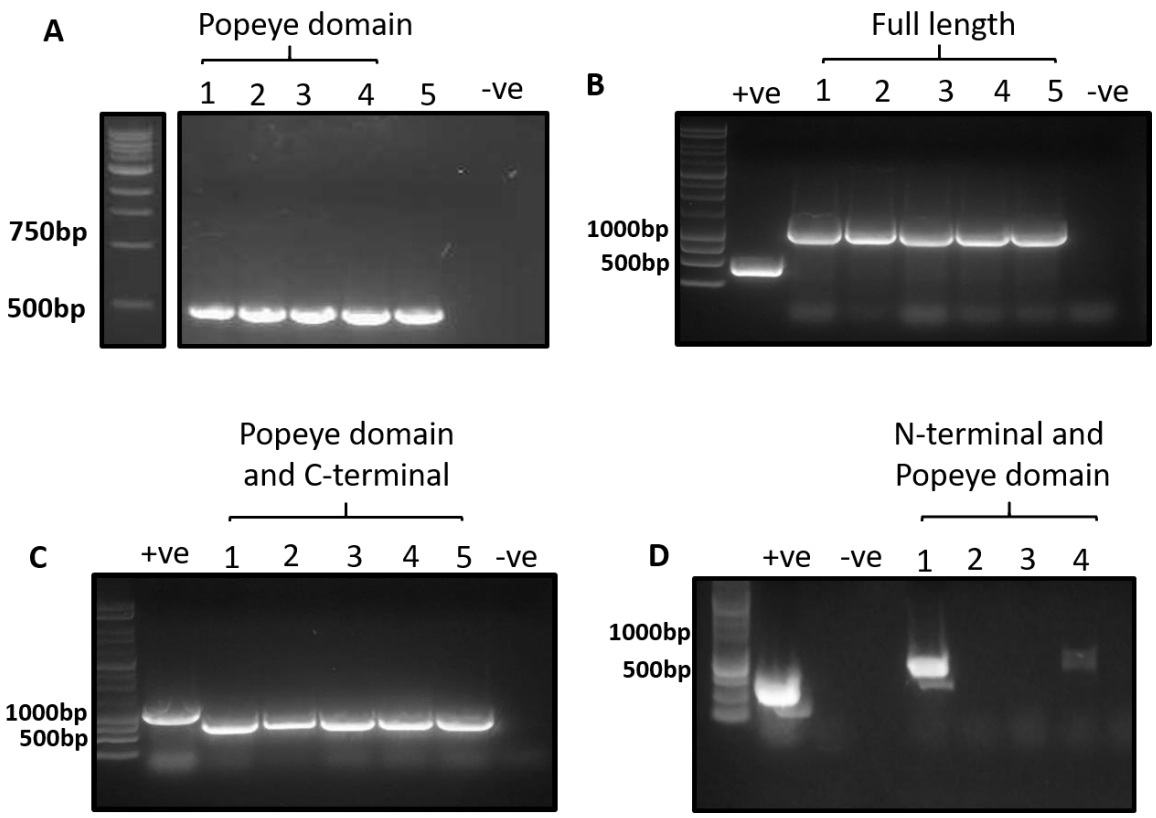

Figure 7.4 Colony PCR to confirm the presence of transformed plasmids containing the POPDC1 constructs. A selection of four or five colonies were taken from each transformation reaction and subjected to colony PCR using the primers that created the original fragment. **A** Colony PCR reactions for 5 colonies transformed with the Popeye domain construct were carried out using Popeye 5' and Popeye 3' primers. **B** Colony PCR reactions for colonies transformed with the full POPDC1 construct were carried out using the Full length 5' and Full length 3' primers. **C** PCR reactions for 5 colonies transformed with the Popeye domain- C-terminal construct were performed using the Popeye 5' and the Full length 3' primers. **D** 5 colony PCR reactions for colonies transformed with the N-terminal – Popeye domain construct were carried out using the Full length 5' and Popeye 3' primers. Negative controls (-ve) were performed using the DNA template without the addition of primers. Positive controls containing a set of known working primers to confirm the reaction was functioning correctly. (Work carried out with the help of Mr Donald Campbell, University of Glasgow).

Correctly sequenced fragments were transformed into BL21 (DE3) (NEB) competent cells for protein expression tests.

7.3.3 Testing conditions for protein expression in *E.coli*

To determine which construct yielded the most promising expression, test cultures were carried out under different growth conditions. The protein expression constructs were tested in 10ml cultures subjected to three IPTG concentrations; 0.1mM, 0.4mM and 1mM, with growth being induced at either 37ºC or 16ºC. Samples were taken from pre and post induction and lysates were analysed via SDS-PAGE to determine protein expression and solubility level.

Expression screening of the full-length construct revealed that this was a difficult protein to produce. With no or little protein being expressed after induction it was decided that the next steps would involve testing of constructs that contained only fragments of POPDC1.

For the construct containing the Popeye domain alone. The presence of a band at the expected molecular weight of 20kDa indicated successful expression (Figure 7.5). The proportion of protein found in the soluble (S) fraction in comparison to the insoluble (P) fraction was used to select subsequent expression conditions. The majority of the Popeye domain protein expressed at 37^{o}C was in the insoluble fraction at all concentrations of IPTG (Figure 7.5 A). At 16^{o}C a larger proportion of the expressed protein was soluble, with the highest levels being found after induction with either 1mM or 0.4mM IPTG, Figure 7.5B). Hence, the expression of the Popeye domain at 16^{o}C for 16 hours induced by 1mM or 0.4mM IPTG were the most promising conditions.

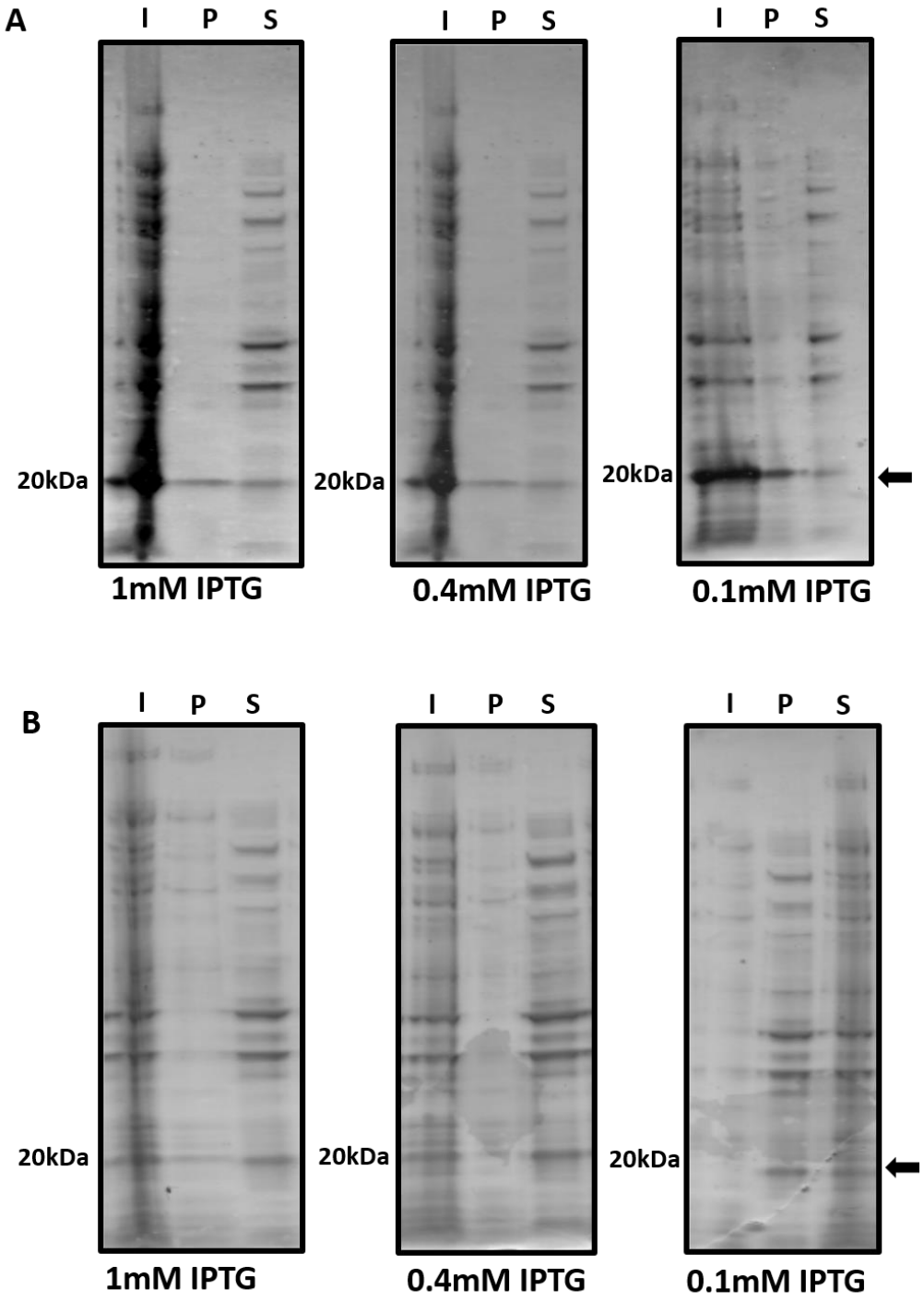

Figure 7.5 SDS-PAGE analysis of Popeye domain construct test cultures to determine optimum expression conditions. Expression of the Popeye domain was carried out under two different induction temperatures (37ºC and 16ºC) and three different concentrations of IPTG (1mM, 0.4mM and 0.1mM) (noted below SDS-PAGE). **A** *E.coli* containing the Popeye induced with different concentrations of IPTG at 37ºC for 3 hours or **B** at 16ºC for 16 hours. For all conditions, samples represent; the total protein after induction (I), the insoluble fraction (P) and the soluble fraction (S). For analysis gels were treated with Coomassie stain to visualise proteins present in each sample. The arrow position corresponds to the molecular weight predicted for the protein expressed from the Popeye domain construct.

The N-terminus-Popeye domain construct was tested, using identical conditions to those outlined above to allow for a direct comparison to be made. At 37°C (Figure 7.6 A), there was little evidence of a soluble expression of the construct shown by a faint band present at ~37kDa in the soluble (S) lane. Weak expression in the total protein samples before or after induction was observed with all concentrations of IPTG. Expression could be seen at 16°C judged by the darker band at the protein's expected molecular weight at each of the IPTG concentrations (Figure 7.6 B). However, the majority of the expressed protein was in the insoluble (P) fraction. In comparison to the Popeye domain alone, the expression levels were lower at all conditions tested, leading to the decision that this construct should not be used in further large-scale protein purification experiments.

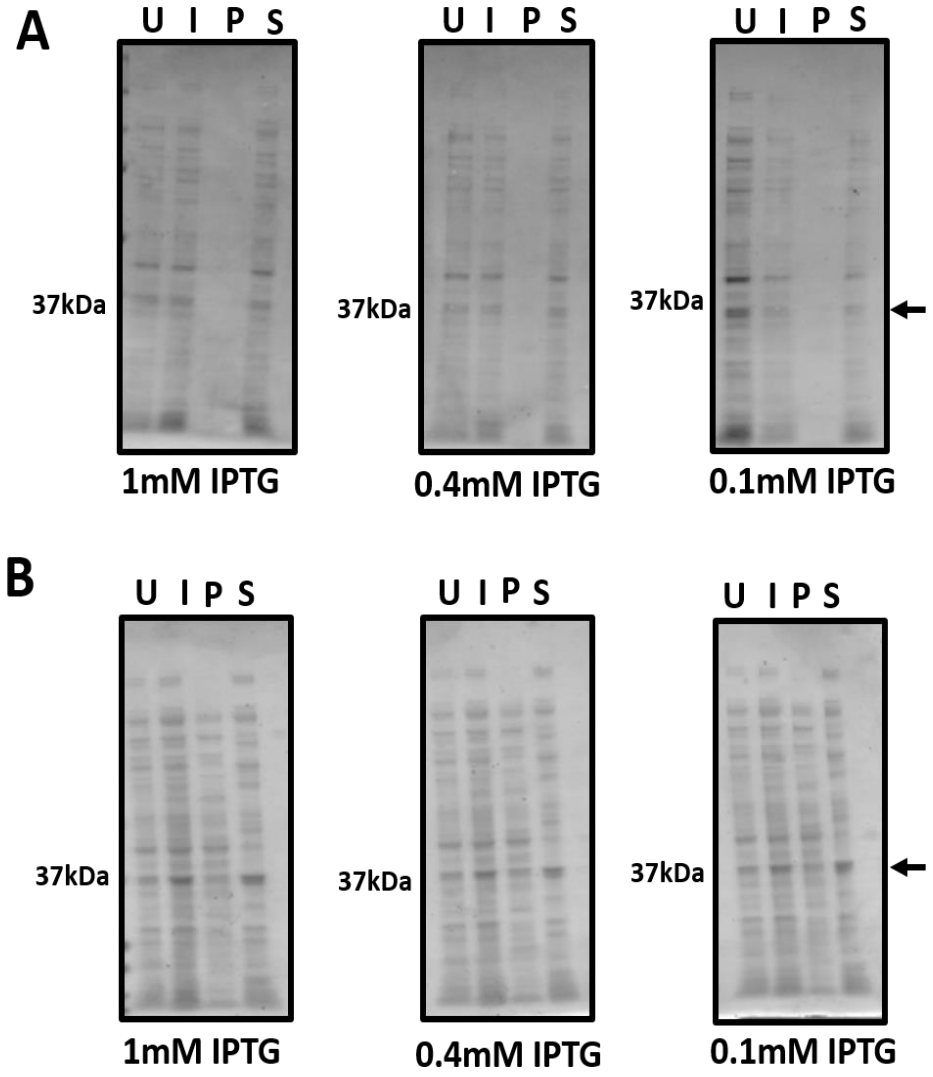

Figure 7.6 SDS-PAGE analysis of test expression conditions for N-terminus - Popeye domain construct. The expression of the N-terminal of POPDC1 coupled to the Popeye domain was carried out under two different induction temperatures (37ºC and 16ºC) and three different concentrations of IPTG (1mM, 0.4mM and 0.1mM) (noted below SDS-PAGE). **A** *E.coli* containing the tagged construct were induced with varying concentrations of IPTG at 37ºC for 3 hours. **B** The N-terminal domain and Popeye domain protein induced expression was carried out at 16ºC for 16 hours using the noted IPTG concentrations. For all conditions, samples were taken for; the total protein before (U) and after induction (I), the insoluble fraction (P) and the soluble fraction (S). For analysis gels were treated with Coomassie stain to visualise proteins present in each sample. The arrow denotes the band that corresponds to the correct molecular weight predicted for the N-terminal coupled Popeye domain construct.

The Popeye domain-C-terminal construct showed a higher expression of protein at 37ºC growth conditions at all concentrations of IPTG (Figure 7.7 A, Lane I). However, the majority of the protein was in the insoluble fraction (P) at 37ºC, a situation that was only slightly improved when the induction temperature was dropped to 16ºC (Figure 7.7B). There appeared to be no significant change in the level of protein produced at any of the IPTG concentrations at an induction

temperature of 16°C. In comparison to the Popeye domain alone, the Popeye domain- C-terminus construct was more highly expressed, but the ratio of soluble to insoluble protein was more favourable in the Popeye domain construct.

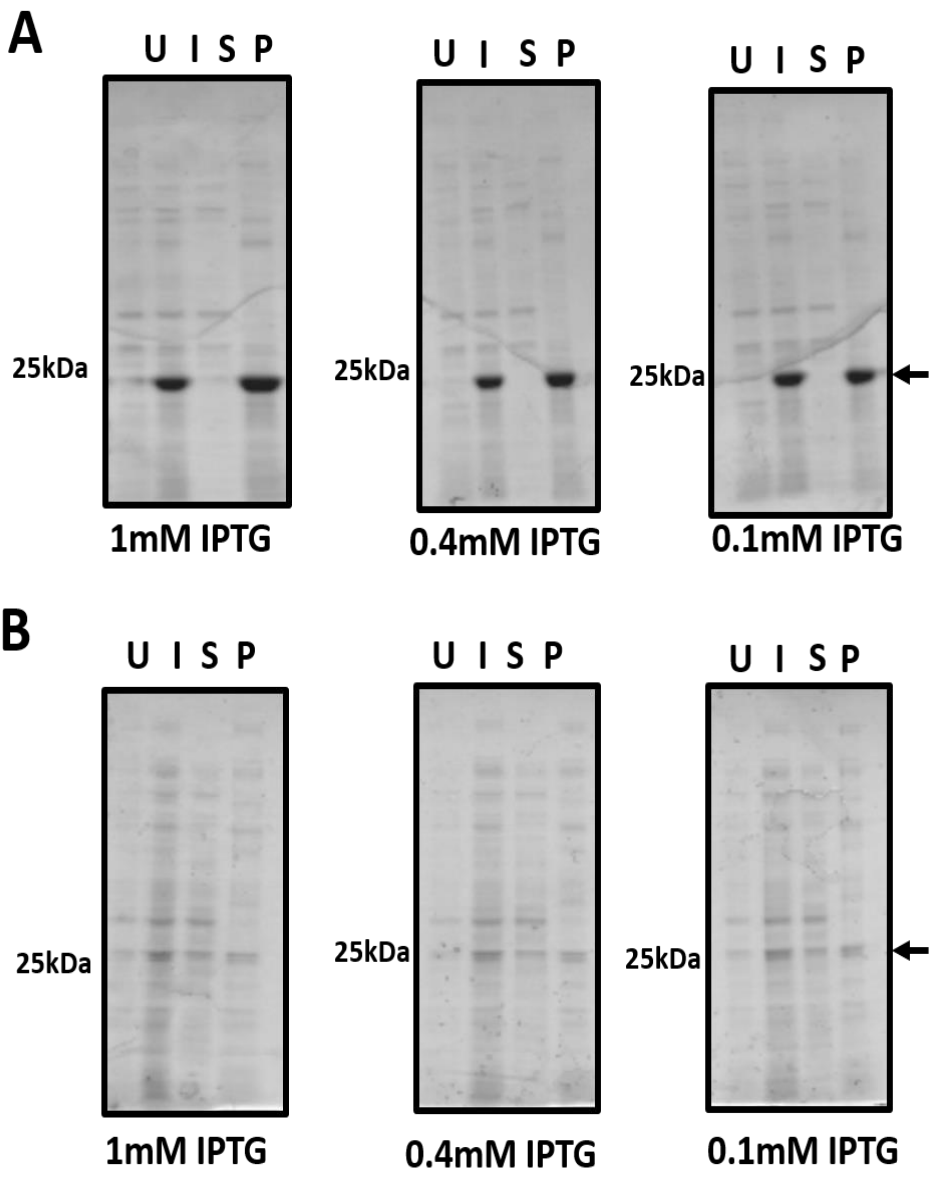

Figure 7.7 SDS-PAGE analysis of Popeye domain - C-terminal construct test cultures to determine optimum expression conditions. The expression of the Popeye domain-C-terminal construct was carried out under two different induction temperatures (37°C and 16°C) and three different concentrations of IPTG (1mM, 0.4mM and 0.1mM) (noted below SDS-PAGE). **A** *E.coli* containing the tagged construct were induced with different concentrations of IPTG at 37°C for 3 hours or **B** at 16°C for 16 hours using the noted IPTG concentrations. For all conditions, samples were taken for; the total protein before (U) and after induction (I), the insoluble fraction (P) and the soluble fraction (S). For analysis gels were treated with Coomassie stain to visualise proteins present in each sample. The arrow denotes the band that corresponds to the correct molecular weight predicted for the Popeye domain-C-terminal construct.

7.3.4 Large scale Protein purification of the Popeye domain

Based on the information gained from the test cultures, it was clear that the Popeye domain construct was the best construct to begin large scale purification trials with the hope of using samples for structural analysis. From the conditions explored the most promising option was inducing protein expression at 16^{o}C supplemented with 1mM IPTG.

Large scale protein purification was carried out using Ni^{2+} affinity chromatography which captures the His_6 tagged Popeye domain. Successful expression of the Popeye domain was detected by the presence of a band at around 20kDa seen in both Coomassie® stain and immunoblotting for the His_6 tag (Figure 7.8A and B, E1-E6 lanes, respectively). As expected, the large-scale production resulted in a good yield of Popeye domain protein being expressed seen in both the SDS-PAGE and Western blotting analysis in comparison (Figure 7.8A and B). Although soluble Popeye domain was obtained, the SDS-PAGE analysis (Figure 7.8A) identified that there was contaminants that were identified not to be the Popeye domain through Western blotting. The second band seen in the Western blot appeared to be approximately 40kDa, a weight corresponding to a dimeric Popeye domain protein (Figure 7.8B).

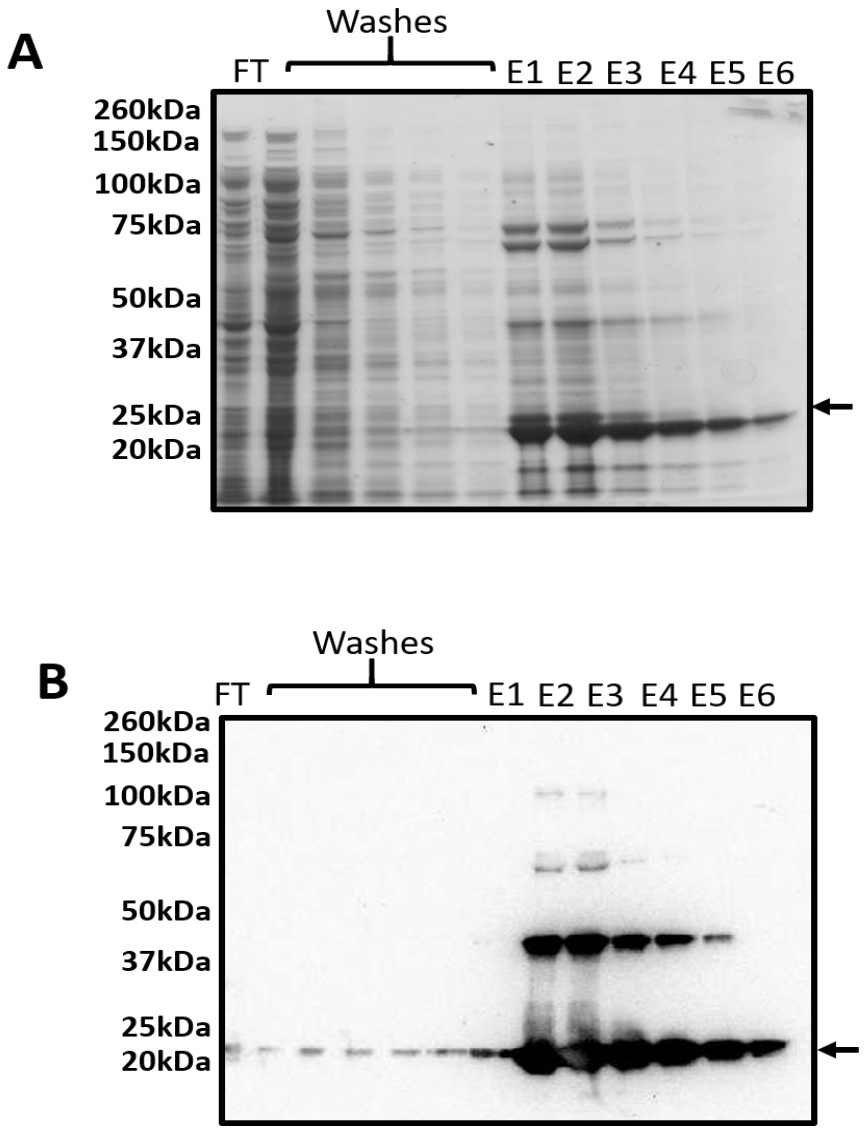

Figure 7.8 Initial large-scale purification of the Popeye domain analysed using Coomassie® stain and immunoblotting for the histidine tag on the construct. A. A sample of the flow through of lysate from a Ni^{2+} affinity column was separated by SDS-PAGE along with samples taken from the column washes. Wash buffer contained 20mM Imidazole to remove weak binding proteins from the Ni^{2+} affinity beads. Elution of the bound protein was carried out using Elution buffer containing 300mM Imidazole. Elution fractions were collected in 500µL aliquots and 10µL samples were analysed via SDS-PAGE. **B.** Samples were subjected to Western blotting for the histidine tag on the Popeye domain construct. The expected size of the monomeric recombinant protein is denoted by the black arrow.

In an attempt to improve the yield of monomeric Popeye domain protein, the addition of a reducing reagent was trialled. Tris(2-carboxyethyl) phosphine (TCEP) was added to prevent the formation of inter-molecular disulphide bonds. TCEP has been shown to be efficient at reducing disulphide bonds, that are commonly a source of aggregation, over a long period of time due to its long half-life (Getz et al., 1999). Initially, 5mM TCEP was added to the lysis buffer and affinity chromatography buffers used in the purification process. In addition,

the Ni^{2+} affinity resin was not capturing all the Popeye domain, as judged by the presence of a band in the FT and wash fractions on the Western blot meaning some of the Popeye domain protein may be lost. Therefore, two Ni^{2+} affinity columns were stacked, and lysed cells were allowed to flow through one into the other to capture the highest purity and concentration of protein. The elution step was carried out for each column separately in order to identify the purest fractions. Samples of each elution taken from column A and column B were analysed via SDS-PAGE (Figure 7.9A and C, respectively). The first five elution's from each column contained high amounts of contaminants but a single band was observed in the later fractions at the correct molecular weight for the Popeye domain recombinant protein (~20kDa) (Figure 7.9). The elution behaviour of this protein is unusual as tagged protein would normally elute in first few elution fractions at high imidazole however, the Popeye domain protein is seen to be eluting slowly from the column implying that it has a higher than usual affinity for the column. This implies either multimerization of the protein, avidity effect from multiple tags on the same molecular entity, or that the protein binds to the resin in a His_6-tag independent manner. Immunoblotting for the His_6 tag on the construct further confirmed the purity of the elution fractions, in particular the last six samples (Figure 7.9 B and D). The Western blot also revealed the lack of dimer band, showing that the addition of TCEP had prevented the dimerization of the Popeye domain. The samples noted below the bracket in Figure 7.9 were deemed the purest and were taken into further structural analysis.

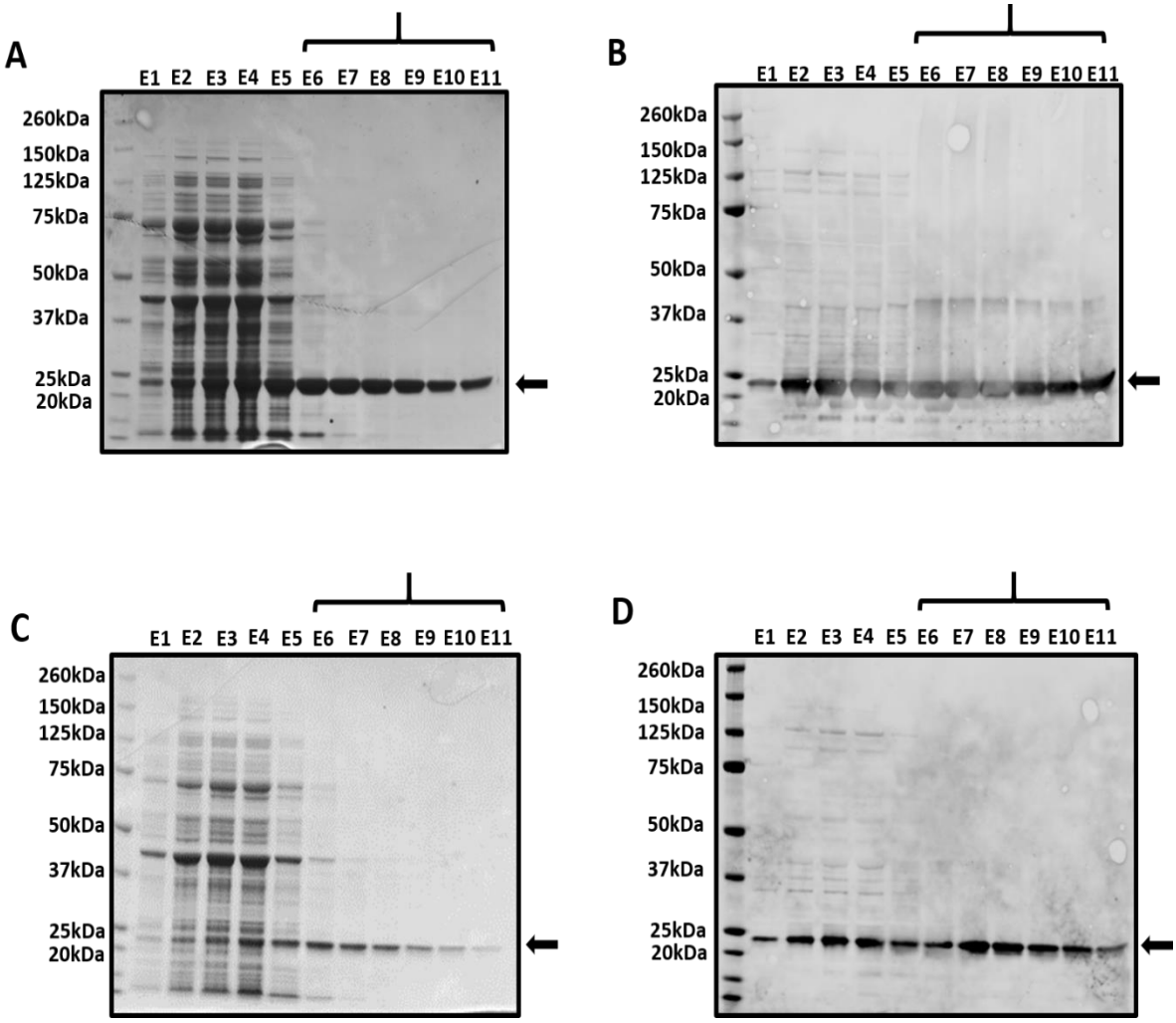

Figure 7.9 SDS-PAGE and Western blot analysis of large scale purification of the Popeye domain in the presence of 5mM TCEP. Large-scale production of the Popeye domain carried out at 16^{o}C for 16 hours and induced using 1mM IPTG. The Popeye domain was purified using Ni^{2+} affinity chromatography. Two columns were stacked, and lysed cells were allowed to flow through. Elution fractions were collected in 500µl aliquots. **A.** 10µl of each fraction from column A were analysed via SDS-PAGE and **B.** confirmed through Western blotting for His_6. The sample analysis was carried out for column B. **C.** Analysis via SDS-PAGE and **D.** Western blotting for histidine identified the presence of the Popeye domain in the second column. The correct band for recombinant Popeye domain was identified by the black arrow. Samples that were carried forward to further experiments are denoted under the bracket.

7.3.5 Analysis of the recombinant Popeye domain

Numerous attempts were made to remove the imidazole and concentrate the elution fractions, however, the protein reacted unfavourably by binding to the membrane of dialysis devices or aggregating in solution. Although it is not normally favourable to study proteins in high imidazole, this prompted the decision to leave the Popeye domain protein in the elution buffer with imidazole to keep the recombinant protein stable.

Dynamic light scattering (DLS) analysis is routinely used in protein characterisation studies. It can provide information on the presence of aggregates, determine size of proteins and study protein complexes (Stetefeld et al., 2016, Lorber et al., 2012). Samples composed of a monomeric Popeye domain population were collected for further analysis. From the DLS data, the mean hydrodynamic radius can be estimated and the polydispersity of the population determined allowing a judgement of whether the protein is monomeric or forming aggregates to be made (Bishop et al., 1991, Stetefeld et al., 2016).

In an aqueous solution maintained at a constant temperature, collision with the surrounding water molecules leads to the displacement of the molecules dissolved in it, this is known as Brownian motion. Smaller molecules move at a much faster rate than larger molecules (Figure 7.10 B). Illumination of the sample with monochromatic light gives rise to scattering of the light at different angles. The intensity of light scattering varies in a time-dependant manner as different size particles diffuse through the observation window with larger particles such as the dissolved protein scattering more strongly than the solvent molecules, and with aggregates scattering more strongly still (Lorber et al., 2012, Stetefeld et al., 2016). The velocity of this Brownian motion is defined as the translational diffusion coefficient (D). This coefficient is used in the Stokes-Einstein equation ($d(H) = \frac{\kappa T}{3\pi\eta D}$, where; *d(H)* = hydrodynamic diameter, D = translational coefficient, κ = Boltzmann's constant, *T* = absolute temperature and η = viscosity) to calculate the hydrodynamic diameter of the protein (Figure 7.10 B, graph).

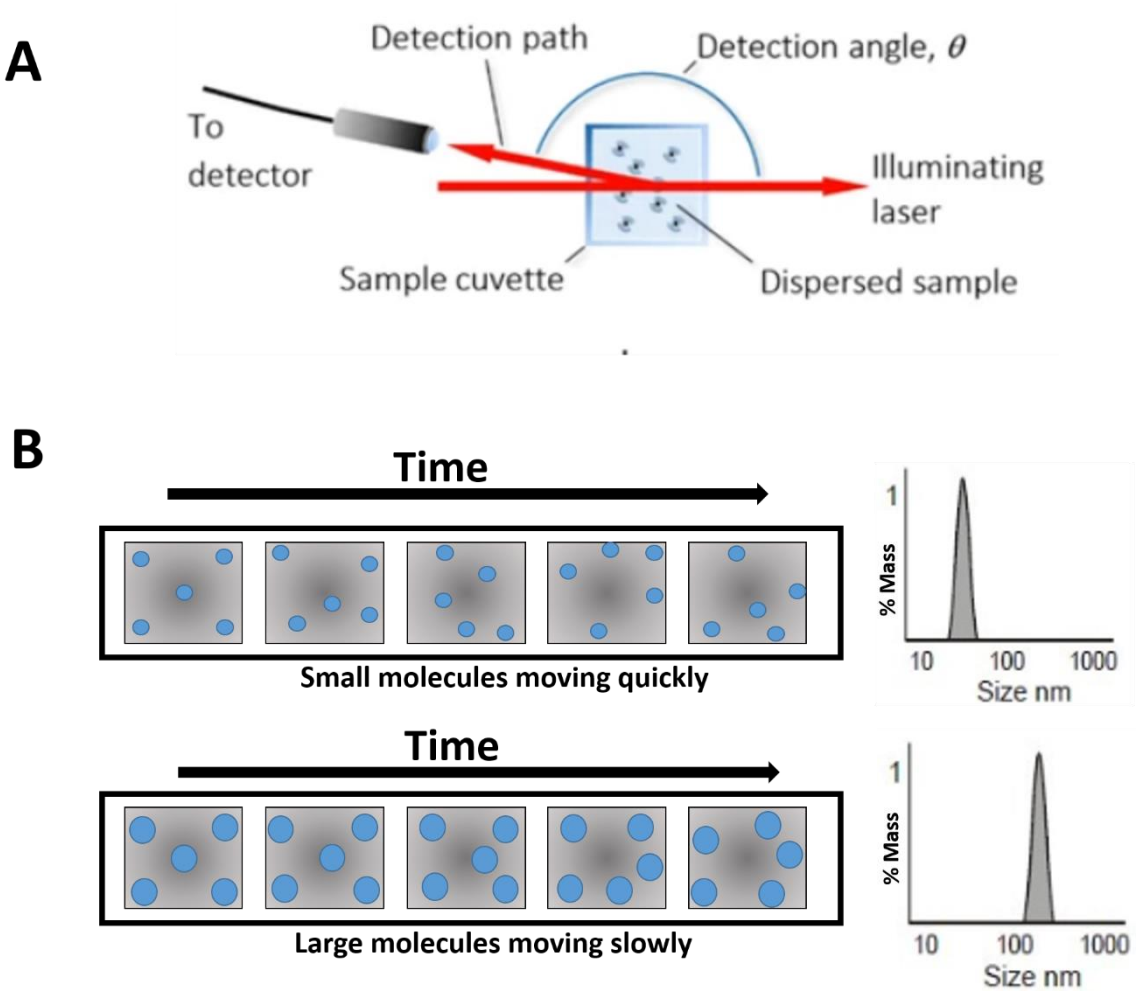

Figure 7.10 Particle dynamics in DLS elucidate to the size and morphology of the protein. A Schematic of a typical DLS instrument set up that is configured to detect backscattered light from a dispersed sample. **B** DLS measures Brownian motion and relates this to the size of the particles in the sample. Brownian motion is the random movement of particles due to the bombardment by the solvent molecules that they are surrounded by. The smaller molecules are "kicked" further by the solvent molecules which move them more rapidly. Large molecules result in a slower Brownian motion. The velocity of the Brownian motions can be defined by a property known as the translational diffusion coefficient. The size of the particle is calculated from the translational diffusion coefficient by using the Stokes-Einstein equation.

The scattered light is detected over a period of time to monitor the movement of the protein within a given sample. As mentioned, smaller particles move at higher speeds which present with faster fluctuations, with the opposite being seen for large molecules. These intensity fluctuations contain information on the time scale of the movement of light scattering, which can be fitted with an autocorrelation function. Taken alongside the translational diffusion coefficient (D_t), which describes the ease with of which a particle is displaced inside a buffer by diffusion, the decay of the autocorrelation function relates to the dimensions of the protein (Koppel, 1972, Stetefeld et al., 2016).

These initial intensity traces are used to generate an auto-correlation function which describes how long the particle remains in the same spot. The exponential decay of the auto-correlation function depicts the movement of the molecule before it returns to a baseline. The decay of the function represents an indirect measure of the time needed for a particle to change its relative position with small particles movement decaying quickly and larger ones more slowly. Measurements are taken over various delay times with results being plotted over a logarithmic time axis (Stetefeld et al., 2016). The signal-to-noise ratio in these measurements can be calculated from the plateau value of the correlation function at the smaller delay times, known as 'the intercept'. If there is not enough signal from the protein within the sample, then the difference between the intercept and the baseline will be low therefore no meaningful correlation function can be produced (Stetefeld et al., 2016, Lorber et al., 2012).

Elutions of the Popeye domain protein (Figure 7.9, bracket) were analysed by a DLS to determine whether there was monomeric Popeye domain present that could be utilised for further experiments. Of the samples tested, only one resulted in a trace that gave a conventional autocorrelation trace (Figure 7.11A). The clear difference between intercept at 1.1 and the baseline at 1, combined with the steep descent allows the autocorrelation function to be fitted with parameters that imply the protein is small, in a relatively high concentration and in a stable condition without the presence of large particulates that were present in the other elutions (Figure 7.11A). The regularization analysis suggests that around 80% of the protein population was in a single species of radius ~3.4 nm (Figure 7.11). This would estimate the molecular weight of the Popeye domain in the buffer to be 58kDa suggesting that the Popeye domain protein is at least a dimer in solution. Precise interpretation of this data is difficult due to the presence of the N-terminal affinity tag and protease cleavage site, which are expected to be disordered and contribute to the hydrodynamic drag on the particles, and the high concentration of imidazole, which act as a surfactant contributing to the total molecular weight of the particles. However, a molecular weight in this range is consistent with the expectation that POPDCs are reportedly found in homo- and hetero-dimeric interactions (Figure 7.11B). The data also indicates the presence of larger particulates or aggregates in the sample above 100 nm in radius with a

predicted molecular weight of several hundred kDa (Figure 7.11B). Given that POPDC1 normally dimerises this aggregation may act to stabilise the Popeye domain construct in solution.

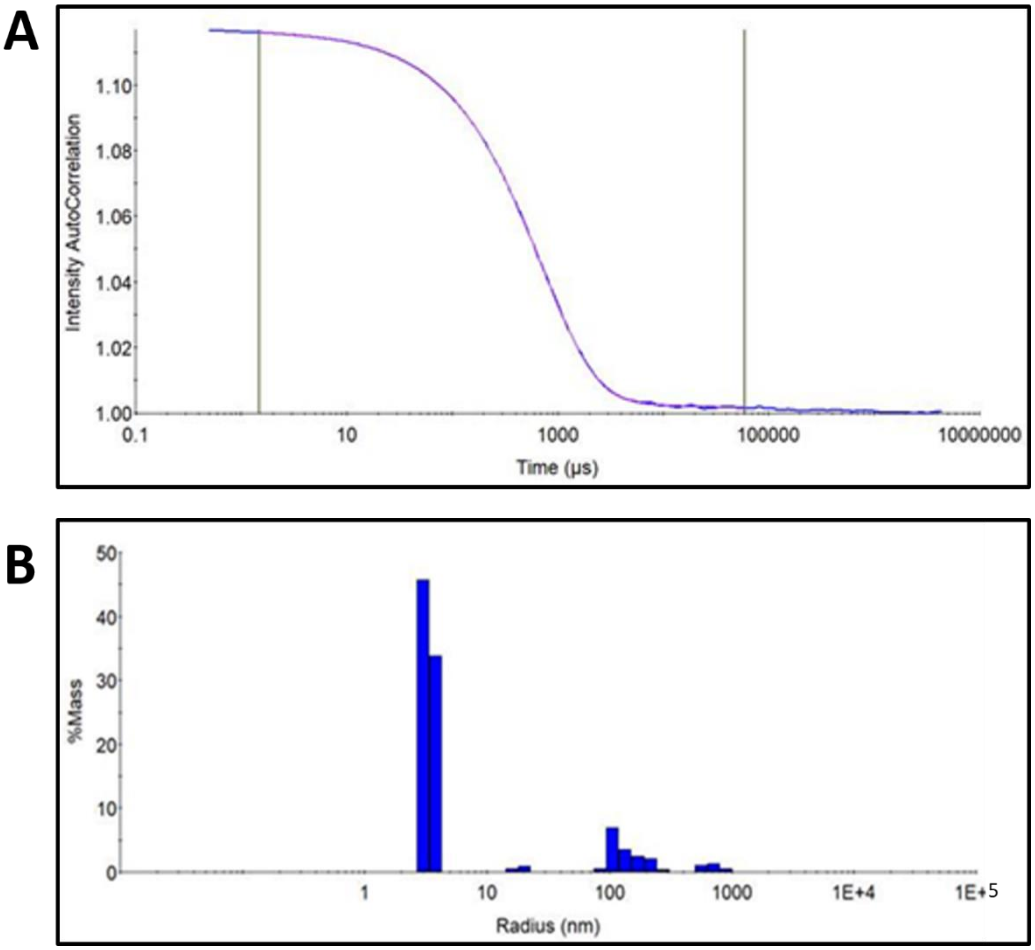

Figure 7.11 DLS data for Popeye domain elution fraction 7 depicting state and size of protein. A Auto-correlation function for Popeye domain protein. **B** Regularization analysis. Bars in the histogram indicate the mass weighted composition of the particles present in solution that would give rise to the recorded autocorrelation function (Experiments undertaken with the help of Ms June Southall, University of Glasgow).

7.3.6 Determining whether the Popeye domain recombinant protein is functional

Although recombinant Popeye domain protein could be purified in soluble form and maintained in solution in high imidazole buffer, it remained to be determined whether the protein was correctly folded and functional. To test the protein's ability to bind cAMP, cAMP conjugated beads were utilised to capture recombinant Popeye domain protein (Figure 7.12). POPDC1 has an EC_{50} of 300 nM for cAMP so a final concentration of 10mM free cAMP was added to one of the

samples to compete any functional Popeye domain off the cAMP agarose beads (Figure 7.12) (Froese et al., 2012). A negative control was performed using Protein g agarose beads, without the presence of cAMP, to determine whether the recombinant protein bound to the agarose beads non-specifically. The recombinant Popeye domain protein was seen to bind to both Protein g and cAMP-conjugated agarose beads as indicated by the presence of a band in all lanes (Figure 7.12). The addition of free cAMP lead to no reduction in the level of captured Popeye domain (Figure 7.12, last lane). Therefore, it could be suggested that the protein was interacting non-specifically with the agarose beads.

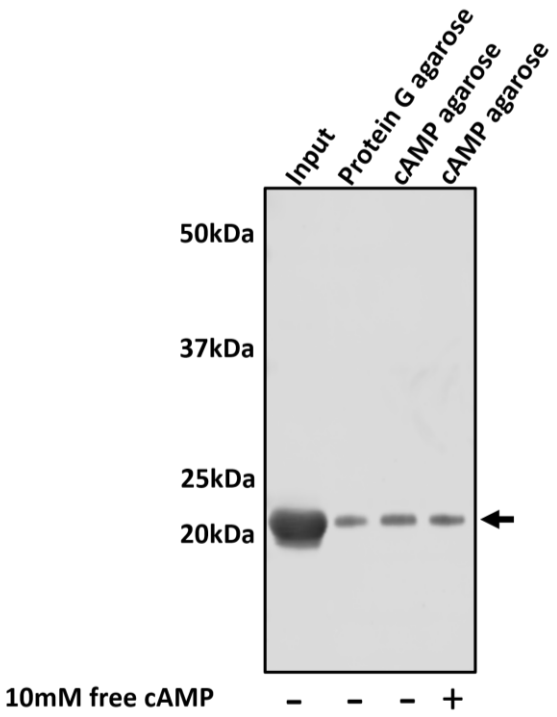

Figure 7.12 Determination of the functionality of recombinant Popeye domain protein using cAMP conjugated agarose beads. 10 µg of purified recombinant protein were diluted in 750µL binding buffer with either Protein G beads or cAMP agarose beads. One cAMP agarose capture experiment was supplemented with 10mM free soluble cAMP. Beads were pelleted and washed n times before being suspended in Laemmli loading buffer. Samples were analysed by SDS-PAGE and Western blotting for the histidine tag on the recombinant protein. The black arrow indicates the correct molecular weight for the Popeye domain. Image representative of n=3.

7.4 Discussion

7.4.1 Solubility issues prevent POPDC1 structural analysis

This chapter illustrates the difficulties in producing a soluble and active POPDC1 protein suitable for structural studies. Only one of the four tested constructs produced an acceptable level of soluble protein that would allow for further experimentation (Figure 7.5, Figure 7.6, Figure 7.7 and Figure 7.9), and the protein produced could not be maintained in solution without high concentrations of imidazole. Therefore, there is a need for further development of methods that would lead to production of amenable protein from other constructs or expression systems. Although the full-length construct was not necessarily expected to be soluble given that it contains predicted hydrophobic transmembrane domains, constructs containing more of the N-terminal regions may be useful given our lack of knowledge of the precise topology of the predicted transmembrane region of the protein. I have shown here that the expression of N-terminus containing constructs is possible in *E. coli* but the yield of soluble protein is not favourable (Figure 7.6) and requires further analysis. Additional constructs were designed and are being produced that express POPDC1 fragments starting at the N-terminus of each of the proposed transmembrane domains and include either just the Popeye domain or the full C-terminal region. Time constraints during this project meant that they could not be carried forward to the solubility testing, but this should be an immediate focus of investigation moving forward.

Although the data presented in this chapter has shown that constructs containing fragments of POPDC1 could be expressed, there was issues maintaining the recombinant protein's solubility. The extraction of integral membrane proteins can be challenging in terms of keeping the protein soluble and is mostly achieved through the use of detergents in the purification buffers. Detergents are amphipathic molecules which contain both hydrophobic and hydrophilic moieties and can form micelles. If the concentration of detergent is too high, micelles can form without inclusion of the protein, this is known as the critical micelle concentration. Le Maire et al., have described that the detergents function to stabilise the protein by forming cooperative interactions that are below the critical micelle concentration (CMC) (le Maire et al., 2000). Within

this study, the addition of the detergent CHAPs was trialled with little success in stabilising the construct (data not shown). However, there are numerous other detergents with elaborate chemical properties that should be investigated to determine if a more appropriate solubilizing detergent should be discovered. For example, CHAPs is known as a type B detergent, meaning it is more rigid and possesses a cholesterol-based structure (reviewed in (Helenius and Simons, 1975) and (Ohlendieck, 2004)). It may be that this protein requires a Type A detergent, such as Dodecyl 4-O-α-D-Glucopyranosyl-ß-D-Glucopyranoside (DDM), which has dual hydrophobic/hydrophilic properties. The hydrophobic part of the detergent masks the hydrophobic part of the membrane protein preventing their aggregation. This type of detergent would allow for experimentation on larger constructs that contain more of the POPDC1 protein.

Furthermore, different tags for the recombinant protein could be trialled. For example, *E.coli* maltose-binding protein (MBP) has been widely recognized as an effective solubilizing agent, which has been shown to increase the yield, enhance solubility and promote proper folding of proteins (Kapust and Waugh, 1999, Fox et al., 2003, Esposito and Chatterjee, 2006). The drawback with using this as a tag is the poor binding capacity of amylose resin, as well as the high level of persistent contaminants (Lichty et al., 2005, Pryor and Leiting, 1997, Nallamsetty et al., 2005). It has been shown that a His_6 tag can be added to the N-terminus of MBP without affecting the solubility of the fused protein (Nallamsetty et al., 2005). This would circumvent the lack of affinity for amylose resin yet improve the solubility of the protein.

The co-expression of either chaperones or foldases may also help to stabilise proteins allowing for improved solubility and hence greater protein yield. Molecular chaperones are known to promote the proper isomerisation and targeting of expressed proteins by interacting with folding intermediates. There are a number of established chaperone systems within *E.coli* including GroES-GroEL, DnaK-DnaJ-GrpE and ClpB (Kumamoto, 1991, Hartl, 1996, Squires and Squires, 1992, Schröder et al., 1993). In addition, there has been evidence that the expression of single subunit of protein complexes can be prone to aggregation in the absence of their natural binding partners (Tan, 2001). Stabilisation of the protein may be gained either by the co-expression of both

POPDC1 and an interaction partner such as PDE4A or by the addition of a peptide containing the binding site of one of said partners. Tan has shown that a modular polycistronic expression system could be used to co-express up to four genes successfully in *E.coli* therefore allowing the reconstitution of protein complexes within the cell (Tan, 2001). This could prove a method of creating a stable, soluble construct that could be used to create a co-crystal structure of POPDC1 and PDE4A. Furthermore, the whole interacting protein may not be required to elicit stability. During this project it has been shown that 25mer cell penetrating peptides can interact with the PDE4A protein and disrupt its interaction with the POPDC1 protein (see Figure 4.7, Figure 4.8, Figure 4.9, Figure 4.11, and Figure 4.13) . Therefore, a possible next step could be to add a peptide containing the 25mer of PDE4A, that is known to interact with POPDC1, to the cells during protein induction. Foldases may be used in conjunction with chaperones or independently to increase stability of proteins. The addition of foldases accelerate the rate limiting steps throughout the folding pathway. For example, peptidyl-prolyl isomerases (PPI), which are ubiquitously expressed proteins in both eukaryotic and prokaryotic cells whose primary function is to facilitate the *cis-trans* isomerisation of peptide bonds to proline residues within the polypeptide chain. It has also been shown to have chaperone properties that could further stabilise the recombinant protein (Kruse et al., 1995, Shaw, 2002, Schmid, 1995). Furthermore, the simultaneous use of both molecular chaperones and foldases can act to prevent and actively reverse protein misfolding and aggregation which may occur accidentally in the native-folding pathway of recombinant protein expression in a foreign environment (reviewed in (Baneyx and Mujacic, 2004)).

Despite the fact that I have produced a soluble protein, testing its functionality as a cAMP binder did not give a definitive answer (Figure 7.12). As POPDC1 is known to be a cAMP effector protein, a means of testing whether the Popeye domain was folded and functioning correctly was developed using cAMP agarose capture. Given that the recombinant Popeye domain was bound to both the cAMP and Protein G beads it could be suggested that the protein may be folded correctly but has a high level of unspecific binding. However, the addition of free excess cAMP did not outcompete the interaction with POPDC1 bound to the cAMP agarose beads; therefore, it remains unclear as to whether a functional

protein has been produced (Figure 7.12). Other methods should be used to further identify whether the pure protein is functional e.g. conducting co-immunoprecipitations using PDE4A and the Popeye domain such as carried out in previous chapters. Confirming whether the recombinant protein still had the capability to bind to its interaction partner would provide support for the protein being correctly folded. This step should be repeated for each construct developed before it is taken onto structural analysis.

Following on from the successful production of a soluble protein, more substantial structural analysis should be carried out including nuclear magnetic resonance spectroscopy (NMR) or protein X-ray crystallography studies. This would provide information that is critical in solving the structure of the POPDC protein family. If a complex of POPDC1 and PDE4A is developed this would allow for the use of transmission electron cryo-microscopy (cryoEM) to investigate protein structure. Advances in cyroEM have made it possible to gain 3-dimensional structural determination that are too heterogenous to be investigated by NMR or X-ray crystallisation (Jonic and Vénien-Bryan, 2009). In order to prepare the protein for cryoEM it would be appropriate to express and purify the Popeye domain from mammalian cells. Either way, the solving of POPDC1's structure would provide unmatched insight into how the protein forms interactions and is modulate by cAMP binding.

7.4.2 Conclusion

The successful expression of a soluble Popeye domain has created a partially optimised protocol as well as identifying potential avenues that will improve solubility giving direction to any further experimentation. The development of fragments of the POPDC1 protein that encompass the full protein sequence has been suggested to be the most promising strategy. Future projects will need to focus on the development of said constructs and optimise methods of maintaining the protein's stability during the purification process. Means by which solubility could be maintained have been outlined here but I believe that the addition of chaperone proteins, whether that be through the systems mentioned or by the co-expression of an interaction partner, will be the most successful strategy to pursue.

8 Discussion

8.1 Background

The discovery of the blood vessel epicardial substance or Popeye domain-containing protein 1 (BVES/POPDC1) by two independent groups in 1999 heralded a new cAMP effector protein that was localised to numerous areas in the heart including the pace-making centres (Reese et al., 1999, Andrée et al., 2000). The first ten years of research have focused on characterising the interactome of POPDC1 in an attempt to determine its cellular role in a number of tissues, however, most initial work has been carried out in the heart. Latter studies have attempted to unpick the complex role of POPDC1 signalling processes, which is where this work lies.

POPDC1 is a largely membrane bound signalling protein that has particular relevance in SA and AV nodes. Loss of function experiments in mice and zebrafish have established an important role for POPDC1 in the maintenance of regular heartbeat, stress signalling and regeneration of skeletal muscle (Schindler et al., 2016b, Alcalay et al., 2013, Froese et al., 2012, Schindler et al., 2012b). *POPDC1*$^{-/-}$ mice have been reported to develop stress-induced bradycardia in response to physical exercise, mental stress or stimulation by injection of isoproterenol (Froese et al., 2012). In addition, it has been shown that POPDC1 protein and mRNA levels are decreased during myocardial I/R injury (Alcalay et al., 2013). In humans, POPDC1 mutations, such as *POPDC1*^{S201F} have been identified leading to the presentation of cardiac arrythmia coupled with limb-girdle muscular dystrophy (Schindler et al., 2016b). Functional analysis of POPDC1 has therefore suggested a crucial role for the protein in the development and maintenance of proper electrical conductance within the heart and skeletal muscle (Froese et al., 2012). More recently, POPDC1 has been shown to be expressed in a number of epithelial cells and can function to control proliferation, migration, invasion and metastasis in a variety of cancers (Amunjela and Tucker, 2017b, Amunjela and Tucker, 2017a, Kim et al., 2010, Han et al., 2015, Williams et al., 2011). With an expanding list of interaction partners, determination of the molecular mechanism(s) of POPDC1 function is a complex task.

Although many interactors for POPDC1 have been found, little is known about how the interactions and hence functions of POPDC1 are controlled. Given its status as the newest cAMP effector protein to be discovered and the knowledge that all other known cAMP effector proteins interact with a phosphodiesterase, it was hypothesised that POPDC1 would also form a complex containing a PDE (Froese et al., 2012). PDE4 has been extensively researched in the cardiovascular system making it an attractive putative target for this study (reviewed in (Fertig and Baillie, 2018)). The spatial and temporal regulation of cAMP by such a localised PDE could provide a means of tightly controlling the actions of POPDC1.

Post-translational modifications to the POPDC family have not been investigated in depth. Currently, there have been hundreds of PTMs identified that result in functional and structural changes to the proteome, triggering changes in protein-protein interactions, cellular location and activity (reviewed in (Prabakaran et al., 2012)). Therefore, POPDC1 function and interaction may be, in part, directed by post-translational modifications.

8.2 POPDC1 creates a signalling complex with PDE4A

The first aim of this project involved the investigation of a potential interaction between POPDC1 and PDE4. Interestingly, the data showed that Popdc1 could interact with PDE4A, PDE4B and PDE4D in endogenously expressing NRVM. This data was not reciprocated in overexpressing HEK293 cells, where POPDC1 only formed an interaction with PDE4A. Within the heart, PDE4A levels are markedly lower than those of the other isoforms (Richter et al., 2011). Despite the lower level of PDE4A in the heart, it displayed the highest affinity for Popdc1 as seen in PLA data (see Figure 3.11) therefore, selected as the main focus for further interaction. Identification of protein binding sites and subsequent development of a cell-penetrating disruptor peptide allowed investigation into the PDE4A-Popdc1 complex. The disruptor reduced the interaction between Popdc1 and PDE4A in both NRVM and HEK293 cells. This data supports the hypothesis that POPDC1 is being controlled by a PDE which acts to shape to cAMP gradient around the effector protein (Figure 8.1).

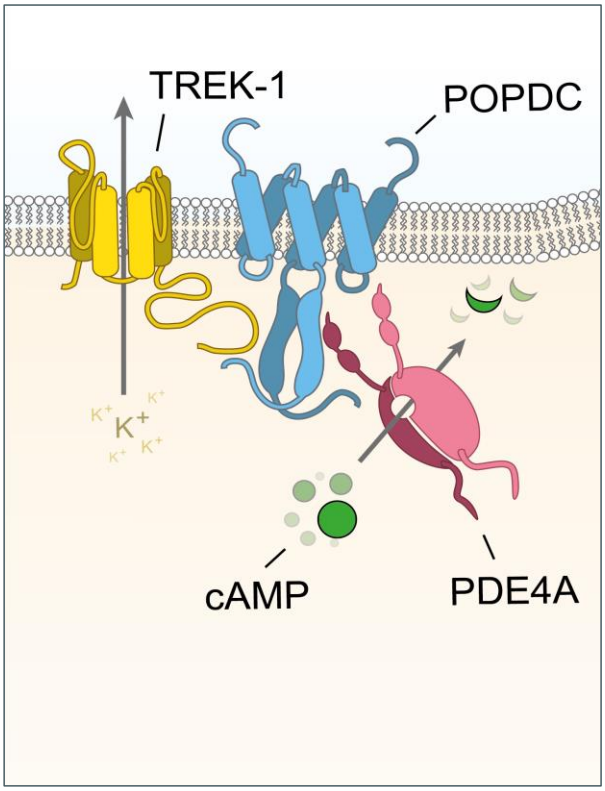

Figure 8.1 The POPDC1/PDE4A complex. POPDC1 is bound to the potassium channel, TREK1 at basal levels of cAMP increasing the efflux of K+ ions. As cAMP levels rise, POPDC1 bind cAMP and dissociates from TREK1. PDE4A functions within this complex to modulate the cAMP gradient. By degrading cAMP in the vicinity of POPDC1, PDE4A can regulate its interaction with TREK1

Given that PDEs can operate within distinct domains within the cell, it may be that the POPDC1 localised to the plasma membrane may interact specifically with PDE4A4/5 as it possesses membrane localisation domains (Beard et al., 1999). It is possible that at other cellular locations where PDE4A is not prevalent then POPDC1 can form interactions with the other isoforms. In addition, there are several proteins that are known to interact with multiple PDE isoforms but maintain a higher affinity for one specific member. For example, multiple PDE4 isoforms are known to associate with the β_1 and β_2 adrenergic receptors and can control the termination of their signalling processes (De Arcangelis et al., 2009b, Baillie et al., 2003, Richter et al., 2008). In isolated murine cardiomyocytes, the depletion of PDE4B and PDE4D were shown to lead to a dysregulation of cardiac contractibility and Ca^{2+} cycling (Leroy et al., 2011). Although β_1 and β_2 can form signalling complexes with isoforms from both PDE4B and PDE4D families, it has been reported that β_1 shows preferential binding to PDE4D8 whereas β_2 has higher affinity for PDE4D5 (Richter et al., 2008). This provides a precedent for the model outlined for POPDC1. The binding of multiple isoforms may also have

a compensatory function. Distinct binding regions may exist for the various PDE4 isoforms on POPDC1 meaning if there was a mutation at one site, for example the *POPDC1*^{R172H} mutation which lies directly in the PDE4A interacting region, another PDE4 may still be able to bind and regulate POPDC1s activity. Different binding regions for multiple PDE isoforms is a concept that has already been shown in the CNS protein, Disrupted in *Schizophrenia* (DISC1). DISC1 was reported to interact with both PDE4B and PDE4D. Mapping of DISC1 binding sites on PDE4B and PDE4D identified two common binding regions for both isoforms and in addition, a further two PDE4B specific sites (Murdoch et al., 2007). For POPDC1, further analysis would have to be carried out using peptide array technology to discover isoform specific binding regions of other PDE4 isoforms.

Despite homology predicting that the identified PDE4A binding site on POPDC1 is only partially accessible, its close proximity of this site to the cAMP binding motif creates a possible means of controlling formation of the interaction. Increased cellular cAMP allows for POPDC1 to bind cAMP close to the surface of the plasma membrane which has been proposed to elicit a conformational change (Froese et al., 2012). In turn, the previously masked residues may become exposed allowing for the binding of PDE4A and consequently leading to a reduction in local cAMP concentration. cAMP bound to POPDC1 is hydrolysed by PDE4A and it returns to its ligand-free conformation, breaking the interaction with PDE4A. This hypothesis may also explain the relatively low levels of endogenous Popdc-PDE4 interaction seen in immunopurification experiments, which were carried out under basal cAMP conditions. This is the first instance of a PDE being associated with the control of the novel cAMP effector protein POPDC1. However, as the structure of POPDC1 has not yet been determined, only predictions can be made around how this interaction may form.

Distinct signalling complexes such as those described in this work are not uncommon in the heart and act to ensure normal cardiac function. PDE4D3 has been reported to form a complex with the RyR2 complex to act as a key regulator in the PKA-dependent phosphorylation of RyR2 (Lehnart et al., 2005). Further examination showed that the complete knock-out of *PDE4D* led to the development of age-dependent cardiomyopathy due to hyperphosphorylation of RyR2 and severe contractile dysfunction. As POPDC1 interactions can be altered

by cellular levels of cAMP, it would not be presumptuous to suggest that the interaction with PDE4A is a regulatory mechanism which controls POPDC1s interactions through the degradation of cAMP. My work has described that the loss of the POPDC1-PDE4 complex resulted in an increased repolarisation event (Figure 4.13) which, has the potential to knock the calcium cycle out of rhythm if a prolonged disruption of the complex was to occur. In addition, POPDC1 mutations have been shown in humans, mouse and zebrafish to lead to the onset of cardiac arrythmias (Froese et al., 2012, Schindler et al., 2016b, De Ridder et al., 2019) and this may in part be due to the loss of control of cAMP dynamics through loss of PDE4 interaction.

There is a variety of conceptual models that have been developed to illustrate possible modes of POPDC1 function within the cell (reviewed in ((Swan et al., 2019)). Two of these models tend to fit with the conclusions from my work. **Firstly,** the switch model provides the simplest of explanation of POPDC1 activity by suggesting that it functions as a molecular switch. In the absence of cAMP binding, POPDC1 is bound to its interaction partners e.g. TREK1. In this instance, there is an increase in the efflux of K^+ ions out of the cell via this channel (Froese et al., 2012). Upon cAMP binding, POPDC1 and TREK1 dissociate and the channel there is a reduction in this efflux of K^+ ions. My addition to this model would be, that with cAMP bound to POPDC1, the obstructed PDE4A binding site to become accessible allowing PDE4 to bind. Subsequently there is a reduction in local cAMP levels allowing POPDC1 to reinstate its interaction with TREK1. This mechanism would function to maintain steady cardiac pace-making (Unudurthi et al., 2016). Where mutations in the binding region of PDE4A in POPDC1 occur, this control would potentially be lost leading to a dysregulation of TREK1 output and the onset of cardiac arrythmia. **Secondly,** the shield model is based on the switch model but suggests that the binding of cAMP may lead to an indirect downstream effect. For example, the binding of POPDC to one of its partners such as TREK1 would create a shield preventing the bound partner from being targeted by kinases such as PKA. When cAMP is bound to POPDC1, either the interaction between the two proteins is disrupted or the shielding mechanism is no longer efficient and therefore the protection elicited by POPDC1 is lost. The protein would now be accessible by kinases and phosphorylation events could occur. In this model, PDE4 would again function to

desensitise the mechanism. So, although my work is consistent with two of the proposed models it does not allow discrimination between them or point to which model is correct.

To summarise, there are many examples of cAMP effector proteins in complex with PDEs but, this is the first instance of POPDC1 forming such an interaction. In the future it is likely that this novel and exciting finding will allow greater insight into the cellular functions of POPDC1 and aid understanding of how the cAMP-specific actions of POPDC1 are controlled.

8.3 Identification of a novel therapeutic target

The cAMP signalling system has been repeatedly shown to coordinate precise and directed cellular responses that are underpinned by numerous protein-protein interactions (reviewed in (Lissandron and Zaccolo, 2006)). In the heart, such compartmentalised cAMP signalling is vital for numerous process, including the fine control of excitation-contraction coupling, which is critical to the maintenance of normal cardiac function. As the only enzyme known to degrade cAMP, PDEs have been repeatedly shown to act as a crucial control mechanism for cardiac signalling (reviewed in (Fertig and Baillie, 2018)). Extensive research has shown that highly compartmentalised cAMP signals result in discrete receptor-specific physiological changes within cardiomyocytes and when these are dysregulated, the result is a loss control that results in the onset of various cardiovascular diseases (Zaccolo, 2009, Fischmeister et al., 2006). As such, these signalling complexes have long been regarded as potential therapeutic targets (Lugnier, 2006). The issue that is posed by targeting proteins such as PDEs, EPAC and PKA, which are all key components of compartmentalised cAMP signalling mechanisms, is that they are ubiquitous signalling proteins that undertake extensive and often unrelated functions in a cell. Targeting protein-protein interactions non-specifically could have serious off-target effects leading to a worsening condition. In this light, targeting specific protein-protein interactions that underpin distinct and highly localised cardiac functions would constitute a novel method of isolating single “pools” of these enzymes allowing better targeted therapeutic changes.

It has been widely accepted that inhibitors targeted against the active site of PDE4 isoforms have immense potential in the treatment of many diseases from asthma to depression (reviewed in (Houslay et al., 2005) and (Francis et al., 2011b)). The main issue with broadly targeting PDE4 is the side effects which limit their maximal dosage rendering them ineffective for clinical treatment (Zhang et al., 2005). Simultaneously inhibiting all PDE4s has been shown to cause headaches, emesis and diarrhoea yet despite this, the PDE4 inhibitor roflumilast has been approved for the treatment of late stage chronic obstructive pulmonary disease (COPD) (Zhang et al., 2005, Fabbri et al., 2010, Gupta, 2012). Specific targeting of single PDE isoforms has been attempted in several ways including siRNA knockdown (Lynch et al., 2005) and dominant negative constructs (McCahill et al., 2005, Henderson et al., 2014). However, for PDE4 family members, such as PDE4D5, which possess multiple non-redundant functions within the cell, all subpopulations of any single isoform would be inhibited creating potentially disastrous dysregulation of signalling crosstalk (Lynch et al., 2007). Therefore, targeting individual PDE4 interactions that anchor the enzymes to a distinct location via the peptide interference approach has the advantage of not affecting global PDE4 activity while at the same time influencing cAMP signals at the nano-level (Smith et al., 2007). Generation of binding maps that chart the binding sites of a set of interacting proteins can act as a blueprint for the development of cell penetrating peptides that can disrupt a specific protein-protein interaction. This disruption approach has been used extensively to investigate cAMP signalling complexes such as the interaction between PDE4 and the signalling proteins RACK1, ß-arrestin and the cardioprotective HSP20 (Bolger et al., 2006, Bolger et al., 2003, Sin et al., 2011).

A large body of evidence has shown that ß-arrestin orchestrates the redistribution of PDE4D5 in response to $ß_2$-adrenergic receptor activation (Le Jeune et al., 2002, Mongillo et al., 2004, Willoughby et al., 2007, Trian et al., 2011, Perry et al., 2002, Billington et al., 2008). The ß-arrestin/PDE4D complex is translocated to activated $ß_2$-adrenergic receptors meaning that an active pool of PDEs are present to initiate the desensitisation process (Houslay et al., 2007). This process essentially resets the receptor to allow for another round of antagonist interaction. Fine mapping of the binding region identified the

minimal sequence required to promote an interaction between ß-arrestin/PDE4D and this was the first 'proof of concept' of a cell penetrating peptide that altered local cAMP signalling. The peptide attenuated recruitment of PDE4D5 to the activated $ß_2$-adrenergic receptor leading to the hyperphosphorylation of the receptor after stimulation and altered receptor activity (Smith et al., 2007). Moreover, the same steps have been carried out with a cAMP effector protein signalling complex containing PDE4D5 and EPAC (Rampersad et al., 2010). Treatment with the PDE4D5-EPAC disruptor peptide lead to a reduction in vascular endothelial cell permeability due to compartmentalised cAMP changes at cell-cell contact points.

Data presented in this thesis has shown that peptide disruption is now a technique that can be used to probe POPDC1 function in primary cell cultures. My results have shown that there is a distinct delay in repolarisation events after treatment with the Popdc1-PDE4 disruptor. POPDC1 has been predicted to act as a hub gene for atrial fibrillation as well as a novel determinant of the length of QT interval (Tan et al., 2013). This is interesting as the cell-penetrating peptide, designed in this thesis, increased the time taken between the start of the depolarisation event and the end of the repolarisation phase in the ventricle. To date, numerous POPDC1 mutations found in humans have been linked to the onset of cardiac arrythmias (Schindler et al., 2016b). Included in this group is the *POPDC1*^{R172H} mutation which changes the arginine at position 172 to a histidine and, as mentioned, this site falls within the mapped binding region that associates with PDE4A. The use of the disruptor peptide could represent a means by which to investigate the functional outcomes of this mutation if it were to affect the binding between POPDC1 and PDE4A in disease. Similarly, other mutations may lead to increase in binding of PDE4A or an inability to sever the interaction after cAMP levels have returned to basal. In this scenario, disrupting the interaction could prove a useful therapeutic strategy (Figure 8.2).

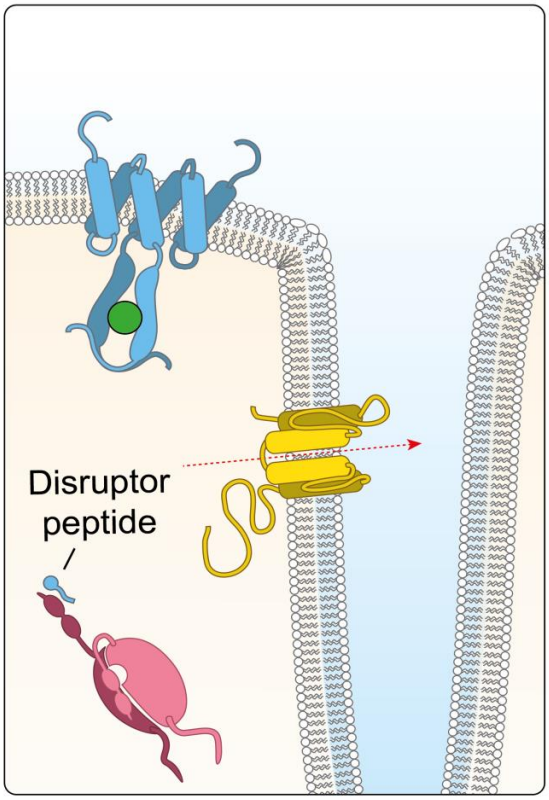

Figure 8.2 The disruptor peptide, designed in this project, blocks the interaction of POPDC1 and PDE4A. In turn, this leads to persistently high levels of cAMP surrounding POPDC1. As cAMP is not degraded in the vicinity of POPDC1, the interaction between POPDC1 and TREK1 remains dissociated. (Image created by Dr Gonzalo Tejeda, University of Glasgow).

Although several peptide based drugs have reached market there is generally low stability and membrane permeability (Craik et al., 2013). Therefore, nonpeptidic agents such as peptidomimetics and small molecules have offered a promising alternative (Schächterle et al., 2015). Fluorescence polarisation (FP) is an extremely versatile technique that is widely used to screen for small molecules that can be utilised in drug development (Lea and Simeonov, 2011). FP is based on the observations taken when a fluorescently labelled peptide is excited by polarized light. The peptide emits light with a degree of polarisation that is inversely proportional to the rate at which the probe is rotating (Moerke, 2009). When the peptide is bound to another protein the rate of rotation and therefore, the fluorescent signal is altered. The level of change in fluorescence can determine the affinity of the peptide for an interacting protein (Moerke, 2009). This process can be utilised for a competition assay allowing for the screening of small molecules which may break the interaction. The sequence used to develop the cell penetrating peptide could be conjugated to a

fluorophore and used to screen small molecules that will elicit the same effect as the peptide. A library of bioactive compounds and 'drug-like' small molecules can be screened to generate hits that can be followed up in secondary assays to assess chemical properties. Desirable properties can create leads in the development of a pharmaceutically relevant drug. There are numerous small molecules that have been shown to interfere with protein-protein interactions. For example, the interaction between AKAP and PKA has been mapped to a 14-18 amino acid sequence on AKAPs that allow for the anchoring of PKAs regulatory subunit (Christian et al., 2011). Peptide inhibitors of AKAP-PKA interactions have proved to be a successful way of studying the role of these proteins in disease but, as mentioned, the poor membrane permeability and inability to be given orally has capped their therapeutic potential. As such, a small molecule screen was undertaken by Christian and colleagues using the defined binding regions of PKA on AKAPs (Christian et al., 2011). This identified the small molecules 3,3′-diamino-4,4′-dihydroxydiphenylmethane (FMP-API-1) and its derivatives that can disrupt the PKA-AKAP complex both biochemically, using recombinant proteins, and functionally, using cultured cardiomyocytes(Christian et al., 2011). This process could be utilised to investigate small molecules that could provide therapeutic intervention by targeting the POPDC1/PDE4A complex given its role in cardiac and skeletal muscle diseases. Such an approach to target the inhibition or activation of this complex would be the first such endeavour involving POPDC1.

8.4 Final Conclusions

My work demonstrates that there is a novel signalling complex containing both POPDC1 and PDE4A and that this has an important function in action potential generation. Since its identification, there has been little research on the control of POPDC1 function and this study identifies the interaction with PDE4A as a POPDC1 control mechanism. In addition to the identification of binding sites and the development of cell penetrating disruptor peptides, I have shown that this interaction can be disrupted in a highly specific manner to effect change in functional outcomes. It is still unclear whether this interaction can be targeted therapeutically, but my work has provided a promising indication that it may be possible. Further experimentation is required to validate whether this interaction is relevant in whole organisms and animal studies using the peptide

could be set up to investigate this. Similar studies have shown promise with peptides designed to disrupt the PDE4D-HSP20 complex in the heart (Martin et al., 2014, Sin et al., 2011, Sin et al., 2015). Overall, my work has opened up new possibilities for research into POPDC1 by firstly discovering the POPDC1-PDE4A interaction and secondly developing novel tools to investigate the function of the complex in primary cells and animals.

Appendix

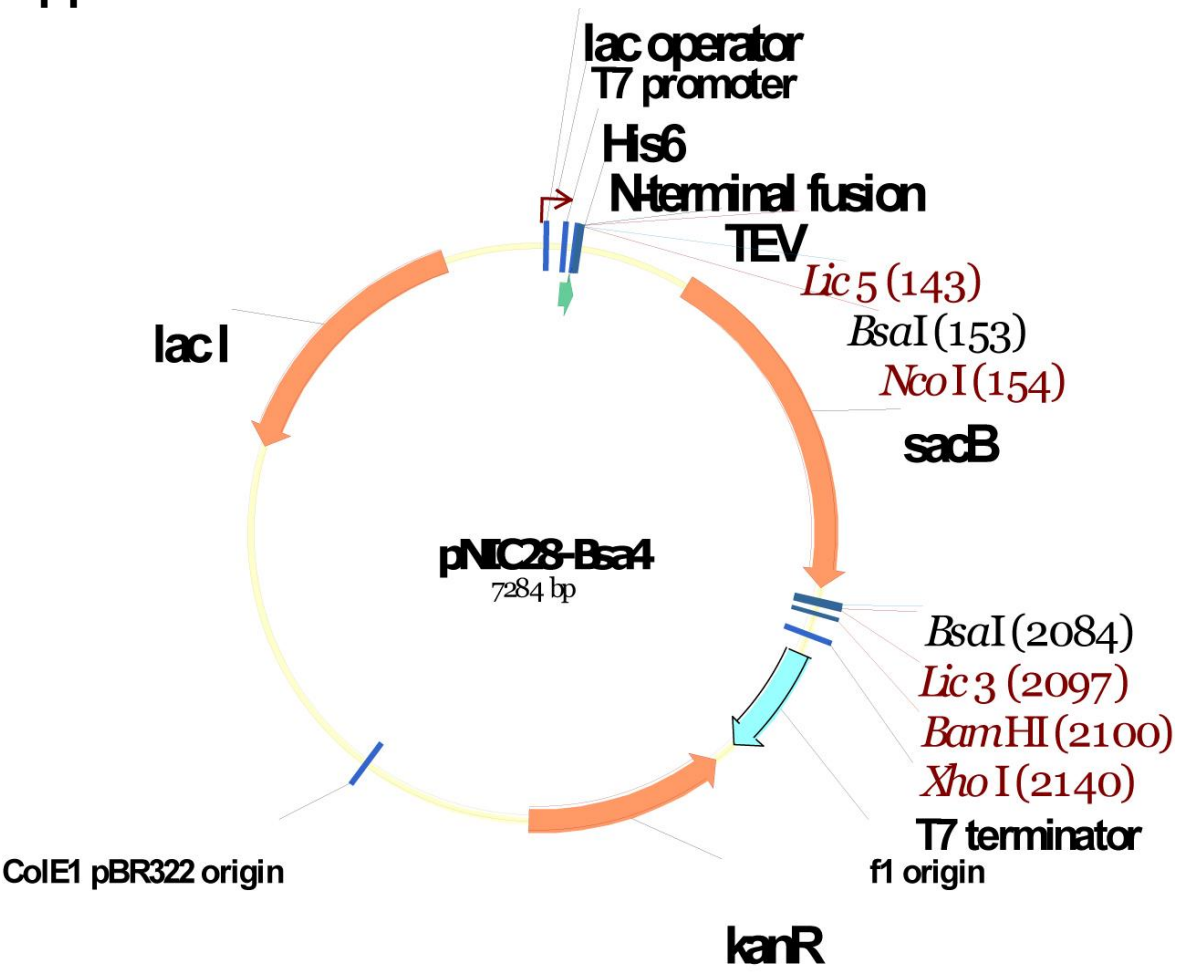

Appendix Figure 1: pNIC28-Bsa4 vector backbone used for *E.coli* expression construct generation. The vector was linearized using the BsaI sites to allow for the insertion of fragments of POPDC1. (Plasmid map taken from (Savitsky et al., 2010)).

References

ABI-GERGES, A., RICHTER, W., LEFEBVRE, F., MATEO, P., VARIN, A., HEYMES, C., SAMUEL, J.-L., LUGNIER, C., CONTI, M., FISCHMEISTER, R. & VANDECASTEELE, G. 2009. Decreased expression and activity of cAMP phosphodiesterases in cardiac hypertrophy and its impact on beta-adrenergic cAMP signals. *Circulation research,* 105**,** 784-792.

ADAMS, J. A., MCGLONE, M. L., GIBSON, R. & TAYLOR, S. S. 1995. Phosphorylation modulates catalytic function and regulation in the cAMP-dependent protein kinase. *Biochemistry,* 34**,** 2447-54.

AL-SALAM, S. & HASHMI, S. 2014. Galectin-1 in Early Acute Myocardial Infarction. *PLOS ONE,* 9**,** e86994.

ALBERTS, B., JOHNSON, A., LEWIS, J., RAFF, M., ROBERTS, K. & WALTER, P. 2002. Molecular biology or the cell. *Molecular biology or the cell.*

ALCALAY, Y., HOCHHAUSER, E., KLIMINSKI, V., DICK, J., ZAHALKA, M. A., PARNES, D., SCHLESINGER, H., ABASSI, Z., SHAINBERG, A., SCHINDLER, R. F. R., BRAND, T. & KESSLER-ICEKSON, G. 2013. Popeye domain containing 1 (Popdc1/Bves) is a caveolae-associated protein involved in ischemia tolerance. *PloS one,* 8**,** e71100-e71100.

ALESSI, D. R., BARRY CAUDWELL, F., ANDJELKOVIC, M., HEMMINGS, B. A. & COHEN, P. 1996. Molecular basis for the substrate specificity of protein kinase B; comparison with MAPKAP kinase-1 and p70 S6 kinase. *FEBS Letters,* 399**,** 333-338.

AMUNJELA, J. N., SWAN, A. H. & BRAND, T. 2019. The Role of the Popeye Domain Containing Gene Family in Organ Homeostasis. *Cells,* 8.

AMUNJELA, J. N. & TUCKER, S. J. 2016a. Loss of Popdc protein expression promotes a more malignant phenotype in glioblastoma and breast cancer cells. *European Journal of Cancer,* 61**,** S46.

AMUNJELA, J. N. & TUCKER, S. J. 2016b. POPDC proteins as potential novel therapeutic targets in cancer. *Drug Discovery Today,* 21**,** 1920-1927.

AMUNJELA, J. N. & TUCKER, S. J. 2017a. Dysregulation of POPDC1 promotes breast cancer cell migration and proliferation. *Bioscience reports,* 37**,** BSR20171039.

AMUNJELA, J. N. & TUCKER, S. J. 2017b. POPDC1 is suppressed in human breast cancer tissues and is negatively regulated by EGFR in breast cancer cell lines. *Cancer Letters,* 406**,** 81-92.

ANDJELKOVIĆ, M., JAKUBOWICZ, T., CRON, P., XIU-FEN, M., HAN, J. & HEMMINGS, B. A. 1996. Activation and phosphorylation of a pleckstrin homology domain containing protein kinase (RAC-PK/PKB) promoted by serum and protein phosphatase inhibitors. . *Proceedings of the National Academy of Sciences of the United States of America,* 93**,** 5699-704.

ANDRÉE, B., FLEIGE, A., ARNOLD, H.-H. & BRAND, T. 2002a. Mouse Pop1 Is Required for Muscle Regeneration in Adult Skeletal Muscle. *Molecular and Cellular Biology,* 22**,** 1504.

ANDRÉE, B., FLEIGE, A., HILLEMANN, T., ARNOLD, H.-H., KESSLER-ICEKSON, G. & BRAND, T. 2002b. Molecular and functional analysis of Popeye genes: A novel family of transmembrane proteins preferentially expressed in heart and skeletal muscle. *Experimental and clinical cardiology,* 7**,** 99-103.

ANDRÉE, B., HILLEMANN, T., KESSLER-ICEKSON, G., SCHMITT-JOHN, T., JOCKUSCH, H., ARNOLD, H.-H. & BRAND, T. 2000. Isolation and Characterization of the Novel Popeye Gene Family Expressed in Skeletal Muscle and Heart. *Developmental Biology,* 223**,** 371-382.

ANELLI, T. & SITIA, R. 2008. Protein quality control in the early secretory pathway. *The EMBO Journal,* 27**,** 315-327.

ANVERSA, P., OLIVETTI, G., MEGGS, L. G., SONNENBLICK, E. H. & CAPASSO, J. M. 1993. Cardiac anatomy and ventricular loading after myocardial infarction. *Monograph-American Heart Association,* 87**,** VII. 22-VII. 27.

ARAI, M., ALPERT, N. R., MACLENNAN, D. H., BARTON, P. & PERIASAMY, M. 1993. Alterations in sarcoplasmic reticulum gene expression in human heart failure. A possible mechanism for alterations in systolic and diastolic properties of the failing myocardium. *Circulation Research,* 72**,** 463-469.

ARDITO, F., GIULIANI, M., PERRONE, D., TROIANO, G. & LO MUZIO, L. 2017. The crucial role of protein phosphorylation in cell signaling and its use as targeted therapy (Review). *International journal of molecular medicine,* 40**,** 271-280.

ASSAYAG, P., CARRÉ, F., CHEVALIER, B., DELCAYRE, C., MANSIER, P. & SWYNGHEDAUW, B. 1997. Compensated cardiac hypertrophy: arrhythmogenicity and the new myocardial phenotype. I. Fibrosis. *Cardiovascular Research,* 34**,** 439-444.

AVERAIMO, S. & NICOL, X. 2014. Intermingled cAMP, cGMP and calcium spatiotemporal dynamics in developing neuronal circuits. *Frontiers in Cellular Neuroscience,* 8**,** 376.

AZEVEDO, M. F., FAUCZ, F. R., BIMPAKI, E., HORVATH, A., LEVY, I., DE ALEXANDRE, R. B., AHMAD, F., MANGANIELLO, V. & STRATAKIS, C. A. 2014. Clinical and molecular genetics of the phosphodiesterases (PDEs). *Endocrine reviews,* 35**,** 195-233.

AZEVEDO, P. S., POLEGATO, B. F., MINICUCCI, M. F., PAIVA, S. A. R. & ZORNOFF, L. A. M. 2016. Cardiac Remodeling: Concepts, Clinical Impact, Pathophysiological Mechanisms and Pharmacologic Treatment. *Arquivos brasileiros de cardiologia,* 106**,** 62-69.

BACHOVCHIN, D. A., JI, T., LI, W., SIMON, G. M., BLANKMAN, J. L., ADIBEKIAN, A., HOOVER, H., NIESSEN, S. & CRAVATT, B. F. 2010. Superfamily-wide portrait of serine hydrolase inhibition achieved by library-versus-library screening. *Proceedings of the National Academy of Sciences of the United States of America,* 107**,** 20941-20946.

BACKX, P. H. & MARBAN, E. 1993. Background potassium current active during the plateau of the action potential in guinea pig ventricular myocytes. *Circulation Research,* 72**,** 890-900.

BAILEY, C. H., BARTSCH, D. & KANDEL, E. R. 1996. Toward a molecular definition of long-term memory storage. *Proceedings of the National Academy of Sciences,* 93**,** 13445-13452.

BAILLIE, G. S. 2009. Compartmentalized signalling: spatial regulation of cAMP by the action of compartmentalized phosphodiesterases. *The FEBS Journal,* 276**,** 1790-1799.

BAILLIE, G. S., ADAMS, D. R., BHARI, N., HOUSLAY, T. M., VADREVU, S., MENG, D., LI, X., DUNLOP, A., MILLIGAN, G., BOLGER, G. B., KLUSSMANN, E. & HOUSLAY, M. D. 2007. Mapping binding sites for the PDE4D5 cAMP-specific phosphodiesterase to the N- and C-domains of beta-arrestin using spot-immobilized peptide arrays. *The Biochemical journal,* 404**,** 71-80.

BAILLIE, G. S., HUSTON, E., SCOTLAND, G., HODGKIN, M., GALL, I., PEDEN, A. H., MACKENZIE, C., HOUSLAY, E. S., CURRIE, R., PETTITT, T. R., WALMSLEY, A. R., WAKELAM, M. J. O., WARWICKER, J. & HOUSLAY, M. D. 2002. TAPAS-1, a Novel Microdomain within the Unique N-terminal Region of the PDE4A1 cAMP-specific Phosphodiesterase That Allows Rapid, Ca2+-

triggered Membrane Association with Selectivity for Interaction with Phosphatidic Acid. *Journal of Biological Chemistry,* 277**,** 28298-28309.

BAILLIE, G. S., SOOD, A., MCPHEE, I., GALL, I., PERRY, S. J., LEFKOWITZ, R. J. & HOUSLAY, M. D. 2003. ß-Arrestin-mediated PDE4 cAMP phosphodiesterase recruitment regulates ß-adrenoceptor switching from Gs to Gi. *Proceedings of the National Academy of Sciences,* 100**,** 940-945.

BAILLIE, G. S., TEJEDA, G. S. & KELLY, M. P. 2019. Therapeutic targeting of 3′,5′-cyclic nucleotide phosphodiesterases: inhibition and beyond. *Nature Reviews Drug Discovery,* 18**,** 770-796.

BALDA, M. S., GARRETT, M. D. & MATTER, K. 2003. The ZO-1-associated Y-box factor ZONAB regulates epithelial cell proliferation and cell density. *The Journal of cell biology,* 160**,** 423-432.

BALDA, M. S. & MATTER, K. 2009. Tight junctions and the regulation of gene expression. *Biochimica et Biophysica Acta (BBA) - Biomembranes,* 1788**,** 761-767.

BANEYX, F. 1999. Recombinant protein expression in Escherichia coli. *Current Opinion in Biotechnology,* 10**,** 411-421.

BANEYX, F. & MUJACIC, M. 2004. Recombinant protein folding and misfolding in Escherichia coli. *Nature Biotechnology,* 22**,** 1399-1408.

BARBER, R., BAILLIE, G. S., BERGMANN, R., SHEPHERD, M. C., SEPPER, R., HOUSLAY, M. D. & HEEKE, G. V. 2004. Differential expression of PDE4 cAMP phosphodiesterase isoforms in inflammatory cells of smokers with COPD, smokers without COPD, and nonsmokers. *American Journal of Physiology-Lung Cellular and Molecular Physiology,* 287**,** L332-L343.

BARBER, T. D., BARBER, M. C., TOMESCU, O., BARR, F. G., RUBEN, S. & FRIEDMAN, T. B. 2002. Identification of Target Genes Regulated by PAX3 and PAX3–FKHR in Embryogenesis and Alveolar Rhabdomyosarcoma. *Genomics,* 79**,** 278-284.

BAREFIELD, D. & SADAYAPPAN, S. 2010. Phosphorylation and function of cardiac myosin binding protein-C in health and disease. *Journal of Molecular and Cellular Cardiology,* 48**,** 866-875.

BARTOS, D. C., GRANDI, E. & RIPPLINGER, C. M. 2015. Ion Channels in the Heart. *Comprehensive Physiology,* 5**,** 1423-1464.

BARYSHNIKOVA, O. K., LI, M. X. & SYKES, B. D. 2008. Modulation of Cardiac Troponin C Function by the Cardiac-Specific N-Terminus of Troponin I: Influence of PKA Phosphorylation and Involvement in Cardiomyopathies. *Journal of Molecular Biology,* 375**,** 735-751.

BAYER, T. S., BOOTH, L. N., KNUDSEN, S. M. & ELLINGTON, A. D. 2005. Arginine-rich motifs present multiple interfaces for specific binding by RNA. *RNA (New York, N.Y.),* 11**,** 1848-1857.

BEARD, M. B., HUSTON, E., CAMPBELL, L., GALL, I., MCPHEE, I., YARWOOD, S., SCOTLAND, G. & HOUSLAY, M. D. 2002. In addition to the SH3 binding region, multiple regions within the N-terminal noncatalytic portion of the cAMP-specific phosphodiesterase, PDE4A5, contribute to its intracellular targeting. *Cellular Signalling,* 14**,** 453-465.

BEARD, M. B., O'CONNELL, J. C., BOLGER, G. B. & HOUSLAY, M. D. 1999. The unique N-terminal domain of the cAMP phosphodiesterase PDE4D4 allows for interaction with specific SH3 domains. *FEBS Letters,* 460**,** 173-177.

BEAVO, J. A. & BRUNTON, L. L. 2002. Cyclic nucleotide research — still expanding after half a century. *Nature Reviews Molecular Cell Biology,* 3**,** 710-717.

BECA, S., HELLI, P. B., SIMPSON, J. A., ZHAO, D., FARMAN, G. P., JONES, P., TIAN, X., WILSON, L. S., AHMAD, F., CHEN, S. R. W., MOVSESIAN, M. A., MANGANIELLO, V., MAURICE, D. H., CONTI, M. & BACKX, P. H. 2011. Phosphodiesterase 4D regulates baseline sarcoplasmic reticulum Ca2+ release and cardiac contractility, independently of L-type Ca2+ current. *Circulation research,* 109**,** 1024-1030.

BEERI, R., YOSEFY, C., GUERRERO, J. L., NESTA, F., ABEDAT, S., CHAPUT, M., DEL MONTE, F., HANDSCHUMACHER, M. D., STROUD, R., SULLIVAN, S., PUGATSCH, T., GILON, D., VLAHAKES, G. J., SPINALE, F. G., HAJJAR, R. J. & LEVINE, R. A. 2008. Mitral Regurgitation Augments Post-Myocardial Infarction Remodeling: Failure of Hypertrophic Compensation. *Journal of the American College of Cardiology,* 51**,** 476-486.

BELLUCCI, A., NAVARRIA, L., FALARTI, E., ZALTIERI, M., BONO, F., COLLO, G., SPILLANTINI, M. G., MISSALE, C. & SPANO, P. 2011. Redistribution of DAT/α-synuclein complexes visualized by "in situ" proximity ligation assay in transgenic mice modelling early Parkinson's disease. *PloS one,* 6**,** e27959-e27959.

BELTRAMI, C. A., FINATO, N., ROCCO, M., FERUGLIO, G. A., PURICELLI, C., CIGOLA, E., SONNENBLICK, E. H., OLIVETTI, G. & ANVERSA, P. 1995. The cellular basis of dilated cardiomyopathy in humans. *Journal of molecular and cellular cardiology,* 27**,** 291-305.

BELTRAO, P., ALBANÈSE, V., KENNER, L. R., SWANEY, D. L., BURLINGAME, A., VILLÉN, J., LIM, W. A., FRASER, J. S., FRYDMAN, J. & KROGAN, N. J. 2012. Systematic functional prioritization of protein posttranslational modifications. *Cell,* 150**,** 413-425.

BELTRAO, P., BORK, P., KROGAN, N. J. & VAN NOORT, V. 2013. Evolution and functional cross-talk of protein post-translational modifications. *Molecular systems biology,* 9**,** 714-714.

BENARROCH, E. E. 2013. HCN channels. *Neurology,* 80**,** 304.

BENATAR, M. 2000. Neurological potassium channelopathies. *QJM: An International Journal of Medicine,* 93**,** 787-797.

BENDER, A. T. & BEAVO, J. A. 2006. Cyclic Nucleotide Phosphodiesterases: Molecular Regulation to Clinical Use. *Pharmacological Reviews,* 58**,** 488.

BENESH, E. C., MILLER, P. M., PFALTZGRAFF, E. R., GREGA-LARSON, N. E., HAGER, H. A., SUNG, B. H., QU, X., BALDWIN, H. S., WEAVER, A. M. & BADER, D. M. 2013. Bves and NDRG4 regulate directional epicardial cell migration through autocrine extracellular matrix deposition. *Molecular biology of the cell,* 24**,** 3496-3510.

BERRIDGE, M. J. 1984. Inositol trisphosphate and diacylglycerol as second messengers. *Biochemical Journal,* 220**,** 345-360.

BERS, D. M. 2002. Cardiac excitation–contraction coupling. *Nature,* 415**,** 198-205.

BEUCKELMANN, D. J., NÄBAUER, M. & ERDMANN, E. 1992. Intracellular calcium handling in isolated ventricular myocytes from patients with terminal heart failure. *Circulation,* 85**,** 1046-1055.

BHARDWAJ, N., STAHELIN, R. V., LANGLOIS, R. E., CHO, W. & LU, H. 2006. Structural Bioinformatics Prediction of Membrane-binding Proteins. *Journal of Molecular Biology,* 359**,** 486-495.

BIANCO, C., TORTORA, G., BALDASSARRE, G., CAPUTO, R., FONTANINI, G., CHINÈ, S., BIANCO, A. R. & CIARDIELLO, F. 1997. 8-Chloro-cyclic AMP inhibits autocrine and angiogenic growth factor production in human colorectal and breast cancer. *Clinical Cancer Research,* 3**,** 439.

BIJLMAKERS, M.-J. & MARSH, M. 2003. The on–off story of protein palmitoylation. *Trends in Cell Biology,* 13**,** 32-42.

BILLINGTON, C. K., JEUNE, I. R. L., YOUNG, K. W. & HALL, I. P. 2008. A Major Functional Role for Phosphodiesterase 4D5 in Human Airway Smooth Muscle Cells. *American Journal of Respiratory Cell and Molecular Biology,* 38**,** 1-7.

BISHOP, J. B., MARTIN, J. C. & ROSENBLUM, W. M. 1991. A light scattering method for qualitatively monitoring aggregation rates in macromolecular systems. *Journal of Crystal Growth,* 110**,** 164-170.

BLOKLAND, A., VAN DUINEN, M. A., SAMBETH, A., HECKMAN, P. R., TSAI, M., LAHU, G., UZ, T. & PRICKAERTS, J. 2019. Acute treatment with the PDE4 inhibitor roflumilast improves verbal word memory in healthy old individuals: a double-blind placebo-controlled study. *Neurobiology of aging,* 77**,** 37-43.

BOBIN, P., BELACEL-OUARI, M., BEDIOUNE, I., ZHANG, L., LEROY, J., LEBLAIS, V., FISCHMEISTER, R. & VANDECASTEELE, G. 2016. Cyclic nucleotide phosphodiesterases in heart and vessels: A therapeutic perspective. *Archives of Cardiovascular Diseases,* 109**,** 431-443.

BOLGER, G., MICHAELI, T., MARTINS, T., ST JOHN, T., STEINER, B., RODGERS, L., RIGGS, M., WIGLER, M. & FERGUSON, K. 1993. A family of human phosphodiesterases homologous to the dunce learning and memory gene product of Drosophila melanogaster are potential targets for antidepressant drugs. *Molecular and Cellular Biology,* 13**,** 6558.

BOLGER, G. B., BAILLIE, G. S., LI, X., LYNCH, M. J., HERZYK, P., MOHAMED, A., MITCHELL, L. H., MCCAHILL, A., HUNDSRUCKER, C., KLUSSMANN, E., ADAMS, D. R. & HOUSLAY, M. D. 2006. Scanning peptide array analyses identify overlapping binding sites for the signalling scaffold proteins, beta-arrestin and RACK1, in cAMP-specific phosphodiesterase PDE4D5. *The Biochemical journal,* 398**,** 23-36.

BOLGER, G. B., DUNLOP, A. J., MENG, D., DAY, J. P., KLUSSMANN, E., BAILLIE, G. S., ADAMS, D. R. & HOUSLAY, M. D. 2015. Dimerization of cAMP phosphodiesterase-4 (PDE4) in living cells requires interfaces located in both the UCR1 and catalytic unit domains. *Cellular signalling,* 27**,** 756-769.

BOLGER, G. B., MCCAHILL, A., HUSTON, E., CHEUNG, Y.-F., MCSORLEY, T., BAILLIE, G. S. & HOUSLAY, M. D. 2003. The Unique Amino-terminal Region of the PDE4D5 cAMP Phosphodiesterase Isoform Confers Preferential Interaction with β-Arrestins. *Journal of Biological Chemistry,* 278**,** 49230-49238.

BOLLEN, E. & PRICKAERTS, J. 2012. Phosphodiesterases in neurodegenerative disorders. *IUBMB Life,* 64**,** 965-970.

BOOZ, G. W. & BAKER, K. M. 1996. Role of Type 1 and Type 2 Angiotensin Receptors in Angiotensin II–Induced Cardiomyocyte Hypertrophy. *Hypertension,* 28**,** 635-640.

BRAAKMAN, I. & HEBERT, D. N. 2013. Protein folding in the endoplasmic reticulum. *Cold Spring Harbor perspectives in biology,* 5**,** a013201-a013201.

BRADY, S. 2011. *Basic neurochemistry: principles of molecular, cellular, and medical neurobiology*, Academic press.

BRAND, T. 2018. *The Popeye Domain Containing Genes and Their Function as cAMP Effector Proteins in Striated Muscle*.

BRAND, T. & SCHINDLER, R. 2017. New kids on the block: The Popeye domain containing (POPDC) protein family acting as a novel class of cAMP effector proteins in striated muscle. *Cellular signalling,* 40**,** 156-165.

BRETSCHER, A., EDWARDS, K. & FEHON, R. G. 2002. ERM proteins and merlin: integrators at the cell cortex. *Nature reviews Molecular cell biology,* 3**,** 586-599.

BRISTOW, M. R., GINSBURG, R., MINOBE, W., CUBICCIOTTI, R. S., SAGEMAN, W. S., LURIE, K., BILLINGHAM, M. E., HARRISON, D. C. & STINSON, E. B. 1982. Decreased Catecholamine Sensitivity and ß-Adrenergic-Receptor Density in Failing Human Hearts. *New England Journal of Medicine,* 307**,** 205-211.

BROWN, R. D., AMBLER, S. K., MITCHELL, M. D. & LONG, C. S. 2005. The cardiac fibroblast: therapeutic target in myocardial remodeling and failure. *Annu Rev Pharmacol Toxicol,* 45**,** 657-87.

BRYANT, S., KIMURA, T. E., KONG, C. H. T., WATSON, J. J., CHASE, A., SULEIMAN, M. S., JAMES, A. F. & ORCHARD, C. H. 2014. Stimulation of ICa by basal PKA activity is facilitated by caveolin-3 in cardiac ventricular myocytes. *Journal of molecular and cellular cardiology,* 68**,** 47-55.

BRYANT, S. M., KONG, C. H. T., WATSON, J. J., GADEBERG, H. C., ROTH, D. M., PATEL, H. H., CANNELL, M. B., JAMES, A. F. & ORCHARD, C. H. 2018. Caveolin-3 KO disrupts t-tubule structure and decreases t-tubular ICa density in mouse ventricular myocytes. *American Journal of Physiology-Heart and Circulatory Physiology,* 315**,** H1101-H1111.

BÜNEMANN, M., GERHARDSTEIN, B. L., GAO, T. & HOSEY, M. M. 1999. Functional Regulation of L-type Calcium Channels via Protein Kinase A-mediated Phosphorylation of the ß2 Subunit. *Journal of Biological Chemistry,* 274**,** 33851-33854.

BURGERING, B. M. T. & COFFER, P. J. 1995. Protein kinase B (c-Akt) in phosphatidylinositol-3-OH kinase signal transduction. *Nature,* 376**,** 599-602.

BURGIN, A. B., MAGNUSSON, O. T., SINGH, J., WITTE, P., STAKER, B. L., BJORNSSON, J. M., THORSTEINSDOTTIR, M., HRAFNSDOTTIR, S., HAGEN, T., KISELYOV, A. S., STEWART, L. J. & GURNEY, M. E. 2010. Design of phosphodiesterase 4D (PDE4D) allosteric modulators for enhancing cognition with improved safety. *Nature Biotechnology,* 28**,** 63-70.

BYRNE, A. M., ELLIOTT, C., HOFFMANN, R. & BAILLIE, G. S. 2015. The activity of cAMP-phosphodiesterase 4D7 (PDE4D7) is regulated by protein kinase A-dependent phosphorylation within its unique N-terminus. *FEBS letters,* 589**,** 750-755.

CAHILL, T. J. & KHARBANDA, R. K. 2017. Heart failure after myocardial infarction in the era of primary percutaneous coronary intervention: Mechanisms, incidence and identification of patients at risk. *World journal of cardiology,* 9**,** 407-415.

CALAGHAN, S. & WHITE, E. 2006. Caveolae modulate excitation–contraction coupling and ß2-adrenergic signalling in adult rat ventricular myocytes. *Cardiovascular Research,* 69**,** 816-824.

CAMBY, I., LE MERCIER, M., LEFRANC, F. & KISS, R. 2006. Galectin-1: a small protein with major functions. *Glycobiology,* 16**,** 137R-157R.

CARLSON, E. D., GAN, R., HODGMAN, C. E. & JEWETT, M. C. 2012. Cell-free protein synthesis: applications come of age. *Biotechnology advances,* 30**,** 1185-1194.

CARMELIET, E. 1999. Cardiac Ionic Currents and Acute Ischemia: From Channels to Arrhythmias. *Physiological Reviews,* 79**,** 917-1017.

CAUTHRON, R. D., CARTER, K. B., LIAUW, S. & STEINBERG, R. A. 1998. Physiological phosphorylation of protein kinase A at Thr-197 is by a protein kinase A kinase. *Molecular and cellular biology,* 18**,** 1416-1423.

CHAROLLAIS, J. & VAN DER GOOT, F. G. 2009. Palmitoylation of membrane proteins (Review). *Molecular Membrane Biology,* 26**,** 55-66.

CHAZAUD , B. N. D., SONNET , C., LAFUSTE , P., BASSEZ , G., RIMANIOL , A.-C. C., PORON , F. O., AUTHIER , F. O.-J. R. M., DREYFUS , P. A. & GHERARDI , R. K. 2003. Satellite cells attract monocytes and use macrophages as a support to escape apoptosis and enhance muscle growth. *Journal of Cell Biology,* 163**,** 1133-1143.

CHEMIN, J., PATEL, A. J., DUPRAT, F., LAURITZEN, I., LAZDUNSKI, M. & HONORÉ, E. 2005. A phospholipid sensor controls mechanogating of the K+ channel TREK-1. *The EMBO Journal,* 24**,** 44-53.

CHENG, J. B., COOPER, K., DUPLANTIER, A. J., EGGLER, J. F., KRAUS, K. G., MARSHALL, S. C., MARFAT, A., MASAMUNE, H., SHIRLEY, J. T., TICKNER, J. E. & UMLAND, J. P. 1995. Synthesis and in vitro profile of a novel series of catechol benzimidazoles. The discovery of potent, selective phosphodiesterase type IV inhibitors with greatly attenuated affinity for the [3H]rolipram binding site. *Bioorganic & Medicinal Chemistry Letters,* 5**,** 1969-1972.

CHENG, X., JI, Z., TSALKOVA, T. & MEI, F. 2008. Epac and PKA: a tale of two intracellular cAMP receptors. *Acta biochimica et biophysica Sinica,* 40**,** 651-662.

CHENG, X., MA, Y., MOORE, M., HEMMINGS, B. A. & TAYLOR, S. S. 1998. Phosphorylation and activation of cAMP-dependent protein kinase by phosphoinositide-dependent protein kinase. *Proceedings of the National Academy of Sciences of the United States of America,* 95**,** 9849-9854.

CHO, W. 2001. Membrane targeting by C1 and C2 domains. *Journal of Biological Chemistry,* 276**,** 32407-32410.

CHRISTIAN, F., SZASZÁK, M., FRIEDL, S., DREWIANKA, S., LORENZ, D., GONCALVES, A., FURKERT, J., VARGAS, C., SCHMIEDER, P., GÖTZ, F., ZÜHLKE, K., MOUTTY, M., GÖTTERT, H., JOSHI, M., REIF, B., HAASE, H., MORANO, I., GROSSMANN, S., KLUKOVITS, A., VERLI, J., GÁSPÁR, R., NOACK, C., BERGMANN, M., KASS, R., HAMPEL, K., KASHIN, D., GENIESER, H.-G., HERBERG, F. W., WILLOUGHBY, D., COOPER, D. M. F., BAILLIE, G. S., HOUSLAY, M. D., VON KRIES, J. P., ZIMMERMANN, B., ROSENTHAL, W. & KLUSSMANN, E. 2011. Small molecule AKAP-protein kinase A (PKA) interaction disruptors that activate PKA interfere with compartmentalized cAMP signaling in cardiac myocytes. *The Journal of biological chemistry,* 286**,** 9079-9096.

COLLINS, D. M., MURDOCH, H., DUNLOP, A. J., CHARYCH, E., BAILLIE, G. S., WANG, Q., HERBERG, F. W., BRANDON, N., PRINZ, A. & HOUSLAY, M. D. 2008. Ndel1 alters its conformation by sequestering cAMP-specific phosphodiesterase-4D3 (PDE4D3) in a manner that is dynamically regulated through Protein Kinase A (PKA). *Cellular Signalling,* 20**,** 2356-2369.

CONTI, M. & BEAVO, J. 2007. Biochemistry and Physiology of Cyclic Nucleotide Phosphodiesterases: Essential Components in Cyclic Nucleotide Signaling. *Annual Review of Biochemistry,* 76**,** 481-511.

CONTI, M., RICHTER, W., MEHATS, C., LIVERA, G., PARK, J.-Y. & JIN, C. 2003. Cyclic AMP-specific PDE4 Phosphodiesterases as Critical Components of Cyclic AMP Signaling. *Journal of Biological Chemistry,* 278**,** 5493-5496.

COWLING, V. H. & COLE, M. D. 2007. E-cadherin repression contributes to c-Myc-induced epithelial cell transformation. *Oncogene,* 26**,** 3582-3586.

CRAIK, D. J., FAIRLIE, D. P., LIRAS, S. & PRICE, D. 2013. The future of peptide-based drugs. *Chemical biology & drug design,* 81**,** 136-147.

CRICK, S. J., SHEPPARD, M. N., HO, S. Y., GEBSTEIN, L. & ANDERSON, R. H. 1998. Anatomy of the pig heart: comparisons with normal human cardiac structure. *Journal of anatomy,* 193 (Pt 1)**,** 105-119.

CROSS, D. A. E., ALESSI, D. R., COHEN, P., ANDJELKOVICH, M. & HEMMINGS, B. A. 1995. Inhibition of glycogen synthase kinase-3 by insulin mediated by protein kinase B. *Nature,* 378**,** 785-789.

CURRAN, M. E., SPLAWSKI, I., TIMOTHY, K. W., VINCEN, G. M., GREEN, E. D. & KEATING, M. T. 1995. A molecular basis for cardiac arrhythmia: HERG mutations cause long QT syndrome. *Cell,* 80**,** 795-803.

DAAKA, Y., LUTTRELL, L. M. & LEFKOWITZ, R. J. 1997. Switching of the coupling of the ß 2-adrenergic receptor to different G proteins by protein kinase A. *Nature,* 390**,** 88-91.

DAS, R., ESPOSITO, V., ABU-ABED, M., ANAND, G. S., TAYLOR, S. S. & MELACINI, G. 2007. cAMP activation of PKA defines an ancient signaling mechanism. *Proceedings of the National Academy of Sciences of the United States of America,* 104**,** 93-98.

DASH, R., KADAMBI, V. J., SCHMIDT, A. G., TEPE, N. M., BINIAKIEWICZ, D., GERST, M. J., CANNING, A. M., ABRAHAM, W. T., HOIT, B. D., LIGGETT, S. B., LORENZ, J. N., DORN, G. W. & KRANIAS, E. G. 2001. Interactions Between Phospholamban and B2-Adrenergic Drive May Lead to Cardiomyopathy and Early Mortality. *Circulation,* 103**,** 889-896.

DAVIES, C. H., DAVIA, K., BENNETT, J. G., PEPPER, J. R., POOLE-WILSON, P. A. & HARDING, S. E. 1995. Reduced Contraction and Altered Frequency Response of Isolated Ventricular Myocytes From Patients With Heart Failure. *Circulation,* 92**,** 2540-2549.

DE ARCANGELIS, V., LIU, R., SOTO, D. & XIANG, Y. 2009a. Differential association of phosphodiesterase 4D isoforms with beta2-adrenoceptor in cardiac myocytes. *The Journal of biological chemistry,* 284**,** 33824-33832.

DE ARCANGELIS, V., LIU, R., SOTO, D. & XIANG, Y. 2009b. Differential Association of Phosphodiesterase 4D Isoforms with ß2-Adrenoceptor in Cardiac Myocytes. *Journal of Biological Chemistry,* 284**,** 33824-33832.

DE RIDDER, W., NELSON, I., ASSELBERGH, B., DE PAEPE, B., BEUVIN, M., BEN YAOU, R., MASSON, C., BOLAND, A., DELEUZE, J.-F., MAISONOBE, T., EYMARD, B., SYMOENS, S., SCHINDLER, R., BRAND, T., JOHNSON, K., TÖPF, A., STRAUB, V., DE JONGHE, P., DE BLEECKER, J. L., BONNE, G. & BAETS, J. 2019. Muscular dystrophy with arrhythmia caused by loss-of-function mutations in BVES. *Neurology Genetics,* 5**,** e321.

DE ROOIJ, J., ZWARTKRUIS, F. J. T., VERHEIJEN, M. H. G., COOL, R. H., NIJMAN, S. M. B., WITTINGHOFER, A. & BOS, J. L. 1998. Epac is a Rap1 guanine-nucleotide-exchange factor directly activated by cyclic AMP. *Nature,* 396**,** 474-477.

DEÁK, F., SHIN, O.-H., KAVALALI, E. T. & SÜDHOF, T. C. 2006. Structural Determinants of Synaptobrevin 2 Function in Synaptic Vesicle Fusion. *The Journal of Neuroscience,* 26**,** 6668.

DEBERG, H. A., BRZOVIC, P. S., FLYNN, G. E., ZAGOTTA, W. N. & STOLL, S. 2016. Structure and Energetics of Allosteric Regulation of HCN2 Ion Channels by Cyclic Nucleotides. *The Journal of biological chemistry,* 291**,** 371-381.

DEDMAN, A., SHARIF-NAEINI, R., FOLGERING, J. H. A., DUPRAT, F., PATEL, A. & HONORÉ, E. 2009. The mechano-gated K2P channel TREK-1. *European Biophysics Journal,* 38**,** 293-303.

DELGADO, R. M., 3RD & WILLERSON, J. T. 1999. Pathophysiology of heart failure: a look at the future. *Tex Heart Inst J,* 26**,** 28-33.

DEWALD, O., ZYMEK, P., WINKELMANN, K., KOERTING, A., REN, G., ABOU-KHAMIS, T., MICHAEL, L. H., ROLLINS, B. J., ENTMAN, M. L. & FRANGOGIANNIS, N. G. 2005. CCL2/Monocyte Chemoattractant Protein-1 Regulates Inflammatory Responses Critical to Healing Myocardial Infarcts. *Circulation Research,* 96**,** 881-889.

DICHTL, W., NILSSON, L., GONCALVES, I., ARES, M. P. S., BANFI, C., CALARA, F., HAMSTEN, A., ERIKSSON, P. & NILSSON, J. 1999. Very Low-Density Lipoprotein Activates Nuclear Factor-κB in Endothelial Cells. *Circulation Research,* 84**,** 1085-1094.

DIETZEN, D. J., HASTINGS, W. R. & LUBLIN, D. M. 1995. Caveolin Is Palmitoylated on Multiple Cysteine Residues: PALMITOYLATION IS NOT NECESSARY FOR LOCALIZATION OF CAVEOLIN TO CAVEOLAE. *Journal of Biological Chemistry,* 270**,** 6838-6842.

DIFRANCESCO, D. & BORER, J. S. 2007. The Funny Current. *Drugs,* 67**,** 15-24.

DIFRANCESCO, D. & TORTORA, P. 1991. Direct activation of cardiac pacemaker channels by intracellular cyclic AMP. *Nature,* 351**,** 145-147.

DJILLANI, A., MAZELLA, J., HEURTEAUX, C. & BORSOTTO, M. 2019. Role of TREK-1 in Health and Disease, Focus on the Central Nervous System. *Frontiers in Pharmacology,* 10.

DJILLANI, A., PIETRI, M., MORENO, S., HEURTEAUX, C., MAZELLA, J. & BORSOTTO, M. 2017. Shortened Spadin Analogs Display Better TREK-1 Inhibition, In Vivo Stability and Antidepressant Activity. *Frontiers in pharmacology,* 8**,** 643-643.

DODGE, K. L., KHOUANGSATHIENE, S., KAPILOFF, M. S., MOUTON, R., HILL, E. V., HOUSLAY, M. D., LANGEBERG, L. K. & SCOTT, J. D. 2001. mAKAP assembles a protein kinase A/PDE4 phosphodiesterase cAMP signaling module. *The EMBO Journal,* 20**,** 1921-1930.

DONAHUE, J. K., KIKKAWA, K., THOMAS, A. D., MARBAN, E. & LAWRENCE, J. H. 1998. Acceleration of widespread adenoviral gene transfer to intact rabbit hearts by coronary perfusion with low calcium and serotonin. *Gene Therapy,* 5**,** 630-634.

DUAN, G. & WALTHER, D. 2015. The roles of post-translational modifications in the context of protein interaction networks. *PLoS computational biology,* 11**,** e1004049-e1004049.

DUPAYS, L., SHANG, C., WILSON, R., KOTECHA, S., WOOD, S., TOWERS, N. & MOHUN, T. 2015. Sequential Binding of MEIS1 and NKX2-5 on the Popdc2 Gene: A Mechanism for Spatiotemporal Regulation of Enhancers during Cardiogenesis. *Cell Reports,* 13**,** 183-195.

DZAU, V. J. 1993. The role of mechanical and humoral factors in growth regulation of vascular smooth muscle and cardiac myocytes. *Current Opinion in Nephrology and Hypertension,* 2**,** 27-32.

EDAVETTAL, S. C., HUNTER, M. J. & SWANSON, R. V. 2012. Genetic Construct Design and Recombinant Protein Expression for Structural Biology. *In:* TARI, L. W. (ed.) *Structure-Based Drug Discovery*. Totowa, NJ: Humana Press.

EGERSTEDT, A., BERNTSSON, J., SMITH, M. L., GIDLÖF, O., NILSSON, R., BENSON, M., WELLS, Q. S., CELIK, S., LEJONBERG, C., FARRELL, L., SINHA, S.,

SHEN, D., LUNDGREN, J., RÅDEGRAN, G., NGO, D., ENGSTRÖM, G., YANG, Q., WANG, T. J., GERSZTEN, R. E. & SMITH, J. G. 2019. Profiling of the plasma proteome across different stages of human heart failure. *Nature Communications,* 10**,** 5830.

EISENBERG, L. M., BURNS, L. & EISENBERG, C. A. 2003. Hematopoietic cells from bone marrow have the potential to differentiate into cardiomyocytes in vitro. *The Anatomical Record Part A: Discoveries in Molecular, Cellular, and Evolutionary Biology,* 274A**,** 870-882.

EKHOLM, D., BELFRAGE, P., MANGANIELLO, V. & DEGERMAN, E. 1997. Protein kinase A-dependent activation of PDE4 (cAMP-specific cyclic nucleotide phosphodiesterase) in cultured bovine vascular smooth muscle cells. *Biochimica et Biophysica Acta (BBA) - Molecular Cell Research,* 1356**,** 64-70.

ENCODE-PROJECT-CONSORTIUM 2012. An integrated encyclopedia of DNA elements in the human genome. *Nature,* 489**,** 57-74.

ERL, W., HANSSON, G. K., MARTIN, R. D., DRAUDE, G., WEBER, K. S. C. & WEBER, C. 1999. Nuclear Factor-kBa Regulates Induction of Apoptosis and Inhibitor of Apoptosis Protein-1 Expression in Vascular Smooth Muscle Cells. *Circulation Research,* 84**,** 668-677.

ESPOSITO, D. & CHATTERJEE, D. K. 2006. Enhancement of soluble protein expression through the use of fusion tags. *Current opinion in biotechnology,* 17**,** 353-358.

ETIENNE-MANNEVILLE, S. & HALL, A. 2002. Rho GTPases in cell biology. *Nature,* 420**,** 629-635.

FABBRI, L. M., BEGHÉ, B., YASOTHAN, U. & KIRKPATRICK, P. 2010. Roflumilast. *Nature Reviews Drug Discovery,* 9**,** 761-762.

FABER, G. M. & RUDY, Y. 2000. Action potential and contractility changes in [Na(+)](i) overloaded cardiac myocytes: a simulation study. *Biophysical journal,* 78**,** 2392-2404.

FEINER, E., CHUNG, P., JASMIN, J., ZHANG, J., WHITAKER-MENEZES, D., MYERS, V., SONG, J., FELDMAN, E., FUNAKOSHI, H., DEGEORGE, B., YELAMARTY, R., KOCH, W., LISANTI, M., MCTIERNAN, C., CHEUNG, J., BRISTOW, M., CHAN, T. & FELDMAN, A. 2011. Left Ventricular Dysfunction in Murine Models of Heart Failure and in Failing Human Heart is Associated With a Selective Decrease in the Expression of Caveolin-3. *Journal of cardiac failure,* 17**,** 253-63.

FENTEANY, G., JANMEY, P. A. & STOSSEL, T. P. 2000. Signaling pathways and cell mechanics involved in wound closure by epithelial cell sheets. *Current Biology,* 10**,** 831-838.

FERDINANDY, P., SCHULZ, R. & BAXTER, G. F. 2007. Interaction of Cardiovascular Risk Factors with Myocardial Ischemia/Reperfusion Injury, Preconditioning, and Postconditioning. *Pharmacological Reviews,* 59**,** 418.

FERGUSON, K. M., KAVRAN, J. M., SANKARAN, V. G., FOURNIER, E., ISAKOFF, S. J., SKOLNIK, E. Y. & LEMMON, M. A. 2000. Structural basis for discrimination of 3-phosphoinositides by pleckstrin homology domains. *Molecular cell,* 6**,** 373-384.

FERLITO, M., FULTON, W. B., ZAUHER, M. A., MARBÁN, E., STEENBERGEN, C. & LOWENSTEIN, C. J. 2010. VAMP-1, VAMP-2, and syntaxin-4 regulate ANP release from cardiac myocytes. *Journal of Molecular and Cellular Cardiology,* 49**,** 791-800.

FERRARI, R., GUARDIGLI, G., CICCHITELLI, G., VALGIMIGLI, M., MERLI, E., SOUKHOMORSKAIA, O. & CECONI, C. 2002. Angiotensin II overproduction:

enemy of the vessel wall. *European Heart Journal Supplements,* 4**,** A26-A30.

FERTIG, B. 2019. *Characterising the phosphorylation and SUMOylation of cardiac troponin I in heart failure*. University of Glasgoe.

FERTIG, B. A. & BAILLIE, G. S. 2018. PDE4-Mediated cAMP Signalling. *Journal of cardiovascular development and disease,* 5**,** 8.

FIELDS, G. B. & NOBLE, R. L. 1990. Solid phase peptide synthesis utilizing 9-fluorenylmethoxycarbonyl amino acids. *International Journal of Peptide and Protein Research,* 35**,** 161-214.

FILIPPA, N., SABLE, C. L., FILLOUX, C., HEMMINGS, B. & VAN OBBERGHEN, E. 1999. Mechanism of protein kinase B activation by cyclic AMP-dependent protein kinase. *Molecular and cellular biology,* 19**,** 4989-5000.

FISCHMEISTER, R., CASTRO, L. R. V., ABI-GERGES, A., ROCHAIS, F., JUREVIČIUS, J., LEROY, J. & VANDECASTEELE, G. 2006. Compartmentation of Cyclic Nucleotide Signaling in the Heart. *Circulation Research,* 99**,** 816-828.

FORRESTER, M. T., HESS, D. T., THOMPSON, J. W., HULTMAN, R., MOSELEY, M. A., STAMLER, J. S. & CASEY, P. J. 2011. Site-specific analysis of protein S-acylation by resin-assisted capture. *Journal of Lipid Research,* 52**,** 393-398.

FOX, J. D., ROUTZAHN, K. M., BUCHER, M. H. & WAUGH, D. S. 2003. Maltodextrin-binding proteins from diverse bacteria and archaea are potent solubility enhancers. *FEBS letters,* 537**,** 53-57.

FRAGASSO, G. 2016. Deranged Cardiac Metabolism and the Pathogenesis of Heart Failure. *Cardiac failure review,* 2**,** 8-13.

FRANCIS, H., KENNEDY, L. & ALPINI, G. 2018. Dual ablation of ß- and γ-catenin: Critical regulators of junctions and their functions. *Hepatology (Baltimore, Md.),* 67**,** 2079-2081.

FRANCIS, S. H., BLOUNT, M. A. & CORBIN, J. D. 2011a. Mammalian Cyclic Nucleotide Phosphodiesterases: Molecular Mechanisms and Physiological Functions. *Physiological Reviews,* 91**,** 651-690.

FRANCIS, S. H., HOUSLAY, M. D. & CONTI, M. 2011b. Phosphodiesterase Inhibitors: Factors That Influence Potency, Selectivity, and Action. *In:* FRANCIS, S. H., CONTI, M. & HOUSLAY, M. D. (eds.) *Phosphodiesterases as Drug Targets*. Berlin, Heidelberg: Springer Berlin Heidelberg.

FRANK, R. 2002. The SPOT-synthesis technique: Synthetic peptide arrays on membrane supports—principles and applications. *Journal of Immunological Methods,* 267**,** 13-26.

FREY, U., HUANG, Y. & KANDEL, E. 1993. Effects of cAMP simulate a late stage of LTP in hippocampal CA1 neurons. *Science,* 260**,** 1661-1664.

FRIDOLFSSON, H. N. & PATEL, H. H. 2013. Caveolin and caveolae in age associated cardiovascular disease. *Journal of geriatric cardiology : JGC,* 10**,** 66-74.

FROESE, A., BREHER, S. S., WALDEYER, C., SCHINDLER, R. F. R., NIKOLAEV, V. O., RINNÉ, S., WISCHMEYER, E., SCHLUETER, J., BECHER, J., SIMRICK, S., VAUTI, F., KUHTZ, J., MEISTER, P., KREISSL, S., TORLOPP, A., LIEBIG, S. K., LAAKMANN, S., MÜLLER, T. D., NEUMANN, J., STIEBER, J., LUDWIG, A., MAIER, S. K., DECHER, N., ARNOLD, H.-H., KIRCHHOF, P., FABRITZ, L. & BRAND, T. 2012. Popeye domain containing proteins are essential for stress-mediated modulation of cardiac pacemaking in mice. *The Journal of Clinical Investigation,* 122**,** 1119-1130.

FUKATA, M., FUKATA, Y., ADESNIK, H., NICOLL, R. A. & BREDT, D. S. 2004. Identification of PSD-95 palmitoylating enzymes. *Neuron,* 44**,** 987-996.

FUKUDA, N., GRANZIER, H. L., ISHIWATA, S. I. & KURIHARA, S. 2008. Physiological Functions of the Giant Elastic Protein Titin in Mammalian Striated Muscle. *The Journal of Physiological Sciences,* 58**,** 151-159.

FULLER, M. D., EMRICK, M. A., SADILEK, M., SCHEUER, T. & CATTERALL, W. A. 2010. Molecular mechanism of calcium channel regulation in the fight-or-flight response. *Science signaling,* 3**,** ra70-ra70.

GALBIATI, F., ENGELMAN, J. A., VOLONTE, D., ZHANG, X. L., MINETTI, C., LI, M., HOU, H., KNEITZ, B., EDELMANN, W. & LISANTI, M. P. 2001. Caveolin-3 Null Mice Show a Loss of Caveolae, Changes in the Microdomain Distribution of the Dystrophin-Glycoprotein Complex, and T-tubule Abnormalities. *Journal of Biological Chemistry,* 276**,** 21425-21433.

GALISSON, F., MAHROUCHE, L., COURCELLES, M., BONNEIL, E., MELOCHE, S., CHELBI-ALIX, M. K. & THIBAULT, P. 2011. A novel proteomics approach to identify SUMOylated proteins and their modification sites in human cells. *Molecular & cellular proteomics : MCP,* 10**,** M110.004796-M110.004796.

GAREAU, J. R. & LIMA, C. D. 2010. The SUMO pathway: emerging mechanisms that shape specificity, conjugation and recognition. *Nature reviews. Molecular cell biology,* 11**,** 861-871.

GAUTEL, M. 2011. The sarcomeric cytoskeleton: who picks up the strain? *Current Opinion in Cell Biology,* 23**,** 39-46.

GAZZERRO, E., SOTGIA, F., BRUNO, C., LISANTI, M. P. & MINETTI, C. 2010. Caveolinopathies: from the biology of caveolin-3 to human diseases. *European journal of human genetics : EJHG,* 18**,** 137-145.

GEORGIADIS, A., TSCHERNUTTER, M., BAINBRIDGE, J. W. B., BALAGGAN, K. S., MOWAT, F., WEST, E. L., MUNRO, P. M. G., THRASHER, A. J., MATTER, K., BALDA, M. S. & ALI, R. R. 2010. The tight junction associated signalling proteins ZO-1 and ZONAB regulate retinal pigment epithelium homeostasis in mice. *PloS one,* 5**,** e15730-e15730.

GETZ, E. B., XIAO, M., CHAKRABARTY, T., COOKE, R. & SELVIN, P. R. 1999. A Comparison between the Sulfhydryl Reductants Tris(2-carboxyethyl)phosphine and Dithiothreitol for Use in Protein Biochemistry. *Analytical Biochemistry,* 273**,** 73-80.

GILLEEN, J., FARAH, Y., DAVISON, C., KERINS, S., VALDEARENAS, L., UZ, T., LAHU, G., TSAI, M., OGRINC, F. & REICHENBERG, A. 2018. An experimental medicine study of the phosphodiesterase-4 inhibitor, roflumilast, on working memory-related brain activity and episodic memory in schizophrenia patients. *Psychopharmacology***,** 1-11.

GINGOLD-BELFER, R., BERGMAN, M., ALCALAY, Y., SCHLESINGER, H., ARAVOT, D., BERMAN, M., SALMAN, H., BRAND, T. & KESSLER-ICEKSON, G. 2011. Popeye domain-containing 1 is down-regulated in failing human hearts. *International Journal of Molecular Medicine,* 27.

GOLD, M. G., LYGREN, B., DOKURNO, P., HOSHI, N., MCCONNACHIE, G., TASKÉN, K., CARLSON, C. R., SCOTT, J. D. & BARFORD, D. 2006. Molecular Basis of AKAP Specificity for PKA Regulatory Subunits. *Molecular Cell,* 24**,** 383-395.

GOODWIN, J. S., DRAKE, K. R., ROGERS, C., WRIGHT, L., LIPPINCOTT-SCHWARTZ, J., PHILIPS, M. R. & KENWORTHY, A. K. 2005. Depalmitoylated Ras traffics to and from the Golgi complex via a nonvesicular pathway. *The Journal of cell biology,* 170**,** 261-272.

GOONETILLEKE, L. & QUAYLE, J. 2012. TREK-1 K+ Channels in the Cardiovascular System: Their Significance and Potential as a Therapeutic Target. *Cardiovascular Therapeutics,* 30**,** e23-e29.

GRANT, A. O. 2009. Cardiac Ion Channels. *Circulation: Arrhythmia and Electrophysiology,* 2, 185-194.

GUO, X., STAFFORD, L. J., BRYAN, B., XIA, C., MA, W., WU, X., LIU, D., SONGYANG, Z. & LIU, M. 2003. A Rac/Cdc42-specific Exchange Factor, GEFT, Induces Cell Proliferation, Transformation, and Migration. *Journal of Biological Chemistry,* 278, 13207-13215.

GUPTA, S. 2012. Side-effects of roflumilast. *The Lancet,* 379, 710-711.

HADJEM, M. & NAÏT-ABDESSELAM, F. 2015. *An ECG T-wave Anomalies Detection Using a Lightweight Classification Model for Wireless Body Sensors*.

HAGER, H. A. & BADER, D. M. 2009. Bves: ten years after. *Histology and histopathology,* 24, 777-787.

HAGER, H. A., ROBERTS, R. J., CROSS, E. E., PROUX-GILLARDEAUX, V. & BADER, D. M. 2010. Identification of a novel Bves function: regulation of vesicular transport. *The EMBO Journal,* 29, 532-545.

HAN, J., LIM, C. J., WATANABE, N., SORIANI, A., RATNIKOV, B., CALDERWOOD, D. A., PUZON-MCLAUGHLIN, W., LAFUENTE, E. M., BOUSSIOTIS, V. A., SHATTIL, S. J. & GINSBERG, MARK H. 2006. Reconstructing and Deconstructing Agonist-Induced Activation of Integrin αIIbβ3. *Current Biology,* 16, 1796-1806.

HAN, P., FU, Y., LIU, J., WANG, Y., HE, J., GONG, J., LI, M., TAN, Q., LI, D., LUO, Y., HAN, J., LIU, J., TU, W., WANG, Y., TIAN, D. & YAN, W. 2015. Netrin-1 promotes cell migration and invasion by down-regulation of BVES expression in human hepatocellular carcinoma. *American journal of cancer research,* 5, 1396-1409.

HAN, P., LEI, Y., LI, D., LIU, J., YAN, W. & TIAN, D. 2019. Ten years of research on the role of BVES/ POPDC1 in human disease: a review. *OncoTargets and therapy,* 12, 1279-1291.

HAN, Z.-J., FENG, Y.-H., GU, B.-H., LI, Y.-M. & CHEN, H. 2018. The post-translational modification, SUMOylation, and cancer (Review). *International journal of oncology,* 52, 1081-1094.

HANNOUN, Z., GREENHOUGH, S., JAFFRAY, E., HAY, R. T. & HAY, D. C. 2010. Post-translational modification by SUMO. *Toxicology,* 278, 288-93.

HARTL, F. U. 1996. Molecular chaperones in cellular protein folding. *Nature,* 381, 571-580.

HAYAT, M. A. 2016. Chapter 1 - Overview of Autophagy. *In:* HAYAT, M. A. (ed.) *Autophagy: Cancer, Other Pathologies, Inflammation, Immunity, Infection, and Aging*. Academic Press.

HAYES, J. S. & BRUNTON, L. L. 1982. Functional compartments in cyclic nucleotide action. *J Cyclic Nucleotide Res,* 8, 1-16.

HAYES, J. S., BRUNTON, L. L. & MAYER, S. E. 1980. Selective activation of particulate cAMP-dependent protein kinase by isoproterenol and prostaglandin E1. *Journal of Biological Chemistry,* 255, 5113-5119.

HAYNES, L. & YAU, K.-W. 1985. Cyclic GMP-sensitive conductance in outer segment membrane of catfish cones. *Nature,* 317, 61-64.

HEIN, S., SCHOLZ, D., FUJITANI, N., RENNOLLET, H., BRAND, T., FRIEDL, A. & SCHAPER, J. 1994. Altered Expression of Titin and Contractile Proteins in Failing Human Myocardium. *Journal of Molecular and Cellular Cardiology,* 26, 1291-1306.

HEINRICH, R., NEEL, B. G. & RAPOPORT, T. A. 2002. Mathematical Models of Protein Kinase Signal Transduction. *Molecular Cell,* 9, 957-970.

HELENIUS, A. & SIMONS, K. 1975. Solubilization of membranes by detergents. *Biochimica et Biophysica Acta (BBA) - Reviews on Biomembranes,* 415**,** 29-79.

HEMSLEY, P. A., WEIMAR, T., LILLEY, K. S., DUPREE, P. & GRIERSON, C. S. 2013. A proteomic approach identifies many novel palmitoylated proteins in A rabidopsis. *New Phytologist,* 197**,** 805-814.

HENDERSON, D. J. P., BYRNE, A., DULLA, K., JENSTER, G., HOFFMANN, R., BAILLIE, G. S. & HOUSLAY, M. D. 2014. The cAMP phosphodiesterase-4D7 (PDE4D7) is downregulated in androgen-independent prostate cancer cells and mediates proliferation by compartmentalising cAMP at the plasma membrane of VCaP prostate cancer cells. *British Journal of Cancer,* 110**,** 1278-1287.

HERMANN, A. & WALKER, R. H. 2015. Diagnosis and treatment of chorea syndromes. *Current neurology and neuroscience reports,* 15**,** 1.

HEROLD, J., PIPP, F., FERNANDEZ, B., XING, Z., HEIL, M., TILLMANNS, H. & BRAUN-DULLAEUS, R. C. 2004. Transplantation of monocytes: a novel strategy for in vivo augmentation of collateral vessel growth. *Hum Gene Ther,* 15**,** 1-12.

HERSHBERGER, R. E., MORALES, A. & SIEGFRIED, J. D. 2010. Clinical and genetic issues in dilated cardiomyopathy: a review for genetics professionals. *Genetics in Medicine,* 12**,** 655-667.

HEURTEAUX, C., GUY, N., LAIGLE, C., BLONDEAU, N., DUPRAT, F., MAZZUCA, M., LANG-LAZDUNSKI, L., WIDMANN, C., ZANZOURI, M., ROMEY, G. & LAZDUNSKI, M. 2004. TREK-1, a K+ channel involved in neuroprotection and general anesthesia. *The EMBO Journal,* 23**,** 2684-2695.

HIETAKANGAS, V., ANCKAR, J., BLOMSTER, H. A., FUJIMOTO, M., PALVIMO, J. J., NAKAI, A. & SISTONEN, L. 2006. PDSM, a motif for phosphorylation-dependent SUMO modification. *Proceedings of the National Academy of Sciences of the United States of America,* 103**,** 45-50.

HOCHSTRASSER, M. 2001. SP-RING for SUMO: New Functions Bloom for a Ubiquitin-like Protein. *Cell,* 107**,** 5-8.

HOFFMANN, R., BAILLIE, G. S., MACKENZIE, S. J., YARWOOD, S. J. & HOUSLAY, M. D. 1999. The MAP kinase ERK2 inhibits the cyclic AMP-specific phosphodiesterase HSPDE4D3 by phosphorylating it at Ser579. *The EMBO Journal,* 18**,** 893-903.

HOLLAND, A. & OHLENDIECK, K. 2013. Proteomic profiling of the contractile apparatus from skeletal muscle. *Expert Review of Proteomics,* 10**,** 239-257.

HOLMES, K. C. 1997. The swinging lever-arm hypothesis of muscle contraction. *Current Biology,* 7**,** R112-R118.

HONORÉ, E. 2007. The neuronal background K2P channels: focus on TREK1. *Nature Reviews Neuroscience,* 8**,** 251-261.

HOOVER, K. B., LIAO, S. Y. & BRYANT, P. J. 1998. Loss of the tight junction MAGUK ZO-1 in breast cancer: relationship to glandular differentiation and loss of heterozygosity. *The American journal of pathology,* 153**,** 1767-1773.

HORNBERG, J. J., BRUGGEMAN, F. J., BINDER, B., GEEST, C. R., DE VAATE, A. J. M. B., LANKELMA, J., HEINRICH, R. & WESTERHOFF, H. V. 2005. Principles behind the multifarious control of signal transduction. *The FEBS Journal,* 272**,** 244-258.

HOUSLAY, K. F., CHRISTIAN, F., MACLEOD, R., ADAMS, D. R., HOUSLAY, M. D. & BAILLIE, G. S. 2017. Identification of a multifunctional docking site on the

catalytic unit of phosphodiesterase-4 (PDE4) that is utilised by multiple interaction partners. *The Biochemical journal,* 474**,** 597-609.

HOUSLAY, M. D. 1996. The N-terminal alternately spliced regions of PDE4A cAMP-specific phosphodiesterases determine intracellular targeting and regulation of catalytic activity. *Biochem Soc Trans,* 24**,** 980-6.

HOUSLAY, M. D. 2010. Underpinning compartmentalised cAMP signalling through targeted cAMP breakdown. *Trends in Biochemical Sciences,* 35**,** 91-100.

HOUSLAY, M. D. & ADAMS, D. R. 2003. PDE4 cAMP phosphodiesterases: modular enzymes that orchestrate signalling cross-talk, desensitization and compartmentalization. *Biochemical Journal,* 370**,** 1-18.

HOUSLAY, M. D. & ADAMS, D. R. 2010. Putting the lid on phosphodiesterase 4. *Nature Biotechnology,* 28**,** 38-40.

HOUSLAY, M. D., BAILLIE, G. S. & MAURICE, D. H. 2007. cAMP-Specific phosphodiesterase-4 enzymes in the cardiovascular system: a molecular toolbox for generating compartmentalized cAMP signaling. *Circ Res,* 100**,** 950-66.

HOUSLAY, M. D., SCHAFER, P. & ZHANG, K. Y. J. 2005. Keynote review: Phosphodiesterase-4 as a therapeutic target. *Drug Discovery Today,* 10**,** 1503-1519.

HOWIE, J., REILLY, L., FRASER, N. J., VLACHAKI WALKER, J. M., WYPIJEWSKI, K. J., ASHFORD, M. L. J., CALAGHAN, S. C., MCCLAFFERTY, H., TIAN, L., SHIPSTON, M. J., BOGUSLAVSKYI, A., SHATTOCK, M. J. & FULLER, W. 2014. Substrate recognition by the cell surface palmitoyl transferase DHHC5. *Proceedings of the National Academy of Sciences,* 111**,** 17534.

HUANG, H., XIE, M., GAO, L., ZHANG, W., ZHU, X., WANG, Y., LI, W., WANG, R., CHEN, K., BOUTJDIR, M. & CHEN, L. 2019. Rolipram, a PDE4 Inhibitor, Enhances the Inotropic Effect of Rat Heart by Activating SERCA2a. *Frontiers in Pharmacology,* 10.

HUANG, K., YANAI, A., KANG, R., ARSTIKAITIS, P., SINGARAJA, R. R., METZLER, M., MULLARD, A., HAIGH, B., GAUTHIER-CAMPBELL, C. & GUTEKUNST, C.-A. 2004. Huntingtin-interacting protein HIP14 is a palmitoyl transferase involved in palmitoylation and trafficking of multiple neuronal proteins. *Neuron,* 44**,** 977-986.

HUANG, T. T., WUERZBERGER-DAVIS, S. M., WU, Z.-H. & MIYAMOTO, S. 2003. Sequential Modification of NEMO/IKKγ by SUMO-1 and Ubiquitin Mediates NF-κB Activation by Genotoxic Stress. *Cell,* 115**,** 565-576.

HUNTER, T. 2009. Tyrosine phosphorylation: thirty years and counting. *Current Opinion in Cell Biology,* 21**,** 140-146.

HUSTON, E., BEARD, M., MCCALLUM, F., J PYNE, N., VANDENABEELE, P., SCOTLAND, G. & HOUSLAY, M. 2000a. *The cAMP-specific phosphodiesterase PDE4A5 is cleaved downstream of its SH3 interaction domain by caspase-3: Consequence for altered intracellular distribution*.

HUSTON, E., BEARD, M., MCCALLUM, F., PYNE, N. J., VANDENABEELE, P., SCOTLAND, G. & HOUSLAY, M. D. 2000b. The cAMP-specific Phosphodiesterase PDE4A5 Is Cleaved Downstream of Its SH3 Interaction Domain by Caspase-3: Consequences for altered intracellular distribution. *Journal of Biological Chemistry,* 275**,** 28063-28074.

IBRAHIM, M., SIEDLECKA, U., BUYANDELGER, B., HARADA, M., RAO, C., MOSHKOV, A., BHARGAVA, A., SCHNEIDER, M., YACOUB, M. H., GORELIK, J., KNÖLL, R. & TERRACCIANO, C. M. 2013. A critical role for Telethonin in regulating t-tubule structure and function in the mammalian heart. *Human molecular genetics,* 22**,** 372-383.

IBRAHIM, Z., BUSCH, J., AWWAD, M., WAGNER, R., WELLS, K. & COOPER, D. K. C. 2006. Selected physiologic compatibilities and incompatibilities between human and porcine organ systems. *Xenotransplantation,* 13**,** 488-499.

INAMDAR, A. A. & INAMDAR, A. C. 2016. Heart Failure: Diagnosis, Management and Utilization. *Journal of clinical medicine,* 5**,** 62.

JAKOBS, A., KOEHNKE, J., HIMSTEDT, F., FUNK, M., KORN, B., GAESTEL, M. & NIEDENTHAL, R. 2007. Ubc9 fusion–directed SUMOylation (UFDS): a method to analyze function of protein SUMOylation. *Nature Methods,* 4**,** 245-250.

JARVIS, D. 2014. Recombinant Protein Expression in Baculovirus-Infected Insect Cells. *Methods in enzymology,* 536**,** 149-63.

JARVIS, D. L. 2009. Chapter 14 Baculovirus–Insect Cell Expression Systems. *In:* BURGESS, R. R. & DEUTSCHER, M. P. (eds.) *Methods in Enzymology.* Academic Press.

JAYAGOPAL, A., YANG, J.-L., HASELTON, F. R. & CHANG, M. S. 2011. Tight Junction–Associated Signaling Pathways Modulate Cell Proliferation in Uveal Melanoma. *Investigative Ophthalmology & Visual Science,* 52**,** 588-593.

JENNINGS, B. C. & LINDER, M. E. 2012. DHHC protein S-acyltransferases use similar ping-pong kinetic mechanisms but display different acyl-CoA specificities. *The Journal of biological chemistry,* 287**,** 7236-7245.

JOHNSON, E. S. 2004. Protein Modification by SUMO. *Annual Review of Biochemistry,* 73**,** 355-382.

JONES, P. P., MENG, X., XIAO, B., CAI, S., BOLSTAD, J., WAGENKNECHT, T., LIU, Z. & CHEN, S. W. 2008. Localization of PKA phosphorylation site, Ser2030, in the three-dimensional structure of cardiac ryanodine receptor. *Biochemical Journal,* 410**,** 261-270.

JONIC, S. & VÉNIEN-BRYAN, C. 2009. Protein structure determination by electron cryo-microscopy. *Current Opinion in Pharmacology,* 9**,** 636-642.

JOST, N. 2009. Transmembrane ionic currents underlying cardiac action potential in mammalian hearts.

KAMISAGO, M., SHARMA, S. D., DEPALMA, S. R., SOLOMON, S., SHARMA, P., MCDONOUGH, B., SMOOT, L., MULLEN, M. P., WOOLF, P. K., WIGLE, E. D., SEIDMAN, J. G. & SEIDMAN, C. E. 2000. Mutations in sarcomere protein genes as a cause of dilated cardiomyopathy. *N Engl J Med,* 343**,** 1688-96.

KANAANI, J., PATTERSON, G., SCHAUFELE, F., LIPPINCOTT-SCHWARTZ, J. & BAEKKESKOV, S. 2008. A palmitoylation cycle dynamically regulates partitioning of the GABA-synthesizing enzyme GAD65 between ER-Golgi and post-Golgi membranes. *Journal of cell science,* 121**,** 437-449.

KANDEL, E. R. 2012. The molecular biology of memory: cAMP, PKA, CRE, CREB-1, CREB-2, and CPEB. *Molecular brain,* 5**,** 14.

KANG, R., WAN, J., ARSTIKAITIS, P., TAKAHASHI, H., HUANG, K., BAILEY, A. O., THOMPSON, J. X., ROTH, A. F., DRISDEL, R. C. & MASTRO, R. 2008. Neural palmitoyl-proteomics reveals dynamic synaptic palmitoylation. *Nature,* 456**,** 904-909.

KAPUST, R. B. & WAUGH, D. S. 1999. Escherichia coli maltose-binding protein is uncommonly effective at promoting the solubility of polypeptides to which it is fused. *Protein Science,* 8**,** 1668-1674.

KAUPP, U. B. & SEIFERT, R. 2002. Cyclic Nucleotide-Gated Ion Channels. *Physiological Reviews,* 82**,** 769-824.

KAWASAKI, H., SPRINGETT, G. M., MOCHIZUKI, N., TOKI, S., NAKAYA, M., MATSUDA, M., HOUSMAN, D. E. & GRAYBIEL, A. M. 1998. A Family of cAMP-Binding Proteins That Directly Activate Rap1. *Science,* 282**,** 2275.

KAWASE, Y. & HAJJAR, R. J. 2008. The cardiac sarcoplasmic/endoplasmic reticulum calcium ATPase: a potent target for cardiovascular diseases. *Nature Clinical Practice Cardiovascular Medicine,* 5**,** 554-565.

KEATES, T., COOPER, C., SAVITSKY, P., ALLERSTON, C., PHILLIPS, C., HAMMARSTRÖM, M., DAGA, N., BERRIDGE, G., MAHAJAN, P., BURGESS-BROWN, N., MÜLLER, S., GRASLUND, S. & GILEADI, O. 2011. Expressing the human proteome for affinity proteomics: Optimising expression of soluble protein domains and in vivo biotinylation. *New biotechnology,* 29**,** 515-25.

KELLEY, L. A., MEZULIS, S., YATES, C. M., WASS, M. N. & STERNBERG, M. J. E. 2015. The Phyre2 web portal for protein modeling, prediction and analysis. *Nature Protocols,* 10**,** 845-858.

KEMP, B. E., BYLUND, D. B., HUANG, T. S. & KREBS, E. G. 1975. Substrate specificity of the cyclic AMP-dependent protein kinase. *Proceedings of the National Academy of Sciences,* 72**,** 3448.

KENTISH, J. C., MCCLOSKEY, D. T., LAYLAND, J., PALMER, S., LEIDEN, J. M., MARTIN, A. F. & SOLARO, R. J. 2001. Phosphorylation of Troponin I by Protein Kinase A Accelerates Relaxation and Crossbridge Cycle Kinetics in Mouse Ventricular Muscle. *Circulation Research,* 88**,** 1059-1065.

KHO, C., LEE, A., JEONG, D., OH, J. G., CHAANINE, A. H., KIZANA, E., PARK, W. J. & HAJJAR, R. J. 2011. SUMO1-dependent modulation of SERCA2a in heart failure. *Nature,* 477**,** 601-605.

KHO, C., LEE, A., JEONG, D., OH, J. G., GORSKI, P. A., FISH, K., SANCHEZ, R., DEVITA, R. J., CHRISTENSEN, G., DAHL, R. & HAJJAR, R. J. 2015. Small-molecule activation of SERCA2a SUMOylation for the treatment of heart failure. *Nature Communications,* 6**,** 7229.

KIM, D. & CLAPHAM, D. E. 1989. Potassium channels in cardiac cells activated by arachidonic acid and phospholipids. *Science,* 244**,** 1174.

KIM, E. T., KIM, K. K., MATUNIS, M. J. & AHN, J.-H. 2009. Enhanced SUMOylation of proteins containing a SUMO-interacting motif by SUMO-Ubc9 fusion. *Biochemical and Biophysical Research Communications,* 388**,** 41-45.

KIM, M., JANG, H.-R., HAAM, K., KANG, T.-W., KIM, J.-H., KIM, S.-Y., NOH, S.-M., SONG, K.-S., CHO, J.-S., JEONG, H.-Y., KIM, J. C., YOO, H.-S. & KIM, Y. S. 2010. Frequent silencing of popeye domain-containing genes, BVES and POPDC3 , is associated with promoter hypermethylation in gastric cancer. *Carcinogenesis,* 31**,** 1685-1693.

KIRCHMAIER, B. C., POON, K. L., SCHWERTE, T., HUISKEN, J., WINKLER, C., JUNGBLUT, B., STAINIER, D. Y. & BRAND, T. 2012. The Popeye domain containing 2 (popdc2) gene in zebrafish is required for heart and skeletal muscle development. *Developmental Biology,* 363**,** 438-450.

KITTLESON, M. M., MINHAS, K. M., IRIZARRY, R. A., YE, S. Q., EDNESS, G., BRETON, E., CONTE, J. V., TOMASELLI, G., GARCIA, J. G. N. & HARE, J. M. 2005. Gene expression analysis of ischemic and nonischemic cardiomyopathy: shared and distinct genes in the development of heart failure. *Physiological Genomics,* 21**,** 299-307.

KLIMINSKI, V., UZIEL, O. & KESSLER-ICEKSON, G. 2017. Popdc1/Bves Functions in the Preservation of Cardiomyocyte Viability While Affecting Rac1 Activity and Bnip3 Expression. *Journal of Cellular Biochemistry,* 118**,** 1505-1517.

KLINKE, D. J., 2ND, HORVATH, N., CUPPETT, V., WU, Y., DENG, W. & KANJ, R. 2015. Interlocked positive and negative feedback network motifs regulate

ß-catenin activity in the adherens junction pathway. *Molecular biology of the cell,* 26**,** 4135-4148.

KNIGHT, R. F., BADER, D. M. & BACKSTROM, J. R. 2003. Membrane Topology of Bves/Pop1A, a Cell Adhesion Molecule That Displays Dynamic Changes in Cellular Distribution during Development. *Journal of Biological Chemistry,* 278**,** 32872-32879.

KNIPSCHEER, P., FLOTHO, A., KLUG, H., OLSEN, J. V., VAN DIJK, W. J., FISH, A., JOHNSON, E. S., MANN, M., SIXMA, T. K. & PICHLER, A. 2008. Ubc9 Sumoylation Regulates SUMO Target Discrimination. *Molecular Cell,* 31**,** 371-382.

KOFRON , M., HEASMAN , J., LANG , S. A. & WYLIE , C. C. 2002. Plakoglobin is required for maintenance of the cortical actin skeleton in early Xenopus embryos and for cdc42-mediated wound healing. *Journal of Cell Biology,* 158**,** 695-708.

KONG, C. H. T., BRYANT, S. M., WATSON, J. J., ROTH, D. M., PATEL, H. H., CANNELL, M. B., JAMES, A. F. & ORCHARD, C. H. 2019. Cardiac-specific overexpression of caveolin-3 preserves t-tubular I(Ca) during heart failure in mice. *Experimental physiology,* 104**,** 654-666.

KOO, S. H., KWON, K. C., SHIN, S. Y., JEON, Y. M., PARK, J. W., KIM, S. H. & NOH, S. M. 2000. Genetic Alterations of Gastric Cancer: Comparative Genomic Hybridization and Fluorescence In Situ Hybridization Studies. *Cancer Genetics and Cytogenetics,* 117**,** 97-103.

KOPPEL, D. E. 1972. Analysis of Macromolecular Polydispersity in Intensity Correlation Spectroscopy: The Method of Cumulants. *The Journal of Chemical Physics,* 57**,** 4814-4820.

KOSTIN, S., RIEGER, M., DAMMER, S., HEIN, S., RICHTER, M., KLÖVEKORN, W.-P., BAUER, E. P. & SCHAPER, J. 2003. Gap junction remodeling and altered connexin43 expression in the failing human heart. *In:* KARDAMI, E., HRYSHKO, L. & MESAELI, N. (eds.) *Cardiac Cell Biology*. Boston, MA: Springer US.

KOUDSTAAL, S., JANSEN OF LORKEERS, S., GHO, J. M. I. H., VAN HOUT, G. P. J., JANSEN, M. S., GRÜNDEMAN, P. F., PASTERKAMP, G., DOEVENDANS, P. A., HOEFER, I. E. & CHAMULEAU, S. A. J. 2014. Myocardial infarction and functional outcome assessment in pigs. *Journal of visualized experiments : JoVE***,** 51269.

KRAMER, A. & SCHNEIDER-MERGENER, J. 1998. Synthesis and Screening of Peptide Libraries on Continuous Cellulose Membrane Supports. *In:* CABILLY, S. (ed.) *Combinatorial Peptide Library Protocols.* Totowa, NJ: Humana Press.

KROETZ, M. B. 2005. SUMO: a ubiquitin-like protein modifier. *The Yale journal of biology and medicine,* 78**,** 197-201.

KRUPINSKI, J., COUSSEN, F., BAKALYAR, H. A., TANG, W. J., FEINSTEIN, P. G., ORTH, K., SLAUGHTER, C., REED, R. R. & GILMAN, A. G. 1989. Adenylyl cyclase amino acid sequence: possible channel- or transporter-like structure. *Science,* 244**,** 1558.

KRUPNICK, J. G. & BENOVIC, J. L. 1998. The role of receptor kinases and arrestins in G protein–coupled receptor regulation. *Annual review of pharmacology and toxicology,* 38**,** 289-319.

KRUSE, M., BRUNKE, M., ESCHER, A., SZALAY, A. A., TROPSCHUG, M. & ZIMMERMANN, R. 1995. Enzyme assembly after de novo synthesis in rabbit reticulocyte lysate involves molecular chaperones and immunophilins. *Journal of Biological Chemistry,* 270**,** 2588-2594.

KUMAMOTO, C. A. 1991. Molecular chaperones and protein translocation across the Escherichia coli inner membrane. *Molecular Microbiology,* 5, 19-22.

KUREPA, J., WALKER, J. M., SMALLE, J., GOSINK, M. M., DAVIS, S. J., DURHAM, T. L., SUNG, D.-Y. & VIERSTRA, R. D. 2003. The Small Ubiquitin-like Modifier (SUMO) Protein Modification System in Arabidopsis : ACCUMULATION OF SUMO1 AND -2 CONJUGATES IS INCREASED BY STRESS. *Journal of Biological Chemistry,* 278, 6862-6872.

KUROKAWA, J., MOTOIKE, H. K., RAO, J. & KASS, R. S. 2004. Regulatory actions of the A-kinase anchoring protein Yotiao on a heart potassium channel downstream of PKA phosphorylation. *Proceedings of the National Academy of Sciences of the United States of America,* 101, 16374.

LACHAUD, Q. 2019. *Development of a medium-high throughputelectrophysiology method to study cellular heterogeneity in the rabbitheart*. PhD University of Glasgow.

LAKICS, V., KARRAN, E. H. & BOESS, F. G. 2010. Quantitative comparison of phosphodiesterase mRNA distribution in human brain and peripheral tissues. *Neuropharmacology,* 59, 367-374.

LALEVÉE, N., MONIER, B., SÉNATORE, S., PERRIN, L. & SÉMÉRIVA, M. 2006. Control of Cardiac Rhythm by ORK1, a Drosophila Two-Pore Domain Potassium Channel. *Current Biology,* 16, 1502-1508.

LALIBERTÉ, F., LIU, S., GORSETH, E., BOBECHKO, B., BARTLETT, A., LARIO, P., GRESSER, M. J. & HUANG, Z. 2002. In vitro PKA phosphorylation-mediated human PDE4A4 activation. *FEBS Letters,* 512, 205-208.

LE JEUNE, I. R., SHEPHERD, M., VAN HEEKE, G., HOUSLAY, M. D. & HALL, I. P. 2002. Cyclic AMP-dependent Transcriptional Up-regulation of Phosphodiesterase 4D5 in Human Airway Smooth Muscle Cells: IDENTIFICATION AND CHARACTERIZATION OF A NOVEL PDE4D5PROMOTER. *Journal of Biological Chemistry,* 277, 35980-35989.

LE MAIRE, M., CHAMPEIL, P. & MØLLER, J. V. 2000. Interaction of membrane proteins and lipids with solubilizing detergents. *Biochimica et Biophysica Acta (BBA) - Biomembranes,* 1508, 86-111.

LEA, W. A. & SIMEONOV, A. 2011. Fluorescence polarization assays in small molecule screening. *Expert Opinion on Drug Discovery,* 6, 17-32.

LEE, A., JEONG, D., MITSUYAMA, S., OH, J. G., LIANG, L., IKEDA, Y., SADOSHIMA, J., HAJJAR, R. J. & KHO, C. 2014. The Role of SUMO-1 in Cardiac Oxidative Stress and Hypertrophy. *Antioxidants & Redox Signaling,* 21, 1986-2001.

LEE, L. C. Y., MAURICE, D. H. & BAILLIE, G. S. 2013. Targeting protein–protein interactions within the cyclic AMP signaling system as a therapeutic strategy for cardiovascular disease. *Future Medicinal Chemistry,* 5, 451-464.

LEHNART, S. E., WEHRENS, X. H. T., REIKEN, S., WARRIER, S., BELEVYCH, A. E., HARVEY, R. D., RICHTER, W., JIN, S. L. C., CONTI, M. & MARKS, A. R. 2005. Phosphodiesterase 4D deficiency in the ryanodine-receptor complex promotes heart failure and arrhythmias. *Cell,* 123, 25-35.

LELOVAS, P. P., KOSTOMITSOPOULOS, N. G. & XANTHOS, T. T. 2014. A comparative anatomic and physiologic overview of the porcine heart. *Journal of the American Association for Laboratory Animal Science : JAALAS,* 53, 432-438.

LEMMON, M. A. & FERGUSON, K. M. 2000. Signal-dependent membrane targeting by pleckstrin homology (PH) domains. *Biochemical Journal,* 350, 1-18.

LEOR, J., ROZEN, L., ZULOFF-SHANI, A., FEINBERG, M. S., AMSALEM, Y., BARBASH, I. M., KACHEL, E., HOLBOVA, R., MARDOR, Y., DANIELS, D., OCHERASHVILLI, A., ORENSTEIN, A. & DANON, D. 2006. Ex Vivo Activated Human Macrophages Improve Healing, Remodeling, and Function of the Infarcted Heart. *Circulation,* 114, I-94-I-100.

LEROY, J., RICHTER, W., MIKA, D., CASTRO, L. R. V., ABI-GERGES, A., XIE, M., SCHEITRUM, C., LEFEBVRE, F., SCHITTL, J., MATEO, P., WESTENBROEK, R., CATTERALL, W. A., CHARPENTIER, F., CONTI, M., FISCHMEISTER, R. & VANDECASTEELE, G. 2011. Phosphodiesterase 4B in the cardiac L-type Ca2+ channel complex regulates Ca2+ current and protects against ventricular arrhythmias in mice. *The Journal of Clinical Investigation,* 121, 2651-2661.

LEVENTAL, I., GRZYBEK, M. & SIMONS, K. 2010. Greasing their way: lipid modifications determine protein association with membrane rafts. *Biochemistry,* 49, 6305-6316.

LI, D., TAPSCOFT, T., GONZALEZ, O., BURCH, P. E., QUIÑONES, M. A., ZOGHBI, W. A., HILL, R., BACHINSKI, L. L., MANN, D. L. & ROBERTS, R. 1999. Desmin mutation responsible for idiopathic dilated cardiomyopathy. *Circulation,* 100, 461-4.

LI, H., ZUO, J. & TANG, W. 2018. Phosphodiesterase-4 Inhibitors for the Treatment of Inflammatory Diseases. *Frontiers in pharmacology,* 9, 1048-1048.

LI, J., BIGELOW, D. J. & SQUIER, T. C. 2004. Conformational changes within the cytosolic portion of phospholamban upon release of Ca-ATPase inhibition. *Biochemistry,* 43, 3870-3879.

LI, X., VADREVU, S., DUNLOP, A., DAY, J., ADVANT, N., TROEGER, J., KLUSSMANN, E., JAFFREY, E., HAY, RON T., ADAMS, DAVID R., HOUSLAY, MILES D. & BAILLIE, GEORGE S. 2010. Selective SUMO modification of cAMP-specific phosphodiesterase-4D5 (PDE4D5) regulates the functional consequences of phosphorylation by PKA and ERK. *Biochemical Journal,* 428, 55-65.

LICHTY, J. J., MALECKI, J. L., AGNEW, H. D., MICHELSON-HOROWITZ, D. J. & TAN, S. 2005. Comparison of affinity tags for protein purification. *Protein expression and purification,* 41, 98-105.

LIEBELT, F. & VERTEGAAL, A. C. O. 2016. Ubiquitin-dependent and independent roles of SUMO in proteostasis. *American journal of physiology. Cell physiology,* 311, C284-C296.

LIMA, W. R., PARREIRA, K. S., DEVUYST, O., CAPLANUSI, A., N'KULI, F., MARIEN, B., VAN DER SMISSEN, P., ALVES, P. M. S., VERROUST, P., CHRISTENSEN, E. I., TERZI, F., MATTER, K., BALDA, M. S., PIERREUX, C. E. & COURTOY, P. J. 2010. ZONAB Promotes Proliferation and Represses Differentiation of Proximal Tubule Epithelial Cells. *Journal of the American Society of Nephrology,* 21, 478.

LIN, S., ZHAO, D. & BOWNES, M. 2007. Blood vessel/epicardial substance (bves) expression, essential for embryonic development, is down regulated by Grk/EFGR signalling. *Int J Dev Biol,* 51, 37-44.

LINDER, M. E., MIDDLETON, P., HEPLER, J. R., TAUSSIG, R., GILMAN, A. G. & MUMBY, S. M. 1993. Lipid modifications of G proteins: alpha subunits are palmitoylated. *Proceedings of the National Academy of Sciences of the United States of America,* 90, 3675-3679.

LINDSKOG, C. 2016. The Human Protein Atlas - an important resource for basic and clinical research. *Expert Rev Proteomics,* 13, 627-9.

LISSANDRON, V. & ZACCOLO, M. 2006. Compartmentalized cAMP/PKA signalling regulates cardiac excitation–contraction coupling. *Journal of Muscle Research & Cell Motility,* 27**,** 399-403.

LIU, B., LIAO, J., RAO, X., KUSHNER, S. A., CHUNG, C. D., CHANG, D. D. & SHUAI, K. 1998. Inhibition of Stat1-mediated gene activation by PIAS1. *Proceedings of the National Academy of Sciences,* 95**,** 10626.

LIU, B. & SHUAI, K. 2008. Targeting the PIAS1 SUMO ligase pathway to control inflammation. *Trends in pharmacological sciences,* 29**,** 505-509.

LIU, F.-T. & RABINOVICH, G. A. 2010. Galectins: regulators of acute and chronic inflammation. *Annals of the New York Academy of Sciences,* 1183**,** 158-182.

LIU, M., CHEN, T.-Y., AHAMED, B., LI, J. & YAU, K.-W. 1994. Calcium-Calmodulin Modulation of the Olfactory Cyclic Nucleotide-Gated Cation Channel. *Science,* 266**,** 1348.

LOBO, S., GREENTREE, W. K., LINDER, M. E. & DESCHENES, R. J. 2002. Identification of a Ras palmitoyltransferase in Saccharomyces cerevisiae. *Journal of Biological Chemistry,* 277**,** 41268-41273.

LÖHN, M., FÜRSTENAU, M., SAGACH, V., ELGER, M., SCHULZE, W., LUFT, F. C., HALLER, H. & GOLLASCH, M. 2000. Ignition of Calcium Sparks in Arterial and Cardiac Muscle Through Caveolae. *Circulation Research,* 87**,** 1034-1039.

LOPASCHUK, G. D., USSHER, J. R., FOLMES, C. D. L., JASWAL, J. S. & STANLEY, W. C. 2010. Myocardial Fatty Acid Metabolism in Health and Disease. *Physiological Reviews,* 90**,** 207-258.

LOPES, C. M. B., ROHÁCS, T., CZIRJÁK, G., BALLA, T., ENYEDI, P. & LOGOTHETIS, D. E. 2005. PIP2 hydrolysis underlies agonist-induced inhibition and regulates voltage gating of two-pore domain K+ channels. *The Journal of Physiology,* 564**,** 117-129.

LORBER, B., FISCHER, F., BAILLY, M., ROY, H. & KERN, D. 2012. Protein analysis by dynamic light scattering: Methods and techniques for students. *Biochemistry and Molecular Biology Education,* 40**,** 372-382.

LU, L., LIU, M., SUN, R., ZHENG, Y. & ZHANG, P. 2015. Myocardial Infarction: Symptoms and Treatments. *Cell Biochemistry and Biophysics,* 72**,** 865-867.

LUDWIG, A., ZONG, X., JEGLITSCH, M., HOFMANN, F. & BIEL, M. 1998. A family of hyperpolarization-activated mammalian cation channels. *Nature,* 393**,** 587-591.

LUFTMAN, K., HASAN, N., DAY, P., HARDEE, D. & HU, C. 2009. Silencing of VAMP3 inhibits cell migration and integrin-mediated adhesion. *Biochemical and Biophysical Research Communications,* 380**,** 65-70.

LUGNIER, C. 2006. Cyclic nucleotide phosphodiesterase (PDE) superfamily: A new target for the development of specific therapeutic agents. *Pharmacology & Therapeutics,* 109**,** 366-398.

LUK, A., AHN, E., SOOR, G. S. & BUTANY, J. 2009. Dilated cardiomyopathy: a review. *Journal of Clinical Pathology,* 62**,** 219.

LYNCH, M. J., BAILLIE, G. S. & HOUSLAY, M. D. 2007. cAMP-specific phosphodiesterase-4D5 (PDE4D5) provides a paradigm for understanding the unique non-redundant roles that PDE4 isoforms play in shaping compartmentalized cAMP cell signalling. *Biochemical Society Transactions,* 35**,** 938-941.

LYNCH, M. J., BAILLIE, G. S., MOHAMED, A., LI, X., MAISONNEUVE, C., KLUSSMANN, E., VAN HEEKE, G. & HOUSLAY, M. D. 2005. RNA Silencing Identifies PDE4D5 as the Functionally Relevant cAMP Phosphodiesterase

Interacting with ßArrestin to Control the Protein Kinase A/AKAP79-mediated Switching of the ß2-Adrenergic Receptor to Activation of ERK in HEK293B2 Cells. *Journal of Biological Chemistry,* 280**,** 33178-33189.

MAASS, P. G., AYDIN, A., LUFT, F. C., SCHÄCHTERLE, C., WEISE, A., STRICKER, S., LINDSCHAU, C., VAEGLER, M., QADRI, F., TOKA, H. R., SCHULZ, H., KRAWITZ, P. M., PARKHOMCHUK, D., HECHT, J., HOLLFINGER, I., WEFELD-NEUENFELD, Y., BARTELS-KLEIN, E., MÜHL, A., KANN, M., SCHUSTER, H., CHITAYAT, D., BIALER, M. G., WIENKER, T. F., OTT, J., RITTSCHER, K., LIEHR, T., JORDAN, J., PLESSIS, G., TANK, J., MAI, K., NARAGHI, R., HODGE, R., HOPP, M., HATTENBACH, L. O., BUSJAHN, A., RAUCH, A., VANDEPUT, F., GONG, M., RÜSCHENDORF, F., HÜBNER, N., HALLER, H., MUNDLOS, S., BILGINTURAN, N., MOVSESIAN, M. A., KLUSSMANN, E., TOKA, O. & BÄHRING, S. 2015. PDE3A mutations cause autosomal dominant hypertension with brachydactyly. *Nature Genetics,* 47**,** 647-653.

MACKENZIE, KIRSTY F., WALLACE, DEREK A., HILL, ELAINE V., ANTHONY, DIANA F., HENDERSON, DAVID J. P., HOUSLAY, DANIEL M., ARTHUR, J. SIMON C., BAILLIE, GEORGE S. & HOUSLAY, MILES D. 2011. Phosphorylation of cAMP-specific PDE4A5 (phosphodiesterase-4A5) by MK2 (MAPKAPK2) attenuates its activation through protein kinase A phosphorylation. *Biochemical Journal,* 435**,** 755-769.

MACKENZIE, S. J., BAILLIE, G. S., MCPHEE, I., MACKENZIE, C., SEAMONS, R., MCSORLEY, T., MILLEN, J., BEARD, M. B., VAN HEEKE, G. & HOUSLAY, M. D. 2002. Long PDE4 cAMP specific phosphodiesterases are activated by protein kinase A-mediated phosphorylation of a single serine residue in Upstream Conserved Region 1 (UCR1). *British journal of pharmacology,* 136**,** 421-433.

MACLENNAN, D. H. & KRANIAS, E. G. 2003. Phospholamban: a crucial regulator of cardiac contractility. *Nature Reviews Molecular Cell Biology,* 4**,** 566-577.

MAILLET, M., LYNCH, J. M., SANNA, B., YORK, A. J., ZHENG, Y. & MOLKENTIN, J. D. 2009. Cdc42 is an antihypertrophic molecular switch in the mouse heart. *The Journal of clinical investigation,* 119**,** 3079-3088.

MAINGRET, F., HONORÉ, E., LAZDUNSKI, M. & PATEL, A. J. 2002. Molecular Basis of the Voltage-Dependent Gating of TREK-1, a Mechano-Sensitive K+ Channel. *Biochemical and Biophysical Research Communications,* 292**,** 339-346.

MAINGRET, F., LAURITZEN, I., PATEL, A. J., HEURTEAUX, C., REYES, R., LESAGE, F., LAZDUNSKI, M. & HONORÉ, E. 2000. TREK-1 is a heat-activated background K(+) channel. *The EMBO journal,* 19**,** 2483-2491.

MANN, D. L. & BRISTOW, M. R. 2005. Mechanisms and Models in Heart Failure. *Circulation,* 111**,** 2837-2849.

MARCHMONT, R. J. & HOUSLAY, M. D. 1980. Insulin triggers cyclic AMP-dependent activation and phosphorylation of a plasma membrane cyclic AMP phosphodiesterase. *Nature,* 286**,** 904-906.

MARTIN, T. P., HORTIGON-VINAGRE, M. P., FINDLAY, J. E., ELLIOTT, C., CURRIE, S. & BAILLIE, G. S. 2014. Targeted disruption of the heat shock protein 20–phosphodiesterase 4D (PDE4D) interaction protects against pathological cardiac remodelling in a mouse model of hypertrophy. *FEBS Open Bio,* 4**,** 923-927.

MATCHKOV, V. V. & KRIVOI, I. I. 2016. Specialized Functional Diversity and Interactions of the Na,K-ATPase. 7.

MATTANOVICH, D., BRANDUARDI, P., DATO, L., GASSER, B., SAUER, M. & PORRO, D. 2012. Recombinant Protein Production in Yeasts. *In:* LORENCE, A. (ed.) *Recombinant Gene Expression.* Totowa, NJ: Humana Press.

MATTIAZZI, A., HOVE-MADSEN, L. & BERS, D. M. 1994. Protein kinase inhibitors reduce SR Ca transport in permeabilized cardiac myocytes. *American Journal of Physiology-Heart and Circulatory Physiology,* 267**,** H812-H820.

MATULEF, K. & ZAGOTTA, W. N. 2003. Cyclic Nucleotide-Gated Ion Channels. *Annual Review of Cell and Developmental Biology,* 19**,** 23-44.

MAURICE, D. H., KE, H., AHMAD, F., WANG, Y., CHUNG, J. & MANGANIELLO, V. C. 2014. Advances in targeting cyclic nucleotide phosphodiesterases. *Nature reviews. Drug discovery,* 13**,** 290-314.

MCCAHILL, A., MCSORLEY, T., HUSTON, E., HILL, E. V., LYNCH, M. J., GALL, I., KERYER, G., LYGREN, B., TASKEN, K., VAN HEEKE, G. & HOUSLAY, M. D. 2005. In resting COS1 cells a dominant negative approach shows that specific, anchored PDE4 cAMP phosphodiesterase isoforms gate the activation, by basal cyclic AMP production, of AKAP-tethered protein kinase A type II located in the centrosomal region. *Cellular Signalling,* 17**,** 1158-1173.

MCCAHILL, A. C., HUSTON, E., LI, X. & HOUSLAY, M. D. 2008. PDE4 Associates with Different Scaffolding Proteins: Modulating Interactions as Treatment for Certain Diseases. *In:* KLUSSMANN, E. & SCOTT, J. (eds.) *Protein-Protein Interactions as New Drug Targets.* Berlin, Heidelberg: Springer Berlin Heidelberg.

MCCARTHY, M. 2006. Allen Brain Atlas maps 21 000 genes of the mouse brain. *The Lancet Neurology,* 5**,** 907-908.

MCGRATH, M. F. & DE BOLD, A. J. 2009. Transcriptional analysis of the mammalian heart with special reference to its endocrine function. *BMC Genomics,* 10**,** 254.

MCPHEE, I., POOLEY, L., LOBBAN, M., BOLGER, G. & HOUSLAY, M. D. 1995. Identification, characterization and regional distribution in brain of RPDE-6 (RNPDE4A5), a novel splice variant of the PDE4A cyclic AMP phosphodiesterase family. *The Biochemical journal,* 310 (Pt 3)**,** 965-974.

MCPHEE, I., YARWOOD, S. J., SCOTLAND, G., HUSTON, E., BEARD, M. B., ROSS, A. H., HOUSLAY, E. S. & HOUSLAY, M. D. 1999. Association with the SRC Family Tyrosyl Kinase LYN Triggers a Conformational Change in the Catalytic Region of Human cAMP-specific Phosphodiesterase HSPDE4A4B: CONSEQUENCES FOR ROLIPRAM INHIBITION. *Journal of Biological Chemistry,* 274**,** 11796-11810.

MENCACCI, N. E., KAMSTEEG, E.-J., NAKASHIMA, K., R'BIBO, L., LYNCH, D. S., BALINT, B., WILLEMSEN, M. A. A. P., ADAMS, M. E., WIETHOFF, S., SUZUKI, K., DAVIES, C. H., NG, J., MEYER, E., VENEZIANO, L., GIUNTI, P., HUGHES, D., RAYMOND, F. L., CARECCHIO, M., ZORZI, G., NARDOCCI, N., BARZAGHI, C., GARAVAGLIA, B., SALPIETRO, V., HARDY, J., PITTMAN, A. M., HOULDEN, H., KURIAN, M. A., KIMURA, H., VISSERS, L. E. L. M., WOOD, N. W. & BHATIA, K. P. 2016. De Novo Mutations in PDE10A Cause Childhood-Onset Chorea with Bilateral Striatal Lesions. *American journal of human genetics,* 98**,** 763-771.

MEYER, D. & BIRCHMEIER, C. 1995. Multiple essential functions of neuregulin in development. *Nature,* 378**,** 386-390.

MILLER, M. L., JENSEN, L. J., DIELLA, F., JØRGENSEN, C., TINTI, M., LI, L., HSIUNG, M., PARKER, S. A., BORDEAUX, J., SICHERITZ-PONTEN, T., OLHOVSKY, M., PASCULESCU, A., ALEXANDER, J., KNAPP, S., BLOM, N.,

BORK, P., LI, S., CESARENI, G., PAWSON, T., TURK, B. E., YAFFE, M. B., BRUNAK, S. & LINDING, R. 2008. Linear motif atlas for phosphorylation-dependent signaling. *Science signaling,* 1, ra2-ra2.

MINATOGUCHI, S., TAKEMURA, G., CHEN, X.-H., WANG, N., UNO, Y., KODA, M., ARAI, M., MISAO, Y., LU, C., SUZUKI, K., GOTO, K., KOMADA, A., TAKAHASHI, T., KOSAI, K., FUJIWARA, T. & FUJIWARA, H. 2004. Acceleration of the Healing Process and Myocardial Regeneration May Be Important as a Mechanism of Improvement of Cardiac Function and Remodeling by Postinfarction Granulocyte Colony–Stimulating Factor Treatment. *Circulation,* 109, 2572-2580.

MINTY, A., DUMONT, X., KAGHAD, M. & CAPUT, D. 2000. Covalent Modification of p73α by SUMO-1: TWO-HYBRID SCREENING WITH p73 IDENTIFIES NOVEL SUMO-1-INTERACTING PROTEINS AND A SUMO-1 INTERACTION MOTIF. *Journal of Biological Chemistry,* 275, 36316-36323.

MITCHELL, D. A., MITCHELL, G., LING, Y., BUDDE, C. & DESCHENES, R. J. 2010. Mutational analysis of Saccharomyces cerevisiae Erf2 reveals a two-step reaction mechanism for protein palmitoylation by DHHC enzymes. *The Journal of biological chemistry,* 285, 38104-38114.

MOERKE, N. J. 2009. Fluorescence Polarization (FP) Assays for Monitoring Peptide-Protein or Nucleic Acid-Protein Binding. *Current Protocols in Chemical Biology,* 1, 1-15.

MONGILLO, M., MCSORLEY, T., EVELLIN, S., SOOD, A., LISSANDRON, V., TERRIN, A., HUSTON, E., HANNAWACKER, A., LOHSE, M. J., POZZAN, T., HOUSLAY, M. D. & ZACCOLO, M. 2004. Fluorescence Resonance Energy Transfer–Based Analysis of cAMP Dynamics in Live Neonatal Rat Cardiac Myocytes Reveals Distinct Functions of Compartmentalized Phosphodiesterases. *Circulation Research,* 95, 67-75.

MOORE, M. J., ADAMS, J. A. & TAYLOR, S. S. 2003. Structural basis for peptide binding in protein kinase A. Role of glutamic acid 203 and tyrosine 204 in the peptide-positioning loop. *J Biol Chem,* 278, 10613-8.

MOORTHY, B. S., GAO, Y. & ANAND, G. S. 2011. Phosphodiesterases catalyze hydrolysis of cAMP-bound to regulatory subunit of protein kinase A and mediate signal termination. *Molecular & cellular proteomics : MCP,* 10, M110.002295-M110.002295.

MØRK, H. K., SJAASTAD, I., SANDE, J. B., PERIASAMY, M., SEJERSTED, O. M. & LOUCH, W. E. 2007. Increased cardiomyocyte function and Ca2+ transients in mice during early congestive heart failure. *Journal of Molecular and Cellular Cardiology,* 43, 177-186.

MUKHOPADHYAY, D. & DASSO, M. 2007. Modification in reverse: the SUMO proteases. *Trends in Biochemical Sciences,* 32, 286-295.

MÜLLER, S., HOEGE, C., PYROWOLAKIS, G. & JENTSCH, S. 2001. Sumo, ubiquitin's mysterious cousin. *Nature Reviews Molecular Cell Biology,* 2, 202-210.

MÜLLER, T., ENGELS, P. & FOZARD, J. R. 1996. Subtypes of the type 4 cAMP phosphodiesterases: structure, regulation and selective inhibition. *Trends in Pharmacological Sciences,* 17, 294-298.

MUNTONI, F., CAU, M., GANAU, A., CONGIU, R., ARVEDI, G., MATEDDU, A., MARROSU, M. G., CIANCHETTI, C., REALDI, G., CAO, A. & ET AL. 1993. Brief report: deletion of the dystrophin muscle-promoter region associated with X-linked dilated cardiomyopathy. *N Engl J Med,* 329, 921-5.

MURBARTIÁN, J., LEI, Q., SANDO, J. J. & BAYLISS, D. A. 2005. Sequential Phosphorylation Mediates Receptor- and Kinase-induced Inhibition of

TREK-1 Background Potassium Channels. *Journal of Biological Chemistry,* 280, 30175-30184.

MURDOCH, H., MACKIE, S., COLLINS, D. M., HILL, E. V., BOLGER, G. B., KLUSSMANN, E., PORTEOUS, D. J., MILLAR, J. K. & HOUSLAY, M. D. 2007. Isoform-Selective Susceptibility of DISC1/Phosphodiesterase-4 Complexes to Dissociation by Elevated Intracellular cAMP Levels. *The Journal of Neuroscience,* 27, 9513.

NAG, A. C. 1980. Study of non-muscle cells of the adult mammalian heart: a fine structural analysis and distribution. *Cytobios,* 28, 41-61.

NAGAYAMA, T., TAKIMOTO, E., SADAYAPPAN, S., MUDD, J. O., SEIDMAN, J. G., ROBBINS, J. & KASS, D. A. 2007. Control of in vivo left ventricular [correction] contraction/relaxation kinetics by myosin binding protein C: protein kinase A phosphorylation dependent and independent regulation. *Circulation,* 116, 2399-408.

NALEFSKI, E. A. & FALKE, J. J. 1996. The C2 domain calcium-binding motif: structural and functional diversity. *Protein Science,* 5, 2375-2390.

NALLAMSETTY, S., AUSTIN, B. P., PENROSE, K. J. & WAUGH, D. S. 2005. Gateway vectors for the production of combinatorially-tagged His6-MBP fusion proteins in the cytoplasm and periplasm of Escherichia coli. *Protein Science,* 14, 2964-2971.

NEELY, J. R., ROVETTO, M. J. & ORAM, J. F. 1972. Myocardial utilization of carbohydrate and lipids. *Progress in Cardiovascular Diseases,* 15, 289-329.

NELSON, I., BEUVIN, M., BEN-YAOU, R., MASSON, C., BOLAND, A., SCHINDLER, R., BRAND, T., EYMARD, B. & BONNE, G. 2017. P.142 - Novel recessive splice site mutation in POPDC1 (BVES) is associated with first-degree atrioventricular block and muscular dystrophy. *Neuromuscular Disorders,* 27, S139-S140.

NEWTON, A. C., BOOTMAN, M. D. & SCOTT, J. D. 2016. Second Messengers. *Cold Spring Harbor perspectives in biology,* 8, a005926.

NIKOLAEV, V. O., BÜNEMANN, M., HEIN, L., HANNAWACKER, A. & LOHSE, M. J. 2004. Novel Single Chain cAMP Sensors for Receptor-induced Signal Propagation. *Journal of Biological Chemistry,* 279, 37215-37218.

NIKOLAEV, V. O. & LOHSE, M. J. 2006. Monitoring of cAMP Synthesis and Degradation in Living Cells. *Physiology,* 21, 86-92.

NISHI, H., SHAYTAN, A. & PANCHENKO, A. R. 2014. Physicochemical mechanisms of protein regulation by phosphorylation. *Frontiers in genetics,* 5, 270-270.

NOBES, C. D. 2000. Rho GTPases and cell migration-fibroblast wound healing. *In:* BALCH, W. E., DER, C. J. & HALL, A. (eds.) *Methods in Enzymology.* Academic Press.

NOORMAN, M., VAN DER HEYDEN, M. A. G., VAN VEEN, T. A. B., COX, M. G. P. J., HAUER, R. N. W., DE BAKKER, J. M. T. & VAN RIJEN, H. V. M. 2009. Cardiac cell–cell junctions in health and disease: Electrical versus mechanical coupling. *Journal of Molecular and Cellular Cardiology,* 47, 23-31.

O'CONNELL, J. C., MCCALLUM, J. F., MCPHEE, I., WAKEFIELD, J., HOUSLAY, E. S., WISHART, W., BOLGER, G., FRAME, M. & HOUSLAY, M. D. 1996. The SH3 domain of Src tyrosyl protein kinase interacts with the N-terminal splice region of the PDE4A cAMP-specific phosphodiesterase RPDE-6 (RNPDE4A5). *Biochemical Journal,* 318, 255-261.

OBATA, T., YAFFE, M. B., LEPARC, G. G., PIRO, E. T., MAEGAWA, H., KASHIWAGI, A., KIKKAWA, R. & CANTLEY, L. C. 2000. Peptide and Protein Library

Screening Defines Optimal Substrate Motifs for AKT/PKB. *Journal of Biological Chemistry,* 275, 36108-36115.

OHLENDIECK, K. 2004. Extraction of Membrane Proteins. *In:* CUTLER, P. (ed.) *Protein Purification Protocols.* Totowa, NJ: Humana Press.

OHNO, Y., KIHARA, A., SANO, T. & IGARASHI, Y. 2006. Intracellular localization and tissue-specific distribution of human and yeast DHHC cysteine-rich domain-containing proteins. *Biochimica et Biophysica Acta (BBA) - Molecular and Cell Biology of Lipids,* 1761, 474-483.

OLSON, T. M., MICHELS, V. V., THIBODEAU, S. N., TAI, Y. S. & KEATING, M. T. 1998. Actin mutations in dilated cardiomyopathy, a heritable form of heart failure. *Science,* 280, 750-2.

OMORI, K. & KOTERA, J. 2007. Overview of PDEs and Their Regulation. *Circulation Research,* 100, 309-327.

ONG, S. H., WHITLEY, T. H., STOWE, N. W. & STEINER, A. L. 1975. Immunohistochemical localization of 3'5'-cyclic AMP and 3'5'-cyclic GMP in rat liver, intestine, and testis. *Proceedings of the National Academy of Sciences,* 72, 2022.

OPTHOF, T. 1988. The mammalian sinoatrial node. *Cardiovasc Drugs Ther,* 1, 573-97.

OSLER, M. E., CHANG, M. S. & BADER, D. M. 2005. Bves modulates epithelial integrity through an interaction at the tight junction. *Journal of Cell Science,* 118, 4667.

OSTERRIEDER, W. 1988. Modification of K+ conductance of heart cell membrane by BRL 34915. *Naunyn-Schmiedeberg's Archives of Pharmacology,* 337, 93-97.

PACKER, M., CARVER, J. R., RODEHEFFER, R. J., IVANHOE, R. J., DIBIANCO, R., ZELDIS, S. M., HENDRIX, G. H., BOMMER, W. J., ELKAYAM, U., KUKIN, M. L., MALLIS, G. I., SOLLANO, J. A., SHANNON, J., TANDON, P. K. & DEMETS, D. L. 1991. Effect of Oral Milrinone on Mortality in Severe Chronic Heart Failure. *New England Journal of Medicine,* 325, 1468-1475.

PAGE, P. 2014. Beyond statistical significance: clinical interpretation of rehabilitation research literature. *International journal of sports physical therapy,* 9, 726-736.

PALATINUS, J. A., O'QUINN, M. P., BARKER, R. J., HARRIS, B. S., JOURDAN, J. & GOURDIE, R. G. 2010. ZO-1 determines adherens and gap junction localization at intercalated disks. *American Journal of Physiology-Heart and Circulatory Physiology,* 300, H583-H594.

PALVIMO, J. J. 2007. PIAS proteins as regulators of small ubiquitin-related modifier (SUMO) modifications and transcription. *Biochemical Society Transactions,* 35, 1405-1408.

PARANG, B., KAZ, A. M., BARRETT, C. W., SHORT, S. P., NING, W., KEATING, C. E., MITTAL, M. K., NAIK, R. D., WASHINGTON, M. K., REVETTA, F. L., SMITH, J. J., CHEN, X., WILSON, K. T., BRAND, T., BADER, D. M., TANSEY, W. P., CHEN, R., BRENTNALL, T. A., GRADY, W. M. & WILLIAMS, C. S. 2017. BVES regulates c-Myc stability via PP2A and suppresses colitis-induced tumourigenesis. *Gut,* 66, 852-862.

PARNES, D., JACOBY, V., SHARABI, A., SCHLESINGER, H., BRAND, T. & KESSLER-ICEKSON, G. 2007. The Popdc gene family in the rat: Molecular cloning, characterization and expression analysis in the heart and cultured cardiomyocytes. *Biochimica et Biophysica Acta (BBA) - Gene Structure and Expression,* 1769, 586-592.

PATEL, A. J. & HONORÉ, E. 2001. Properties and modulation of mammalian 2P domain K+ channels. *Trends in Neurosciences,* 24**,** 339-346.

PATEL, A. J., HONORÉ, E., MAINGRET, F., LESAGE, F., FINK, M., DUPRAT, F. & LAZDUNSKI, M. 1998. A mammalian two pore domain mechano-gated S-like K+ channel. *The EMBO Journal,* 17**,** 4283-4290.

PATEL, H. H., MURRAY, F. & INSEL, P. A. 2008. Caveolae as organizers of pharmacologically relevant signal transduction molecules. *Annual review of pharmacology and toxicology,* 48**,** 359-391.

PATTERSON, C., RUEF, J., MADAMANCHI, N. R., BARRY-LANE, P., HU, Z., HORAIST, C., BALLINGER, C. A., BRASIER, A. R., BODE, C. & RUNGE, M. S. 1999. Stimulation of a Vascular Smooth Muscle Cell NAD(P)H Oxidase by Thrombin: EVIDENCE THAT p47 phox MAY PARTICIPATE IN FORMING THIS OXIDASE IN VITRO AND IN VIVO. *Journal of Biological Chemistry,* 274**,** 19814-19822.

PÉREZ-TORRES, S., MIRÓ, X., PALACIOS, J. M., CORTÉS, R., PUIGDOMÉNECH, P. & MENGOD, G. 2000. Phosphodiesterase type 4 isozymes expression in human brain examined by in situ hybridization histochemistry and [3H]rolipram binding autoradiography: Comparison with monkey and rat brain. *Journal of Chemical Neuroanatomy,* 20**,** 349-374.

PERRY, S. J., BAILLIE, G. S., KOHOUT, T. A., MCPHEE, I., MAGIERA, M. M., ANG, K. L., MILLER, W. E., MCLEAN, A. J., CONTI, M., HOUSLAY, M. D. & LEFKOWITZ, R. J. 2002. Targeting of Cyclic AMP Degradation to ß2-Adrenergic Receptors by ß-Arrestins. *Science,* 298**,** 834-836.

PETER, A. K., BJERKE, M. A. & LEINWAND, L. A. 2016. Biology of the cardiac myocyte in heart disease. *Molecular biology of the cell,* 27**,** 2149-2160.

PHROMMINTIKUL, A. & CHATTIPAKORN, N. 2006. Roles of cardiac ryanodine receptor in heart failure and sudden cardiac death. *International journal of cardiology,* 112**,** 142-152.

PIERCE, K. L., PREMONT, R. T. & LEFKOWITZ, R. J. 2002. Seven-transmembrane receptors. *Nature Reviews Molecular Cell Biology,* 3**,** 639-650.

PIERRE, S., ESCHENHAGEN, T., GEISSLINGER, G. & SCHOLICH, K. 2009. Capturing adenylyl cyclases as potential drug targets. *Nature Reviews Drug Discovery,* 8**,** 321-335.

PINNELL, J., TURNER, S. & HOWELL, S. 2007. Cardiac muscle physiology. *Continuing Education in Anaesthesia Critical Care & Pain,* 7**,** 85-88.

PORTER, B., VAN DUIJVENBODEN, S., BISHOP, M. J., ORINI, M., CLARIDGE, S., GOULD, J., SIENIEWICZ, B. J., SIDHU, B., RAZAVI, R., RINALDI, C. A., GILL, J. S. & TAGGART, P. 2018. Beat-to-Beat Variability of Ventricular Action Potential Duration Oscillates at Low Frequency During Sympathetic Provocation in Humans. *Frontiers in Physiology,* 9.

POULSEN, H., NISSEN, P., MOURITSEN, O. G. & KHANDELIA, H. 2012. Protein Kinase A (PKA) Phosphorylation of Na+/K+-ATPase Opens Intracellular C-terminal Water Pathway Leading to Third Na+-binding site in Molecular Dynamics Simulations. *Journal of Biological Chemistry,* 287**,** 15959-15965.

POZZI, A. & ZENT, R. 2010. ZO-1 and ZONAB interact to regulate proximal tubular cell differentiation. *Journal of the American Society of Nephrology : JASN,* 21**,** 388-390.

PRABAKARAN, S., LIPPENS, G., STEEN, H. & GUNAWARDENA, J. 2012. Post-translational modification: nature's escape from genetic imprisonment and the basis for dynamic information encoding. *WIREs Systems Biology and Medicine,* 4**,** 565-583.

PROUX-GILLARDEAUX, V., GAVARD, J., IRINOPOULOU, T., MÈGE, R.-M. & GALLI, T. 2005. Tetanus neurotoxin-mediated cleavage of cellubrevin impairs epithelial cell migration and integrin-dependent cell adhesion. *Proceedings of the National Academy of Sciences of the United States of America,* 102**,** 6362.

PRYOR, K. D. & LEITING, B. 1997. High-Level Expression of Soluble Protein inEscherichia coliUsing a His6-Tag and Maltose-Binding-Protein Double-Affinity Fusion System. *Protein expression and purification,* 10**,** 309-319.

PUTILINA, T., WONG, P. & GENTLEMAN, S. 1999. The DHHC domain: a new highly conserved cysteine-rich motif. *Molecular and cellular biochemistry,* 195**,** 219-226.

QI, C., SORRENTINO, S., MEDALIA, O. & KORKHOV, V. M. 2019. The structure of a membrane adenylyl cyclase bound to an activated stimulatory G protein. *Science,* 364**,** 389.

RABABA'H, A. M., BSOUL, R. W., ALKHATATBEH, M. J., ALZOUBI, K. H. & KHABOUR, O. F. 2019. Waterpipe tobacco smoke distresses cardiovascular biomarkers in mice: alterations in protein expression of metalloproteinases, endothelin and myeloperoxidase. *Inhalation Toxicology,* 31**,** 99-106.

RABE, K. F. 2011. Update on roflumilast, a phosphodiesterase 4 inhibitor for the treatment of chronic obstructive pulmonary disease. *British Journal of Pharmacology,* 163**,** 53-67.

RALL, T. W. & WEST, T. C. 1963. THE POTENTIATION OF CARDIAC INOTROPIC RESPONSES TO NOREPINEPHRINE BY THEOPHYLLINE. *Journal of Pharmacology and Experimental Therapeutics,* 139**,** 269.

RAMPERSAD, S. N., OVENS, J. D., HUSTON, E., UMANA, M. B., WILSON, L. S., NETHERTON, S. J., LYNCH, M. J., BAILLIE, G. S., HOUSLAY, M. D. & MAURICE, D. H. 2010. Cyclic AMP phosphodiesterase 4D (PDE4D) Tethers EPAC1 in a vascular endothelial cadherin (VE-Cad)-based signaling complex and controls cAMP-mediated vascular permeability. *The Journal of biological chemistry,* 285**,** 33614-33622.

RANGARAJAN, S., ENSERINK, J. M., KUIPERIJ, H. B., DE ROOIJ, J., PRICE, L. S., SCHWEDE, F. & BOS, J. L. 2003. Cyclic AMP induces integrin-mediated cell adhesion through Epac and Rap1 upon stimulation of the beta 2-adrenergic receptor. *The Journal of cell biology,* 160**,** 487-493.

RAYMENT, I., RYPNIEWSKI, W. R., SCHMIDT-BASE, K., SMITH, R., TOMCHICK, D. R., BENNING, M. M., WINKELMANN, D. A., WESENBERG, G. & HOLDEN, H. M. 1993. Three-dimensional structure of myosin subfragment-1: a molecular motor. *Science,* 261**,** 50.

REDDY, V. K., SHORT, S. P., BARRETT, C. W., MITTAL, M. K., KEATING, C. E., THOMPSON, J. J., HARRIS, E. I., REVETTA, F., BADER, D. M., BRAND, T., WASHINGTON, M. K. & WILLIAMS, C. S. 2016. BVES Regulates Intestinal Stem Cell Programs and Intestinal Crypt Viability after Radiation. *Stem cells (Dayton, Ohio),* 34**,** 1626-1636.

REESE, D. E., ZAVALJEVSKI, M., STREIFF, N. L. & BADER, D. 1999. bves:A Novel Gene Expressed during Coronary Blood Vessel Development. *Developmental Biology,* 209**,** 159-171.

REHMANN, H., WITTINGHOFER, A. & BOS, J. L. 2007. Capturing cyclic nucleotides in action: snapshots from crystallographic studies. *Nature Reviews Molecular Cell Biology,* 8**,** 63-73.

RESH, M. D. 1999. Fatty acylation of proteins: new insights into membrane targeting of myristoylated and palmitoylated proteins. *Biochimica et Biophysica Acta (BBA) - Molecular Cell Research,* 1451, 1-16.

RESH, M. D. 2006. Trafficking and signaling by fatty-acylated and prenylated proteins. *Nature Chemical Biology,* 2, 584-590.

RICCIARELLI, R. & FEDELE, E. 2018. cAMP, cGMP and amyloid ß: three ideal partners for memory formation. *Trends in neurosciences,* 41, 255-266.

RICH, T. C. & KARPEN, J. W. 2002. Review Article: Cyclic AMP Sensors in Living Cells: What Signals Can They Actually Measure? *Annals of Biomedical Engineering,* 30, 1088-1099.

RICHTER, W. & CONTI, M. 2002. Dimerization of the Type 4 cAMP-specific Phosphodiesterases Is Mediated by the Upstream Conserved Regions (UCRs). *Journal of Biological Chemistry,* 277, 40212-40221.

RICHTER, W. & CONTI, M. 2004. The Oligomerization State Determines Regulatory Properties and Inhibitor Sensitivity of Type 4 cAMP-specific Phosphodiesterases. *Journal of Biological Chemistry,* 279, 30338-30348.

RICHTER, W., DAY, P., AGRAWAL, R., BRUSS, M. D., GRANIER, S., WANG, Y. L., RASMUSSEN, S. G. F., HORNER, K., WANG, P., LEI, T., PATTERSON, A. J., KOBILKA, B. & CONTI, M. 2008. Signaling from beta1- and beta2-adrenergic receptors is defined by differential interactions with PDE4. *The EMBO journal,* 27, 384-393.

RICHTER, W., XIE, M., SCHEITRUM, C., KRALL, J., MOVSESIAN, M. A. & CONTI, M. 2011. Conserved expression and functions of PDE4 in rodent and human heart. *Basic Research in Cardiology,* 106, 249-262.

RIPLEY, A. N., OSLER, M. E., WRIGHT, C. V. E. & BADER, D. 2006. Bves is a regulator of epithelial movement during early Xenopus laevis development. *Proceedings of the National Academy of Sciences of the United States of America,* 103, 614-619.

RIZO, J. & SÜDHOF, T. C. 1998. C2-domains, structure and function of a universal Ca2+-binding domain. *Journal of Biological Chemistry,* 273, 15879-15882.

ROBERTS, W. C., SIEGEL, R. J. & MCMANUS, B. M. 1987. Idiopathic dilated cardiomyopathy: analysis of 152 necropsy patients. *The American journal of cardiology,* 60, 1340-1355.

ROCHAIS, F., VANDECASTEELE, G., LEFEBVRE, F., LUGNIER, C., LUM, H., MAZET, J.-L., COOPER, D. M. F. & FISCHMEISTER, R. 2004. Negative Feedback Exerted by cAMP-dependent Protein Kinase and cAMP Phosphodiesterase on Subsarcolemmal cAMP Signals in Intact Cardiac Myocytes: AN IN VIVO STUDY USING ADENOVIRUS-MEDIATED EXPRESSION OF CNG CHANNELS. *Journal of Biological Chemistry,* 279, 52095-52105.

ROCKS, O., PEYKER, A., KAHMS, M., VERVEER, P. J., KOERNER, C., LUMBIERRES, M., KUHLMANN, J., WALDMANN, H., WITTINGHOFER, A. & BASTIAENS, P. I. 2005. An acylation cycle regulates localization and activity of palmitoylated Ras isoforms. *Science,* 307, 1746-1752.

RODRIGUEZ, R. D. & SCHOCKEN, D. D. 1990. Update on sick sinus syndrome, a cardiac disorder of aging. *Geriatrics,* 45, 26-30, 33-6.

ROGER, V. L. 2013. Epidemiology of heart failure. *Circulation research,* 113, 646-659.

ROSANO, G. L. & CECCARELLI, E. A. 2014. Recombinant protein expression in Escherichia coli: advances and challenges. *Frontiers in microbiology,* 5, 172-172.

ROSEN, O. M. & ERLICHMAN, J. 1975. Reversible autophosphorylation of a cyclic 3':5'-AMP-dependent protein kinase from bovine cardiac muscle. *Journal of Biological Chemistry,* 250**,** 7788-7794.

ROSENBAUM, D. M., RASMUSSEN, S. G. F. & KOBILKA, B. K. 2009. The structure and function of G-protein-coupled receptors. *Nature,* 459**,** 356-363.

ROSKOSKI, R. 2012. ERK1/2 MAP kinases: Structure, function, and regulation. *Pharmacological Research,* 66**,** 105-143.

ROTH, A. F., FENG, Y., CHEN, L. & DAVIS, N. G. 2002. The yeast DHHC cysteine-rich domain protein Akr1p is a palmitoyl transferase. *The Journal of cell biology,* 159**,** 23-28.

ROTH, A. F., WAN, J., BAILEY, A. O., SUN, B., KUCHAR, J. A., GREEN, W. N., PHINNEY, B. S., YATES III, J. R. & DAVIS, N. G. 2006. Global analysis of protein palmitoylation in yeast. *Cell,* 125**,** 1003-1013.

ROY, S., PLOWMAN, S., ROTBLAT, B., PRIOR, I. A., MUNCKE, C., GRAINGER, S., PARTON, R. G., HENIS, Y. I., KLOOG, Y. & HANCOCK, J. F. 2005. Individual palmitoyl residues serve distinct roles in H-ras trafficking, microlocalization, and signaling. *Molecular and cellular biology,* 25**,** 6722-6733.

RUBIN, S. A., FISHBEIN, M. C. & SWAN, H. J. C. 1983. Compensatory hypertrophy in the heart after myocardial infarction in the rat. *Journal of the American College of Cardiology,* 1**,** 1435-1441.

RUSS, P. K., KUPPERMAN, A. I., PRESLEY, S.-H., HASELTON, F. R. & CHANG, M. S. 2010. Inhibition of RhoA signaling with increased Bves in trabecular meshwork cells. *Investigative ophthalmology & visual science,* 51**,** 223-230.

RUSS, P. K., PINO, C. J., WILLIAMS, C. S., BADER, D. M., HASELTON, F. R. & CHANG, M. S. 2011. Bves Modulates Tight Junction Associated Signaling. *PLOS ONE,* 6**,** e14563.

SACHS, B. D., BAILLIE, G. S., MCCALL, J. R., PASSINO, M. A., SCHACHTRUP, C., WALLACE, D. A., DUNLOP, A. J., MACKENZIE, K. F., KLUSSMANN, E., LYNCH, M. J., SIKORSKI, S. L., NURIEL, T., TSIGELNY, I., ZHANG, J., HOUSLAY, M. D., CHAO, M. V. & AKASSOGLOU, K. 2007. p75 neurotrophin receptor regulates tissue fibrosis through inhibition of plasminogen activation via a PDE4/cAMP/PKA pathway. 177**,** 1119-1132.

SALAUN, C., GREAVES, J. & CHAMBERLAIN, L. H. 2010. The intracellular dynamic of protein palmitoylation. *The Journal of cell biology,* 191**,** 1229-1238.

SANGUINETTI, M. C. & TRISTANI-FIROUZI, M. 2006. hERG potassium channels and cardiac arrhythmia. *Nature,* 440**,** 463-469.

SANTORO, B., LIU, D. T., YAO, H., BARTSCH, D., KANDEL, E. R., SIEGELBAUM, S. A. & TIBBS, G. R. 1998. Identification of a Gene Encoding a Hyperpolarization-Activated Pacemaker Channel of Brain. *Cell,* 93**,** 717-729.

SARASWATHY, N. & RAMALINGAM, P. 2011. 15 - Phosphoproteomics. *In:* SARASWATHY, N. & RAMALINGAM, P. (eds.) *Concepts and Techniques in Genomics and Proteomics.* Woodhead Publishing.

SATOH, M., OGITA, H., TAKESHITA, K., MUKAI, Y., KWIATKOWSKI, D. J. & LIAO, J. K. 2006. Requirement of Rac1 in the development of cardiac hypertrophy. *Proceedings of the National Academy of Sciences,* 103**,** 7432.

SAVITSKY, P., BRAY, J., COOPER, C. D. O., MARSDEN, B. D., MAHAJAN, P., BURGESS-BROWN, N. A. & GILEADI, O. 2010. High-throughput production of human proteins for crystallization: the SGC experience. *Journal of structural biology,* 172**,** 3-13.

SAWADA, N., MURATA, M., KIKUCHI, K., OSANAI, M., TOBIOKA, H., KOJIMA, T. & CHIBA, H. 2003. Tight junctions and human diseases. *Med Electron Microsc,* 36**,** 147-56.

SCHÄCHTERLE, C., CHRISTIAN, F., FERNANDES, J. M. P. & KLUSSMANN, E. 2015. Screening for Small Molecule Disruptors of AKAP–PKA Interactions. *In:* ZACCOLO, M. (ed.) *cAMP Signaling: Methods and Protocols*. New York, NY: Springer New York.

SCHAPER, J., FROEDE, R., HEIN, S., BUCK, A., HASHIZUME, H., SPEISER, B., FRIEDL, A. & BLEESE, N. 1991. Impairment of the myocardial ultrastructure and changes of the cytoskeleton in dilated cardiomyopathy. *Circulation,* 83**,** 504-514.

SCHINDLER, R. 2014. *Protein biochemistry of Popdc1 and -2 in heart and skeletal muscle*. Doctor of Philosophy Imperial College London.

SCHINDLER, R., SIMIRICK, S. & BRAND, T. 2012a. Nuclear localization of members of the popeye domain containing (Popdc) protein family. Cardiovascular Research.

SCHINDLER, R. F., POON, K. L., SIMRICK, S. & BRAND, T. 2012b. The Popeye domain containing genes: essential elements in heart rate control. *Cardiovascular Diagnosis and Therapy,* 2**,** 308-319.

SCHINDLER, R. F., SCOTTON, C., FRENCH, V., FERLINI, A. & BRAND, T. 2016a. The Popeye Domain Containing Genes and their Function in Striated Muscle. *Journal of cardiovascular development and disease,* 3**,** 22-22.

SCHINDLER, R. F. R. & BRAND, T. 2016. The Popeye domain containing protein family--A novel class of cAMP effectors with important functions in multiple tissues. *Progress in biophysics and molecular biology,* 120**,** 28-36.

SCHINDLER, R. F. R., SCOTTON, C., ZHANG, J., PASSARELLI, C., ORTIZ-BONNIN, B., SIMRICK, S., SCHWERTE, T., POON, K.-L., FANG, M., RINNÉ, S., FROESE, A., NIKOLAEV, V. O., GRUNERT, C., MÜLLER, T., TASCA, G., SARATHCHANDRA, P., DRAGO, F., DALLAPICCOLA, B., RAPEZZI, C., ARBUSTINI, E., DI RAIMO, F. R., NERI, M., SELVATICI, R., GUALANDI, F., FATTORI, F., PIETRANGELO, A., LI, W., JIANG, H., XU, X., BERTINI, E., DECHER, N., WANG, J., BRAND, T. & FERLINI, A. 2016b. POPDC1(S201F) causes muscular dystrophy and arrhythmia by affecting protein trafficking. *The Journal of clinical investigation,* 126**,** 239-253.

SCHLÜTER, H., APWEILER, R., HOLZHÜTTER, H.-G. & JUNGBLUT, P. R. 2009. Finding one's way in proteomics: a protein species nomenclature. *Chemistry Central Journal,* 3**,** 11.

SCHMID, F. X. 1995. Protein folding: prolyl isomerases join the fold. *Current Biology,* 5**,** 993-994.

SCHÖNICHEN, A., WEBB, B. A., JACOBSON, M. P. & BARBER, D. L. 2013. Considering protonation as a posttranslational modification regulating protein structure and function. *Annual review of biophysics,* 42**,** 289-314.

SCHRÖDER, H., LANGER, T., HARTL, F. U. & BUKAU, B. 1993. DnaK, DnaJ and GrpE form a cellular chaperone machinery capable of repairing heat-induced protein damage. *The EMBO journal,* 12**,** 4137-4144.

SCHROEDER, H., LEVENTIS, R., REX, S., SCHELHAAS, M., NÄGELE, E., WALDMANN, H. & SILVIUS, J. R. 1997. S-Acylation and plasma membrane targeting of the farnesylated carboxyl-terminal peptide of N-ras in mammalian fibroblasts. *Biochemistry,* 36**,** 13102-13109.

SCHWARTZ, P. A. & MURRAY, B. W. 2011. Protein kinase biochemistry and drug discovery. *Bioorganic Chemistry,* 39**,** 192-210.

SCHWARZ, F., MALL, G., ZEBE, H., BLICKLE, J., DERKS, H., MANTHEY, J. & KÜBLER, W. 1983. Quantitative morphologic findings of the myocardium in idiopathic dilated cardiomyopathy. *The American journal of cardiology,* 51**,** 501-506.

SCICCHITANO, P., CARBONARA, S., RICCI, G., MANDURINO, C., LOCOROTONDO, M., BULZIS, G., GESUALDO, M., ZITO, A., CARBONARA, R., DENTAMARO, I., RICCIONI, G. & CICCONE, M. M. 2012. HCN channels and heart rate. *Molecules (Basel, Switzerland),* 17**,** 4225-4235.

SEELER, J.-S. & DEJEAN, A. 2003. Nuclear and unclear functions of SUMO. *Nature Reviews Molecular Cell Biology,* 4**,** 690-699.

SELZMAN, C. H., SHAMES, B. D., REZNIKOV, L. L., MILLER, S. A., MENG, X., BARTON, H. A., WERMAN, A., HARKEN, A. H., DINARELLO, C. A. & BANERJEE, A. 1999. Liposomal Delivery of Purified Inhibitory-; Inhibits Tumor Necrosis Factor-kBα Induced Human Vascular Smooth Muscle Proliferation. *Circulation Research,* 84**,** 867-875.

SEROPIAN, I. M., CERLIANI, J. P., TOLDO, S., VAN TASSELL, B. W., ILARREGUI, J. M., GONZÁLEZ, G. E., MATOSO, M., SALLOUM, F. N., MELCHIOR, R., GELPI, R. J., STUPIRSKI, J. C., BENATAR, A., GÓMEZ, K. A., MORALES, C., ABBATE, A. & RABINOVICH, G. A. 2013. Galectin-1 Controls Cardiac Inflammation and Ventricular Remodeling during Acute Myocardial Infarction. *The American Journal of Pathology,* 182**,** 29-40.

SETTE, C. & CONTI, M. 1996. Phosphorylation and Activation of a cAMP-specific Phosphodiesterase by the cAMP-dependent Protein Kinase: INVOLVEMENT OF SERINE 54 IN THE ENZYME ACTIVATION. *Journal of Biological Chemistry,* 271**,** 16526-16534.

SHAHINIAN, S. & SILVIUS, J. R. 1995. Doubly-lipid-modified protein sequence motifs exhibit long-lived anchorage to lipid bilayer membranes. *Biochemistry,* 34**,** 3813-3822.

SHAKUR, Y., PRYDE, J. G. & HOUSLAY, M. D. 1993. Engineered deletion of the unique N-terminal domain of the cyclic AMP-specific phosphodiesterase RD1 prevents plasma membrane association and the attainment of enhanced thermostability without altering its sensitivity to inhibition by rolipram. *Biochemical Journal,* 292**,** 677-686.

SHAKUR, Y., WILSON, M., POOLEY, L., LOBBAN, M., GRIFFITHS, S. L., CAMPBELL, A. M., BEATTIE, J., DALY, C. & HOUSLAY, M. D. 1995. Identification and characterization of the type-IVA cyclic AMP-specific phosphodiesterase RD1 as a membrane-bound protein expressed in cerebellum. *Biochemical Journal,* 306**,** 801-809.

SHANNON, R. P., KOMAMURA, K., STAMBLER, B. S., BIGAUD, M., MANDERS, W. T. & VATNER, S. F. 1991. Alterations in myocardial contractility in conscious dogs with dilated cardiomyopathy. *American Journal of Physiology-Heart and Circulatory Physiology,* 260**,** H1903-H1911.

SHAW, P. E. 2002. Peptidyl-prolyl isomerases: a new twist to transcription. *EMBO reports,* 3**,** 521-526.

SHI, J.-W., LIU, W., ZHANG, T.-T., WANG, S.-C., LIN, X.-L., LI, J., JIA, J.-S., SHENG, H.-F., YAO, Z.-F., ZHAO, W.-T., ZHAO, Z.-L., XIE, R.-Y., YANG, S., GAO, F., FAN, Q.-R., ZHANG, M.-Y., YUE, M., YUAN, J., GU, W.-W., YAO, K.-T. & XIAO, D. 2013. The enforced expression of c-Myc in pig fibroblasts triggers mesenchymal-epithelial transition (MET) via F-actin reorganization and RhoA/Rock pathway inactivation. *Cell cycle (Georgetown, Tex.),* 12**,** 1119-1127.

SHOJI, S., TITANI, K., DEMAILLE, J. G. & FISCHER, E. H. 1979. Sequence of two phosphorylated sites in the catalytic subunit of bovine cardiac muscle adenosine 3':5'-monophosphate-dependent protein kinase. *J Biol Chem,* 254, 6211-4.

SICHELSCHMIDT, O. J., HAHNEFELD, C., HOHLFELD, T., HERBERG, F. W. & SCHRÖR, K. 2003. Trapidil protects ischemic hearts from reperfusion injury by stimulating PKAII activity. *Cardiovascular research,* 58, 602-610.

SIN, Y. Y., EDWARDS, H. V., LI, X., DAY, J. P., CHRISTIAN, F., DUNLOP, A. J., ADAMS, D. R., ZACCOLO, M., HOUSLAY, M. D. & BAILLIE, G. S. 2011. Disruption of the cyclic AMP phosphodiesterase-4 (PDE4)–HSP20 complex attenuates the ß-agonist induced hypertrophic response in cardiac myocytes. *Journal of Molecular and Cellular Cardiology,* 50, 872-883.

SIN, Y. Y., MARTIN, T. P., WILLS, L., CURRIE, S. & BAILLIE, G. S. 2015. Small heat shock protein 20 (Hsp20) facilitates nuclear import of protein kinase D 1 (PKD1) during cardiac hypertrophy. *Cell communication and signaling : CCS,* 13, 16-16.

SKALHEGG, B. S. & TASKEN, K. 2000. Specificity in the cAMP/PKA signaling pathway. Differential expression,regulation, and subcellular localization of subunits of PKA. *Front Biosci,* 5, D678-93.

SMITH, K. J., BAILLIE, G. S., HYDE, E. I., LI, X., HOUSLAY, T. M., MCCAHILL, A., DUNLOP, A. J., BOLGER, G. B., KLUSSMANN, E., ADAMS, D. R. & HOUSLAY, M. D. 2007. 1H NMR structural and functional characterisation of a cAMP-specific phosphodiesterase-4D5 (PDE4D5) N-terminal region peptide that disrupts PDE4D5 interaction with the signalling scaffold proteins, ßarrestin and RACK1. *Cellular Signalling,* 19, 2612-2624.

SMITH, T. K. & BADER, D. M. 2006. Characterization of Bves expression during mouse development using newly generated immunoreagents. *Developmental Dynamics,* 235, 1701-1708.

SMITH, T. K., HAGER, H. A., FRANCIS, R., KILKENNY, D. M., LO, C. W. & BADER, D. M. 2008. Bves directly interacts with GEFT, and controls cell shape and movement through regulation of Rac1/Cdc42 activity. *Proceedings of the National Academy of Sciences,* 105, 8298.

SÖDERBERG, O., LEUCHOWIUS, K.-J., GULLBERG, M., JARVIUS, M., WEIBRECHT, I., LARSSON, L.-G. & LANDEGREN, U. 2008. Characterizing proteins and their interactions in cells and tissues using the in situ proximity ligation assay. *Methods,* 45, 227-232.

SONG, K. S., SCHERER, P. E., TANG, Z., OKAMOTO, T., LI, S., CHAFEL, M., CHU, C., KOHTZ, D. S. & LISANTI, M. P. 1996. Expression of Caveolin-3 in Skeletal, Cardiac, and Smooth Muscle Cells: Caveolin-3 is a component of the sarcolemma and co-fractionates with dystrophin and dystrophin-associated glycoproteins. *Journal of Biological Chemistry,* 271, 15160-15165.

SOUDERS, C. A., BOWERS, S. L. K. & BAUDINO, T. A. 2009. Cardiac fibroblast: the renaissance cell. *Circulation research,* 105, 1164-1176.

SOUNESS, J. E., ALDOUS, D. & SARGENT, C. 2000. Immunosuppressive and anti-inflammatory effects of cyclic AMP phosphodiesterase (PDE) type 4 inhibitors. *Immunopharmacology,* 47, 127-162.

SPINA, A., DI MAIOLO, F., ESPOSITO, A., SAPIO, L., CHIOSI, E., SORVILLO, L. & NAVIGLIO, S. 2012. cAMP Elevation Down-Regulates ß3 Integrin and Focal Adhesion Kinase and Inhibits Leptin-Induced Migration of MDA-MB-231 Breast Cancer Cells. *BioResearch open access,* 1, 324-332.

SPINALE, F. G., ZELLNER, J. L., TOMITA, M., CRAWFORD, F. & ZILE, M. 1991. Relation between ventricular and myocyte remodeling with the development and regression of supraventricular tachycardia-induced cardiomyopathy. *Circulation research,* 69**,** 1058-1067.

SQUIRES, C. & SQUIRES, C. L. 1992. The Clp proteins: proteolysis regulators or molecular chaperones? *Journal of bacteriology,* 174**,** 1081-1085.

STAN, R. V. 2005. Structure of caveolae. *Biochimica et Biophysica Acta (BBA) - Molecular Cell Research,* 1746**,** 334-348.

STEINACHER, R. & SCHÄR, P. 2005. Functionality of Human Thymine DNA Glycosylase Requires SUMO-Regulated Changes in Protein Conformation. *Current Biology,* 15**,** 616-623.

STEINBERG, R. A., CAUTHRON, R. D., SYMCOX, M. M. & SHUNTOH, H. 1993. Autoactivation of catalytic (C alpha) subunit of cyclic AMP-dependent protein kinase by phosphorylation of threonine 197. *Mol Cell Biol,* 13**,** 2332-41.

STEINER, A. L., WHITLEY, T. H., ONG, S.-H. H. & STOWE, N. W. 1975. Cyclic AMP and cyclic GMP: Studies utilizing immunohistochemical techniques for the localization of the nucleotides in tissue. *Metabolism,* 24**,** 419-428.

STENMARK, H., AASLAND, R. & DRISCOLL, P. C. 2002. The phosphatidylinositol 3-phosphate-binding FYVE finger. *FEBS letters,* 513**,** 77-84.

STETEFELD, J., MCKENNA, S. A. & PATEL, T. R. 2016. Dynamic light scattering: a practical guide and applications in biomedical sciences. *Biophysical reviews,* 8**,** 409-427.

STUDER, ROMAIN A., DESSAILLY, BENOIT H. & ORENGO, CHRISTINE A. 2013. Residue mutations and their impact on protein structure and function: detecting beneficial and pathogenic changes. *Biochemical Journal,* 449**,** 581-594.

SUSSMAN, M. A., WELCH, S., WALKER, A., KLEVITSKY, R., HEWETT, T. E., PRICE, R. L., SCHAEFER, E. & YAGER, K. 2000. Altered focal adhesion regulation correlates with cardiomyopathy in mice expressing constitutively active rac1. *The Journal of Clinical Investigation,* 105**,** 875-886.

SUTHERLAND, E. W. 1972. Studies on the Mechanism of Hormone Action. *Science,* 177**,** 401.

SUTHERLAND, E. W. & RALL, T. W. 1958. FRACTIONATION AND CHARACTERIZATION OF A CYCLIC ADENINE RIBONUCLEOTIDE FORMED BY TISSUE PARTICLES. *Journal of Biological Chemistry,* 232**,** 1077-1092.

SWAN, A. H., GRUSCHESKI, L., BOLAND, L. A. & BRAND, T. 2019. The Popeye domain containing gene family encoding a family of cAMP-effector proteins with important functions in striated muscle and beyond. *Journal of Muscle Research and Cell Motility,* 40**,** 169-183.

TAKAHASHI, Y., TOH-E, A. & KIKUCHI, Y. 2001. A novel factor required for the SUMO1/Smt3 conjugation of yeast septins. *Gene,* 275**,** 223-231.

TAKEO, S., NIIMURA, M., MIYAKE-TAKAGI, K., NAGAKURA, A., FUKATSU, T., ANDO, T., TAKAGI, N., TANONAKA, K. & HARA, J. 2003. A possible mechanism for improvement by a cognition-enhancer nefiracetam of spatial memory function and cAMP-mediated signal transduction system in sustained cerebral ischaemia in rats. *British journal of pharmacology,* 138**,** 642-654.

TAN, M., SONG, X., ZHANG, G., PENG, A., LI, X., LI, M., LIU, Y. & WANG, C. 2013. Overexpression of adenylate cyclase-associated protein 1 is associated with metastasis of lung cancer. *Oncology reports,* 30**,** 1639-1644.

TAN, S. 2001. A Modular Polycistronic Expression System for Overexpressing Protein Complexes in Escherichia coli. *Protein Expression and Purification,* 21**,** 224-234.

TANAKA, M., FUJIWARA, H., ONODERA, T., WU, D., MATSUDA, M., HAMASHIMA, Y. & KAWAI, C. 1987. Quantitative analysis of narrowings of intramyocardial small arteries in normal hearts, hypertensive hearts, and hearts with hypertrophic cardiomyopathy. *Circulation,* 75**,** 1130-1139.

TANG, W.-J. & HURLEY, J. H. 1998. Catalytic Mechanism and Regulation of Mammalian Adenylyl Cyclases. *Molecular Pharmacology,* 54**,** 231.

TASKEN, K. & AANDAHL, E. M. 2004. Localized Effects of cAMP Mediated by Distinct Routes of Protein Kinase A. *Physiological Reviews,* 84**,** 137-167.

TAYLOR, M. S., BONEV, A. D., GROSS, T. P., ECKMAN, D. M., BRAYDEN, J. E., BOND, C. T., ADELMAN, J. P. & NELSON, M. T. 2003. Altered Expression of Small-Conductance Ca2+-Activated K+(SK3) Channels Modulates Arterial Tone and Blood Pressure. *Circulation Research,* 93**,** 124-131.

TAYLOR, S. S., BUECHLER, J. A. & YONEMOTO, W. 1990. cAMP-dependent protein kinase: Framework for a diverse family of regulatory enzymes. *Annual Review of Biochemistry,* 59**,** 971-1005.

TAYLOR, S. S., YANG, J., WU, J., HASTE, N. M., RADZIO-ANDZELM, E. & ANAND, G. 2004. PKA: a portrait of protein kinase dynamics. *Biochimica et Biophysica Acta (BBA) - Proteins and Proteomics,* 1697**,** 259-269.

TERRENOIRE, C., HOUSLAY, M. D., BAILLIE, G. S. & KASS, R. S. 2009. The Cardiac IKs Potassium Channel Macromolecular Complex Includes the Phosphodiesterase PDE4D3. *Journal of Biological Chemistry,* 284**,** 9140-9146.

TERRENOIRE, C., LAURITZEN, I., LESAGE, F., ROMEY, G. & LAZDUNSKI, M. 2001. A TREK-1 Like Potassium Channel in Atrial Cells Inhibited by B2;-Adrenergic Stimulation and Activated by Volatile Anesthetics. *Circulation Research,* 89**,** 336-342.

TESMER, J. J. G., SUNAHARA, R. K., GILMAN, A. G. & SPRANG, S. R. 1997. Crystal Structure of the Catalytic Domains of Adenylyl Cyclase in a Complex with G_{sα}·GTPγS. *Science,* 278**,** 1907-1916.

TEVOSIAN, S. G., DECONINCK, A. E., TANAKA, M., SCHINKE, M., LITOVSKY, S. H., IZUMO, S., FUJIWARA, Y. & ORKIN, S. H. 2000. FOG-2, a Cofactor for GATA Transcription Factors, Is Essential for Heart Morphogenesis and Development of Coronary Vessels from Epicardium. *Cell,* 101**,** 729-739.

THEIN, E. & HAMMER, C. 2004. Physiologic barriers to xenotransplantation. *Current Opinion in Organ Transplantation,* 9**,** 186-189.

THRELFELL, S. & WEST, A. R. 2013. Modulation of striatal neuron activity by cyclic nucleotide signalling and phosphodiesterase inhibition. *Basal ganglia,* 3**,** 137-146.

TIBBO, A. J., TEJEDA, G. S. & BAILLIE, G. S. 2019. Understanding PDE4's function in Alzheimer's disease; a target for novel therapeutic approaches. *Biochemical Society transactions,* 47**,** 1557-1565.

TILEMANN, L., LEE, A., ISHIKAWA, K., AGUERO, J., RAPTI, K., SANTOS-GALLEGO, C., KOHLBRENNER, E., FISH, K. M., KHO, C. & HAJJAR, R. J. 2013. SUMO-1 Gene Transfer Improves Cardiac Function in a Large-Animal Model of Heart Failure. *Science Translational Medicine,* 5**,** 211ra159.

TOBACMAN, L. S. 1996. Thin Filament-Mediated Regulation of Cardiac Contraction. *Annual Review of Physiology,* 58**,** 447-481.

TONG, C. W., STELZER, J. E., GREASER, M. L., POWERS, P. A. & MOSS, R. L. 2008. Acceleration of crossbridge kinetics by protein kinase A phosphorylation of cardiac myosin binding protein C modulates cardiac function. *Circulation research,* 103**,** 974-982.

TOON, C. W., CHOU, A., CLARKSON, A., DESILVA, K., HOUANG, M., CHAN, J. C. Y., SIOSON, L. L., JANKOVA, L. & GILL, A. J. 2014. Immunohistochemistry for myc predicts survival in colorectal cancer. *PloS one,* 9**,** e87456-e87456.

TORPHY, T. J. 1998. Phosphodiesterase Isozymes. *American Journal of Respiratory and Critical Care Medicine,* 157**,** 351-370.

TRIAL, J., ROSSEN, R. D., RUBIO, J. & KNOWLTON, A. A. 2004. Inflammation and ischemia: macrophages activated by fibronectin fragments enhance the survival of injured cardiac myocytes. *Experimental biology and medicine (Maywood, N.J.),* 229**,** 538-545.

TRIAN, T., BURGESS, J. K., NIIMI, K., MOIR, L. M., GE, Q., BERGER, P., LIGGETT, S. B., BLACK, J. L. & OLIVER, B. G. 2011. ß2-Agonist induced cAMP is decreased in asthmatic airway smooth muscle due to increased PDE4D. *PloS one,* 6**,** e20000-e20000.

TSUBATA, S., BOWLES, K. R., VATTA, M., ZINTZ, C., TITUS, J., MUHONEN, L., BOWLES, N. E. & TOWBIN, J. A. 2000. Mutations in the human delta-sarcoglycan gene in familial and sporadic dilated cardiomyopathy. *J Clin Invest,* 106**,** 655-62.

ULRICH, H. D. 2009. The SUMO System: An Overview. *In:* ULRICH, H. D. (ed.) *SUMO Protocols.* Totowa, NJ: Humana Press.

ULRICH, HELLE D. 2012. Ubiquitin, SUMO, and Phosphate: How a Trio of Posttranslational Modifiers Governs Protein Fate. *Molecular Cell,* 47**,** 335-337.

UNUDURTHI, S. D., WU, X., QIAN, L., AMARI, F., ONAL, B., LI, N., MAKARA, M. A., SMITH, S. A., SNYDER, J., FEDOROV, V. V., COPPOLA, V., ANDERSON, M. E., MOHLER, P. J. & HUND, T. J. 2016. Two-Pore K+ Channel TREK-1 Regulates Sinoatrial Node Membrane Excitability. *Journal of the American Heart Association,* 5**,** e002865-e002865.

VAIDYANATHAN, R., REILLY, L. & ECKHARDT, L. L. 2018. Caveolin-3 Microdomain: Arrhythmia Implications for Potassium Inward Rectifier and Cardiac Sodium Channel. *Frontiers in Physiology,* 9.

VAN ELDIK, W. & PASSIER, R. 2013. Signalling in sarcomeres in development and disease. *Netherlands heart journal : monthly journal of the Netherlands Society of Cardiology and the Netherlands Heart Foundation,* 21**,** 367-371.

VASAVADA, T., DIANGELO, J. & DUNCAN, M. 2004. Developmental Expression of Pop1/Bves. *The journal of histochemistry and cytochemistry : official journal of the Histochemistry Society,* 52**,** 371-7.

VERDE, I., VANDECASTEELE, G., LEZOUALC'H, F. & FISCHMEISTER, R. 1999. Characterization of the cyclic nucleotide phosphodiesterase subtypes involved in the regulation of the L-type Ca2+ current in rat ventricular myocytes. *British Journal of Pharmacology,* 127**,** 65-74.

VERGER, A., PERDOMO, J. & CROSSLEY, M. 2003. Modification with SUMO. A role in transcriptional regulation. *EMBO Rep,* 4**,** 137-42.

VILEIGAS, D. F., HARMAN, V. M., FREIRE, P. P., MARCIANO, C. L. C., SANT'ANA, P. G., DE SOUZA, S. L. B., MOTA, G. A. F., DA SILVA, V. L., CAMPOS, D. H. S., PADOVANI, C. R., OKOSHI, K., BEYNON, R. J., SANTOS, L. D. & CICOGNA, A. C. 2019. Landscape of heart proteome changes in a diet-induced obesity model. *Scientific Reports,* 9**,** 18050.

VOLKOVA, M., GARG, R., DICK, S. & BOHELER, K. R. 2005. Aging-associated changes in cardiac gene expression. *Cardiovascular Research,* 66**,** 194-204.

WACHTEL, H. 1983. Potential antidepressant activity of rolipram and other selective cyclic adenosine 3′,5′-monophosphate phosphodiesterase inhibitors. *Neuropharmacology,* 22**,** 267-272.

WADA, A. M., REESE, D. E. & BADER, D. M. 2001. Bves: prototype of a new class of cell adhesion molecules expressed during coronary artery development. *Development,* 128**,** 2085.

WALSH, D., PERKINS, J. P. & KREBS, E. G. 1968. An adenosine 3', 5'-monophosphate-dependant protein kinase from rabbit skeletal muscle. *Journal of Biological Chemistry,* 243**,** 3763-3765.

WANG, H., PENG, M.-S., CHEN, Y., GENG, J., ROBINSON, H., HOUSLAY, M. D., CAI, J. & KE, H. 2007. Structures of the four subfamilies of phosphodiesterase-4 provide insight into the selectivity of their inhibitors. *The Biochemical journal,* 408**,** 193-201.

WANG, H. D., XU, S., JOHNS, D. G., DU, Y., QUINN, M. T., CAYATTE, A. J. & COHEN, R. A. 2001. Role of NADPH Oxidase in the Vascular Hypertrophic and Oxidative Stress Response to Angiotensin II in Mice. *Circulation Research,* 88**,** 947-953.

WASS, M. N., KELLEY, L. A. & STERNBERG, M. J. E. 2010. 3DLigandSite: predicting ligand-binding sites using similar structures. *Nucleic Acids Research,* 38**,** W469-W473.

WEBER, A. R., SCHUERMANN, D. & SCHÄR, P. 2014. Versatile Recombinant SUMOylation System for the Production of SUMO-Modified Protein. *PLOS ONE,* 9**,** e102157.

WEBER, K. T. 2004. Fibrosis in hypertensive heart disease: focus on cardiac fibroblasts. *J Hypertens,* 22**,** 47-50.

WEI, W. & LIN, H.-K. 2012. The key role of ubiquitination and sumoylation in signaling and cancer: a research topic. *Frontiers in oncology,* 2**,** 187-187.

WEISHAAR, R. E., KOBYLARZ-SINGER, D. C., STEFFEN, R. P. & KAPLAN, H. R. 1987. Subclasses of cyclic AMP-specific phosphodiesterase in left ventricular muscle and their involvement in regulating myocardial contractility. *Circulation Research,* 61**,** 539-547.

WHITE, K. A., RUIZ, D. G., SZPIECH, Z. A., STRAULI, N. B., HERNANDEZ, R. D., JACOBSON, M. P. & BARBER, D. L. 2017. Cancer-associated arginine-to-histidine mutations confer a gain in pH sensing to mutant proteins. *Science signaling,* 10**,** eaam9931.

WILLIAMS, C. S., ZHANG, B., SMITH, J. J., JAYAGOPAL, A., BARRETT, C. W., PINO, C., RUSS, P., PRESLEY, S. H., PENG, D., ROSENBLATT, D. O., HASELTON, F. R., YANG, J.-L., WASHINGTON, M. K., CHEN, X., ESCHRICH, S., YEATMAN, T. J., EL-RIFAI, W., BEAUCHAMP, R. D. & CHANG, M. S. 2011. BVES regulates EMT in human corneal and colon cancer cells and is silenced via promoter methylation in human colorectal carcinoma. *The Journal of clinical investigation,* 121**,** 4056-4069.

WILLOUGHBY, D., BAILLIE, G. S., LYNCH, M. J., CIRUELA, A., HOUSLAY, M. D. & COOPER, D. M. F. 2007. Dynamic Regulation, Desensitization, and Cross-talk in Discrete Subcellular Microdomains during β2-Adrenoceptor and Prostanoid Receptor cAMP Signaling. *Journal of Biological Chemistry,* 282**,** 34235-34249.

WILLOUGHBY, D. & COOPER, D. M. F. 2007. Organization and Ca2+ Regulation of Adenylyl Cyclases in cAMP Microdomains. *Physiological Reviews,* 87**,** 965-1010.

WILLS, L. 2017. *SUMOylation of the B2AR influences receptor internalisation, desensitisation and downstream signalling*. University of Glasgow.

WILLS, L., FERTIG, B. A. & BAILLIE, G. S. 2017. Cardiac cAMP Microdomains and Their Modulation Using Disruptor Peptides. *In:* NIKOLAEV, V. & ZACCOLO, M. (eds.) *Microdomains in the Cardiovascular System*. Cham: Springer International Publishing.

WOLFF, M. R., BUCK, S. H., STOKER, S. W., GREASER, M. L. & MENTZER, R. M. 1996. Myofibrillar calcium sensitivity of isometric tension is increased in human dilated cardiomyopathies: role of altered beta-adrenergically mediated protein phosphorylation. *The Journal of Clinical Investigation,* 98**,** 167-176.

WRIGHT, L. P. & PHILIPS, M. R. 2006. Thematic review series: lipid posttranslational modifications CAAX modification and membrane targeting of Ras. *Journal of lipid research,* 47**,** 883-891.

WU, X., LI, J., ZHU, M., FLETCHER, J. A. & HODI, F. S. 2012a. Protein kinase C inhibitor AEB071 targets ocular melanoma harboring GNAQ mutations via effects on the PKC/Erk1/2 and PKC/NF-κB pathways. *Molecular cancer therapeutics,* 11**,** 1905-1914.

WU, Y.-C., LIU, C.-Y., CHEN, Y.-H., CHEN, R.-F., HUANG, C.-J. & WANG, I.-J. 2012b. Blood Vessel Epicardial Substance (Bves) Regulates Epidermal Tight Junction Integrity through Atypical Protein Kinase C. *Journal of Biological Chemistry,* 287**,** 39887-39897.

WYPIJEWSKI, K. J., TINTI, M., CHEN, W., LAMONT, D., ASHFORD, M. L. J., CALAGHAN, S. C. & FULLER, W. 2015. Identification of Caveolar Resident Proteins in Ventricular Myocytes Using a Quantitative Proteomic Approach: Dynamic Changes in Caveolar Composition Following Adrenoceptor Activation. *Molecular & Cellular Proteomics,* 14**,** 596.

XIANG, Y. K. 2011. Compartmentalization of beta-adrenergic signals in cardiomyocytes. *Circ Res,* 109**,** 231-44.

XUE, Y., LIU, Z., CAO, J., MA, Q., GAO, X., WANG, Q., JIN, C., ZHOU, Y., WEN, L. & REN, J. 2010. GPS 2.1: enhanced prediction of kinase-specific phosphorylation sites with an algorithm of motif length selection. *Protein Engineering, Design and Selection,* 24**,** 255-260.

YANCY, C. W., JESSUP, M., BOZKURT, B., BUTLER, J., CASEY, D. E., DRAZNER, M. H., FONAROW, G. C., GERACI, S. A., HORWICH, T., JANUZZI, J. L., JOHNSON, M. R., KASPER, E. K., LEVY, W. C., MASOUDI, F. A., MCBRIDE, P. E., MCMURRAY, J. J. V., MITCHELL, J. E., PETERSON, P. N., RIEGEL, B., SAM, F., STEVENSON, L. W., TANG, W. H. W., TSAI, E. J. & WILKOFF, B. L. 2013. 2013 ACCF/AHA Guideline for the Management of Heart Failure: A Report of the American College of Cardiology Foundation/American Heart Association Task Force on Practice Guidelines. *Journal of the American College of Cardiology,* 62**,** e147-e239.

YANG, C. & KAZANIETZ, M. G. 2003. Divergence and complexities in DAG signaling: looking beyond PKC. *Trends in pharmacological sciences,* 24**,** 602-608.

YANG, S.-H., GALANIS, A., WITTY, J. & SHARROCKS, A. D. 2006. An extended consensus motif enhances the specificity of substrate modification by SUMO. *The EMBO journal,* 25**,** 5083-5093.

YANG, Y., HE, Y., WANG, X., LIANG, Z., HE, G., ZHANG, P., ZHU, H., XU, N. & LIANG, S. 2017. Protein SUMOylation modification and its associations with disease. *Open Biology,* 7**,** 170167.

YUE, D. T. & MARBAN, E. 1988. A novel cardiac potassium channel that is active and conductive at depolarized potentials. *Pflügers Archiv,* 413**,** 127-133.

ZACCOLO, M. 2009. cAMP signal transduction in the heart: understanding spatial control for the development of novel therapeutic strategies. *British journal of pharmacology,* 158**,** 50-60.

ZACCOLO, M. & POZZAN, T. 2002. Discrete Microdomains with High Concentration of cAMP in Stimulated Rat Neonatal Cardiac Myocytes. *Science,* 295**,** 1711.

ZAK, R. 1974. Development and proliferative capacity of cardiac muscle cells. *Circ Res,* 35**,** suppl II:17-26.

ZATLOUKAL, B., KUFFERATH, I., THUERINGER, A., LANDEGREN, U., ZATLOUKAL, K. & HAYBAECK, J. 2014. Sensitivity and Specificity of In situ Proximity Ligation for Protein Interaction Analysis in a Model of Steatohepatitis with Mallory-Denk Bodies. *PLOS ONE,* 9**,** e96690.

ZHA, J., WEILER, S., OH, K. J., WEI, M. C. & KORSMEYER, S. J. 2000. Posttranslational N-myristoylation of BID as a molecular switch for targeting mitochondria and apoptosis. *Science,* 290**,** 1761-1765.

ZHANG, G., LIU, Y., RUOHO, A. E. & HURLEY, J. H. 1997. Structure of the adenylyl cyclase catalytic core. *Nature,* 386**,** 247-253.

ZHANG, J., MA, Y., TAYLOR, S. S. & TSIEN, R. Y. 2001. Genetically encoded reporters of protein kinase A activity reveal impact of substrate tethering. *Proceedings of the National Academy of Sciences,* 98**,** 14997.

ZHANG, K. Y. J., IBRAHIM, P. N., GILLETTE, S. & BOLLAG, G. 2005. Phosphodiesterase-4 as a potential drug target. *Expert Opinion on Therapeutic Targets,* 9**,** 1283-1305.

ZHANG, M. M. & HANG, H. C. 2017. Protein S-palmitoylation in cellular differentiation. *Biochemical Society transactions,* 45**,** 275-285.

ZHANG, R., YANG, J., ZHU, J. & XU, X. 2009. Depletion of zebrafish Tcap leads to muscular dystrophy via disrupting sarcomere-membrane interaction, not sarcomere assembly. *Human molecular genetics,* 18**,** 4130-4140.

ZHANG, Z., AKHTER, S., MOTTL, S. & JIN, J.-P. 2011. Calcium-regulated conformational change in the C-terminal end segment of troponin I and its binding to tropomyosin. *The FEBS journal,* 278**,** 3348-3359.

ZHENG, M., DILLY, K., CRUZ, J. D. S., LI, M., GU, Y., URSITTI, J. A., CHEN, J., JOHN ROSS, J., CHIEN, K. R., LEDERER, J. W. & WANG, Y. 2004. Sarcoplasmic reticulum calcium defect in Ras-induced hypertrophic cardiomyopathy heart. *American Journal of Physiology-Heart and Circulatory Physiology,* 286**,** H424-H433.